

CRYSTALLIZATION, MORPHOLOGY, THERMAL STABILITY AND ADHESIVE PROPERTIES OF NOVEL HIGH PERFORMANCE SEMICRYSTALLINE POLYIMIDES

by

Varun Ratta

Dissertation submitted to the Faculty of Virginia Polytechnic Institute and State
University in partial fulfillment of the requirements for the degree of

**Doctor of Philosophy
in
Chemical Engineering**

Advisory Committee

Dr. Garth L. Wilkes, Chairman

Dr. James E. McGrath

Dr. Herve Marand

Dr. Richey M. Davis

Dr. Thomas C. Ward

Dr. David F. Cox

April, 1999
Blacksburg, Virginia

Keywords: Polyimides, Crystallization, Morphology, Adhesive, Lap-shear, Thermal
Stability, Crystallization Kinetics

CRYSTALLIZATION, MORPHOLOGY, THERMAL STABILITY AND ADHESIVE PROPERTIES OF NOVEL HIGH PERFORMANCE SEMICRYSTALLINE POLYIMIDES

by

Varun Ratta

Chairman: Garth L. Wilkes

Department of Chemical Engineering

Abstract

It was the objective of this research to develop high temperature and high performance polyimides that also display (a) thermal stability; (b) crystallinity in the initial material and ability to crystallize from the melt; (c) fast crystallization kinetics and (d) melt processability. This unique combination of properties is presently unavailable in any other polyimide. In this regard, the present work investigates the crystallization, morphology and thermal stability of two novel semicrystalline polyimides based on the same diamine, 1,3-bis (4-aminophenoxy) benzene (TPER), but two different dianhydrides, 3,3',4',4'-biphenyltetracarboxylic dianhydride (BPDA) and 3,3',4,4'-benzophenonetetracarboxylic dianhydride (BTDA). Phthalic anhydride was used as an endcapper to improve the thermal stability of the polyimides. The BPDA based polyimide was also tested extensively as a structural adhesive using Ti-6Al-4V coupons. Additionally, these polyimides are based on monomers, that are presently commercially available.

The bulk thermal stability of the polyimides was first evaluated using dynamic and isothermal thermogravimetric experiments. DSC was utilized to test the ability of the polyimides to crystallize from the melt after exposures to varying melt times and temperatures. Exceptional thermal stability was demonstrated by BPDA based polyimide with no change in the melting behavior after 40 min at 430°C or 30 min at 440°C. The semicrystalline morphology of the material was studied using hot stage polarized optical microscopy (OM) and atomic force microscopy. The spherulitic growth rates were

determined as a function of crystallization temperature after quenching from various melt times and temperatures. The effect of crystallization temperature, previous melt time and melt temperature on the morphology was considered. The spherulitic growth rates increased with increasing undercooling in the temperature range studied (nucleation controlled), while the growth rate at a specific crystallization temperature decreased on increasing the previous melt time and temperature. The melting behavior was studied after different crystallization times and temperatures and also as a function of different heating rates. Crystallization kinetics was followed both isothermally and non-isothermally using DSC and OM. Avrami analysis was performed for TPER-BPDA and the obtained results were correlated with microscopic observations. Melt viscosity measurements were carried out as a function of melt temperature, melt time and frequency. The adhesive investigations for TPER-BTDA utilized lap-shear test, wedge test and double cantilever beam tests. The durability of the adhesive and the fracture surface was studied after exposure to various solvents and after high aging and testing temperatures. The polyimide demonstrated very high average room temperature lap-shear strengths (8400 psi or 59 MPa), excellent solvent resistance and durability of strengths at high aging and testing temperatures.

DEDICATION

To

my parents

Reva and D.B. Ratta

without whose sacrifices none of this would be possible

ACKNOWLEDGEMENTS

I am going to cherish my experiences at Virginia Tech for a long time to come. Indeed, this university, along with providing a first class education, has given me several opportunities for both academic and personal growth. In this regard, I am thankful to number of my teachers, colleagues and friends. First and foremost however, I express my gratitude to my advisor, Dr. Garth L. Wilkes, who along with teaching me a great deal about polymer science, also contributed significantly towards my overall professional development. His guidance, patience and encouragement throughout my doctoral work are instrumental in its completion. I am also indebted to him for teaching two marvelous polymer courses.

Thanks are also due to Dr. Hervé Marand for teaching me polymer crystallization and for being a member of my committee. His criticisms, guidance and support have always motivated me to become a better researcher. I also wish to express my gratitude towards Dr. James E. McGrath for giving me a wonderful opportunity to learn more about polymer chemistry, for being able to work with his research group and for serving on my committee. His inputs and support were critical in the successful completion of this work. I am also indebted to Dr. Thomas C. Ward for teaching me two outstanding courses and for being a member of this committee. I also thank him for organizing the NSF summer student program, which provided me an enjoyable opportunity to work with summer students for two successive years. I also express my thanks towards Dr. Richey M. Davis for teaching an excellent course and serving on my committee. I am also grateful to him for several helpful discussions and for allowing me to use his research facilities. I also express my gratitude towards Dr. David. F. Cox for his suggestions and for serving on my committee.

I will also like to acknowledge a number of my friends and colleagues, without whom, this experience would have been incomplete. Firstly, a special thanks to Srivatsan Srinivas for his initial support, friendship and for training me on several research equipment. I specially value the assistance and friendship of many of my colleagues- Amba Ayembem, Ed Stancik, Stefan Williams, Binh Tran, Hari Parvattareddy, Robert

Young, Quin Ji, Rakesh Mehta, Todd Bullions and Slade Gardener. Thanks are also due to several of my friends in our research group including- Chris, Kurt, Hongyi, Ta-Hua, Jianye, David Shelby, Rob, Bryan, Matt Johnson, Matt O'Sickey, David Godshall, Chenghong and now Ashish.

A special thanks to Sandy for all her help in getting things done. I will also like to acknowledge the help of Joyce, Esther, Millie and Laurie in Chemistry. Thanks are also due to Steve McCartney for his help with the AFM and TEM experiments. I also appreciate help of the Department of Chemical Engineering's staff including Diane Cannady, Diane Patty, Carol Stables, Wendall Brown, Riley Chan and the Department Head, Dr. W.L. Conger. The NSF Science and Technology Center at Virginia Tech and the Department of Chemical Engineering are gratefully acknowledged for their financial support.

I will also thank several of my roommates and friends in Blacksburg- Vikram, Vivek, Rakesh, Indi, Rajeev, Raj, Vidhu, Sukhtej, Arun, Neeraj, Rajesh and Prabhu for a great time I had in Blacksburg.

Finally my most important acknowledgments are towards my family who have been the single biggest motivating force in my life. I thank my sister Ekta, and my parents Reva and D.B. Ratta for their encouragement, advice and for the many sacrifices they have made over a number of years. This dissertation is dedicated to them.

Table of Contents

ABSTRACT

ACKNOWLEDGEMENTS

TABLE OF CONTENTS

LIST OF FIGURES

LIST OF TABLES

INTRODUCTION 1

**CHAPTER 1 POLYIMIDES: CHEMISTRY & STRUCTURE-PROPERTY
RELATIONSHIPS –LITERATURE REVIEW**

1.1	Introduction	3
1.2	Two step method for polyimide synthesis	3
1.2.	Formation of poly(amic acids).....	5
1.2.2	<i>Effect of monomer reactivity</i>	<i>6</i>
1.2.3	<i>Effect of reaction conditions and solvents on the synthesis</i>	<i>8</i>
1.2.4	<i>Side reactions and other factors involved in the synthesis.....</i>	<i>9</i>
1.2.5	<i>Thermal imidization of poly(amic acid).....</i>	<i>11</i>
1.2.5.1	Determination of the degree of imidization:.....	12
1.2.5.2	Changes in mechanical properties & molecular weight during thermal imidization:	13
1.2.6	<i>Chemical imidization of the poly(amic acids):</i>	<i>14</i>
1.3	One step method- high temperature solution polymerization:.....	14
1.4	Structure property relationships in linear aromatic polyimides	15
1.4.1	<i>T_g – structure relationships</i>	<i>15</i>
1.4.2	<i>Polyimide chain-chain interactions.....</i>	<i>16</i>

1.4.3	<i>Effect of chain length of the ether diamine on the glass transition</i>	20
1.4.4	<i>Effect of isomeric attachment of the diamine:</i>	22
1.4.5	<i>Effect of the dianhydride structure on the glass transition:</i>	24
1.4.6	<i>Effect of chain structure on the crystallinity:</i>	25

CHAPTER 2 POLYMER CRYSTALLIZATION – LITERATURE REVIEW

2.1	Introduction	29
2.2	Thermodynamics of crystallization and melting	30
2.3	Crystallization in polymers: structure, models & relationships	32
2.4	The fringed micelle model.....	39
2.5	Lamellar models	41
2.6	Gibbs-Thomson equation':.....	44
2.7	Lauritzen-Hoffman secondary nucleation theory'	46
2.8	Growth rate determination and regime kinetics	57
2.9	Primary nucleation:.....	62
2.10	Spherulites	67
2.11	Bulk crystallization kinetics-avrami analysis	69

CHAPTER 3 SEMI-FLEXIBLE SEMICRYSTALLINE POLYIMIDES- LITERATURE REVIEW

3.1	Introduction	80
3.2	Crystallization behavior from the melt.....	81
3.3	Crystallization kinetics	85
3.4	Morphology of semicrystalline polyimides.....	89
3.5	Melting behavior of semicrystalline polyimides	92
3.6	Melt viscosity	94

CHAPTER 4 POLYIMIDES AS ADHESIVES: -LITERATURE REVIEW

4.1	Introduction	102
4.2	Theories of adhesion	103
4.2.1	<i>Mechanical interlocking</i>	103
4.2.2	<i>Molecular inter-diffusion</i>	103
4.2.3	<i>Electronic theory</i>	104
4.2.4	<i>Adsorption theory</i>	104
4.3	Adhesion aspects of the present work	105
4.4	Titanium as an adherend	106
4.5	Some aspects of various adhesion tests	110
4.6	Lap-shear test	110
4.7	Crystallization aspects in adhesion.....	114
4.8	Polyimides as high performance adhesives.....	116

CHAPTER 5 A MELT PROCESSABLE SEMICRYSTALLINE POLYIMIDE STRUCTURAL ADHESIVE BASED ON 1,3-BIS(4- AMINOPHENOXY) BENZENE AND 3,3',4,4'- BIPHENYLTETRACARBOXYLIC DIANHYDRIDE

5.1	Introduction	125
5.2	Experimental	129
5.2.1	<i>Synthesis</i>	129
5.2.2	<i>Characterization:</i>	132
5.2.3	<i>Surface treatment:</i>	134
5.3	Results and Discussion	135
5.3.1	<i>Thermal stability:</i>	135
5.3.2	<i>Melt rheology</i>	138
5.3.3	<i>Morphology of TPER-BPDA-PA:</i>	140
5.3.4	<i>Surface preparation:</i>	148

5.3.5	<i>Optimization of bonding process:</i>	149
5.3.6	<i>Durability studies on lap-shear bonds</i>	158
5.3.7	<i>Effect of various solvents:</i>	164
5.4	Conclusions	166
5.5	Acknowledgments.....	167

CHAPTER 6 THERMAL STABILITY, CRYSTALLIZATION KINETICS AND MORPHOLOGY OF A NEW SEMICRYSTALLINE POLYIMIDE BASED ON 1,3-BIS (4-AMINOPHENOXY) BENZENE AND 3,3', 4,4'-BIPHENYLTETRACARBOXYLIC DIANHYDRIDE

6.1	Introduction	170
6.2	Experimental	172
6.3	Results and Discussion	174
6.3.1	<i>Effect of melt residence time and melt temperature on crystallization kinetics</i>	189
6.3.2	<i>Rheological studies</i>	200
6.3.2.1	Isothermal frequency sweeps at 430°C.....	200
6.3.2.2	Isothermal time sweeps at various melt temperatures	203
6.3.2.3	Complex viscosity on cooling from various melt temperatures	208
6.3.2.4	Activation energy (E_a) values on cooling from various melt temperatures.....	209
6.3.3	<i>Growth rates as a function of melt histories and non-isothermal behavior:</i>	210
6.4	Conclusions	216
6.5	Acknowledgments.....	219

**CHAPTER 7 WEDGE AND DOUBLE CANTILEVER BEAM TESTS ON A
HIGH TEMPERATURE MELT PROCESSABLE POLYIMIDE
ADHESIVE, TPER-BPDA-PA**

7.1	Introduction	221
7.2	Wedge test (experimental methodology):	222
7.3	Double cantilever beam (DCB) Test (experimental methodology):	225
7.4	Experimental:	227
7.5	Results and Discussion	229
	7.5.1 <i>Wedge tests</i>	229
	7.5.2 <i>Double cantilever beam tests</i>	234
7.6	Conclusions	239

**CHAPTER 8 CRYSTALLIZATION AND MULTIPLE MELTING BEHAVIOR
OF A NEW SEMICRYSTALLINE POLYIMIDE BASED ON 1,3-
BIS (4-AMINOPHENOXY) BENZENE (TPER) AND 3,3', 4,4'-
BENZOPHENONETETRACARBOXYLIC DIANHYDRIDE
(BTDA)**

8.1	Introduction	244
8.2	Experimental	249
	8.2.1 <i>Synthesis</i> :	249
	8.2.2 <i>Characterization</i>	251
8.3	Results and Discussion	252
8.4	Conclusions	288

**CHAPTER 9 SUMMARY AND RECOMMENDATIONS FOR FUTURE
WORK**

9.1	Summary	292
9.2	Recommendations for Future Work	294

LIST OF FIGURES

Figure 1.1	Reaction scheme for the preparation of Kapton [®] polyimide (ref 2)	4
Figure 1.2	Generalized reaction mechanism of imide formation (ref 2).....	5
Figure 1.3	Idealized charge transfer complex formation in dianhydrides (ref 31).....	16
Figure 1.4	Idealized polymer chain-chain interaction in the crystalline state (ref 38).	17
Figure 1.5	Packing structure of New-TPI viewed along the b-axis as proposed by Okuyama et al. (ref 39).....	19
Figure 1.6	Effect of isomeric attachment of BTDA based polyimides (ref 33)	22
Figure 2.1	General behavior of thermodynamic variables at the equilibrium melting temperature T_m^∞ (a) gibbs free energy (b) entropy and volume	31
Figure 2.2	(a) Crystallization of macromolecules (i) polymerization, followed by crystallization [(i.e.) separate polymerization and crystallization] (ii) crystallization during polymerization and (b) example of macroscopic single crystal obtained by simultaneous polymerization and crystallization-poly (sulfur nitride) 1 division = 0.5 mm.(ref 3).....	34
Figure 2.3	Schematic representation of orientation induced crystallization. The first three drawings illustrate the orientation and crystallization of random coils while the last two drawings show the growth of folded chain kebabs around the central shish. (ref 10).....	37
Figure 2.4	(a) Shish kebab morphology of polyethylene from solution (from pennings, 1967, Ref 2. (b) shish kebabs of cellulose formed by recrystallizing cellulose II onto valonia microfibrils of high molecular weight (also from ref 2). (ref 3)	37
Figure 2.5	Fringed micelle model (a) model of crystallization as might be visualized in a thermoreversible gel (keller et al. Ref 10) (b) hermann and gerngross model (ref 15) for a semicrystalline polymer. Similar schematics illustrate the general molecular picture in fringed micellar crystallization.	39

Figure 2.6	Single crystals of polyethylene after evaporation of tetrachloroethylene solvent. Pleats form due to crystal collapse. Micrograph is taken from 'Polymer Single Crystals' by P.H. Geil. (ref 19).....	41
Figure 2.7	(A) Schematic of a switchboard model, showing the surface of a lamella, interlamellar region and tie chains between the lamella. (from mandelkern) (B) originally proposed model for melt crystallization in polymers.....	42
Figure 2.8	"Erstarrungsmodell" (a) chain conformation in the melt state (b) alignment of suitable conformations in to the crystal. (ref 36)	44
Figure 2.9	Formation of the physically aligned activated complex and its conversion to first crystallographically attached stem. The first step A_0 is the slowest and rate determining step while the step A_0' is fast. (ref 39)	49
Figure 2.10	Formation of the physically aligned activated complex and its conversion to second crystallographically attached stem. The first step A_0 is the slowest and rate determining step while the step A_0' is fast. The activated state includes a tight fold + the aligned part of the chain. (ref 39)	50
Figure 2.11	Barrier system for the surface nucleation showing both the slow, fast and backward steps possible. A , A_0 , B_1 and B are the rate determining slow steps while A_0' and A' are the fast steps. (ref 32).....	51
Figure 2.12	Free energy with subsequent stem deposition along the substrate for different values of lamellar thickness' ' l '. (ref 30)	52
Figure 2.13	Scheme illustrating the rates of stem deposition during three different regimes of crystallization. ' i ' represents the rate of stem nucleation whereas ' g ' represents the rate of substrate completion.....	59
Figure 2.14	A schematic illustrating the conversion of growth rate data to a L-H plot showing the three regime transitions (ref 38). The values of regime constants are calculated by the slope in various regimes and are used to give the product of surface energy terms $\sigma\sigma_e$. All three regimes or even a single regime transition may not be experimentally observed for many polymers.	61

Figure 2.15	Schematic illustrating the variation of free energy with nucleus size. The initial free energy barrier needs to be crossed for the nucleus to become stable. (ref 5)	63
Figure 2.16	Types of crystal nuclei (a) primary nucleus (b) secondary nucleus (c) tertiary nucleus.....	64
Figure 2.17	Variation of total free energy with size depends upon two opposing factors, the gain being due to increased surface area while the loss due to free energy of crystallization. Also, the critical size for stable nuclei formation as well as the critical free energy barrier decrease with increasing undercooling. (ref 2, 38)	65
Figure 2.18	Tie chains in polyethylene spherulites crystallized in presence of n-paraffin, C ₃₂ H ₆₆ , and then extracted with xylene at room temperature. (keith and padden et al. ref 70)	67
Figure 2.19	Utilization of isothermal crystallization data by either DSC or by volume measurements can give the degree of transformation, which can subsequently be utilized for Avrami analysis. (ref 30)	72
Figure 2.20	The characteristic Avrami plots obtained by isothermal crystallization experiments for a polyimide. The initial slope of the curves gives the Avrami constant 'n', which is related to the crystal shape and nucleation type. (ref 84).....	73
Figure 3.1	(a) Second heat DSC scans of LaRC-CPI after having been previously taken to melt and quenching. While 'A' is the low molecular weight version, others are increasingly of higher mol. wt. (b) first heat DSC scans of variously stoichiometrically offset LaRC-CPI-2 polyimide films. (c) DSC scans of LaRC-CPI-2 films showing changing melting behavior after annealing treatment. (d) First and consecutive heating scans for TPEQ-ODPA polyimide showing sluggish crystallization behavior.....	84
Figure 3.2	First heat and repeat heat DSC scans for the commercial New-TPI. The scans are shown for two different grades (a) high viscosity grade (b) low viscosity grade.....	86

Figure 3.3	Chemical structure and thermal stability of New-TPI polyimide. The 3-D plot illustrates the heat of melting after exposures to different melt temperatures and melt residence times.....	87
Figure 3.4	(a) spherulitic growth rates for New-TPI. (b) negatively birefringent spherulites observed for New-TPI. (c) SAXS for LaRC-CPI-2 samples indicating differently thick lamellae responsible for different endotherms. (d) The hedritic structure obtained for LaRC-CPI by Muellerleile et al. (e) The variation of lamellar thickness for New-TPI observed by Srinivas et al.	91
Figure 3.5	Rheological results for different grades of LaRC-TPI. (a) loss modulus, storage modulus and complex viscosity at 350°C for up to 3 hrs. (b) complex viscosity-frequency profiles at different melt temperatures for two grades of LaRC-TPI. (c) master curves for the two grades constructed using the data in (b).	95
Figure 3.6	(a) Melt rheology of an amorphous polyimide by Hergenrother et al. (b) continuous loss and storage shear modulus for LaRC-8515 polyimide at different melt temperatures (c) melt viscosity vs. time at 360°C for LaRC-IA and -IAX (d) crystallization behavior of LaRC-8515 after annealing at different temperatures.....	97
Figure 3.7	Rheological behavior of (a) New-TPI and (b) TPEQ-ODPA polyimides showing molecular weight changes for both polyimides.	99
Figure 4.1	The surface morphology of the Ti-6Al-4V after various surface treatments (a) gritblasting (b) TURCO 5578 sodium hydroxide etch (c) chromic acid treatment (d) chromic acid treated samples after exposure to water vapor at 300°C.	109
Figure 4.2	Shear strain (& shear stress) in the bond-line and tensile stress on the adherends as given (a) ideally & (b) predicted by Volkersen's analysis. (c) effect of bending moment, which acts along the bondline to give a peel stress, thereby reducing joint strengths. (d) shear strength profile as given by various analysis (e) peel stresses along the bondline as calculated by goland-reissner analysis.....	112

Figure 4.3	Room temperature lap-shear strength of the LaRC-TPI-am adhesive for various bonding temperatures and pressures.	119
Figure 4.4	Lap-shear strengths for LaRC-TPI and effect of adding various additives (to change the melt viscosity) when bonded at 50 psi.....	120
Figure 5.1	Percentage weight loss as a function of increasing temperature in nitrogen and air for TPER-BPDA-PA (15,000 Daltons) when heated at 10°C/minute.	137
Figure 5.2	Consecutive DSC heating scans after heating to 430°C at 10°C/min, holding for 1 min, quenching to 150°C and reheating at 10°C/min.....	138
Figure 5.3	Complex viscosity as a function of increasing temperature for TPER-BPDA (30,000 Daltons) and TPER-BPDA-PA (15,000 Daltons).....	140
Figure 5.4	Polarized optical micrograph of the initial TPER-BPDA-PA film.	142
Figure 5.5	Polarized optical micrograph of TPER-BPDA-PA (15,000 Daltons) after heating at 430°C for 20 minutes and subsequent quenching to various crystallization temperatures.	144
Figure 5.6	Growth rate of spherulites as a function of crystallization temperature for TPER-BPDA-PA (both 15,000 Daltons and 30,000 Daltons molecular weights) after 20 minutes in melt at (▲) 420°C and (●) 430°C.	146
Figure 5.7	Lap-shear strengths as a function of bonding temperature (420°C and 430°C). Bonding pressure and bonding time were kept constant at 300 psi and 20 minutes respectively.....	151
Figure 5.8	Lap-shear strengths as a function of bonding time (10, 20 and 30 minutes). Bonding pressure and bonding temperature were kept constant at 300 psi and 430°C respectively.....	153
Figure 5.9	Lap-shear strengths as a function of bonding pressure (100, 200, 300 and 500 psi). Bonding temperature and bonding time were kept constant at 430°C and 20 minutes respectively.....	154
Figure 5.10	Thermal cycle followed for preparing lap-shear specimens.....	155
Figure 5.11	Scheme illustrating the conditions tried and finally selected for optimization of the bonding process.	156
Figure 5.12	SEM micrographs of the fracture surface of the lap-shear specimens. ...	157

Figure 5.13	Scheme followed in the aging study of the lap-shear bonds.....	159
Figure 5.14	Lap-shear strengths after aging at room temperature for a period of 1,3 and 7 weeks and testing at ambient, 177°C and 232°C.	160
Figure 5.15	Lap-shear strengths after aging at 177°C for a period of 1,3 and 7 weeks and testing at ambient, 177°C and 232°C.....	161
Figure 5.16	Lap-shear strengths after aging at 232°C for a period of 1,3 and 7 weeks and testing at ambient, 177°C and 232°C.....	162
Figure 5.17	Lap-shear strengths shown as function of test temperature for various aging times and aging temperatures.	163
Figure 5.18	Lap-shear strengths of TPER-BPDA-PA (15,000 Daltons) after exposure to different solvents for a period of nine days. Values from other similar studies in literature are also shown for comparison.	165
Figure 6.1	Crystallization exotherms at various crystallization temperatures after 20min residence time at 430°C.....	176
Figure 6.2(a)	Normalized crystalline content as a function of Log (time) at various crystallization temperatures.	177
Figure 6.2(b)	Plot of $\log [-\ln (1-X_c (t))]$ versus $\log (time)$ at various crystallization temperatures.	178
Figure 6.3	Variation of logarithm of transformation rate 'K', and crystallization half time ' $t_{1/2}$ ', as a function of crystallization time after a melt holding conditions of 430°C for 20 minutes.	180
Figure 6.4	Polarized optical micrographs at the indicated crystallization temperatures after being at a melt temperature of 430°C for 20 minutes.	181
Figure 6.5	Evolution of spherulitic growth ranging from a folded-chain single crystal to a fully developed spherulite.	183
Figure 6.6	Radial growth rates of spherulites at various crystallization temperatures after melt temperature of 430°C for 20 minutes. ($M_n=15,000$ Daltons, $M_w=30,000$ Daltons)	185
Figure 6.7	(a) AFM height image of a central part of a spherulite for a sample crystallized at 360°C after a melt temperature of 430°C for 20 minutes. (b) AFM height image of a outward region of a spherulite for a sample	

	crystallized at 360°C after a melt temperature of 430°C for 20 minutes. The center of the spherulite lies toward upper-right of the micrograph.	187
Figure 6.8	Crystallization exotherms at 355°C after various melt residence times at 430°C.	188
Figure 6.9	Plot of $\log [-\ln (1-X_c(t))]$ versus $\log (\text{time})$ at 355°C after various melt residence times at 430°C.	191
Figure 6.10	Variation of logarithm of transformation rate ‘K’, and crystallization half time ‘ $t_{1/2}$ ’ at crystallization temperature of 355°C, as a function of residence time at 430°C.	192
Figure 6.11	Polarized optical micrographs at 355°C after indicated melt residence times at 430°C.	194
Figure 6.12	Crystallization exotherms at 355°C after 20 minutes residence times at various melt temperatures.	196
Figure 6.13	Plot of $\log [-\ln (1-X_c(t))]$ versus $\log (\text{time})$ at 355°C after various melt temperatures and 20 minutes residence time.	197
Figure 6.14	Polarized optical micrographs at 355°C after indicated melt temperatures and 20 minutes residence time.	198
Figure 6.15	Non-newtonian viscosity-frequency profile of TPER-BPDA-PA (initial $M_n=15,000$ Daltons, $M_w=30,000$ Daltons) at 430°C. The plot also indicates the data collection times for consecutive scans at the same temperature.	201
Figure 6.16	Isothermal complex viscosity (1 radians/s) as a function of residence time in the melt at various melt temperatures.	204
Figure 6.17	Non-isothermal complex viscosity (1 radians/s) when cooled at 10°C/min from various melt temperatures after 20 minutes residence time. Inset: Corresponding arrhenius plots for the non-isothermal viscosity profiles when cooled from various melt temperatures. The initial regions prior to crystallization were utilized for estimating value of activation energy using the Andrade-Eyring equation.	208

Figure 6.18	Spherulitic growth rates at 345°C after 20 minutes at various initial melt temperatures.....	213
Figure 6.19	DSC cooling scans at 10°C/min after 10 minutes at various melt temperatures.....	214
Figure 6.20	Polarized optical micrographs illustrating the morphological development when cooled at 20°C/min from the melt at 430°C for 20 minutes. Micrographs taken at (a) 340°C (b) 332°C (c) 323°C.....	217
Figure 7.1	Specimen configuration for the wedge test.	223
Figure 7.2	Crack growth vs. time in various solvents. (a) and (b) represent the data for each of the two samples.	231
Figure 7.3	Fractured wedge test samples in environment (a) acetone (b) boiling water.	233
Figure 7.4	(a) Collected data for the DCB sample for the standard bonding condition (b) Calculation using the compliance method.	235
Figure 7.5	Maximum and arrest strain energy release rates for samples bonded under the standard bonding conditions. Both ASTM and Compliance method are used to calculate the results.....	236
Figure 7.6	Photomicrograph of the fractured DCB specimen that was bonded under the standard bonding conditions.....	236
Figure 7.7	Scanning electron micrographs of the fractured DCB specimen that was bonded under the standard bonding conditions. (a) lower magnification (b) higher magnification.....	237
Figure 7.8	Results for the samples (a) that were only bonded for 2 min and (b) that were quenched to room temperature from the standard bonding conditions.....	238
Figure 7.9	Photomicrograph of the fractured DCB specimen that was bonded for only two minutes.....	241
Figure 7.10	Photomicrograph of the fractured DCB specimen that was held at 365°C for 2 hours before cooling to room temperature.	241
Figure 8.1	Scheme for synthesis of TPER-BTDA-PA polyimide.	250

Figure 8.2	(a) Dynamic heating profiles for weight loss in air and nitrogen when heated at 5°C/min.	253
Figure 8.2	(b) Weight loss profile with time in air and nitrogen when kept at a typical melt temperature of 450°C.....	255
Figure 8.3	Consecutive DSC heating scans after heating to 450°C at 10°C/min, holding for 1 min, quenching to 100°C and reheating at 10°C/min.....	257
Figure 8.4	Second heat DSC scans at 10°C/min after cooling from 450°C, 1 min at different cooling rates.....	259
Figure 8.5	(a and b) Scans from room temperature at 10°C/min after crystallizing at different temperatures from the melt at 450°C, 1 min.	262
Figure 8.6	Peak times for isothermal crystallization exotherms, after quenching from 450°C, 1 min to different crystallization temperatures. The error bars indicate the standard deviation of at least four samples.	266
Figure 8.7	Polarized optical micrographs of sample (a) crystallized at 340°C for 20 min and (b, c, d) held at 370°C for (a) 30s (b) 90s (c) 120s. The error bars indicate 25 microns.	268
Figure 8.8	WAXD patterns of TPER-BTDA-PA –initial film and melt crystallized at different temperatures. Samples were precisely prepared in the DSC...	270
Figure 8.9	Direct DSC heating scans at 10°C/min after crystallizing for various times at (a) 320°C and (b) 360°C.	272
Figure 8.10	DSC heating scans at different heating rates for (a) initial film, (b) crystallized at 320°C, (c) crystallized at 360°C and (d) zinc after calibrating the DSC at different heating rates.....	276
Figure 8.11	Isothermal crystallization at 360°C with respect to logarithm of time (■) heat of melting obtained after heating to melt (▲) the corresponding peak melting points obtained.	283
Figure 8.12	Isothermal crystallization at various temperatures with respect to logarithm of time and the peak melting points obtained on heating for crystallization temperatures of (a) 380°C, (b) 377.5°C, (c) 375°C and (d) 370°C.....	284

LIST OF TABLES

Table 1.1	Electron affinity of common aromatic dianhydrides (ref 2).....	7
Table 1.2	Dependence of glass transition on the chain length of diamines (ref 40).....	21
Table 1.3	Effect of isomeric attachment of the diamine for ODPA based polyimides. (ref 40)	23
Table 1.4	Effect of dianhydride on the T_g of the various ether based diamines (ref 40).....	24
Table 2.1	Values of T_m , ΔH_f and ΔS_f for various polymers. (ref 2)	31
Table 2.2	Exponents of time in the Avrami equation. (ref 82)	71
Table 3.1	Chemical structures and T_g 's and T_m 's of various semicrystalline polyimides. The structures and values for ULTEM, an amorphous polyetherimide, and PEEK are also shown.....	83
Table 4.1	Some selected properties of different metals.....	106
Table 8.1	Previously developed semicrystalline polyimides at Virginia Tech.	246

Introduction

The last twenty-five years of this century have seen a flurry of activity in the synthesis and development of high performance and high temperature polymers. This has been in large part due to need for advanced materials required for a diverse range of applications including aerospace, automotive and microelectronic industries. These applications often demand a unique combination of properties including high glass transition temperatures, toughness, good adhesion, oxidative and thermal stability, and low dielectric constant. In this regard, a large number of polymers have been developed which can be broadly categorized as either thermosets or thermoplastics. Examples of thermosetting materials include epoxies, polyimides and bismaleimides while the example of thermoplastic materials largely consist of poly(sulfones), poly(ether ether ketones) and poly(ether imide).

From an application point of view, thermoplastic materials often possess some distinct advantages such as increased ductility and toughness of the material, ease of processing, and in many cases, potential to recycle the material. Furthermore, presence of crystallinity in thermoplastic polymers provides advantages such as improved solvent resistance, increased dimensional stability at higher temperatures and improved radiation resistance. These features make the development of high-performance and high temperature semicrystalline thermoplastics particularly attractive. From this standpoint, polyimides as a class of materials are very promising due to an array of desirable characteristics that these materials possess including excellent mechanical properties, wear resistance, radiation resistance, inertness to solvents, hydrolytic stability, low dielectric constants and good adhesion strengths.

Indeed significant advances have been made in the diverse field of polyimides in the past five decades and today these versatile materials find use in a broad range of applications. These functions include use as structural adhesive to bond wing panels and fuselage of both civilian and military aircraft, as interlayer dielectrics in microelectronic applications and as coatings in optoelectronic applications. However, one important

research area still lagging behind has been the development of melt processable semicrystalline polyimides. In fact, to this day, the vast majority of polyimides are exclusively processed using the solvent-based methods. In this regard, it is obvious that development of novel melt processable semicrystalline polyimides will be advantageous both from a processing standpoint and also due to many advantages that the presence of crystallinity would provide. This research addresses specifically this issue.

The primary subjects of this research work are two novel semicrystalline polyimides, both of these being based on commercially available monomers. This research thesis presents the encouraging results concerning these two polyimides. In this research effort, several different areas have become important especially in the way they are critically interconnected. This document therefore first reviews the literature in this area with respect to the goals of the conducted research work. The first four chapters thus provide the literature review focussing on the areas of ‘Polyimide Chemistry’, ‘Polymer Crystallization’, ‘Semicrystalline Polyimides’ and ‘Polyimides as Adhesives’ respectively. The next four chapters present the conducted research using the two polyimides.

Chapter 5 discusses the research concerning the melt processable semicrystalline polyimide structural adhesive based on 1,3-bis(4-aminophenoxy) benzene and 3,3',4,4'-biphenyltetracarboxylic dianhydride. Chapter 6 provides the results on the same polyimide concerning its thermal stability, crystallization kinetics and morphology. Chapter 7 discusses the research concerning the crystallization and multiple melting behavior of a new semicrystalline polyimide based on 1,3-bis (4-aminophenoxy) benzene (TPER) and 3,3', 4,4'-benzophenonetetracarboxylic dianhydride (BTDA). Chapter 8 presents the results on the wedge and double cantilever beam tests on a high temperature melt processable polyimide adhesive, TPER-BPDA-PA.

Additionally the later four chapters are presented in the form of journal publications with each chapter including its own abstract, introduction, experimental section, results and discussion and list of references. Also, all the relevant figures are presented together at the end of the respective chapter. All polyimides were synthesized in Dr. McGrath's laboratory in chemistry, with the synthesis for TPER-BPDA being primarily carried out by Dr. Amba Ayambem and, by this author, for TPER-BTDA.

Chapter 1

POLYIMIDES: chemistry & structure-property relationships – literature review

1.1 Introduction

Polyimides are a class of thermally stable polymers that are often based on stiff aromatic backbones. The chemistry of polyimides is in itself a vast area with a large variety of monomers available and several methodologies available for synthesis. However, there has been considerable debate on the various reaction mechanisms involved in different synthesis methods. This review however, covers only the important fundamentals regarding the polyimide synthesis. The focus in this review will rest only on ‘aromatic’ polyimides as they constitute the major category of such materials. Secondly, the properties of polyimides can be dramatically altered by minor variations in the structure. The subtle variations in the structures of the dianhydride and diamine components have a tremendous effect on the properties of the final polyimide. This chapter reviews several such features that are important towards understanding these structure-property relationships. Specifically, the effects of changing the diamines, dianhydrides or the overall flexibility of the chain on the basic parameters like T_g and T_m are also examined.

1.2 Two step method for polyimide synthesis

The most widely practiced procedure in polyimide synthesis is the two-step poly(amic acid) process. It involves reacting a dianhydride and a diamine at ambient conditions in a dipolar aprotic solvent such as N,N-dimethylacetamide (DMAc) or N-methylpyrrolidinone (NMP) to yield the corresponding poly(amic acid), which is then

cyclized into the final polyimide. This process involving a soluble polymer precursor was pioneered by workers at Dupont¹ in 1950's, and to this day, continues to be the primary route by which most polyimides are made. Most polyimides are infusible and insoluble due to their planar aromatic and hetero-aromatic structures and thus usually need to be processed from the solvent route. This method provided the first such solvent based route to process these polyimides. The process also enabled the first polyimide of significant commercial importance-‘KaptonTM’, to enter the market. The process for most extensively developed KaptonTM polyimide utilizes the monomer pyromellitic dianhydride (PMDA) and 4,4'-oxydianiline (ODA) and is illustrated in Figure 1.1.

However, the seemingly simple process involves several elementary reactions that are interrelated in a complex scheme². The course of these reactions can be tremendously effected by a large number of factors that include reaction conditions³ and even the mode of monomer addition⁴. The success of the overall reaction to yield high molecular weight polymers is critically dependent on seemingly subtle details. The ensuing discussion will address several parameters which govern these interrelations with respect to dependence of the synthesis on choice of monomers, solvents, reaction conditions and the importance of various side reactions involved in the synthesis.

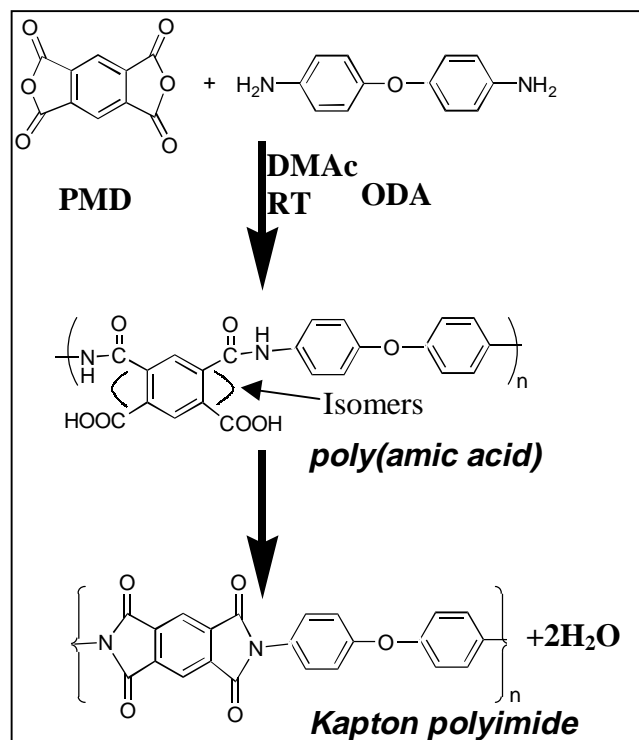


Figure 1.1 Reaction scheme for the preparation of kaptonTM polyimide (ref 2)

1.2.1 Formation of poly(amic acids)

Addition of a dianhydride to a diamine in a dipolar aprotic solvent such as DMAc or NMP at ambient temperatures leads to the formation of the intermediate poly(amic acid) due to the nucleophilic attack of the amino group on the carbonyl carbon of the anhydride group. The scheme that is illustrated in Figure 1.2 involves a reversible reaction leading to opening of the anhydride ring to form an amic acid group⁵. However, the forward rate constant for the reaction is several orders of magnitude larger than the reverse reaction⁶ and thus the reaction often appears irreversible if pure reagents are utilized. The formation of high molecular weight product is also dependent on this large difference in the reaction rate constants and thus it becomes important to examine the driving forces favoring the forward reaction. For the reverse reaction to take place, the carboxyl proton needs to attack the adjacent poly(amic acid) group². Thus any reagent, that hinders this reaction can decrease the rate of backward reaction and thus can shift the equilibrium to the right.

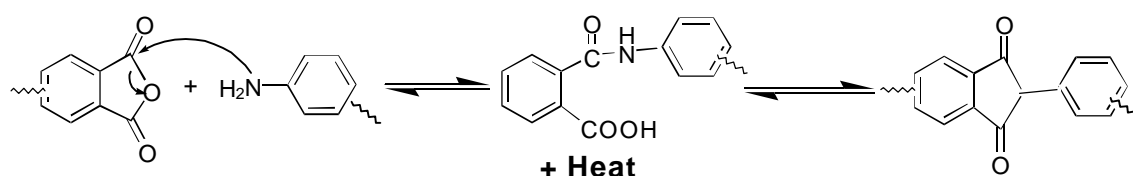


Figure 1.2 Generalized reaction mechanism of aromatic imide formation²

Polar aprotic solvents form strongly hydrogen bonded complexes with the free carboxyl groups and thus lead to equilibrium constants in excess of 10^5 l/mol at ambient conditions⁶. However, if the polymerization reaction is carried out in ether or hydrocarbon solvents, considerable differences in equilibrium constant are observed depending upon the amine's basicity and the dianhydride's electrophilicity⁷.

It is also important to note that the poly(amic acid) formation is exothermic and the equilibrium is favored at lower temperatures⁸. However, the equilibrium is shifted

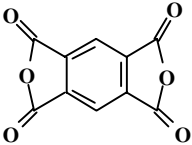
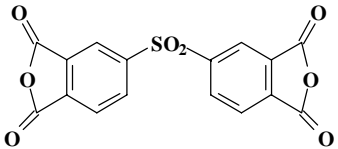
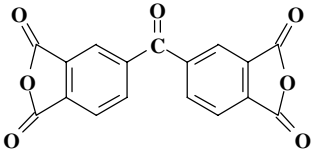
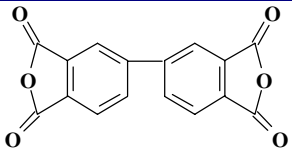
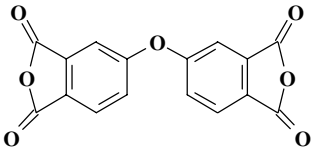
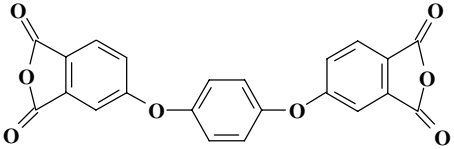
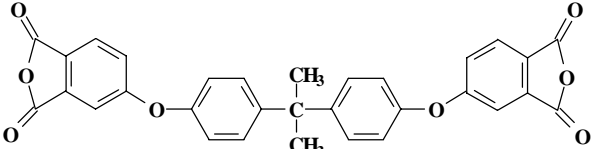
so far to the right at ambient that further lowering of the temperature usually does not show any detectable effect on the reaction. Another important factor effecting the reaction equilibrium is the monomer concentration. As the forward reaction is bimolecular and the reverse reaction unimolecular, increasing the monomer concentration favors high molecular weight products⁸. For the case of very dilute solutions this feature becomes especially important and leads to decreased molecular weight of the poly(amic acid).

1.2.2 Effect of monomer reactivity

As stated earlier, the mechanism of poly(amic acid) formation involves a nucleophilic substitution reaction at the carbonyl carbon atom of the dianhydride with a diamine. Hence the reaction is expected to depend upon the electrophilicity of the carbonyl groups of the dianhydride and the nucleophilicity of the amino nitrogen atom of the diamine. Electrophilicity of the dianhydride is usually gauged in terms of electron affinity (E_a) of the molecule measured by polarographic measurement techniques. PMDA that has the highest E_a , of the common aromatic dianhydrides also usually demonstrates the highest reactivity when reacted with different diamines². For dianhydrides with bridged bisphthalic anhydride structure (i.e. dianhydrides 2,3 and 5 in Table 1), electrophilicity is strongly influenced by the bridging group. In comparison to BPDA, which lacks a bridging group, the electron-withdrawing groups such as SO_2 and $\text{C}=\text{O}$ increases the E_a value substantially whereas electron donating groups such as ethers decrease the E_a value. Due to this difference in reactivity, while ether-containing dianhydrides are not readily effected by atmospheric moisture, PMDA and BTDA have to be handled in strictly moisture free environments at all times.

Attempts at correlating the reactivity of the aromatic diamines with their nucleophilicity have been less successful. However, the reaction rates of the diamines with a given dianhydride usually increase with increasing ionization potential². Also, considerable success has been achieved in quantitatively correlating the diamine basicity with reactivity, with the rate constants increasing with increasing value of pK_a ⁹.

Table 1.1 Electron affinity of common aromatic dianhydrides²

Dianhydride Structure	Name	Electron Affinity (eV)
	PMDA	1.90
	DSDA	1.57
	BTDA	1.55
	BPDA	1.38
	ODPA	1.30
	HQDA	1.19
	BPADA	1.12

The structure of the diamines effects the reaction rate significantly more than the changes in the dianhydride structure. It is often observed that the rate constant differs by four orders of magnitude between diamines with electron-withdrawing substituents and those with electron-donating ones⁸.

1.2.3 Effect of reaction conditions and solvents on polyimide synthesis

Early workers found that using higher concentration of monomers could produce higher molecular weight poly(amic acids)¹⁰. It was also found that the order and the mode of the monomer addition strongly influenced the final molecular weight with the highest molecular weights obtained when solid dianhydrides were added to a solution of diamines^{4,10}. It was reasoned earlier on, that this increase in molecular weights was entirely due to the avoidance of the side reactions¹⁰. Aromatic dianhydrides were known to react with water and other impurities in the amide solvents. However, the reactions with diamines were considerably faster. It was then correctly reasoned¹ that the solid mode of addition of dianhydride reduced its availability for competing reactions with water and other impurities, thus leading to higher molecular weights. Also a slight stoichiometric excess of dianhydride was found to increase the molecular weight. Similar reasoning is also offered to explain the dependence of molecular weight on concentration of monomers. A lower amount of solvent would result in a lower amount of impurities that interfere with the build-up in molecular weight⁸.

Another very important factor to consider is that dianhydrides are usually added as solids to the reaction mixture. This solid mode of addition does not lead to immediate dissolution of the dianhydride¹⁰. The rate of dissolution itself depends on the concentration of monomers and is slow. If both the dianhydride solubility and monomer reactivities are low, then above a certain critical concentration, the process becomes diffusion controlled much like solid-liquid interfacial polymerization^{11,12}. This leads to formation of very high molecular weight product at the beginning of the reaction, long before the dianhydride has completely dissolved and the stoichiometric balance has been

obtained. This kind of reaction can often lead (temporarily) to a polymer with a broad and often binodal distribution of molecular weight⁸.

Early workers in the field also found that the viscosities of poly(amic acids) rapidly decreased when they were stored in a solution after preparation^{4,10}. This was first attributed to the sensitivity of the amic acids to hydrolysis. Later work, however, showed that the phenomenon was associated with the reversibility of the propagation reaction¹¹. Although the rate constants for such reactions are very small, the few such reactions that may take place can have a dramatic effect on the M_w of the polymer.

Solvents utilized in the poly(amic acid) synthesis also play a very important role. Common dipolar aprotic amide solvents utilized are DMF, DMAc, NMP and TMU. All these solvents share a common feature, as they are all Lewis' bases. Interestingly, while the starting reagents for the reaction are weakly basic aromatic amines and nonprotic anhydrides, yet the final product is an acid. Thus, while the starting mixture is basic, the product is acidic. The strong acid-base interaction of this resulting acid with the basic solvent medium is exothermic and one of most important driving forces for the reaction. It is thus expected that the rate of the reaction will be faster for more basic and more polar solvents. This was indeed found to be the case for reaction of phthalic anhydride with 4-phenoxyaniline with the reaction rate increasing in order of the solvent utilized as THF < acetonitrile < DMAc¹³.

1.2.4 Side reactions and other factors involved in polyimide synthesis

There are several side-reactions involved in the poly(amic acid) synthesis, which accompany the main chain reaction. These side-reactions not only lead to undesired side-products, they can also have a tremendous effect on the molecular weight (both M_w and M_n) and the polydispersity of the final product. It is thus desirable to keep these side-reactions to a minimum if suitably high enough molecular weights are to be achieved.

One side reaction that cannot be completely eliminated is the reverse propagation reaction of the poly(amic acid) to yield the dianhydride and the diamine⁸. This intramolecular acidolysis which yields a anhydride is a result of the pendant carboxylic

groups at the ortho-positions². In contrast, the acylation reaction of an amine with benzoic dianhydride is a irreversible reaction. However the former reversible reaction does not prevent the formation of high molecular weight product as the magnitude of the equilibrium constant (K_{eq}) is still very high. In fact, if this was the only side reaction involved, then the expected X_n for most poly(amic acids) would be over 300 ($X_n \sim K_{eq}^{1/2}$)¹⁴. In practice, the values of the X_n of the poly(amic acids) falls in the range of 25 to 275 that corresponds to a M_n in the range of 10,000 to 100,000⁸.

An important side reaction often taking place is that of the dianhydride with water, which also competes, with the propagation reaction. This reaction has been stated to have a dramatic effect on the molecular weight of the poly(amic acid) as it removes the dianhydride from the equilibrium and upsets the monomer stoichiometry⁸. The reaction between dianhydride and water may be primarily driven by the enhanced nucleophilicity of the water in the polar aprotic medium. Also, some authors have speculated (with little or no evidence) that the ortho-dicarboxylic group that is formed is highly stabilized due to the acid-base interaction with the dipolar solvent and thus exists as one of the end groups of the poly(amic acid), thus effectively lowering the molecular weight³. As the anhydride group is consumed more is regenerated by the backward reaction to maintain the equilibrium. The above-discussed factors have lead to some widely practiced methods during the synthesis, namely

- 1) Higher concentrations of the monomers are favored in the poly(amic acid) synthesis.
- 2) The amine is added first and the dianhydride second (the dianhydride that is added second reacts faster with the diamine than with the existing water).
- 3) Sometimes a slight excess of dianhydride is found to be useful in attaining higher molecular weights.

It is important to remember that while the water may be present as an impurity in the monomers or the solvents, it is not the only source of water. While the conversion of a poly(amic acid) to a polyimide is slow at ambient temperatures, some water may form as a side product due to reactions occurring at ambient conditions if poly(amic acid) is left at these conditions for a long time¹⁵. Other solvent impurities like monofunctional 'amines' which may be present in the amide solvents can also have a devastating effect

on the main chain synthesis reaction⁸. These monofunctional impurities if present, would compete with the monomeric diamines throughout the polymerization reaction. These reactions can upset the monomer stoichiometry and lead to unreactive chain ends. Another side reaction speculated to have an important effect is the cyclic conversion of the o-carboxycarboxamide groups to an isoimide¹⁶.

The excess dianhydride that sometimes has to be used to give high molecular weight products can also lead to several damaging side reactions. This is more so the case when highly reactive dianhydrides like PMDA are used as these are strongly dehydrating agents. The excess dianhydride groups attack the amic acid group leading to formation of a diacid and an imide. The ortho-dicarboxylic acid group, which remains as a chain end group, limits the molecular weight of the resulting poly(amic acid).

1.2.5 Thermal imidization of a poly(amic acid)

The intermediate poly(amic acid) is usually converted to the final polyimide by the thermal imidization route. This process is especially useful when the final product is desired in a film or a coating form. Films are first cast on a substrate and then undertaken through a thermal cycle with temperatures ranging from 100°C to 350°C. There has been considerable debate in the literature regarding the exact thermal cycle to be utilized for achieving close to 100% imidization of the poly(amic acids). While the types of thermal cycles utilized are many, they can essentially be divided into two different types

- 1) Heating gradually to 250°C-350°C, depending on the stability and T_g of the polyimide^{2,8,17}.
- 2) Heating the poly(amic acid) mixture to 100°C and holding for one hour, heating from 100°C to 200°C and holding for one hour, heating from 200°C to 300°C and holding for one hour and slow cooling to room temperature from 300°C^{18,19,20,21}.

However, irrespective of the type of thermal cycle utilized, it is important to recognize that there are several complicating factors involved in these seemingly simple thermal imidization processes, which finally determine the degree of imidization of the polyimide product. It needs to be emphasized that the imidization reactions take place in a very

concentrated viscous solution (during initial and intermediate stages) and the presence of residual solvent plays a very important role during imidization at the later stages of the reaction. In this regard, the imidization proceeds faster in the presence of dipolar amide solvents due to several reasons, some of which are;

- 1) Specific solvation allows the favorable conformation of the amic acid group to cyclize²².
- 2) Plasticizing effect of the solvent to increase the mobility of the reacting functional groups⁸.
- 3) The basicity of the amide solvent allows it to accept protons and may be responsible for the specific effect².

A simple kinetic expression for the imidization reaction is often not possible as the overall process involves several interrelated elementary reactions and dynamically changing physical properties such as diffusion rate, chain mobility, solvation and acidity. The rate of imidization is usually faster during the initial stages due to the presence of solvent and shorter chain sizes resulting in increased chain mobility. However, during the later stages of the reaction the rate tapers off due to primarily the reasons listed below:

- 1) Loss of residual solvent which occurs due to the extended heating²³.
- 2) The T_g of the polymer increases as the degree of imidization reaction proceeds and as the T_g approaches the reaction temperature, the imidization rate slows down markedly due to the decreased chain mobility.

Lastly, the rate of imidization may be dependent upon the availability of suitable conformations for the amic acid group to decyclohydrate in to an imide³. The slower rate of imidization during the later stages of imidization is attributed to unfavorable conformations, which have to rearrange to favorable conformations before imidization can take place²³. Such a conformational rearrangement is only possible if the rotation of the adjoining polymer chain and strongly bound solvent molecules takes place.

1.2.5.1 Determination of the degree of imidization:

Infrared spectroscopy continues to be the prominent tool in determining the degree of imidization despite limited agreement on its sensitivity to chemical changes

taking place. The bands most frequently utilized are imide absorption bands near 1780 cm^{-1} (C=O asymmetrical stretching), 1380 cm^{-1} (C-N stretching) and 725 cm^{-1} (C=O bending). The strongest band that occurs at 1720 cm^{-1} (C=O symmetrical stretching) also overlaps with strong carboxylic acid band (1700 cm^{-1} , C=O) of the poly(amic acid). Some overlap of the 1780 and 725 cm^{-1} imide bands is also possible with absorption of anhydrides occurring at 1780 cm^{-1} and 720 cm^{-1} . The carboxylic acid bands of 1700 cm^{-1} (C=O) and $2800\text{-}3200\text{ cm}^{-1}$ (OH) and amide bands at 1660 cm^{-1} (C=O), 1550 cm^{-1} (C-NH) and $3200\text{-}3300\text{ cm}^{-1}$ (N-H) which often appear as broad peaks are also useful for qualitative assessment during imidization process.

1.2.5.2 Changes in mechanical properties & molecular weight during thermal imidization:

Dramatic changes in the mechanical properties occur as the poly(amic acid) sample is converted to the final polyimide. This phenomenon was covered qualitatively in a very early study¹⁰ of thermal imidization and was later confirmed by other workers. The magnitude of the change that occurred depends upon the molecular weight of the starting poly(amic acid). For example, films prepared from polymers with inherent viscosity of less than 0.2 were brittle and remained brittle throughout the curing cycle. Poly(amic acids) with inherent viscosities in the range of 0.2-1.0 produced tough, creasable films that became brittle between 150°C and 200°C and tough and creasable again when heated above 275°C . Films prepared from samples with inherent viscosities greater than 1.0 were also tough and creasable and suffered only a minor and temporary loss in these properties during the cure cycle⁸. These fluctuations in mechanical properties have been attributed to fluctuations in molecular weight. These occur due to a small number of the amic acid groups that cyclize to regenerate anhydride and amine moieties at temperatures in the vicinity of 100°C . As the chains are broken at these points, the molecular weights and the resulting mechanical properties are reduced. As the temperature is increased, the terminal functional groups react and the mechanical properties improve due to increased molecular weight.

1.2.6 Chemical imidization of the poly(amic acids):

The chemical imidization of the poly(amic acids) is a useful technique for manufacturing molding powders⁸. Despite low energy requirements for such a process, it is rarely used for other applications due to the dangerous reagents involved. The process essentially consists of treating the poly(amic acid) with a mixture of aliphatic carboxylic acid dianhydride and tertiary amine at ambient temperatures²⁷⁻³⁰. The common reagents utilized are acetic anhydride, pyridine and triethylamine²⁴.

The mechanism of chemical imidization involves the reaction of the tertiary amine with an anhydride, which is more susceptible to nucleophilic attack. The final polyimide formed is insoluble in the imidization mixture and hence precipitates out. However, the possibility exists that precipitation occurs before all the amic acid groups have cyclized into an imide. The percentage of imidization achieved thus depends on the solubility of the polyimide in the imidization mixture with more soluble polyimides attaining higher degrees of imidization³. In general though, the chemical imidization technique requires a final treatment where the powder is heated briefly to temperatures near 300°C ($>T_g$) to complete the imidization and remove traces of any solvent²⁵. It has been stated that the reverse propagation reaction characteristic of the thermal imidization process does not occur during chemical imidization, which means that the mechanical properties of the polymer do not change much during the conversion process²⁵. This is an important factor in the imidization of films and fibers. However, chemical imidization may lead to substantially higher percentage of 'isoimide' moieties in the final product⁸, which at higher temperatures converts to the more stable imide.

1.3 One step method- high temperature solution polymerization:

This technique is employed for polyimides that are soluble in organic solvents at polymerization temperatures²⁶. The process involves heating a stoichiometric mixture of monomers in a high boiling solvent or a mixture of solvents at 180°C-220°C^{2,3,8}. The imidization proceeds rapidly at these temperatures and water generated due to the reaction is distilled off continuously as an azeotrope along with the solvent. The commonly utilized solvents are nitrobenzene, m-cresol and dipolar aprotic amide solvents. The imidization still proceeds via the amic acid route although the concentration of amic acid at any time is very small. The amic acid group rapidly converts to an imide or reverts back to amine and dianhydride. The high temperature solution polymerization is often performed in the presence of catalysts such as quinoline, tertiary amines, alkali metals and zinc salts of carboxylic acids^{27,28,29,30}. This process is especially useful for polymerization involving unreactive dianhydrides and diamines. An interesting feature of this method is that it often yields materials with a higher degree of crystallinity than can be obtained with two-step methods⁸, which may be due to the increased solubility of the monomers in the solvent medium.

1.4 Structure property relationships in linear aromatic polyimides

1.4.1 T_g – structure relationships:

While the glass transition temperature of linear aromatic polyimides is strongly intertwined with the chemical structure of the polyimide, the exact nature of this relationship is complex due to several factors involved in determining the T_g of the final polyimide. While the chain stiffness is certainly the most important aspect, other factors like chain-chain interactions effect the T_g substantially. Isomeric attachments of the flexible/rigid groups and presence of bulky side groups can also effect both the chain-

stiffness and chain-chain interactions and thus are important in determining the T_g . Other traditional factors like presence of crystallinity and molecular weight (when below a certain critical molecular weight) can also contribute to influencing the T_g . The multitude of factors effecting T_g is certainly one of the reasons why not a single comprehensive study fundamentally addressing the exact T_g -structure relationship of polyimides exists in the literature. The large varieties of monomers used in the synthesis of polyimides have certainly raised the difficulty of any such analysis considerably. The extensive amount of experimental data existing in the literature may sometimes help in crudely predicting the approximate T_g of any new polyimide being developed depending upon the similarity of structure of the proposed polyimide with previously developed polyimides. However, several studies in the literature have addressed the various key features effecting the glass transition behavior of linear aromatic polyimides. The following section will briefly address some of these features:

1.4.2 Polyimide chain-chain interactions

The formation of a charge transfer complex (CTC) formation between the dianhydride and diamine groups in polypyromellitic diimides was first proposed by Kotov et al.³¹ in 1977 using UV spectroscopy. They described the color changes in these materials by a cut-off of optical wavelengths, E_{opt} , which in turn were found to be inversely correlated with the ionization potential of the diamines. The authors attributed these changes to the formation of a CTC. Fryd³² applied a similar reasoning in 1984 when proposing a CTC formation between dianhydride and diamine groups in polyimides being an important reason for high T_g 's of polyimides. The increased inter-chain attractive forces due to such interactions were proposed as effectively increasing the chain rigidity and hence the T_g . It was also proposed that the presence of any bridging group in the dianhydride had a strong influence on the glass transition as it changed its electron affinity and hence promoted the possibility of CTC formation. Table 1.4 later in this report depicts such behavior for a series of polyimides based on ether diamines in which the dianhydrides with varying E_a were utilized.

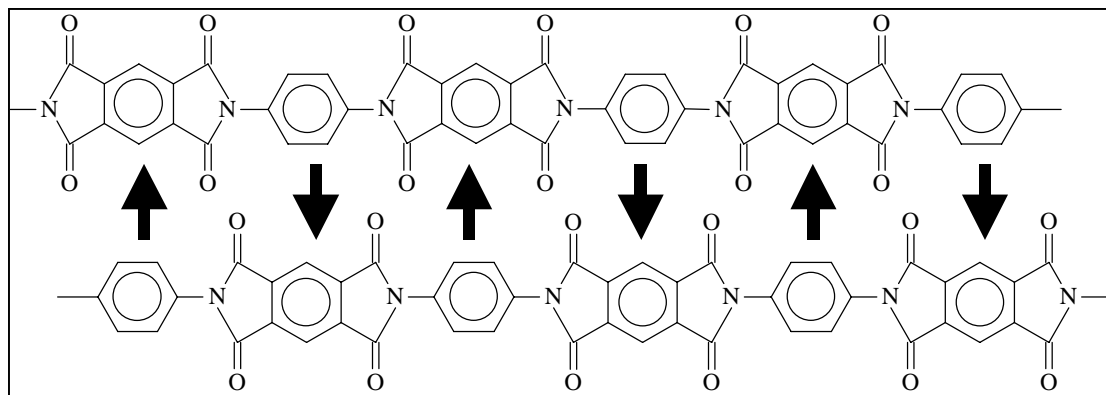


Figure 1.3 Idealized charge transfer complex formation in dianhydrides³¹.

Figure 1.3 shows the idealized form of such an interaction between the dianhydride and diamine groups. However, such alignment of repeat units will not occur over more than a few repeat units. Though the values of E_a cannot be used directly to give a quantitative value for the measure for this interaction, it is clear that the more electron deficient PMDA will have a much larger affinity than ODPA for the electron rich amine-derived center. This type of interaction can also be looked as a Lewis acid-base kind of interaction³³. It has been widely speculated in the literature³³ that the presence of such very strong electronic interactions in polyimides is responsible for their enhanced color³⁴. Several researchers have worked on lessening these interactions in order to develop polyimides with reduced color, increase solubility and to lower the dielectric constant^{35,36,37}. Although the CTC model successfully explains the *qualitative* nature of the relationship between the T_g 's of the polyimides and the E_a 's of the dianhydrides for several polyimides, the T_g seems to become insensitive to E_a of the dianhydride as the bridging group in the dianhydride becomes longer³³.

Another type of idealized chain-chain interaction visualized for polyimide is called the “*Preferred Layer Packing*” arrangement where the dianhydride and the diamine sections of the one chain are correspondingly packed alongside the dianhydride and diamine

sections of another chain³⁸. This type of chain-chain interaction that may exist in the crystalline state is schematically shown in Figure 1.4.

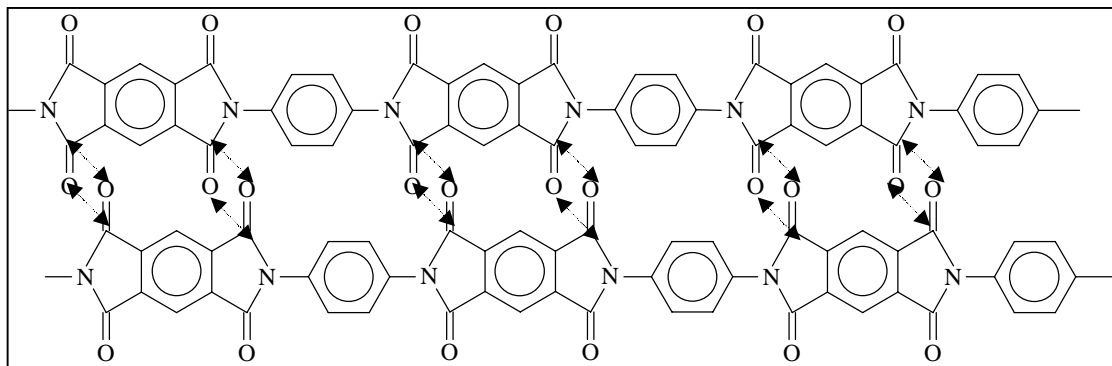


Figure 1.4 Idealized polymer chain-chain interaction in the crystalline state³⁸.

Such chain packing models have also been utilized to qualitatively explain the predominating effect of any bridging groups present in the dianhydride, which then may disrupt the packing arrangement by inhibiting the carbonyl-carbonyl dipolar attractions. The presence of such bridging groups in the diamine has been proposed to only reduce the packing density and thus exerts lesser influence on the final T_g ³⁸. While such explanations provide some degree of qualitative explanation of T_g behavior, they cannot be utilized for any convenient quantification to predict the T_g . Although such ideal chain-chain interactions have been hypothesized, the structural arrangements within any polyimide should be governed by minimum energy conformations. Interestingly the crystal structure determinations of some polyimides have shown the packing arrangement to be dissimilar to any of the packing arrangements shown in Figure 1.3 or Figure 1.4. Figure 1.5 illustrates the crystal packing arrangement for New-TPI as proposed by Okuyama et al³⁹ which does not lend itself to comparison between the two different kind of arrangements but rather seems to be intermediate between the two kinds.

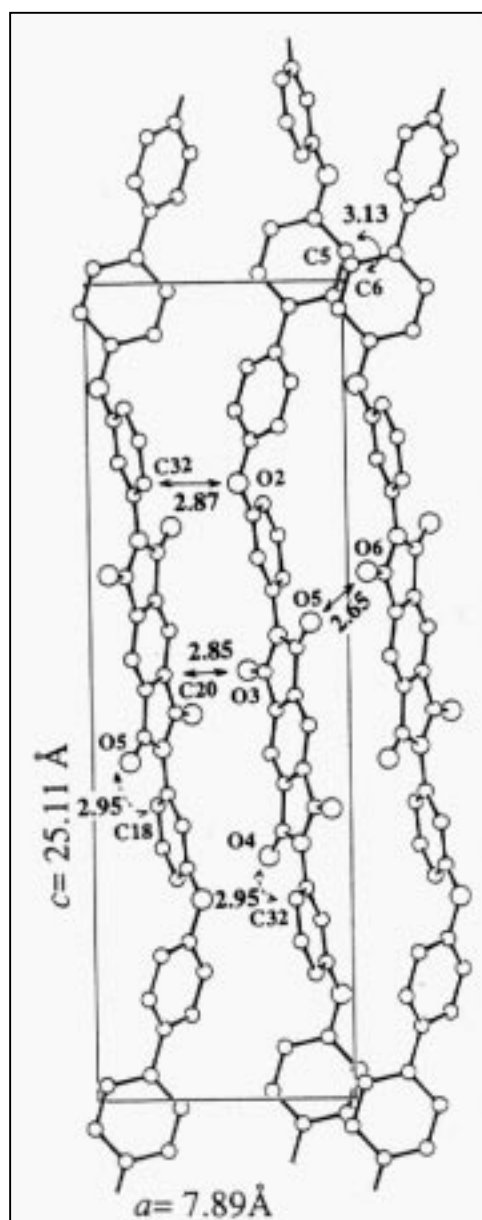
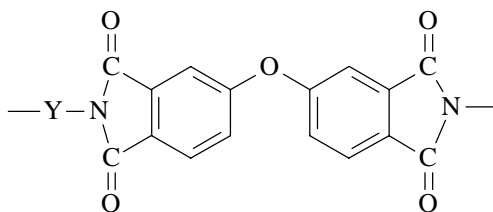


Figure 1.5 Packing structure of New-TPI viewed along the b-axis as proposed by okuyama et al³⁹.

1.4.3 Effect of chain length of the ether diamine on the glass transition:

Tamai et al.⁴⁰ studied the effect on T_g of ODPA based polyimides due to the chain length of the diamine by introducing ether linkages in the diamine component. The inherent viscosity's of the initial poly(amic acids) were kept constant at 0.5 dl/g and the chain ends were endcapped with phthalic anhydride. The results are shown in Table 1.2. It is clear that the chain length of the diamine component can significantly effect the glass transition of the final polyimide significantly. This effect is primarily due to introduction of additional flexible linkages that in effect decreases the persistence length of the polyimide. These shorter and more flexible ether linkages require lesser “ kT ” for the motion to set in. Another feature illustrated in Table 1.2 is that the para-amino-substituted polyimides have a significantly higher T_g for all the polyimides with equal number of benzene rings [i.e. polyimide (b) & (f), (c) & (g), (d) & (h)]. However, the effect of number of benzene rings seems to be more important than the nature of amino substitution. It is also seen that no clear correlation seems to exist regarding the presence of crystallinity, or when it is present, regarding the melting point. The study also illustrates the range of glass transitions (from 181°C to 326°C) and the range of melting points (from 318°C to 491°C) that can be obtained by varying the number of benzene rings in the ether diamine while keeping the dianhydride the same.

Table 1.2 Dependence of glass transition on the chain length of diamines⁴⁰.



Polymer	Dianhydride	Y	T _g (°C)	T _m (°C)
(a)	ODPA		326	ND
(b)	ODPA		242	374
(c)	ODPA		222	428
(d)	ODPA		204	332
(e)	ODPA		261	491
(f)	ODPA		205	ND
(g)	ODPA		189	318
(h)	ODPA		181	ND

1.4.4 Effect of isomeric attachment of the diamine:

The effect of isomeric attachment on T_g is more clearly illustrated in Table 1.3, which shows a series of ether diamines with varying para-, and meta- linkages⁴⁰. It is clear that as degree of para-substitution decreases and that of meta-substitution increases, the glass transition decreases tremendously. Also, it is clear that the nature of amino-substitution is far more important than the type (para- or meta-) of ether linkages inside the diamine. No clear correlation seems to exist for the crystallinity to exist. It is however, no surprise that more flexible chains yield lower melting points. However, as the position of the amino substitution changes to the ortho-position (which are expected to be even more flexible) this general rule is broken and the polyimides show considerably higher T_g 's than just expected from the flexibility of the diamine. This phenomenon is shown in Figure 1.6 which illustrates the effect of isomeric attachment in diaminobenzophenone in a series of BTDA based polyimides⁴¹ of similar molecular weight. The unusually higher T_g of ortho-substituted polyimides is in large part due to the strong dipolar attractions between the imide linkage and the closely placed carbonyl moiety on the diamine.

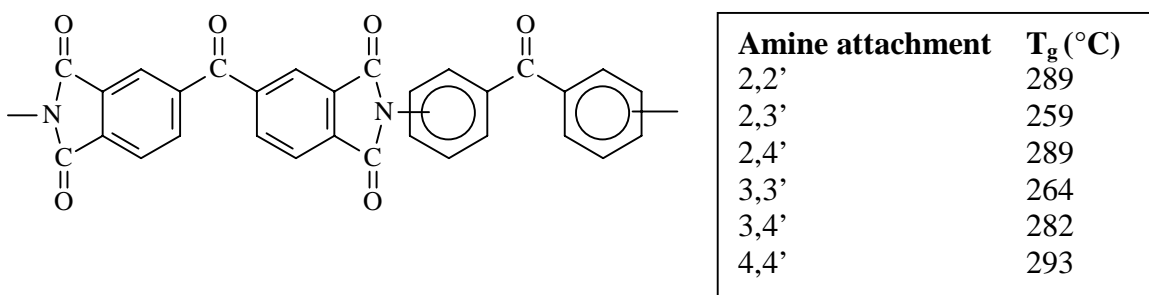
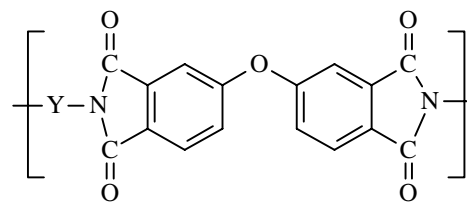


Figure 1.6 Effect of isomeric attachment of BTDA based polyimides³³.

Table 1.3 Effect of isomeric attachment of the diamine for ODPA based polyimides⁴⁰.

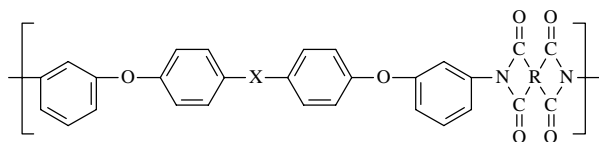


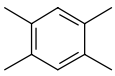
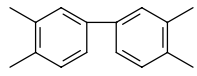
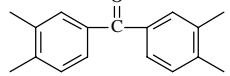
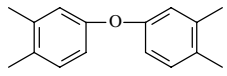
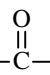
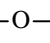
	<i>Diamine Structure</i>	<i>T_g(°C)</i>	<i>T_m(°C)</i>
A		242	374
B		219	325
C		205	ND
D		222	428
E		201	341
F		189	318
G		168	ND

1.4.5 Effect of the dianhydride structure on the glass transition:

The nature of the bridging group in the dianhydride strongly effects its electron affinity (see Table I) and also its T_g . As explained earlier, these factors have been correlated on the basis of the CTC model by many authors i.e. polymers with higher E_a have a much higher propensity for CTC formation and thus display a higher T_g . Although, this general relation seems to hold well for most short chain diamines, discrepancies are often observed for BTDA and BPDA based polyimides

Table 1.4 Effect of dianhydride on the T_g of the various ether diamine based polyimides⁴⁰.



	 PMDA	 BPDA	 BTDA	 ODPA
X				
—	250°C	221°C	216°C	199°C
	230°C	211°C	205°C	193°C
	212°C	199°C	192°C	181°C

1.4.6 Effect of chain structure on the crystallinity:

Although many semicrystalline polyimides have been synthesized, the literature provides only little work on the crystallization behavior of these polyimides, once they are taken above their melt temperatures. While many crystalline polyimides have been reported, it has often been ignored that this initial presence of crystallinity is the result of solvent aided crystallization that occurs in parallel with the later stages of the synthesis reaction. This also has been due to the fact that most of these researchers were not concerned with developing melt-processable polyimides. It is thus difficult to properly ascribe the effects of structural changes on the crystallization behavior from the melt for most of these polyimides. However, few factors appear to be distinctly important for inducing crystallinity (initial) in polyimides. For a given dianhydride (Table 1.3), para-substitution polyimides appear to favor the crystallization while increasing meta-substitution seems to reduce the ability of the polymer to crystallize. Similar behavior is also observed in Table 1.2 where the ether diamines based with all para-substituted positions appear to be much more inclined to crystallization. Another feature related to the ability of the polyimides to crystallize is the nature of the dianhydride. For most polyimides using common dianhydrides, the ability to crystallize often goes with BTDA>PMDA>BPDA~ODPA, although some exceptions to this rule do exist. Also, while para and meta substituted ether linked diamines seem to be the best candidates for inducing crystallinity in the polyimides increasing the flexibility by introducing ortho-substitution often inhibits the presence of crystallinity. This is because the ortho-substitution often contorts the chain symmetry and thus makes it harder for the chain to pack into the crystal lattice. Introduction of bulky bridging groups or pendant side groups along the chain backbone also inhibits crystallinity and is actually often one of the means practiced when developing soluble polyimides⁴². The crystallization behavior from the melt for many crystalline polyimides will now be examined in the next chapter.

References:

-
- ¹ Sroog, C.E., Endrey, A.L., Abramo, S.V., Berr, C.E., Edward, W.M., and Olivier, K.L. *J. Polym. Sci.*, Part A, 1965, **3**, 1373.
- ² Takekoshi, T., *Polyimides- Fundamentals and Applications*, Ed. Ghosh, M.K. and Mittal, K.L., Marcel Dekker, New York, 1996, Chapter 2.
- ³ Bessonov, M.I., Koton, M.M., Kudryavtsev, V.V. and Laius, L.A. *Polyimides: Thermally Stable Polymers*, 2nd edition, Plenum, New York, 1987.
- ⁴ Bower, G.M. and Frost, L. *J. Polym. Sci.*, 1963, **A1**, 3135.
- ⁵ Pravednikov, A.N., Kardash, I.Y., Glukhoyedov, N.P. and Ardashnikov, A.Y., *Polym. Sci. USSR*, 1973, **15** (2), 399.
- ⁶ Kardash, I.Y., Glukhoyedov, N.P. and Ardashnikov, A.Y., *Polym. Sci. USSR*, 1971, **13** (8), 2092.
- ⁷ Kaas, R.L., *J. Polym. Sci.*, Part A, 1981, **19**, 2255.
- ⁸ Harris, F.W., *Polyimides*, Ed. Wilson D., Stenzenberger, H.D., Hergenrother, P.M., Chapman and Hall, New York, 1990, Chapter 1.
- ⁹ Zubkov, V.A., Koton, M.M., Kudryavstev, V.V. and Svetlichnyi, V.M. *Zh. Org. Khim*, English transl. 1982, **17** (8), 1501.
- ¹⁰ Dine-Hart, R.A., Wright, W.W., *J. Appl. Polym. Sci.* 1967, **11**, 609.
- ¹¹ Volksen, W. and Cotts, P.M. *Polyimides: Synthesis, Characterization and Properties*, Vol. 1, Ed. Mittal K.L., Plenum New York, 1984, pg. 163-170.
- ¹² Orwall, R.A., St. Clair, T.L. and Dobbs, K.D. *J. Polym. Sci. Part B*, 1981, **19**, 1385.
- ¹³ Solomin, V.A., Kardash, I.E., Snagovskii, Y.S., Messerle, P.E., Zhubanov, B.A. and Pravendnikov, Dokl. Akad. Nauk USSR, English transl. 1977, **236** (1), 510.
- ¹⁴ Odian, G. *Principles of Polymerization*, 2 edn., Wiley, New York, 1981.
- ¹⁵ Frost L.W. and Kesse I. *J. Appl. Polym. Sci.*, 1964, **8**, 1039.
- ¹⁶ Cotter, R.J., Sauers, C.K. and Whelan, J.M., *J. Org. Chem.* 1961, **26**, 10.
- ¹⁷ Sroog, C.E., *J. Polym. Sci., Macromol. Rev.* 1976, **11**, 161.
- ¹⁸ Brink, M.H., Brandom ,D.K., Wilkes, G.L. and McGrath, J.E., *Polymer*, 1994, **35**, 5018.

-
- ¹⁹ Bell, V.L., Stump, B.L. and Gager, H. *J. Polym. Sci.* 1976, **12**, 2275.
- ²⁰ Bandom, D.K. and Wilkes, G.L. *Polymer* 1994, **35**, 5672.
- ²¹ Woodard, M.H., Rogers, M.E., Bandom, D.K., Wilkes, G.L. and McGRath, J.E. *Polym. Prepr.* 1992, **33** (2) 333.
- ²² Laius, L.A., Bessonov, M.I., Kallistova, Y.V., Adrova, N.A. and Florinskii, F.S. *Polym. Sci. USSR* 1967, **A9** (10), 2470.
- ²³ Kreuz, J.A., Endrey, A.L., Gay, F.P. and Sroog, C.E. *J. Polym. Sci. part A*, 1966, **4**, 2607.
- ²⁴ Vinogradova, S.V., Vygodskii, Voro'bev, V.D., Churochkina, N.A., Chudina, L.I., Sprina, T.N. and Korshak, V.V. *Polym. Sci. USSR* 1974, **A16** (3), 584.
- ²⁵ Cotts, P.M. in *Polyimides: Synthesis, Characterization and Properties*, Vol. 1, Ed. Mittal K.L., Plenum New York, 1984, pg. 223-226.
- ²⁶ Vinogradova, S.V., Vygodskii, Y.S. and Korshak, V.V. *Polym. Sci. USSR*, 1970, 12 (9), 2254.
- ²⁷ Endrey, A.L., US Patent, 3,179,630, 1965, to Dupont Co.
- ²⁸ Endrey, A.L., US Patent, 3,179,631, 1965, to Dupont Co.
- ²⁹ Hendrix, W.R. US Patent, 3,179,632, 1965, to Dupont Co.
- ³⁰ Endrey, A.L., US Patent, 3,179,633, 1965, to Dupont Co.
- ³¹ Kotov, B.V., Gordina, T.V., Kolninov, O.V. and Pravednikov, A.N. *Vysok. Soyed* 15B, 1977, **237** (3), 612.
- ³² Fryd, M. Structure – T_g relationships in Polyimides in *Polyimides: Synthesis, Characterization and Properties*, Vol. 1, Ed. Mittal K.L., Plenum New York, 1984, pg. 377.
- ³³ St. Clair, T.L. in *Polyimides*, Ed. Wilson D., Stenzenberger, H.D., Hergenrother, P.M., Chapman and Hall, New York, 1990, Chapter 2.
- ³⁴ Olivier, K.L. US Patent 3,234,181, 1966.
- ³⁵ Bell, V.L. *Organic Coatings and Plastics* preprint 1973, **33**, 153.
- ³⁶ St. Clair, A.K. and St. Clair, T.L. US Patent 4,595,548, 1986.
- ³⁷ Progar, D.J., Bell, V.L., St. Clair, T.L. US Patent 4,065,345, 1977.
- ³⁸ Lee, C.J. *J. Macromol. Sci.- Rev. Macromol. Chem. Phys.* 1989, **29** (4), 431.

-
- ³⁹ Okuyama, K., Sakaitani, H. and Arikawa, H. *Macromolecules* 1992, **25**, 7261.
- ⁴⁰ Tamai, S., Yamaguchi, A. and Ohta, M. *Polymer*, 1996, **37**, 3683.
- ⁴¹ Bell, V.L., Stump, B.L. and Gager H. *J. Polym. Sci. Part A*, 1976, **14**, 2275.
- ⁴² St. Clair, A.K. and St. Clair, T.L. in *Polymers for High technology*, Ed. Bowden, M.J. and Turner, S.R., *Amer. Chem. Soc. Symposium Series*, 1987, 483.

Chapter 2

Polymer Crystallization – Literature review

2.1 Introduction

While it is not possible to cover the subject of polymer crystallization in a review of this size, it is important in light of author's research to review the fundamental features that are essential to the study of polymer crystallization. The topic itself is central to the present research work, which deals in large part with the crystallization behavior of semicrystalline polyimides. This section thus attempts to cover the important topics in polymer crystallization, the understanding of which is directly or indirectly connected to the present research work. It is also important to look at the fundamental Lauritzen-Hoffman polymer crystallization theory, which was derived originally for flexible polymers like polyethylene. The topics covered in this review encompass several concepts that make the essential foundation on which a significant part of the subsequent research investigation rests.

The Lauritzen-Hoffman theory and its conclusions serve more to establish the general framework for explaining several important observations regarding the crystallization behavior of flexible polymers. While the theory is not readily applicable to more rigid chain polymers like PEEK and aromatic polyimides, it has been used many times without sufficient justification for explaining the crystallization behavior of such rigid chain systems¹. It can only be said that in future, this theory may serve as a good starting point for better explaining the crystallization behavior of rigid chain systems like polyimides.

2.2 Thermodynamics of crystallization and melting

From thermodynamic considerations alone, a crystal is in a lower free energy state than the liquid when the temperature is below the melting point (T_e^∞) for a large crystal of a very high molecular weight polymer. Figure 2.1 shows schematically the changes in the Gibbs free energy of liquid and a crystal with temperature. The necessary (but not sufficient) criterion for any spontaneous phase transformation (for a constant temperature and constant pressure process) is a negative value of ΔG . Hence the process of crystal formation is spontaneous below the equilibrium melting point (T_m^∞)** while the reverse process, i.e. crystal melting to form liquid is spontaneous above T_m^∞ . At T_m^∞ , a condition of equilibrium exists between the crystal and liquid as both phases have the same value of G and $\Delta G = 0$.

For the case of constant temperature process such as fusion at T_m^∞ , $\Delta G_f = 0$ and

$$\Delta G = \Delta H - T\Delta S = 0 \text{ at } T = T_m^\infty \quad \{2.1\}$$

Thus:

$$T_m^\infty = \frac{\Delta H_f}{\Delta S_f} = \frac{H_l - H_{cr}}{S_l - S_{cr}} \quad \{2.2\}$$

Thus both enthalpic and entropic effects will determine the equilibrium melting point for any polymer crystal. While a higher value of ΔH_f leads to a higher T_m^∞ , the entropic effects cannot be ignored and are often dominant in deciding the value of T_m^∞ . Table 2.1² lists the values of T_m , ΔH_f and ΔS_f for a series of polymers and illustrates the effect of

** While T_e^∞ represents the melting point of an infinitely long crystal of an infinite molecular weight polymer, T_m^∞ represents the melting point of an infinitely long crystal of finite molecular weight. In the case $M \rightarrow \infty$, $T_m^\infty \rightarrow T_e^\infty$.

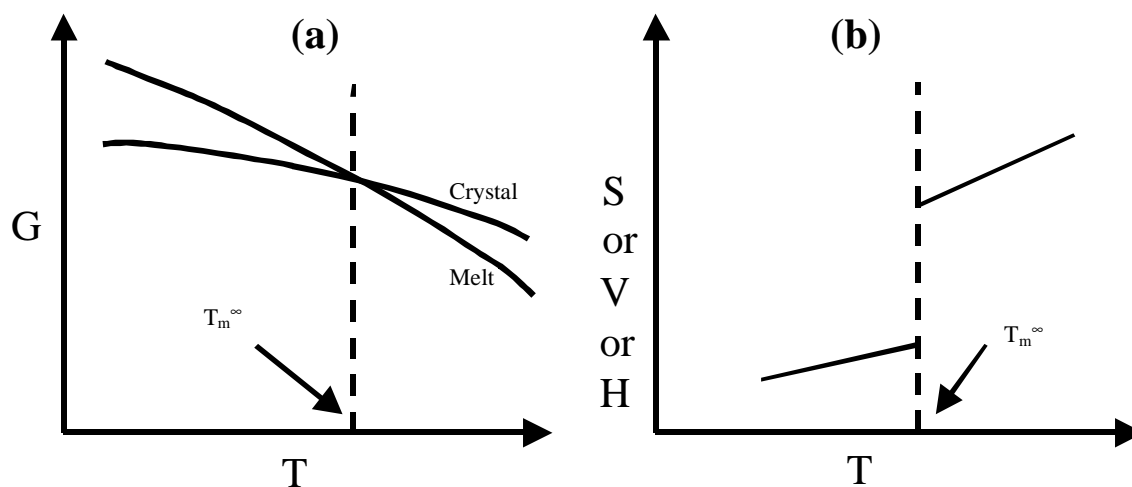


Figure 2.1 General behavior of thermodynamic variables at the equilibrium melting temperature T_m^∞ (a) gibbs free energy (b) entropy and volume.

Table 2.1 Values of T_m , ΔH_f and ΔS_f for various polymers².

Polymer	T_m (°C)	ΔH_f (J/mol)	ΔS_f (J/(K.mol))
Polyethylene	137.5	4,020	9.8
Poly(1,4-cis-isoprene)	28	4,390	14.5
Poly(decamethylene sebacate)	80	50,200	142.3
Poly(decamethylene azetate)	69	41,840	121.3
Poly(decamethylene sebacamide)	216	34,700	71.1
Poly(decamethylene Azelamide)	214	36,800	75.3

varying ΔH_f and ΔS_f . In this regard, it is especially important to visualize the importance of the term ' S_l ', the entropy of the liquid state. As shown in the table, while the values of ΔH_f are lesser for the polyamides, the melting points are higher due to lower ΔS_f . This lower value of ΔS_f is in part due to lower value of entropy (S_l) for the amide in the liquid state. The value of S_l is lower due to presence of hydrogen bonding and increased chain stiffness. Similar effects of lower ' S_l ' and hence lower ΔS_f could also be important for the class of high melting semicrystalline polyimides, the topic of this proposal. Although comprehensive calculations of these fundamental thermodynamic parameters for semicrystalline polyimides is still lacking in literature, it is widely known (as discussed in Chapter 1) that strong intermolecular forces due to CTC formation exist in polyimides. The inherent stiffness of the chain also contributes to a lower value of ' S_l '.

Gibbs free energy change for a particular phase is expressed as

$$dG = V dP - S dT \quad \{2.3\}$$

where V and S are the volume and entropy of the phase respectively. Taking the partial derivatives of 'G' with respect to P & T in the above equation, we obtain:

$$(\partial G/\partial T)_P = -S \quad \& \quad (\partial G/\partial P)_T = V \quad \{2.4\}$$

Figure 2.1(b) shows the idealized response of these variables as a function of temperature and at the transition temperature T_m^∞ . These first derivatives of 'G' show a step change at the transition temperature T_m^∞ and the transition is called a first-order transition. While the above discussion addresses purely thermodynamic considerations, the kinetic issues do not favor formation of an infinitely large crystal in polymers, which are characterized, by the formation of finite sized crystals. The exact nature and morphology of these crystals however, has been one of the most heavily debated topics in polymer science.

2.3 Crystallization in polymers: structure, models & relationships

The crystallization of polymers can be broadly classified under three groups:

- (A) Crystallization during polymerization
- (B) Crystallization induced by orientation and
- (C) Crystallization under quiescent condition. While this discussion will only briefly

address type (A) and (B), the last category (C), will be covered in greater detail as it is more pertinent to the present discussion.

(A) Crystallization during polymerization

A special attribute of this kind of polymerization is the formation of macroscopic single polymer crystals³ (see Figure 2.2 (b)). During such a process the monomers forming a crystal can be joined up into chains by solid state polymerization, while the original “monomer” crystals are preserved. The final polymer crystal is obtained due to chemical reactions at the gas/solid or liquid/solid interface and not just as a consequence of change in physical state of the material as is observed in normal crystallization processes⁴. The final properties of crystals formed by such methods can be very interesting, for e.g. poly (sulfur nitride) crystals formed by such methods conduct electricity like metals along the crystal axis (corresponding to the chain direction) and can even become superconducting at sufficiently low temperatures⁵. The mechanism of such a process can be (a) the simultaneous polymerization and crystallization and (b) successive polymerization and crystallization⁵ (see Figure 2.2 (a)). In (a) the primary and secondary bonds are set at the same time, and in (b) the polymerization and crystallization sites can be separated and thus the nature of the polymer segments as yet uncrystallized becomes important⁵. While macromolecular crystallization can occur from only the melt or solution state, the crystallization during polymerization can occur from the monomer being in either gaseous or condensed state. It is thus also possible to get chain folded crystals below the glass transition temperature of the final polymer (e.g. 100°C below T_g for poly (p-xylylenes)²).

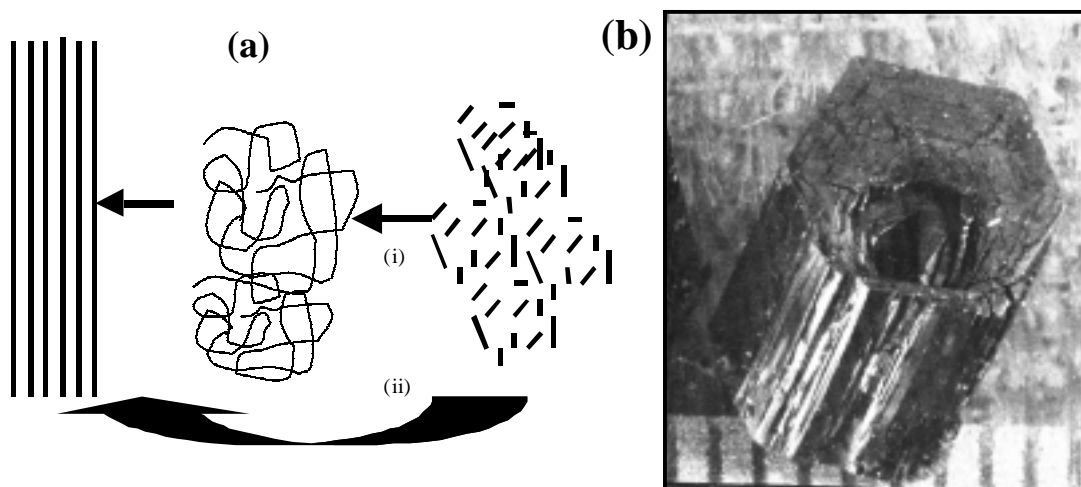


Figure 2.2 (a) Crystallization of macromolecules (i) polymerization followed by crystallization [(i.e.) separate polymerization and crystallization] (ii) crystallization during polymerization⁴ and (b) example of macroscopic single crystal obtained by simultaneous polymerization and crystallization-poly (sulfur nitride) 1 division = 0.5 mm (stejny et al.³)

(B) Crystallization induced by orientation

The schematic of orientation induced crystallization is illustrated in Figure 2.3. The process can be described as stretching of long chains to form fibrous crystals. In fact this is the underlying process governing the formation of fibers though any perfectly smooth and completely elongated chain morphology as illustrated in the schematic is difficult to attain under the most perfect of circumstances. During stretching, the distortion of chains from their most probable conformation results and hence a decrease in the conformational entropy takes place. If this deformation is maintained in this lower conformational entropy state then less conformational entropy needs to be sacrificed by transforming to a crystalline state. This decrease in total entropy of fusion allows the crystallization to occur at higher temperatures than will take place under quiescent conditions. Natural rubber and polyisobutylene are excellent examples of such an effect as they show great propensity to crystallize under stretched conditions whereas they crystallize slowly under quiescent conditions². Also, crystallization in an already oriented polymer results in reduction retractive force² (with respect to oriented state). This can be explained on the basis of rubbery elasticity theory according to which the force exerted by fixed chain ends is inversely proportional to number of statistical elements and the magnitude of end to end distance. The reduction in force results, due to lesser number of statistical units available in the amorphous regions and also because the end to end distance of the amorphous units is smaller than the end to end distance in the crystal. Melting of such elongated crystals lead to contraction and crystallization leads to elongation. Thus macroscopic dimensional changes and changes in retractive force can be related to the crystal-liquid phase transformation².

Normally, the formation of such fibrous morphology is accompanied by formation of an epitaxial layer over⁶ and around the inner fiber giving rise to the so-called 'shish-kebab' kind of morphology⁷. It is well documented^{8,9,11} that the outside 'kebab' like regions are essentially folded chain regions comprised of chains which did not crystallize during the orientation process. Thus, while the inner 'shish' regions form first, the formation of folded chain discs occurs due to nucleation events taking place on

the extended chain surface. It is interesting that though the nature of the nucleating surface is a partially extended chain, and thus a great propensity to crystallize into the thermodynamically more favorable extended chain form exists, subsequent crystallization is still of the folded chain type. This has been used as a strong argument in favor of kinetic theories that argue for the chain folded model of crystallization¹⁰. The lamellar kebabs are usually spaced at distances of ca. 200 to 1000 Å along the chain extended shish. Some researchers have studied the rate of growth perpendicular to the stretch direction and found it to be independent of the percentage extension^{11,12,13} (though the rate of extension was not a factor in these studies). The unaligned chains, which give rise to this undetachable plate like growth, can be the uncrystallized part of the main chain or totally separate chains. Some researchers found that the central shish was of higher molecular weight than the kebabs, while some¹⁴ have demonstrated that a minimum chain length was required for the chain extension process. It has also been argued that the growth of chain folded structures is aided in large part due to the dangling cilia which mostly result along the central fiber like morphology. These cilia, it has been proposed¹⁰, then act as nucleation sites for the chain folded region to develop.

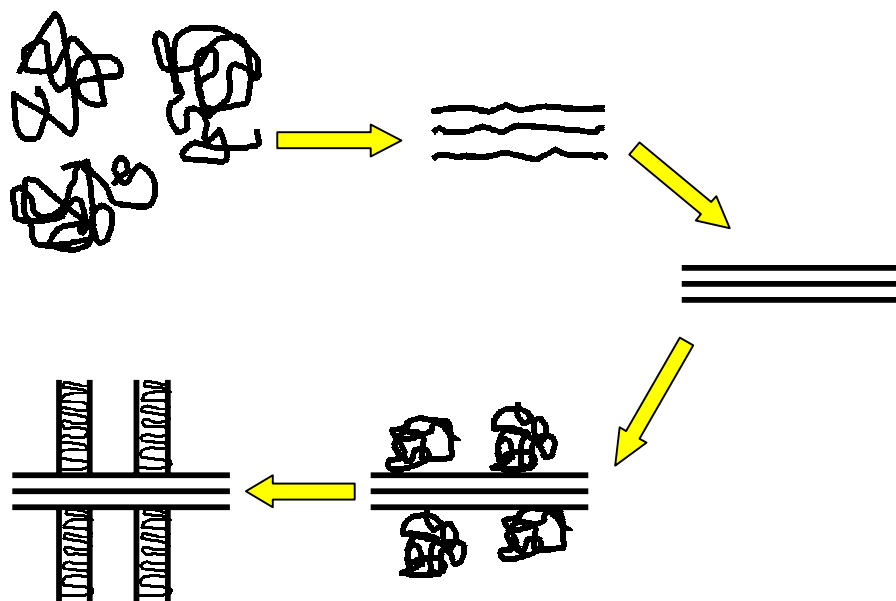


Figure 2.3 Schematic representation of orientation induced crystallization. The first three drawings illustrate the orientation and crystallization of random coils while the last two drawings show the growth of folded chain kebabs around the central shish¹⁰.



Figure 2.4 (a) Shish kebab morphology of polyethylene from solution (from Pennings, 1967³). (b) Shish kebabs of cellulose formed by recrystallizing cellulose II onto microfibrils of high molecular weight³.

(C) Crystallization under quiescent condition

Crystallization of long-chain flexible molecules of sufficient structural regularity is widely observed under quiescent conditions for a large number of macromolecules of both synthetic and natural origin. While it has been long established that similar to low molecular weight compounds, polymers can exhibit considerable long range order in the crystalline regions, the exact nature and morphological form of these crystalline regions (specifically at the molecular level) has been a matter of considerable debate. In this regard it is important to classify the quiescent polymer crystallization into two general types, (1) Crystallization from dilute solutions and (2) Crystallization from the melt. Crystallization from dilute solutions often provides a more fundamental avenue for structural analysis of polymer crystals as these entities can be isolated and precisely studied. Crystallization from the melt is often closer to pragmatic use of the polymer of interest though it adds an additional degree of difficulty to the fundamental structural studies. While this discussion will refer to results and attributes of dilute solution crystallization intermittently, it is crystallization from the melt that is of direct relevance to the present study. The nucleation, growth and kinetics of development of these crystalline regions are of both profound fundamental and practical interest. These characteristics are however directly linked to understanding of the morphological detail of these crystalline regions. On this account, there have been various models proposed over the past five decades- each involving considerable amount of controversy and debate, much of that debate persisting even to date. These models are elucidated below, some of which will be elaborated in more detail in the ensuing discussion. The type of morphology can, however, be first classified into two broad classes¹⁰ (1) the fringed micelle model and (2) lamellar type of morphology. The models of lamellar morphology themselves differ on the basis of the nature of the fold surface, type of reentry of the chains and on accounts of presence of an intermediate region for the chain traveling from the crystal to the amorphous phase.

2.4 The fringed micelle model

Hermann, Gerngross and Abitz¹⁵ first conceived this model in 1930 to explain the structure of gelatin, while the model was later more fully expanded by Flory^{16,17,18}. The fringed micelle model is based on the idea that parts of the polymer segments (either in solution or in the melt) align themselves together to form bundled crystalline regions (Figure 2.5). These bundles can then grow in the direction of chain axis by reeling in adjoining chain segments (of the chains already part of the crystal) into the crystalline region. Lateral growth of these crystalline regions can also take place by accretion of chain segments from other molecules. The growth of these structures however is

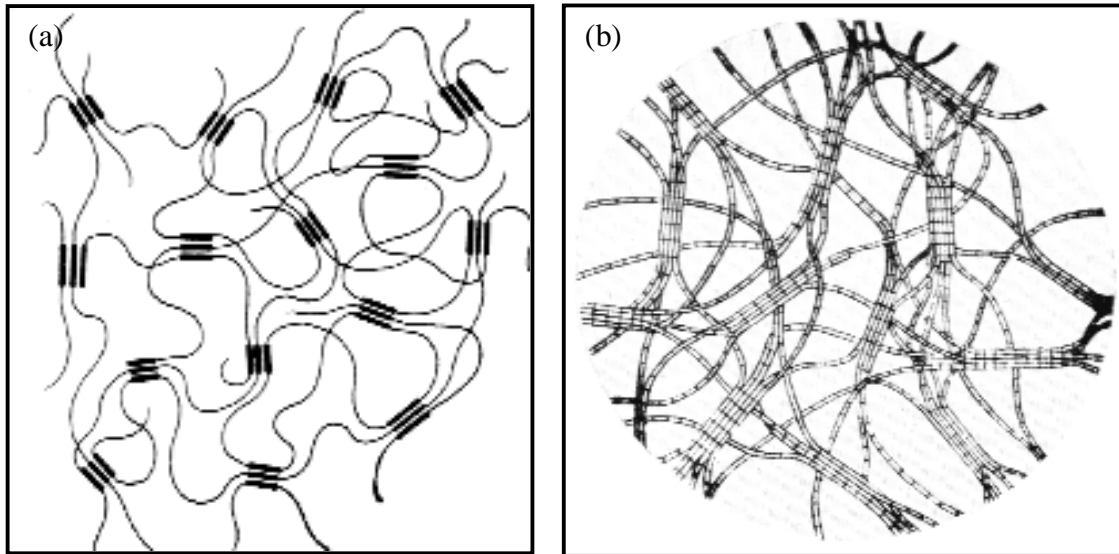


Figure 2.5 Fringed micelle model (a) Model of crystallization as might be visualized in a thermoreversible gel (Keller et al¹⁰.) (b) Hermann and Gerngross model¹⁵ for a semicrystalline polymer. Similar schematics illustrate the general molecular picture in fringed micellar crystallization.

impeded by the presence of entanglements and strained regions, which then constitute the amorphous phase. The “fringes” are the regions of the chains traveling from the crystalline region to the surrounding amorphous regions. The crystalline regions then serve as physical crosslinks.

Some of the first blows to this model of crystallization occurred after collecting evidence of large crystalline superstructures present in such materials, called ‘spherulites’. Such a model could not readily explain the growth of such generally spherically symmetrical structures¹⁹. Also, the birefringence measurements on these spherulites by light microscopy suggested that, for most systems, the polymer chains were more or less tangential in this spherical structure. Although several models were put forward to explain the spherulitic behavior based on this concept²⁰, they were subsequently abandoned in favor of folded chain lamellar models.

While the fringed model has now long been believed to be inaccurate for describing the common quiescent crystallization behavior, its modifications can still be utilized to explain several phenomena occurring in the crystallization of polymers. Several aspects involving the crystallization of thermoreversible gels - where the dilute solution crystallization leads to ‘gelation’ of the overall system have been explained on the basis of this model^{10,21,22}. Lamellar crystallization, it has been debated, would have lead to the presence of individual single crystals or aggregates thereof. This model has also been widely proclaimed to be correct for certain polymers that crystallize during rapid cooling/quenching from the melt, and where the individual spherulitic detail is not discernible from microscopy¹⁰. The use of such a model for describing crystallization of an amorphous polymer just above the T_g has been advocated on the grounds of low thermal energy available to chains at such temperatures¹⁹. At temperatures significantly higher than T_g , these structures will not be stable and will give way to lower energy lamellar form. Additionally the model is utilized to explain the behavior of highly oriented samples like the drawn fibers.

2.5 Lamellar models:

It is a well-established and proven fact that a lamellar crystal is the fundamental structural form by which polymers most generally crystallize, a feature true for the vast majority of semicrystalline polymers crystallized from the bulk (i.e. from solution or from melt). The first report giving evidence of lamellar structures was by Storcks²³ in 1938. He reported electron diffraction results on cast films of gutta-percha and concluded that the films contained microscopic crystals with the molecular axis less than 4° from normal to the plane of the film. He observed that while the electron diffraction results gave only $\{hk0\}$ reflections, the total length of the chains was much greater than the thickness of the films- a recognition that led him to first propose a chain-folded structure to explain the crystallization in such systems. Schlesinger and Leeper²⁴ conducted similar experiments in 1953 on gutta-percha but this time using light microscopy and refractive index measurements. While both these studies were largely

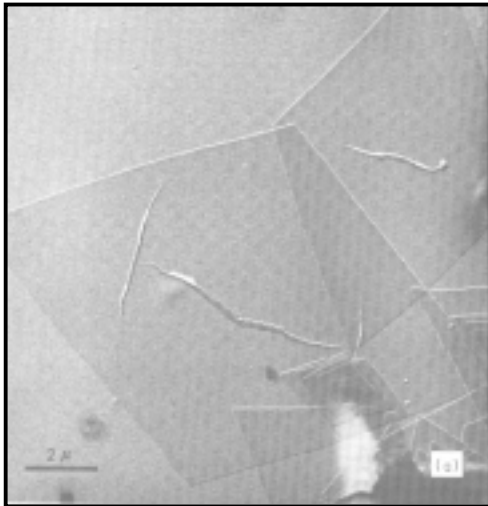


Figure 2.6 Single crystals of Polyethylene after evaporation of tetrachloroethylene solvent. Pleats form due to crystal collapse. Micrograph is taken from 'Polymer Single Crystals' by P.H. Geil¹⁹.

ignored, Jaccodine's report²⁵ of single crystals of polyethylene in 1955 gained attention of several researchers who expanded on his work. In 1957, Till²⁶, Keller²⁷, and Fischer²⁸ independently reported on the growth and identification of single crystals of polyethylene. Since these studies, lamellar crystal habit has been shown to be the dominant structural mode of crystallization for a large number of polymers. The various models proposed for the nature of these structures are:

(1) Random reentry or “Switchboard” folded model.

This model was first proposed by Flory^{17,29,30,31} and consists of chains randomly folding back into the same lamella or even participating in adjoining lamellae. The upper and lower surfaces consist of loops of varying sizes and the amount of adjacent reentry is *small and not a necessity*^{17,29,30,31}. The upper and lower surfaces may consist of transitional regions that constitute a diffuse phase boundary – their density being intermediate between the crystal and purely amorphous regions.

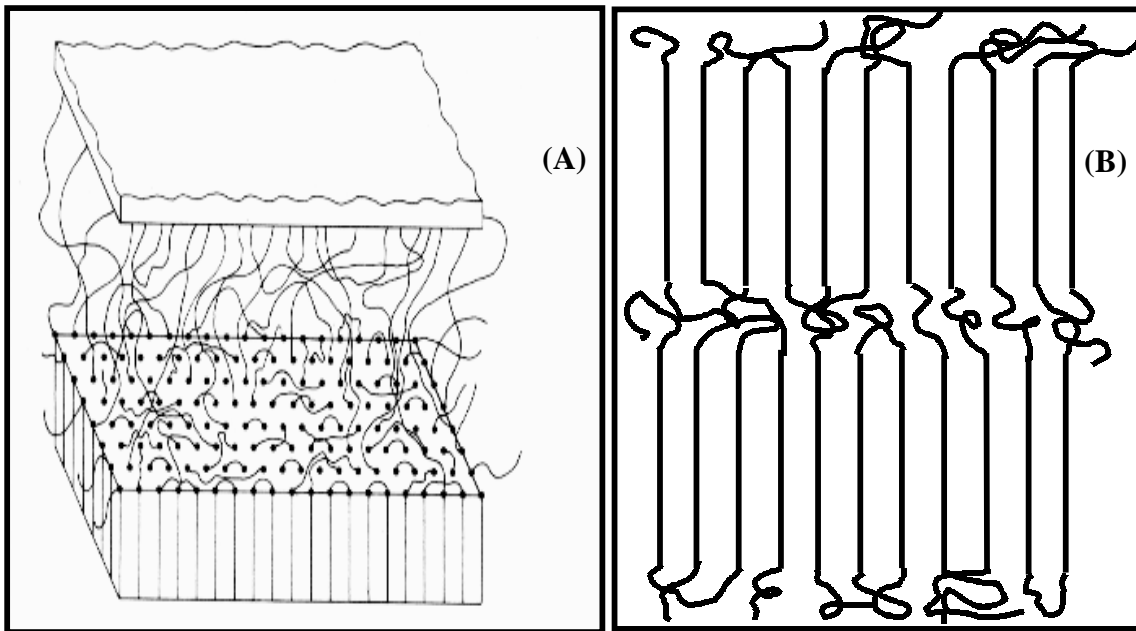
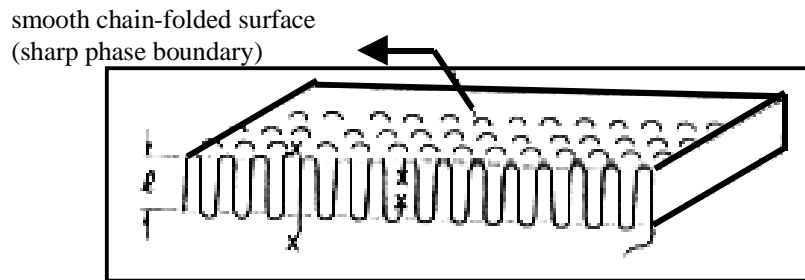


Figure 2.7 (A) Schematic of a Switchboard model, showing the surface of a lamella, interlamellar region and tie chains between the lamella. (From Mandelkern³⁰) (B) originally proposed model for melt crystallization in polymers¹⁷.

(2) **Adjacent reentry chain-folded models (regular folding)**

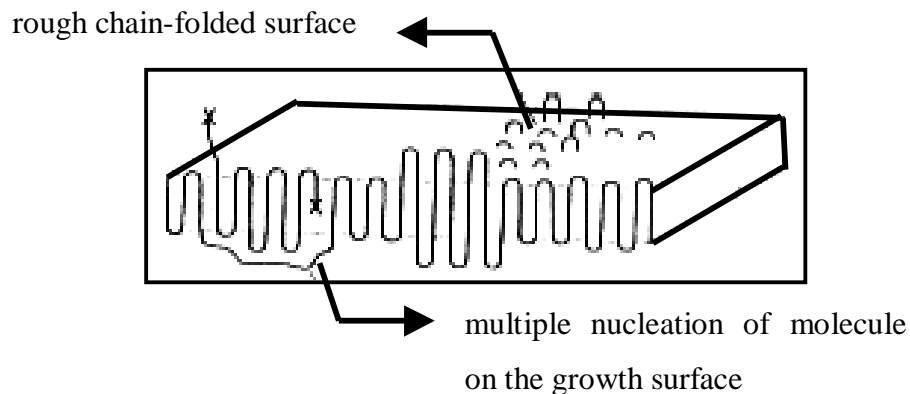
(i) *Smooth surface model*^{32,33}:

This model is characterized by sharp phase boundary between the crystal and the amorphous phase. The mode of reentry of the chains is the adjacent neighbor with only a few exceptions due to multiple nucleation and chain-end defects. This is a very idealized visualization of the chain folding process.



(ii) *Rough surface model*³³:

The reentry of the chain is still in the nearest growth plane, though large variations in the fold length may exist on a local scale. Multiple nucleation and chain-end defects will further contribute to a rough surface. The overall phase boundary is no longer sharp, though local regions may still exhibit such character.



(3) *“Erstarrungsmodell”* (solidification model)^{34,35}

This model was put forward by Fischer & coworkers to explain the constancy of the radius of gyration r_g in the crystalline state (with respect to r_g in the amorphous

state), as detected by small angle neutron scattering (SANS)³⁶. The model is similar in conception to the “fringed micellar” morphology and is visualized in terms of alignment of chains without a long-range diffusion process to give rise to a lamellar morphology. The chain sequences in proper conformations (indicated by thicker lines in the diagram) are incorporated into the crystal without significant reorganization of the chain conformation.

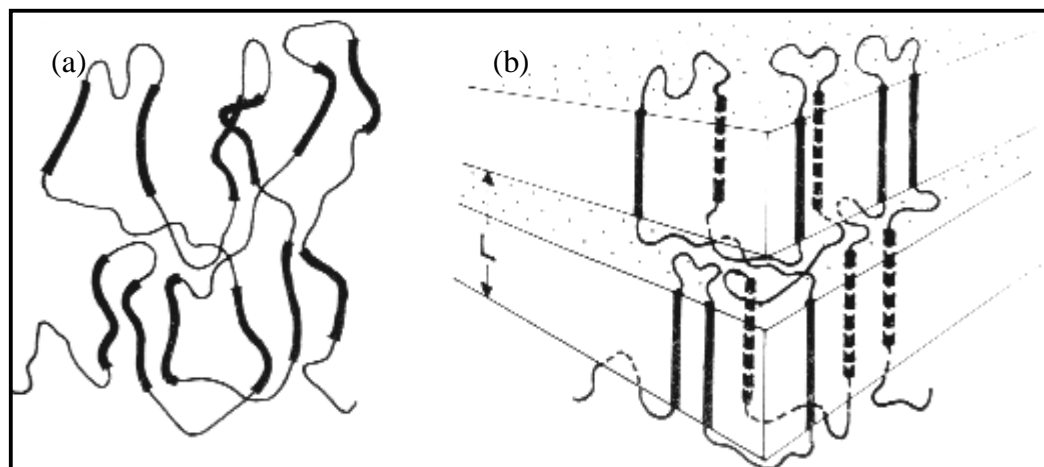
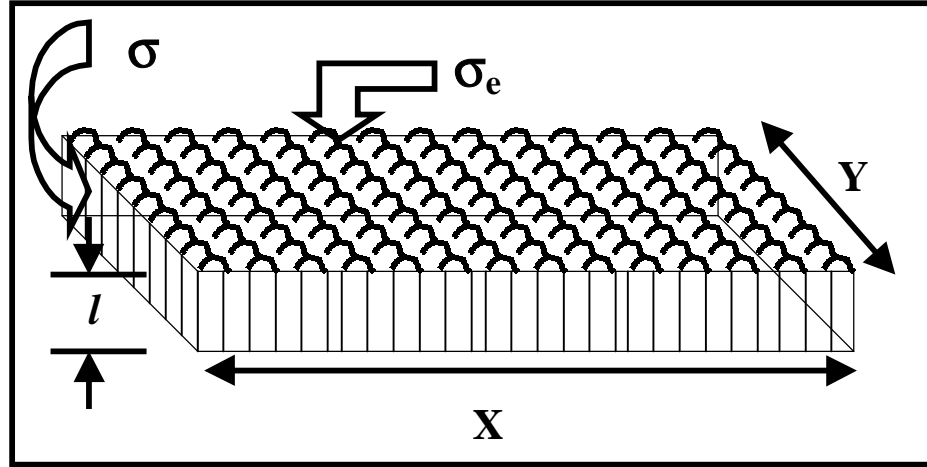


Figure 2.8 “Erstarrungsmodell” (a) chain conformation in the melt state
(b) alignment of suitable conformations into the crystal³⁶.

2.6 Gibbs-Thomson equation^{37,38}:

This well known equation is a simple application of fundamental thermodynamic concepts applied to the above discussed lamellar crystal morphology. The existence of a thin plate lamellae with the thickness much smaller than the lateral dimensions is the primary requirement and not the proof of any particular model thereof. The schematic of a lamellar structure, which is shown in figure below, is thus for the purposes of illustration only and the molecular detail should not be taken literally.



For a finite sized crystal as shown above,

$$\Delta G_{\text{crystal}}(T) = 2XY\sigma_e + 2l[X+Y]\sigma - XYl\Delta G_f^\infty(T) \quad \{2.5\}$$

At the melting point of the crystal, T_m :

$$\Delta G_{\text{crystal}}(T_m) = 0 \quad \{2.6\}$$

Assuming:

- ‘no thickening’
 - $XY \gg l[X+Y]$ {true for thin lamellae with large lateral dimensions}
 - $\sigma_e \gg \sigma$ {true for most polymers}
 - $X \sim Y$ {does not make a difference for large lateral dimensions}

Eq. (2.5) becomes $\Delta G_f^\infty(T_m) = 2\sigma_e/l \quad \{2.7\}$

Now for an infinite sized crystal at T_m° ,

$$\Delta G_f^\infty(T_m^\circ) = \Delta H_f^\infty(T_m^\circ) - T_m^\circ \Delta S_f^\infty(T_m^\circ) = 0 \quad \{2.8\}$$

Hence, $\Delta S_f^\infty(T_m^\circ) = \Delta H_f^\infty(T_m^\circ) / T_m^\circ \quad \{2.9\}$

Now for an infinite sized crystal at T_m ,

$$\Delta G_f^\infty(T_m) = \Delta H_f^\infty(T_m) - T_m \Delta S_f^\infty(T_m) \neq 0 \quad \{2.10\}$$

Assuming * $\Delta H_f^\infty(T_m) = \Delta H_f^\infty(T_m^\circ)$ {small temperature dependence is ignored}

$$* \quad \Delta S_f^\infty(T_m) = \Delta S_f^\infty(T_m^\circ) \quad \{ \text{not a bad assumption for high } T_m \text{'s !} \}$$

it is obtained that,

$$\Delta G_f^\infty(T_m) = \Delta H_f^\infty(T_m^\circ) - T_m \Delta S_f^\infty(T_m^\circ) \quad \{2.11\}$$

$$\text{using eq.(2.9)} \quad \Delta G_f^\infty(T_m) = \Delta H_f^\infty(T_m^\circ) [1 - T_m/T_m^\circ] \quad (\text{important relation}) \quad \{2.12\}$$

comparing eq. (2.7) & eq.(2.12)

$$2\sigma_e/l = \Delta H_f^\infty(T_m^\circ) [1 - T_m/T_m^\circ] \quad \{2.13\}$$

which can be written to give the *Gibbs-Thomson equation*:

$$\boxed{T_m = T_m^\circ \left[1 - \frac{2\sigma_e}{l\Delta H_f^\infty T_m^\circ} \right]} \quad \{2.14\}$$

This equation provides one of the convenient ways for estimating the value of the equilibrium melting point T_m° , and for also obtaining the value of σ_e . Both these quantities are obtained by plotting the observed melting points T_m vs. $1/l$, where the value of σ_e can be learned from the slope and the intercept gives the value of T_m° . The lamellar thickness ' l ' can often be obtained by techniques like SAXS or sometimes TEM whereas T_m is usually obtained using DSC. Many workers^{39,40,41} have elucidated the necessary precautions in this method, some of which are:

- lateral dimensions should be \gg thickness of lamellae
- The melting temperature T_m should correspond to the ' l ', which, however, is usually measured at room temperature⁴² (cause of error for polymers that undergo thickening)⁴².

2.7 Lauritzen-Hoffman secondary nucleation theory^{43,39}

This theory explains the kinetics of crystallization in molecular terms, for linear flexible macromolecules which are crystallized from the melt into chain folded lamellae. This theory⁴³ (and its various modifications^{32,33,39,44-47}) constitutes perhaps the most comprehensive and widely used methodology to interpret and model the crystallization behavior of a large number of polymers. The theory has evolved substantially since it was first proposed and has incorporated several new concepts in order to broaden the

scope of its predictions and also to satiate the objections of other workers in the field³⁹. Though the theory is best suited to describe the chain folded crystallization of polyethylene and other flexible polymers, it has also been applied with some degree of success to model the crystallization behavior of other more rigid chain systems such as PEEK⁴⁸. While it is not possible to fully cover this theory in the present review, the fundamental formalisms and the important deductions will hopefully be succinctly explained in the forthcoming sections.

The original L-H theory and its various modifications account for a broad range of behavior observed for crystallization of linear flexible macromolecules. These are³⁹:

- it accounts for the variation of initial lamellar thickness (l^*) vs. supercooling (ΔT_c)
- parameters can be found that fit the variation of crystal growth rate 'G' vs. ΔT_c
- provides an explanation for break in temperature dependence of G
- explains the origin of σ and σ_e
- the generation and effect of adjacent events (tight folding) and non-adjacent events (e.g. tie chains, loose folds, cilia)
- Variation of (a) the crystal growth rate 'G' and (b) quantified chain folding (i.e. degree of tight chain folding), with the change in molecular weight
- Recent versions have also incorporated the 'reptation' concept into the theory

The various facets of polymer crystallization still not addressed completely by the theory are:

- Explanation for primary nucleation and hence bulk crystallization kinetics
- Development of lamellae from a primary nucleus
- Lamellar branching giving rise to spherulites (other factors like screw dislocations provide some explanation)
- Banding in spherulites due to lamellar twisting
- Quantified estimation of the degree of crystallinity

The treatment starts by first addressing the deposition of a first stem and later treating the deposition of subsequent stems in a stepwise manner. The deposition of the stems is

visualized to take place in two steps. In the first step the part of the chain in proximity to the surface loses conformational entropy and becomes flattened with few crystallographic attachments to the surface. The state of the molecule is visualized as being similar to a weak physically adsorbed system with the possibility of occasional point contacts on the surface. This short section of the molecule, after a series of events, straightens and aligns itself to yield an activated state $\Delta\Phi^*$, where the loss in entropy is equal to $\Delta S_f/C_\infty$ ($= -\Delta S_1^*$). The entropic contribution to the free energy barrier will thus be $T\Delta S_f/C_\infty$ with little/no contribution from the heat of fusion at this stage. The second important aspect of first stem deposition is the creation of two new lateral surfaces with work of building them being equal to $2b_0\sigma l$, where b_0 is the layer thickness while 'l' is the length of the chain attached. The value of 'l' is treated as a variable here and later shown to average out to l_g^* . It is these series of steps to yield an activated state, which are considered to be most difficult and slowest. Subsequent stem deposition from this activated state, with the average length of the stem being l_g^* , takes place without any difficulty. According to this, the free energies for the segment of the chain at various states can be written as:

$$G_{\text{subcooled melt}} = G_{\text{liquid}} \quad \{2.15\}$$

$$G_{\text{activated state}} = \psi G_{\text{crystal}} + (1-\psi) G_{\text{liquid}} + 2b_0\sigma l \quad \{2.16\}$$

$$G_{\text{attached stem}} = G_{\text{crystal}} + 2b_0\sigma l \quad \{2.17\}$$

Also the change in free energy when going from subcooled melt to the activated stem is:

$$\Delta G_c^* = 2b_0\sigma l + \psi [a_0b_0] \Delta G_c \quad \{2.18\}$$

where ΔG_c is the free energy of crystallization/unit volume and ' ψ ' is the apportionment factor, i.e. the fraction of free energy available due to the crystallographic attachment at a finite and few number of sites. The possible values of ' ψ ' can thus be between 0 and 1. The second important formalism is the deposition of second and subsequent stems. The process for second stem deposition is similar in that it also involves an activated complex formation, although the activated stem differs with respect to the surface energy terms. The activated complex for second stem deposition does not lead to creation of any additional lateral surfaces but now consists of a 'single fold' and the 'aligned part of the molecule'. The surface energy and area associated with this tight fold are σ_e and $2a_0b_0$ respectively.

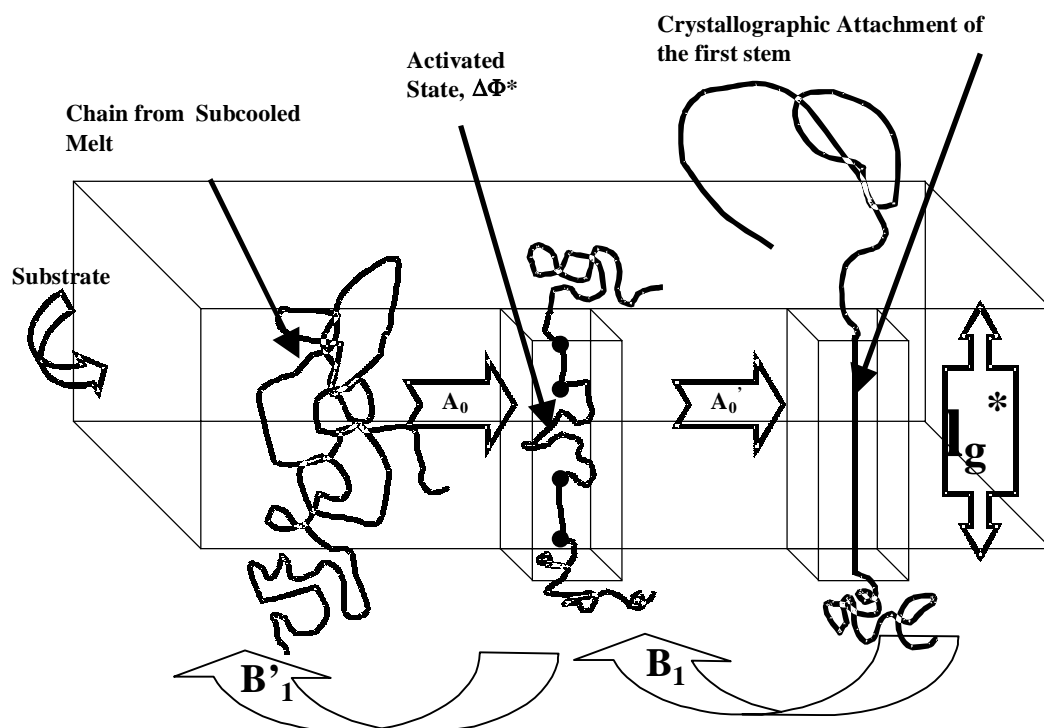


Figure 2.9 Formation of the physically aligned activated complex and its conversion to first crystallographically attached stem. The first step A_0 is the slowest and rate determining step while the step A_0' is fast³⁹.

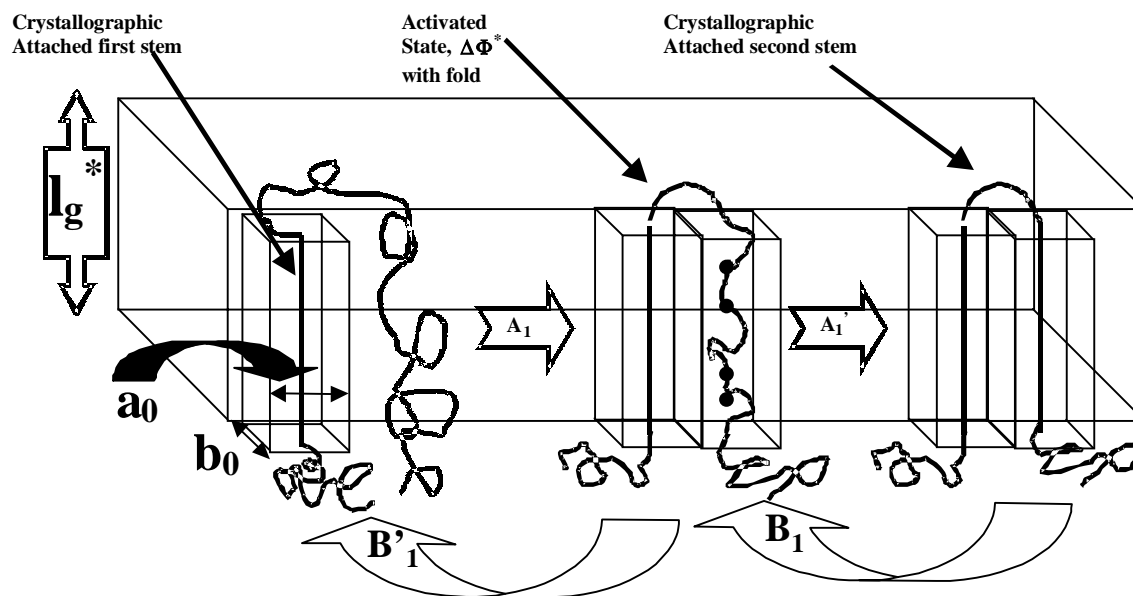


Figure 2.10 Formation of the physically aligned activated complex and its conversion to second crystallographically attached stem. The first step A_0 is the slowest and rate determining step while the step A_0' is fast. The activated state includes a tight fold + the aligned part of the chain³⁹.

The free energy for the unattached part, in the various states is then:

$$G_{\text{initial}} = G_{\text{liquid}} \quad \{2.19\}$$

$$G_{\text{activated state}} = \psi G_{\text{crystal}} + (1-\psi) G_{\text{liquid}} + 2a_0b_0\sigma_e \quad \{2.20\}$$

$$G_{\text{attached stem}} = G_{\text{crystal}} + 2a_0b_0\sigma_e \quad \{2.21\}$$

Also the change in free energy when going from the subcooled melt to the activated state is:

$$\Delta G_c^* = 2a_0b_0\sigma_e + \psi [a_0b_0] \Delta G_c \quad \{2.22\}$$

For the nucleus to become stable, the slope of ΔG vs. v curve should be negative. Thus:

$$2a_0b_0\sigma_e + [a_0b_0] \Delta G_c < 0 \quad \{2.23\}$$

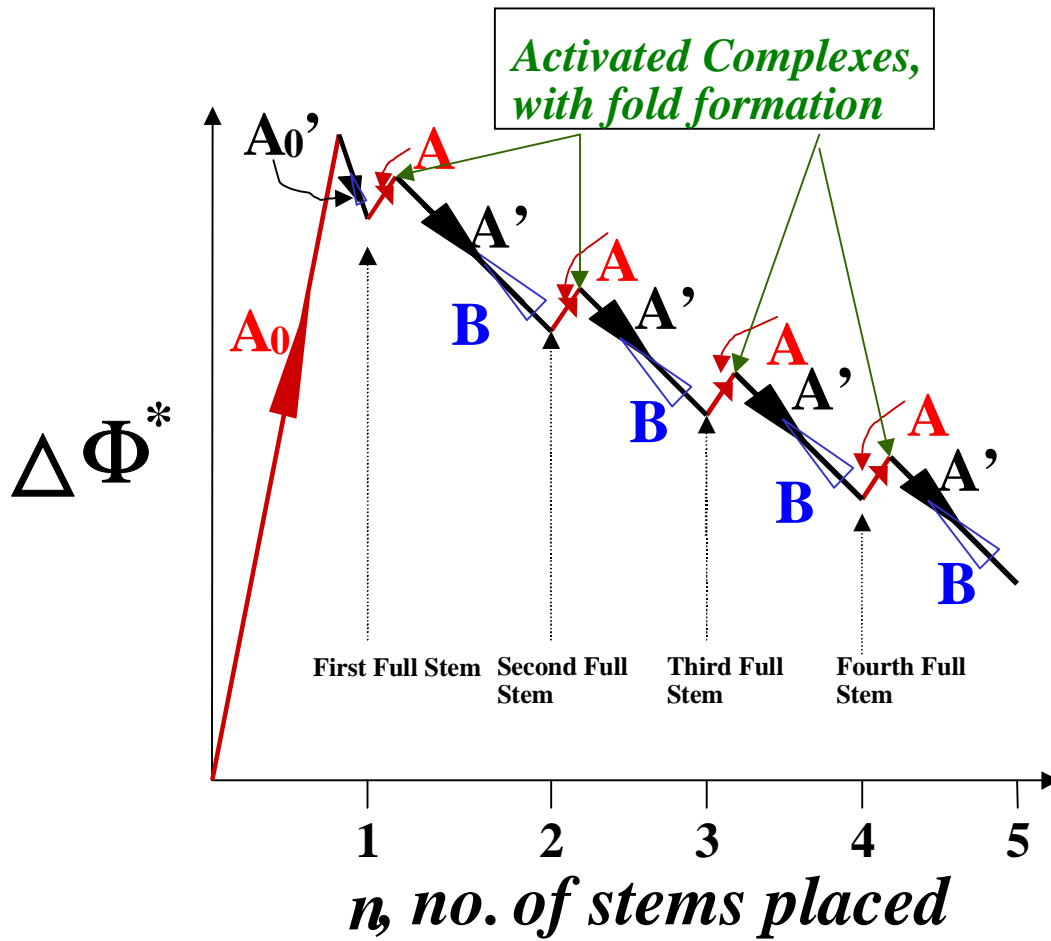


Figure 2.11 Barrier system for the surface nucleation showing both the slow, fast and backward steps possible. A, A₀, B₁ and B are the rate determining slow steps while A₀' and A' are the fast steps³².

$$\Rightarrow l > 2\sigma_e / \Delta G_c$$

for the nucleus to be stable

$$\Rightarrow l > \frac{2\sigma_e T_m}{\Delta H_f \Delta T_c} \quad \{2.24\}$$

This means that $l_{\min} = 2\sigma_e / [\Delta H_f \Delta T_c / T_m]$ is the *critical minimum length* needed to form a thermodynamically stable nucleus. This is schematically illustrated in Figure 2.11 which shows that the free energy actually rises as more and more stems are laid down, thus making the nucleation of those stems thermodynamically unfavorable. The figure also shows the length l_g^* at which the rate of stem deposition is kinetically favored, although it does not mean that the nucleus of such a length is thermodynamically most favored

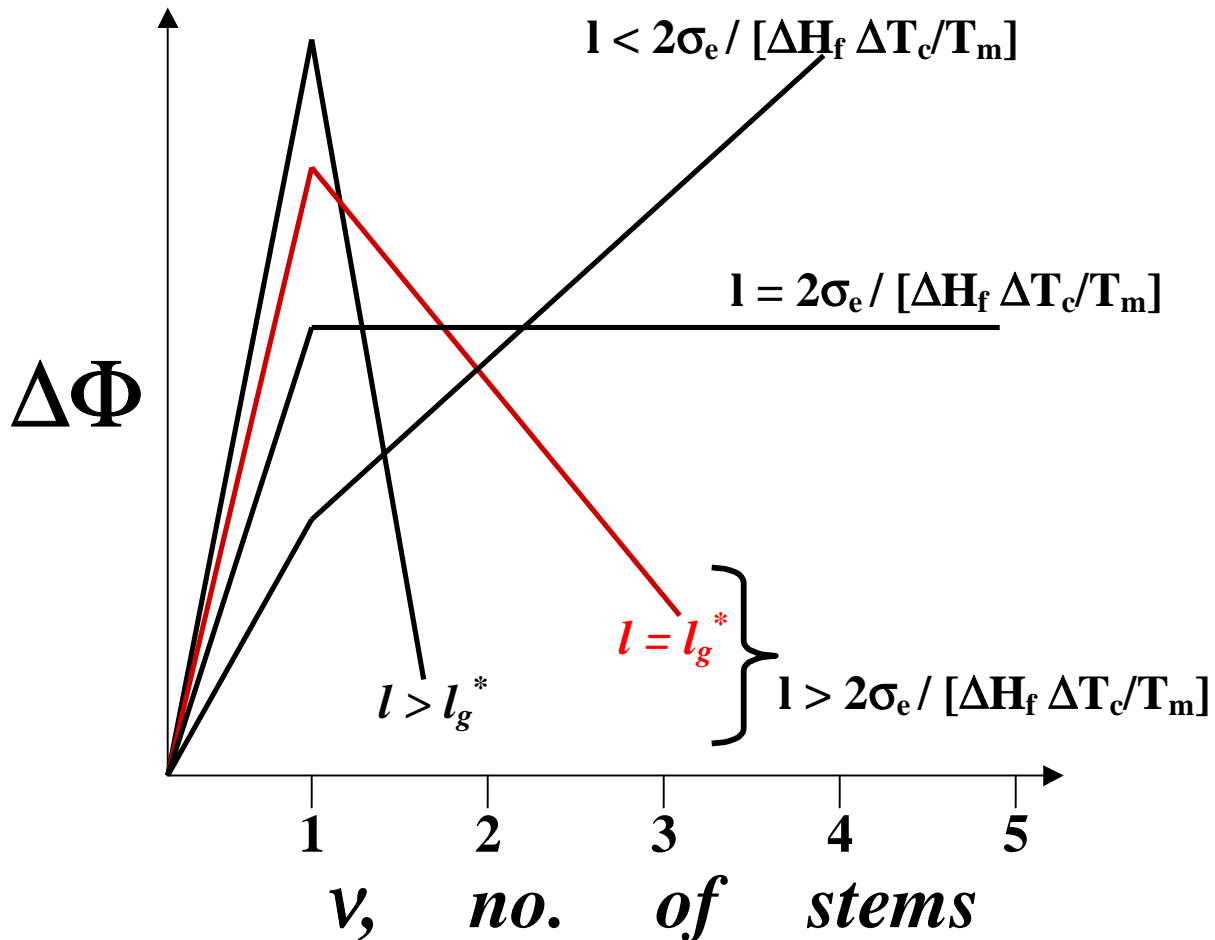


Figure 2.12 Free energy with subsequent stem deposition along the substrate for different values of lamellar thickness' l .³⁰

(fully extended chain crystal will be such a case and not a chain folded one). *Thus the value of l which gives the fastest substrate completion rate and thus the maximum overall crystal growth rate 'G' (at that temperature) is the favored stem length for deposition, the average being l_g^* .* Subsequent flux calculations lead to an expression for l_g^* . It can be shown conveniently by steady state flux calculations that the rate of stem deposition is given by⁴⁹:

$$S(l) = \frac{N_0 A_0 (A - B)}{A - B + B_1} \quad \{2.25\}$$

Where N_0 is the number of initial stems, soon to be involved in the first stem deposition process. The values of the rates along various paths A_0 , A , B_1 and B are estimated by Arrhenius rate expressions, the values of traditional activation energy in these being given by free energy barriers for the respective processes. Thus,

$$A_0 = \beta' \exp \left[\frac{-2b_0 l \sigma + \psi' a_0 b_0 l \Delta G_f}{kT_c} \right] \dots \dots \dots \{2.26\}$$

$$B_1 = \beta' \exp \left[\frac{-(1 - \psi') a_0 b_0 l \Delta G_f}{kT_c} \right] \dots \dots \dots \{2.27\}$$

$$A = \beta \exp \left[\frac{-2b_0 l \sigma_e + \psi a_0 b_0 l \Delta G_f}{kT_c} \right] \dots \dots \dots \{2.28\}$$

$$B = \beta \exp \left[\frac{-(1 - \psi) a_0 b_0 l \Delta G_f}{kT_c} \right] \dots \dots \dots \{2.29\}$$

The above expressions suggested by Marand *et al*^{37,42,50,51} treat the pre-exponential factor (β') and 'apportionment factor' (ψ') for the rates associated with first stem deposition to be different than β and ψ for the second and subsequent stem deposition. However, the traditional L-H theory treats $\beta = \beta'$ and $\psi = \psi'$, in part due to the difficulty associated with finding an analytical solution for the secondary nucleation rate i if these factors are not held equal. While the procedure for using the above equations to give analytical rate expression for i (for two limiting cases) and the implication thereof is outlined by Snyder

et al^{50,51} it is not difficult to visualize that the rationale of assigning different values for first and later stems is based on firmer grounds. While the short-range motions and localized conformational rearrangements (reptation of slack) are expected to govern the placement of the first stem, the later process is more akin to a reptation like motion of the rest of the chain, leading to subsequent stem depositions. In this regard, the molecular weight dependency of β and β' has been assumed to be different, with β' showing little or no dependence on molecular weight⁵⁰ and $\beta^{39,51,52} \propto n^{-1}$. For the traditional L-H treatment the value of β ($=\beta'$) depends upon the value of the friction coefficient per chain repeat unit ζ ³⁹. This monomeric friction coefficient ζ can itself be described by a Arrhenius kind of expression for temperatures greater than T_g+100K and by Vogel-Fulcher type expression for temperatures between T_g and T_g+100K . In these ways the traditional L-H treatment can account for molecular weight dependence and temperature dependence of crystal growth rate 'G' to a reasonable extent.

One problem with the traditional L-H theory has been that it forecasts a critical undercooling $\Delta T^* = 2\sigma T_m / \psi a_0 \Delta H_f$ where the value of l_g^* is predicted to show a relative upswing, a feature not confirmed experimentally for any polymer at any undercooling. Several approaches have been suggested to circumvent or alleviate this dilemma where the barrier to first stem deposition appears to become zero, this problem has been traditionally referred to as the “ δl catastrophe”^{43,53}. This problem is directly related to assignment of the value for ψ and has been circumvented by assigning $\psi=0$ in the traditional L-H theory. Recent modifications have also addressed this problem by stating that if the $\psi \leq 0.2$ the value falls close to absolute zero and is thus not expected to occur³⁹. The low value of ψ has additionally been argued to be justifiable on the basis of a small number of niches expected for the first stem and thus close to nil contribution due to enthalpy of crystallization. Additionally, Marand *et al*⁵¹ have suggested that the “ δl catastrophe” is the mathematical artifact of assuming that ψ for the placement of the first stem and ψ for the placement of subsequent stems are same. Starting with the low ψ formulation in the L-H theory, the initial average lamellar thickness can be calculated as:

$$\langle l \rangle = l_g^* = \frac{\int_{2\sigma_e/\Delta G}^{\infty} l S(l) dl}{\int_{2\sigma_e/\Delta G}^{\infty} S(l) dl} \quad \{2.30\}$$

where the values of $S(l)$ is given by equation (2.25) and the A , A_0 , B_1 and B are given by expressions previously stated with the value of $\psi=\psi'=0$ and $\beta=\beta'$. With some effort, it can then be shown that⁴⁵:

$$l_g^* = \frac{2\sigma_e}{\Delta G_f} + \left[\frac{kT}{2b_0\sigma} \right] \left[\frac{\Delta G_f + 4\sigma a_0}{\Delta G_f + 2\sigma a_0} \right] = l_{\min} + \delta l \quad \{2.31\}$$

where the second term on the right-hand side represents ' δl ', the increment above the minimum lamellar thickness which makes the crystal to enter the thermodynamically stable state at the fastest rate and prevents the anomaly $T_m = T_c$.

Another factor of importance is the thickening of lamellar crystals (1) during the traditional DSC heating scan, i.e. non-isothermal thickening, and also/or (2) when these originally grown crystals are sitting at some temperature (may or may not be T_c) i.e. non-isothermal thickening. These thickening processes occur for a large number of polymers although it has been advocated that a crystalline ' α_c ' relaxation, which involves chain movement along the crystal, is a necessary condition for any thickening to occur in the lamellae^{42,54}. Such thickening, when and if it occurs, will lead to lamellae of different thickness than what had initially formed, the thickening coefficient being defined as:

$$\gamma = l/l_g^* \quad \{2.32\}$$

the thickness of the lamellae at the time of the melting being l . For no thickening the value of γ will obviously be 1 and the value of melting point corresponds to the original lamellae grown at temperature T_c . Now, using the value for l_g^* from the equation (2.31) and incorporating any thickening effects by including equation (2.32) shown above, the previously described Gibbs-Thomson equation (2.14) yields the value of melting point as a function of undercooling ΔT_c .

$$T_m = T_m^\circ \left[1 - \left(\frac{\Delta T_c}{\gamma T_m^\circ} \right) \left(\frac{1}{1 + \frac{\delta l \Delta H_f \Delta T_c}{2 \sigma_e T_m^\circ}} \right) \right] \quad \{2.33\}$$

Now if it is assumed that $\delta l \Delta H_f \Delta T_c \ll 2 \sigma_e T_m^\circ$, and that γ is constant then the equation transforms to the Hoffman-Weeks relation, widely used to determine the value of equilibrium melting point for various polymers.

$$T_m = T_m^{\circ hw} \left(1 - \frac{1}{\gamma^{hw}} \right) + \frac{T_c}{\gamma^{hw}} \quad \{2.34\}$$

where $T_m^{\circ hw}$ and γ^{hw} are the respective value of equilibrium melting point and the thickening coefficient as determined by a Hoffman-Weeks plot. It is clear from the above equations that this method of estimating T_m° , although providing an approximation, is incorrect on rigorous grounds due to two major assumptions mentioned above. Specifically let us address the use of this technique for the more rigid and aromatic based systems such as PEEK and some semicrystalline polyimides. These polymers have shown plenty of evidence for the existence of lamellar structures and exhibit other similarities in crystallization behavior with flexible chain polymers, thus inviting the assumption from many workers that many features of the L-H treatment can be reasonably applied. However, it is important to note that the main assumption of L-H model of an adjacent reentry is not observed for this rigid chain polymers. Also, for most of these polymers, the assumption of a constant thickening coefficient holds well. The problems arise however due to the first assumption of $\delta l \Delta H_f \Delta T_c \ll 2 \sigma_e T_m^\circ$, which in effect pictures the contribution due to the δl term to be small in comparison to the overall lamellar thickness in contributing to the melting point. While this assumption holds better for flexible polymers like polyethylene, there is not much evidence to support this view for more rigid chain systems. Unlike polyethylene which consists of short repeating units and thus the δl increment can consist of several of these units, more rigid polymers display significantly longer repeat units. Thus for these polymers, even if the δl term

consists of one such additional unit, then the contribution of δl term in increasing lamellar thickness and hence the melting point cannot be ignored. The traditional objections for a Hoffman-Weeks analysis then become even more severe for polymers similar to ones utilized in the current project. Therefore such analysis can only serve as a coarse estimate in attaining the value of T_m° . A recent work addresses in some detail the efficiency of this analysis for flexible chain polymers, given the degree of acceptable error⁵⁴.

2.8 Growth rate determination and regime kinetics

The above-discussed concepts lead us to calculations involving the lateral substrate completion rate, S_T as given by equation (2.35) below. The steady state flux S_T is

$$S_T = \frac{1}{l_u} \int_{2\sigma_e/\Delta G}^{\infty} S(l) dl \quad \{2.35\}$$

where l_u is the monomer length.

This allows us to calculate the rate of stem deposition ‘i’, i.e. the surface nucleation rate in terms of stems s⁻¹ cm⁻¹ by the simple relation³⁹

$$i = S_T / L = S_T / n_l a_0 \quad \{2.36\}$$

where n_l is the number of stems of width a_0 which make up the substrate of length L . The second important parameter leading up to the crystal growth rate ‘G’ is given by the substrate completion rate ‘g’. The substrate completion rate is given by

$$g = a_0 (A-B) \quad \{2.37\}$$

Together the substrate nucleation rate ‘i’, and substrate completion rate ‘g’ decide the crystal growth rate ‘G’, the exact nature of this relation being given by relative rates of i vs. g. This issue and the relationship between i, g & G are illustrated in Figure 2.12.

Thus, three regimes of crystallization are considered in this problem. In Regime I^{53,55}, the growing crystal nucleus sweeps completely across the crystalline interface before any new nuclei are laid down. In Regime II^{53,55}, the relative rates of *i* vs. *g* are similar, thus allowing for the new nuclei to form even before the previous layer has completely been filled. In Regime III^{56,57}, a large amount of nucleation events occur and hence little or no substrate completion takes place. These three regimes have been experimentally observed for a large number of polymers and the undercooling dependencies of the growth rates in accordance with the above analysis has been confirmed (when using some adjustable fitting parameters).

Quantifying the analysis further, from the relations shown (Equations 2.35, 2.36 and 2.37 above and Equations 2.28, 2.29 and 2.31 shown previously) one obtains the substrate nucleation rate *i* and substrate completion rate *g* as⁵⁰:

$$i = \frac{N_0 \beta}{n_l a_0 l_u} \left[\frac{kT}{2b_0 \sigma} - \frac{kT}{2b_0 \sigma + \Delta G_f} \right] \exp \left[\frac{-4b_0 \sigma_e \sigma}{\Delta G_f kT} \right] \quad \{2.38\}$$

$$g = a_0 \beta \left[1 - \exp \left(\frac{a_0 b_0 \delta l \Delta G_f}{kT} \right) \right] \exp \left[\frac{-2a_0 b_0 \sigma_e}{kT} \right]$$

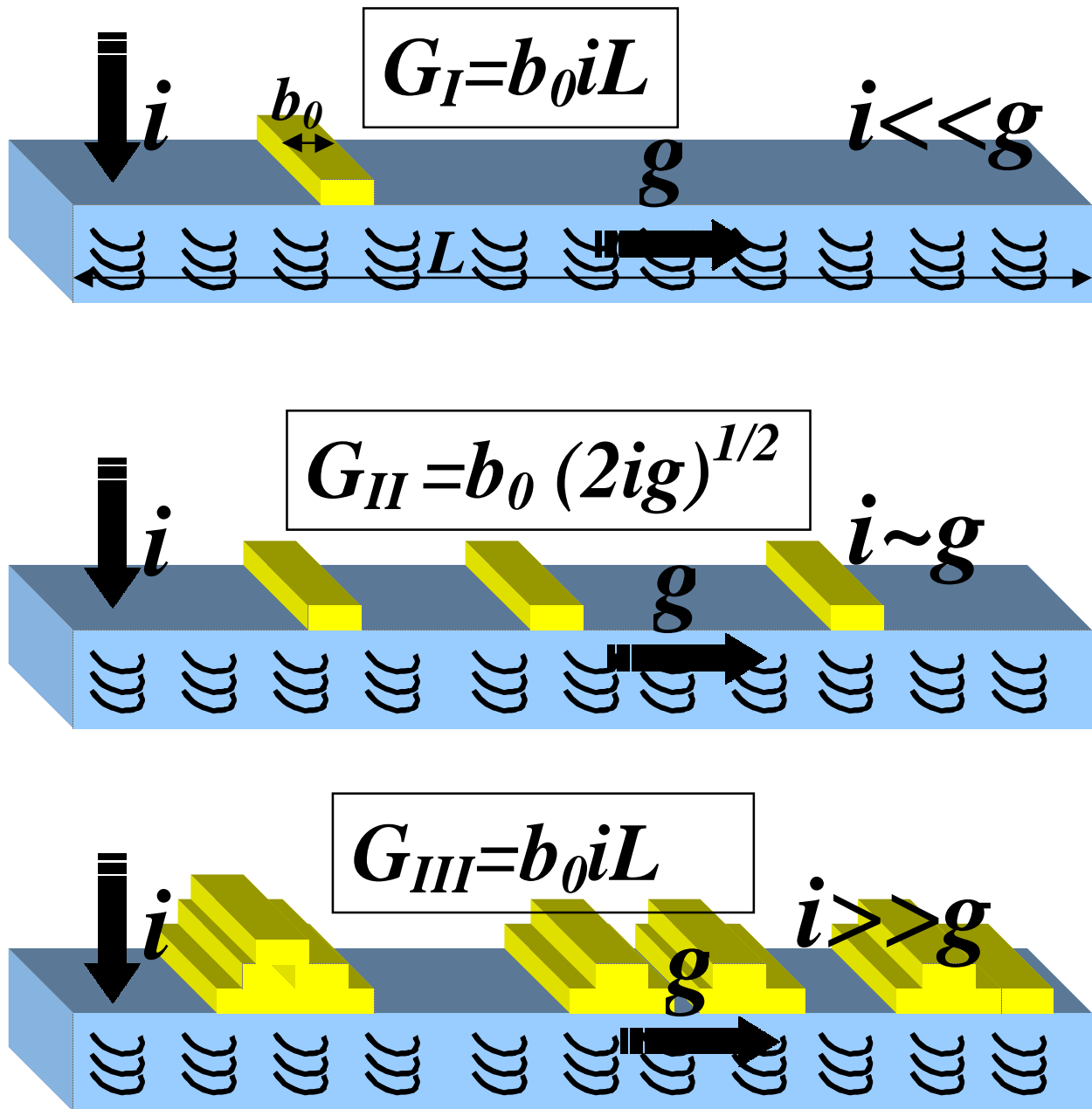


Figure 2.13 Scheme illustrating the rates of stem deposition during three different regimes of crystallization. ‘ i ’ represents the rate of stem nucleation whereas ‘ g ’ represents the rate of substrate completion.

As has been discussed before the parameter β in the above relations can be given by Vogel-Fulcher or Arrhenius type expressions. In the Arrhenius region, this factor can be described as:

$$\beta = J \exp \left[\frac{-U^*}{R(T-T_\infty)} \right] \quad \{2.39a\}$$

where U^* is the activation energy and J is a factor with some degree of temperature dependence. In the recent version of the theory³⁹ it is given as:

$$J = \frac{\kappa}{n} \left(\frac{kT}{h} \right) \quad \{2.39b\}$$

Here ' kT/h ' is the frequency factor in events per second and ' n ' is the number of repeat units. ' κ ' is a numerical constant which is evaluated from the monomeric friction coefficient. These equations when substituted in the relations shown in the schematic give the crystal growth rate ' G ' for the three different regimes as:

$$G_I = G_{0I} \exp (-U^*/R (T-T_\infty)) \exp (-K_{gI}/T\Delta T_c) \quad \{2.40a\}$$

$$G_{II} = G_{0II} \exp (-U^*/R (T-T_\infty)) \exp (-K_{gII}/T\Delta T_c) \quad \{2.40b\}$$

$$G_{III} = G_{0III} \exp (-U^*/R (T-T_\infty)) \exp (-K_{gIII}/T\Delta T_c) \quad \{2.40c\}$$

Where,

$$G_{0i} = \frac{N_0 b_0 J}{l_u} \left[\frac{kT}{b_0 \sigma} - \frac{kT}{2b_0 \sigma + a_0 b_0 \Delta G_f} \right] \quad \{2.41\}$$

$$K_{gI} = K_{gII} = 2K_{gIII} = \frac{4\sigma\sigma_e T_m}{k\Delta H_f} \quad \{2.42\}$$

The value of the nucleation constants K_{gI} , K_{gIII} , K_{gII} and G_{0i} can thus be determined by plotting the spherulitic growth rate data in the form $\ln G + U^*/R (T-T_\infty)$ vs. $1/T\Delta T_c$. These types of plots are usually referred to as L-H plots and Figure 2.13 illustrates the typical plots for polymers showing these transitions. The first exponential term in equation (2.40), $\exp (-U^*/R (T-T_\infty))$ accounts for the chain transport effects to the interface while the second term $\exp (-K_{gi}/T\Delta T_c)$, accounts for the secondary nucleation effects. The widely utilized values for U^* and T_∞ are 1500 cal/mol and T_g-30K for a

large number of polymers^{39,43}. L-H plots have also been widely utilized to obtain values for $\sigma\sigma_e$ if the values of T_m° , ΔH_f and b_0 are known^{40,58,59,60}, or otherwise sometimes to obtain T_m° ^{54,61,62}.

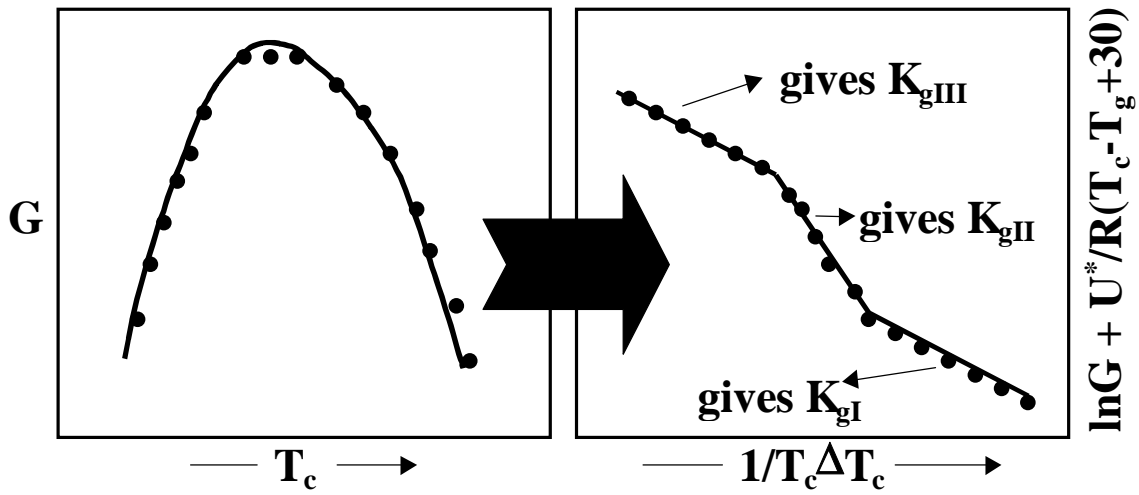


Figure 2.14 A schematic illustrating the conversion of growth rate data to a L-H plot showing the three regime transitions³⁸. The values of regime constants are calculated by the slope in various regimes and are used to give the product of surface energy terms $\sigma\sigma_e$. All three regimes or even a single regime transition may not be experimentally observed for many polymers.

2.9 Primary nucleation:

For polymer crystallization to start, the primary nucleation first needs to take place. The nucleation itself can be defined as formation of a small amount of crystalline material due to fluctuations in density or order in the supercooled melt⁶³. The formation of these initial or primary nuclei is the first step inaugurating crystallization and the phenomenon is called primary nucleation. The continuation of crystallization on the growth surface by induction of more and more polymer molecules is referred to as secondary nucleation and the previously discussed L-H theory addresses this issue. Another way of classifying nucleation is by invoking the prerequisite for the original site where the nucleation occurs. If no second surface or existing nuclei (i.e. any type of second phase) is present and the nuclei formation takes place spontaneously only due to supercooling the phenomenon is referred to as homogenous nucleation. However, if any second phase is required (it may be a foreign particle or surface from the same polymer nuclei/crystal), then the nucleation is termed heterogeneous nucleation. Wunderlich *et al.*⁵ based on an earlier work⁶⁴ have further advocated the subdivision of this classification by incorporating the third category called *self-nucleation*. This nucleation is due to preexisting/residual nuclei that survived the initial melt conditions (or the dissolution conditions if it is solution crystallization). Later studies covered in this report will show results, which indicate that this *self-nucleation* is very important with respect to understanding the melt crystallization behavior of semicrystalline polyimides, the subject of this study. It should be clear that while primary nucleation can be either homogenous or heterogeneous, secondary nucleation by its very definition is heterogeneous in origin. Yet another way of categorizing primary nucleation is on the basis of time dependent effects at any temperature. If the nucleation is such that all nuclei start forming at approximately the same time then the nucleation is referred to as *athermal* nucleation. One aspect of such nucleation is that it leads to spherulites of roughly the same size during isothermal crystallization. If the nucleation on the other hand is such that new nuclei form throughout the crystallization at a particular temperature, and thus different spherulitic (crystal) sizes are obtained than the nucleation is referred to as *thermal*

nucleation. It thus may not be difficult to visualize that homogenous nucleation is often of the thermal type (the converse is not true) whereas the heterogeneous nucleation may be thermal or athermal. In the case of self-nucleation, the nucleation type has generally been observed as athermal although work in the present project has confirmed that this is not a necessary condition.

For the formation of stable nuclei to take place (primary or secondary), the free energy barrier to crystallization needs to be overcome. The size of this critical nucleus required obviously depends upon this free energy barrier, larger critical nuclei requiring longer times to form. The concept is very similar to one discussed in L-H theory previously and is illustrated in Figure 2.14.

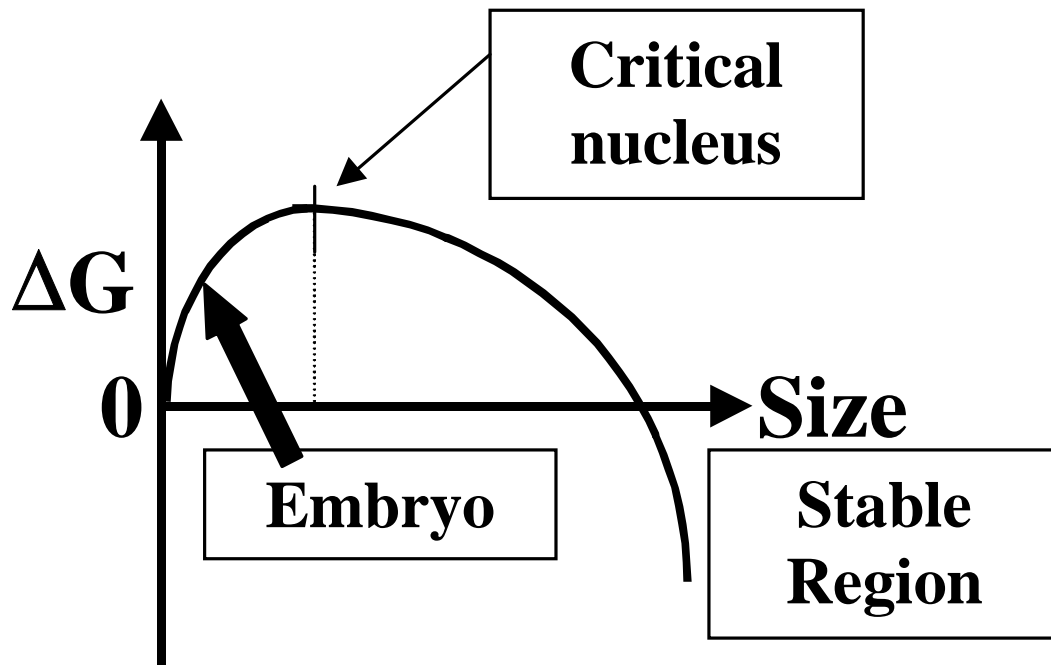


Figure 2.15 Schematic illustrating the variation of free energy with nucleus size. The initial free energy barrier needs to be crossed for the nucleus to become stable⁵.

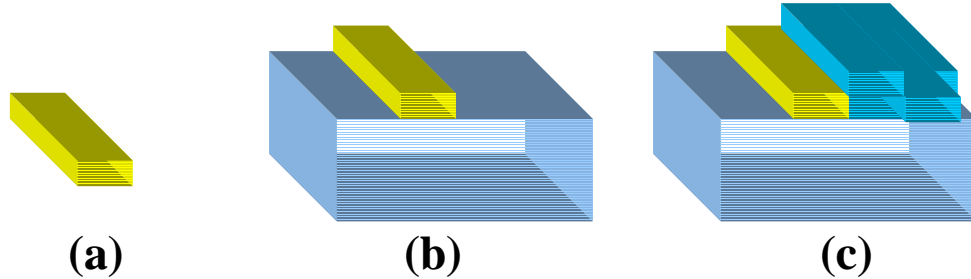


Figure 2.16 Types of Crystal Nuclei (a) Primary nucleus (b) Secondary Nucleus (c) Tertiary Nucleus

In any nucleation process, the free energy of the nucleation process (crystallization) is given by:

$$\Delta G = \Delta G_c + \sum \gamma^* A \quad \{2.43\}$$

where the specific surface free energy is given by γ^* . Primary nucleation involves the largest specific area while the area is somewhat reduced for secondary nucleation on the surface. Tertiary nucleation, which can be defined as nucleation at an edge, involves yet lesser specific area. Thus, in terms of difficulty of the nucleation process, it goes as⁵:

Primary nucleation > Secondary Nucleation > Tertiary Nucleation.

The large specific area to volume ratio of such entities offsets the decrease in free energy that can be obtained by crystallizing the small volume element of the nucleus. The fundamentals of such a nucleation process can be investigated by performing free energy calculations on the incipient nucleus. In this regard, for the general case of a spherical nucleus of radius 'r', the free energy change can be expressed as:

$$\Delta G = 4/3\pi r^3 \Delta G_c + 4\pi r^2 \gamma^* \quad \{2.44\}$$

These two opposing contributions to the free energy lead to an initial rise in ΔG till a certain critical maximum in free energy surface is reached at ' r^* ', beyond which there is a

precipitous drop in the free energy leading to formation of a stable nucleus. The critical point is found out by differentiating the above equation w.r.t. 'r' and equating it with zero. The values for such critical points thus obtained are²:

$$r = r^* = \frac{2\sigma}{\Delta G_c} = \frac{2\sigma T_m^{\circ}}{\Delta H_f \Delta T_c} \quad \{2.45\}$$

$$\Delta G = \Delta G^* = \frac{16\pi\sigma^3}{3\Delta G_c^2} = \frac{16\pi\sigma^3 T_m^{\circ 2}}{3\Delta H_f^2 \Delta T_c^2} \quad \{2.46\}$$

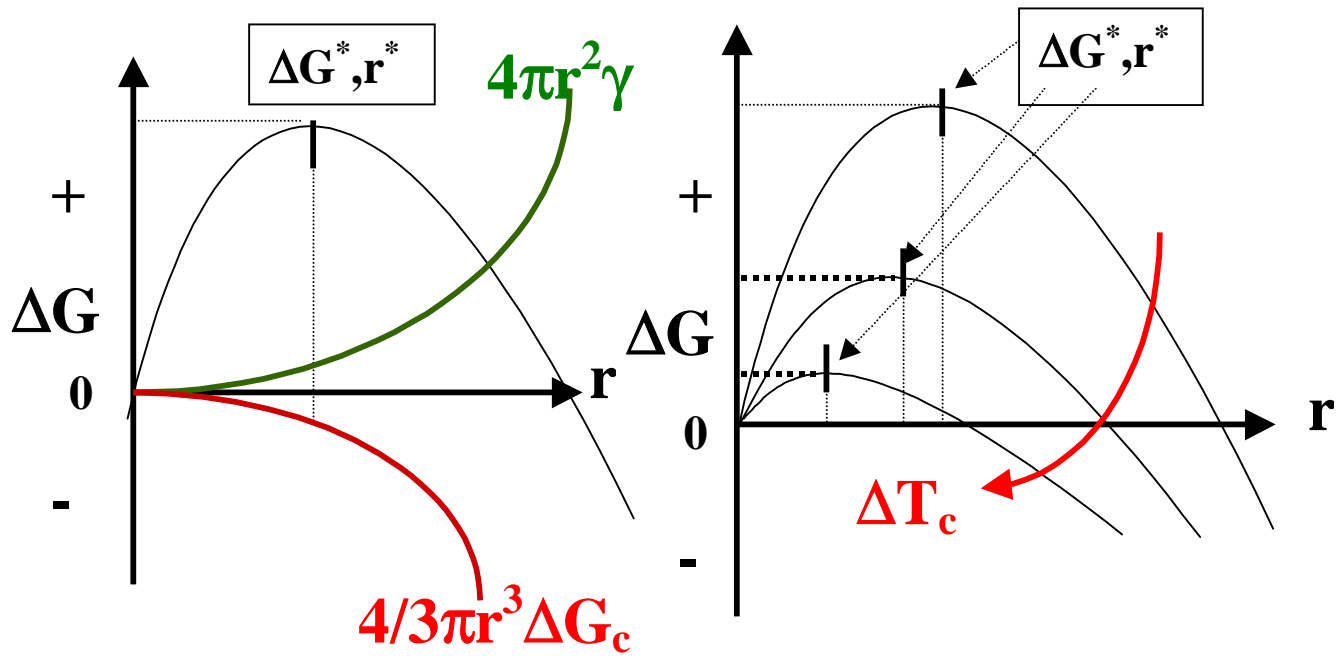


Figure 2.17 Variation of total free energy with size depends upon two opposing factors, the gain being due to increased surface area while the loss due to free energy of crystallization. Also, the critical size for stable nuclei formation as well as the critical free energy barrier decrease with increasing undercooling^{2,38}.

The critical size ' r^* ', and the critical free energy barrier are strongly dependent upon the undercooling ΔT_c . While $r^* \propto 1/\Delta T_c$, the free energy barrier $\Delta G^* \propto 1/\Delta T_c^2$. While the above analysis is for a spherical nuclei, the problems for other shapes such as cylindrical are more suited to polymeric nucleation and expressions for those can be similarly derived. It is very important to mention here that the shape of the nucleus will govern the final morphology of the crystallite, with the initial thickness of the crystallite being related to the critical size of the nucleus². Turnbull and Fisher gave the steady state rate of nucleation per unit volume and time on the basis of transition state theory as⁶⁵:

$$\dot{N} = N_0 \exp \left[-\frac{E_D + \Delta G^*}{RT} \right] \quad \{2.47\}$$

where $N_0 = n_1 kT/h$ is the number of molecules in a unit volume of the liquid. In this expression, ΔG^* is the activation energy derived above and E_D is akin to the free energy of activation for diffusion of chain segments to the phase boundary. The temperature dependence of the transport term E_D , is similar to that of viscosity with it remaining nearly constant at high temperatures and increasing rapidly at temperatures close to the glass transition. Till moderate undercoolings, the nucleation is dominated by the ΔG^* term which is $\propto 1/\Delta T_c^2$. Thus the nucleation rate is zero at T_m and has a large negative temperature coefficient just below T_m due to $\exp(-\Delta G^*/RT)$. At still larger undercoolings the influence of E_D term begins to increase and the nucleation rate reaches a maximum. At temperatures below the maximum, the nucleation rate is dominated by the transport term and has a large positive temperature coefficient with the rate falling to zero at temperatures below the glass transition. The above discussion can be applied with little modifications to heterogeneous nucleation with only the value of the constants varying². The important geometry's of the heterogeneous type nucleation to which this type of analysis can be applied are fringed micelle and folded chain type nuclei. It is also important to recognize that various facets of the nucleation theory predict the experimentally observed features like, the negative temperature coefficient, and the variation of critical nucleus size (and hence the crystallite thickness) with undercooling. These predictions, however, are based on the most general premises, and thus do not

depend on the form, structure or chain disposition within the nucleus. The application of nucleation theory to the chain folded nucleus (L-H treatment), on its own, is thus not the proof of chain folded crystallization being prevalent^{2,31,30}.

2.10 Spherulites

The existence of these large (i.e. micron level) three dimensional supramolecular structures usually possessing three dimensional symmetry is a common occurrence not only in polymers but also in a large variety of inorganic substances and metals^{66,67}. In fact, these kinds of structures have been found in rock specimens from the moon, which indicates that they grow during formation in rock strata⁶⁸! In the case of polymers, these types of structures are conveniently observed in polarized optical microscope and consist of radial fibrils originating from a primary nucleus at the center. The large varieties of such structures that have been experimentally observed prohibit a strict definition though some general features can be summarized. The spherical shape arises usually due to small angle branching and splaying microstructure⁶⁹. The initial stages of such a structure may not be spherical but rather may resemble a sheaf kind of morphology.

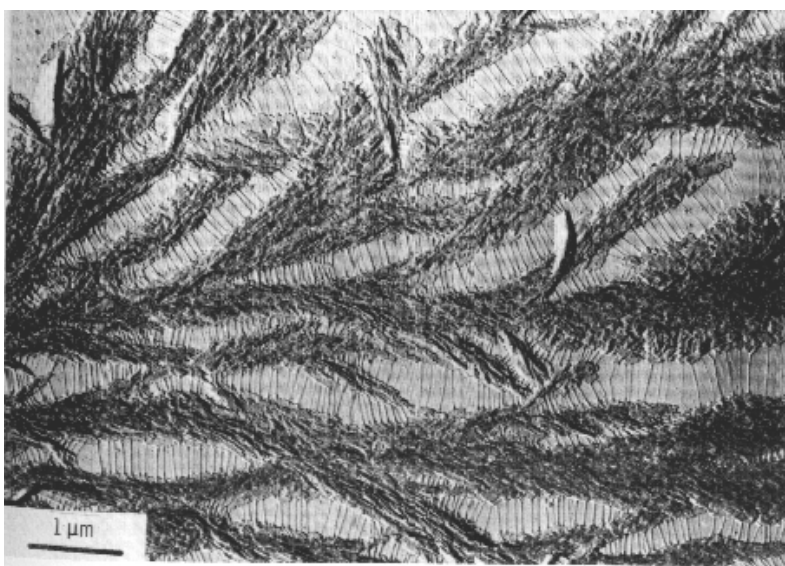


Figure 2.18 Tie chains in polyethylene spherulites crystallized in presence of n-paraffin, $C_{32}H_{66}$, and then extracted with xylene at room temperature. (Keith and Padden⁷⁰ et al.)

Although the radial equivalency of this structure is usually a good approximation, this may not be true for the central core and also when the overall morphology becomes very coarse. The fibrils consist of lamellae radiating outward with the chain folding direction generally being transverse to the growth direction. Tie chains between these lamellae play an important role in improving the mechanical properties with these bridging units being both interlamellar and interspherulitic in origin. These links (Figure 2.17 from Keith and Padden⁷⁰) help in maintaining the interlamellar connections when the polymer is drawn. On the basis of birefringence, the spherulites can be divided into the following categories⁷¹:

- (a) Negatively birefringent: These are the most prevalent types of spherulites present in polymeric materials and are characterized by their refractive index along the transverse direction being greater than along the growth direction⁷². This optical character is due to the chain direction on an average being in transverse direction, this being a result of chain disposition within a lamella and lamellar arrangement within a spherulite.
- (b) Positively Birefringent: These type of spherulites are observed when the refractive index along the radial direction exceeds that along the transverse direction. These types of spherulites are less common as the polarizability along the chain direction usually exceeds than along the other two principal directions. Such spherulites have been observed for polymers that have strong dipoles at large angle to the chain backbone and also exhibit chain tilt with respect to the growth direction.
- (c) Zero birefringence: These type of spherulites are sometimes when the optic axis of the spherulites is aligned parallel to the viewing direction⁷³. Random distribution of crystallites within the spherulite may also lead to such a structure.
- (d) Chain-extended spherulites: These type have been observed during high pressure crystallization of polyethylene⁷⁴.

It has been traditionally believed⁷⁵ that smaller spherulitic sizes result in better impact strength and higher elongation to break. However, experimental studies supporting such conclusions continue to be scarce. Sharples⁷⁶ observed that the yield stress in Nylon 66 samples increased by 30% as the spherulitic size was decreased from 50 microns to 3 microns. Kargin *et al*⁷⁷. demonstrated over a wide range of spherulitic sizes that the

mechanical properties deteriorated by 2-3 times whereas the elongation to break decreased from 500% to 25% as the spherulitic sizes were increased. Way *et al*⁷⁸. showed that the yield stress of isotactic polypropylene goes through a maximum and then drops precipitously as the average spherulitic size was increased. This transition was concluded as being a result of deformation mechanism shifting from intraspherulitic yield to interspherulitic yield. Reinshagen⁷⁹ observed that isotactic polypropylene samples prepared under lower undercooling gave brittle interspherulitic fracture whereas samples prepared under larger undercoolings showed strain whitening and yielding before fracture.

2.11 Bulk crystallization kinetics-avrami analysis

Avrami Analysis^{80,2,5} continues to remain the most popular method for obtaining bulk crystallization kinetics information. Its widespread use to obtain quantitative bulk crystallization kinetics knowledge is in part due to the relative ease with which the analysis can be applied. Unfortunately, this method has often been utilized without recognizing the assumptions and limitations of such an analysis, resulting in wrongful interpretations of experimental data. Before applying this analysis and correctly interpreting the data, it is important to understand the grounds on which this procedure was derived and the recognition of the assumptions that are involved. The mathematical foundation of this analysis is based on the famous raindrop problem first solved by Poisson⁸¹ in 1837, which states that for raindrops falling randomly, the probability of a point being passed over by exactly F wavefronts is given by

$$P(F) = \frac{e^{-\bar{F}} \bar{F}^F}{F!} \quad \{2.48\}$$

where \bar{F} is the average number of such wavefronts passing through a point. Thus considering these wavefronts as spherulites in bulk crystallization, the probability of any point not being run over by a spherulite is given by value of P(F) at F=0. Thus

$$P(0) = e^{-\bar{F}} \quad \{2.49\}$$

$P(0)$ also represents the points which are still amorphous and not been run over by the spherulites and thus is equal to amorphous fraction $1-\theta$, where θ is the amount of fraction crystallized.

$$\begin{aligned} 1-\theta &= P(0) = e^{-\bar{F}} \\ \Rightarrow \ln \frac{1}{1-\theta} &= \bar{F} \\ \Rightarrow \theta &= 1 - \exp(-\bar{F}) \end{aligned} \quad \{2.50\}$$

Now the problem reduces to obtaining the form of the function \bar{F} for different types of geometries that may be involved. The time dependency of the crystalline fraction in the above analysis enters due to time dependency of the function \bar{F} , the average number of wavefronts passing in time 't'. For some particular cases, this function can be calculated to give the following relations^{5,82}:

(a) 2-dimensional case of growing discs starting at the same time

$$\bar{F} = \pi G^2 N t^2 \quad \{2.51\}$$

where G is the growth rate of growing discs, N is the average number of such discs/area and t is the elapsed time.

(b) 2-dimensional case of growing discs forming at a rate \dot{N}

$$\bar{F} = \frac{\pi}{3} G^2 \dot{N} t^3 \quad \{2.52\}$$

(c) 3-dimensional case of growing spheres starting at the same time

$$\bar{F} = \frac{4}{3} \pi G^3 N t^3 \quad \{2.53\}$$

(d) 3-dimensional case of growing spheres forming at a rate \dot{N}

$$\bar{F} = \frac{\pi}{3} G^3 \dot{N} t^4 \quad \{2.54\}$$

In general then, the form of the equation is of the type

$$\boxed{\theta = 1 - \exp(-K t^n)} \quad \{2.55\}$$

which is the famous Avrami equation and the 'K' & 'n' are the two Avrami parameters usually referred to as the bulk crystallization constant (K) and Avrami exponent (n). As should be clear from the above analysis, 'K' is dependent on the *shape* of the growing crystalline entities and the *amount* and *type* of nucleation. The exponent 'n' is dependent

upon the nucleation *type* and growth *geometry* but not on the amount of nucleation. In the cases illustrated above it was tacitly assumed that the nucleation at the growth surface of the growing discs or spheres was the only governing factor in maintaining the growth rate G . In many instances, transport factors (like transport of heat of crystallization or transport of crystallizable molecules to the interface) become rate determining in controlling the rate of growth. These kind of problems involve a moving interface across which the transport phenomenon need to be considered and are usually referred to as Stefan problems⁸³ who applied it to study the thickness of polar ice caps. An example of this in polymers is the transcrystallization where nucleation is not the rate-determining factor. The solution to these kinds of problems is usually of the type^{5,82}

$$G = \left[\frac{2\kappa}{t} \right]^{1/2} \quad \{2.56\}$$

where κ is the diffusion constant. Thus the exponent of the time decreases by $\times 0.5$ for G^r present in the equation if the rate-determining step is transport/diffusion controlled. The various Avrami exponents associated with different nucleation types and crystal geometry's are shown in table 2.

Table 2.2. Avrami exponents for various types of crystal growth geometry's⁸².

Avrami Exponent	Crystal Geometry	Nucleation Type	Rate Determination
0.5	Rod	Athermal	Diffusion
1	Rod	Athermal	Nucleation
1.5	Rod	Thermal	Diffusion
2	Rod	Thermal	Nucleation
1	Disc	Athermal	Diffusion
2	Disc	Athermal	Nucleation
2	Disc	Thermal	Diffusion
3	Disc	Thermal	Nucleation
1.5	Sphere	Athermal	Diffusion
2.5	Sphere	Thermal	Diffusion
3	Sphere	Athermal	Nucleation
4	Sphere	Thermal	Nucleation

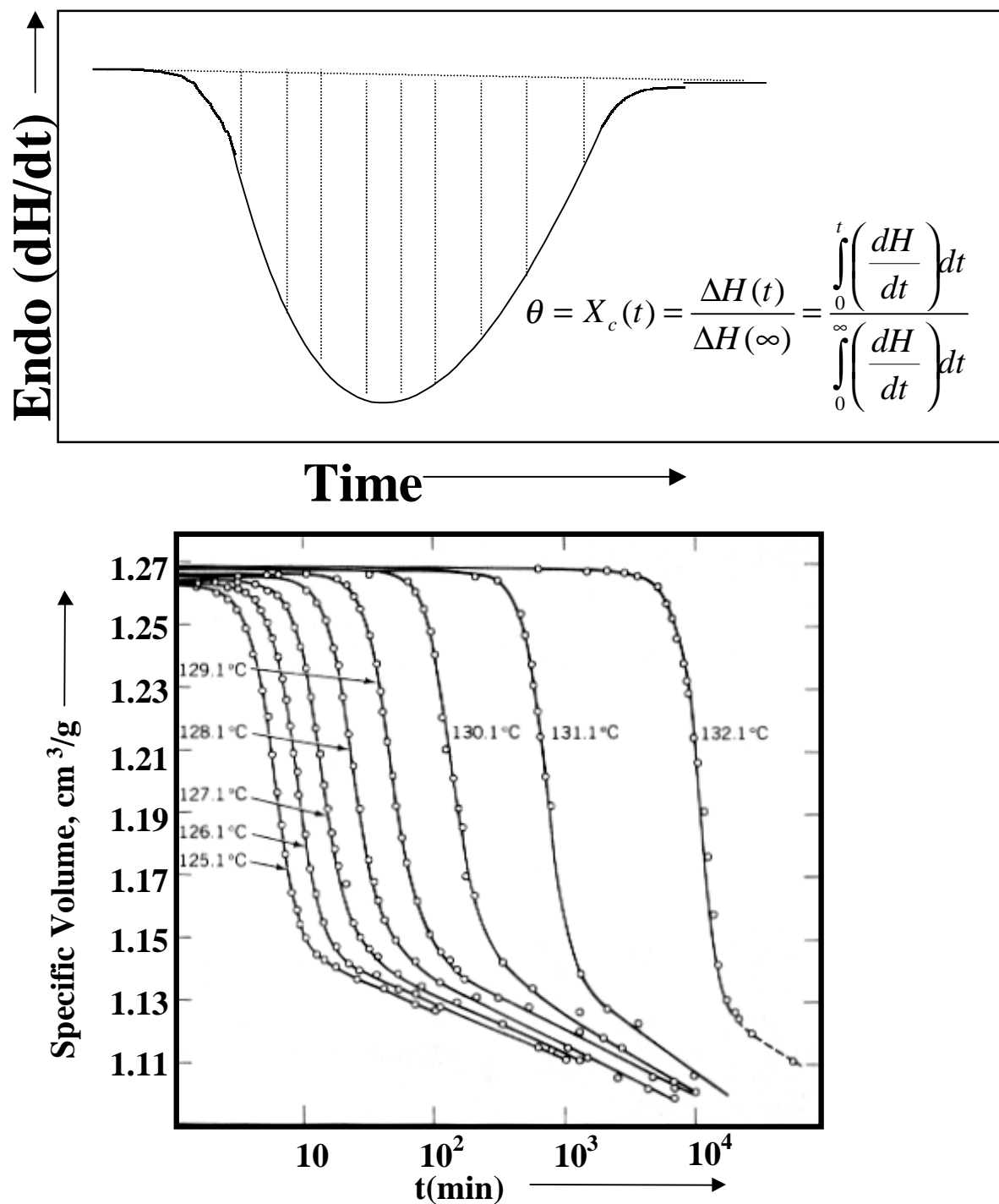


Figure 2.19 Utilization of isothermal crystallization data by either DSC or by volume³⁰ measurements can give the degree of transformation, which can subsequently be utilized for Avrami analysis.

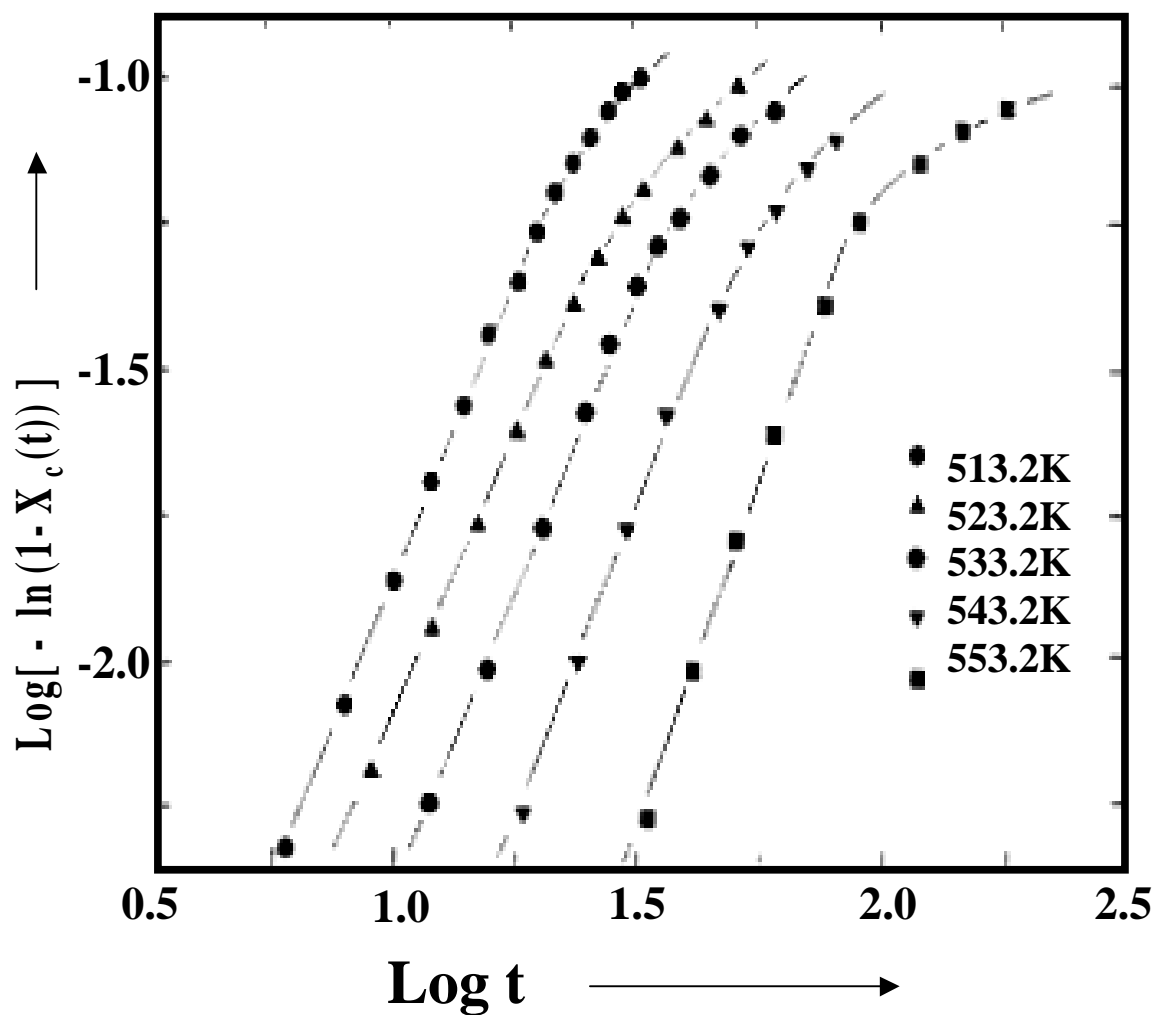


Figure 2.20 The characteristic Avrami plots obtained by isothermal crystallization experiments for a polyimide⁸⁴. The initial slope of the curves gives the Avrami constant 'n', which is related to the crystal shape and nucleation type.

The traditionally utilized methods for measuring the crystalline fraction θ , have been the volume measurements and DSC in which the fraction θ is given respectively as:

$$\text{Volume measurements:} \quad \theta = \frac{V_t - V_0}{V_\infty - V_0} \quad \{2.57\}$$

$$\text{DSC measurements} \quad \theta = \frac{\Delta H(t)}{\Delta H(\infty)} \quad \{2.58\}$$

Where the V_t, V_0 and V_∞ represent the sample volume at time t , $t=0$ and at infinite time respectively. $\Delta H(t)$ and $\Delta H(\infty)$ represent the heat of crystallization obtained at time t and after infinite time. Figure 2.18(a) and Figure 2.18(b) illustrate the type of data obtained by the calorimetric and volumetric techniques and Figure 2.19⁸⁴ illustrates the conversion of such a data to give the characteristic Avrami plot. The Avrami equation (2.55) is analyzed by taking the double logarithm and writing in the form:

$$\text{Log}[-\ln(1-\theta)] = \text{Log}K + n\text{Log}t \quad \{2.59\}$$

The crystalline fraction θ , is plotted in the form $\text{Log}[-\ln(1-\theta)]$ vs. $\text{Log}(t)$ to yield the characteristic Avrami plot. The initial slope of this plot (such as the one shown in Figure 2.19) gives the Avrami constant 'n'. The value of K is usually obtained by using the value of θ at $t=t_{1/2}$ and substituting in equation (2.56). With little effort, equation (2.56) yields:

$$K = \frac{\ln 2}{t_{1/2}^n} \quad \{2.60\}$$

However before these techniques are utilized and interpretations regarding the crystallization kinetics made with the values of 'K' and 'n', it is important to recognize the inherent problems in Avrami analysis. The problems with the basic Avrami Analysis are^{85,86,87,88}:

- (a) The Avrami equation rigorously applies only to problems where the volume does not change. This is never the case with crystallization in polymers.

- (b) It assumes constancy in the shape of growing disc/rod/sphere
- (c) Constant radial growth is assumed ($G \sim t^{-1/2}$ has also been considered)
- (d) The analysis does not account for the presence of an induction time
- (e) The nucleation mode is assumed to be unique i.e. thermal or athermal but not both
- (f) Complete crystallinity of the sample
- (g) Random distribution of nuclei
- (h) Constant value of radial density in the growing structures which is assumed in the derivation does not usually occur experimentally
- (i) Holds well for primary crystallization only
- (j) Does not account for absence of overlap between growing crystallization fronts

It is thus not surprising that non-integer values of n are often obtained. As shown in Table 2, it is not difficult to assign the experimentally obtained value of n by selecting an appropriate geometry. This kind of attribution of the exponent 'n', without independent microscopical evidence is one of the major pitfalls of most studies in the literature utilizing this analysis. *Independent microscopical evidence is critical before assignment of 'n' to a particular geometry can be justified.*

References:

-
- ¹ Cebe, P. and Hong, S.D., *Polymer*, 1986, **27**, 1183.
 - ² Mandelkern, L. *Crystallization of Polymers*, McGraw-Hill, New York, 1964.
 - ³ Stejny, J., Dlugosz, J., and Keller A., *J. Mater. Sci.*, pg. 1291, Vol. 14, 1977.
 - ⁴ Wegner, G., Organization of the Macromolecules in the condensed Phase, pg. 494, *Faraday Discussions of the Royal Society of Chemistry*, n68, 1979.
 - ⁵ Wunderlich, B., *Macromolecular Physics*, Vol. 2, Crystal Nucleation, Growth, Annealing, Academic Press, New York, 1976.
 - ⁶ Chanzy, H., quoted in *Treatise on Materials Science and Technology*, Vol. 10, Part A, Ed. Schultz, J.M., 1977.
 - ⁷ Pennings, A.J., "Crystal Growth", pg 389, Pergamon, Oxford, 1967.

-
- ⁸ Pennings, A.J. and Kiel, A.M. *Kolloid Z.* 1965, **205**, 160
- ⁹ Pennings, A.J. and Pijpers, M.F.J. *Macromolecules* 1970, **3**, 261.
- ¹⁰ Keller, A., Organization of the Macromolecules in the condensed Phase, pg145, *Faraday Discussions of the Royal Society of Chemistry*, n68, 1979.
- ¹¹ Andrews, A.H., *Proceedings of the Royal Society (London)*, A270, 232, 1962.
- ¹² Kobayashi, T. and Broutman, L.J., *Polym. Eng. Sci.* , 14, 260, 1974.
- ¹³ Lindenmayer, P.H., *Molecular Composites: The future high performance plastics*. NSF August Rep., Washington D.C., 1974.
- ¹⁴ McHugh, A.J., and Forest, E.H., *J. Macromol. Sci. Phys.* B11, 219, 1975.
- ¹⁵ Herman, K., Gerngross, O. and Abitz, W. *Z. Phys. Chem.* 1930, **B10**, 371.
- ¹⁶ Flory, P.J. *J. Chem. Phys.* 1949, **17**, 223.
- ¹⁷ Flory, P.J. *J. Amer. Chem. Soc.* 1962, 84, 2857.
- ¹⁸ Yoon, D.Y. and Flory, P.J. Organization of the Macromolecules in the condensed Phase, pg. 288, *Faraday Discussions of the Royal Society of Chemistry*, n68, 1979.
- ¹⁹ Geil, P.H. in *Polymer Single Crystals*, 1963, John Wiley & Sons, New York, pg 9.
- ²⁰ Keller, A. *J. Polym. Sci.* 1955, **17**, 351.
- ²¹ Girolamo, M., Keller, A., Miyasaka, K.K. and Overbergh, N. *J. Polym. Sci. Part B*, 1976, **14**, 39.
- ²² Benson, R., Maxfield, J., Axelson, D.E. and Mandelkern, L. *J. Polym. Sci. Part B*, 1978, **19**, 1583.
- ²³ Storcks, K.H. *J. Am. Chem. Soc.* 1938, **60**, 1753.
- ²⁴ Schlesinger, W. and Leeper, H.M. *J. Polym. Sci.* 1953, **11**, 203.
- ²⁵ Jaccodine, R. *Nature* 1955, **176**, 305.
- ²⁶ Till, P.H. *J. Polym. Sci.* 1957, **24**, 301.
- ²⁷ Keller, A. *Phil. Mag.* 1957, **2**, 1171.
- ²⁸ Fischer, E.W. *Z. Naturforsch.* 1957, **12a**, 753.
- ²⁹ Flory, P.J. in *Structural Orders in Polymers* Ed. Ciardelli, F. and Gusti, P. 1981 Permagon Press, New York.
- ³⁰ Mandelkern, L. in *Characterization of Materials in Research: Ceramics and Polymers*, Syracuse Univ. Press, Syracuse, New York, 1975, pg. 369.

-
- ³¹ Mandelkern, L., Organization of the Macromolecules in the condensed Phase, *Faraday Discussions of the Royal Society of Chemistry*, n68, 1979, 310.
- ³² Hoffman, J.D. and Lauritzen, J.I., Jr. *J. Research NBS*, 1961, **65A**, 297.
- ³³ Hoffman, J.D. *SPE Transactions*, Oct 1964, 315.
- ³⁴ Fischer, E.W. *Pure Appl. Chem.* 1978, **50**, 1319.
- ³⁵ Fischer, E.W. Stamm, M., Dettenmair, M. and Herchenroder, P. *ACS Pol. Prepr.* 1979, **20**, 1, 219.
- ³⁶ Fischer, E.W. Stamm, M. and Dettenmair, M. Organization of the Macromolecules in the condensed Phase, *Faraday Discussions of the Royal Society of Chemistry*, n68, 1979, 263.
- ³⁷ Class Notes- “Physical Chemistry of Polymers”, H. Marand, Virginia Tech, 1998.
- ³⁸ Class Notes- “Polymer Morphology”, G.L. Wilkes, Virginia Tech, 1997.
- ³⁹ Hoffman, J.D. and Miller, R.L. *Polymer* 1997, **38**, 3151.
- ⁴⁰ Marand, H and Hoffman, J.D. *Macromolecules* 1990, **23**, 3682.
- ⁴¹ Wunderlich, B., *Macromolecular Physics, Vol. 3, Crystal Melting*, Academic Press, New York, 1980.
- ⁴² Marand, H., Xu, J. and Srinivas, S. *Macromolecules* 1998, *in print*.
- ⁴³ Hoffman, J.D., Davis, G.T. and Lauritzen, J.I. *Treatise on Solid State Chemistry*, Ed. Hannay, N.B., Plenum Press, New York, 1976, Vol. **3**, Chapter 7.
- ⁴⁴ Hoffman, J.D. and Miller, R.L. *Macromolecules* 1988, **21**, 3038.
- ⁴⁵ Hoffman, J.D. and Miller, R.L., Marand, H. and Roitman, D.B.. *Macromolecules* 1992, **25**, 2221.
- ⁴⁶ Hoffman, J.D., *Polymer* 1991, **32**, 2828.
- ⁴⁷ Mansfield, M.L. *J. Phys. Chem.* 1990, **94**, 6144.
- ⁴⁸ Lovinger, A.J. and Davis, D.D. *J. Appl. Phys.* 1985, **58**, 2843.
- ⁴⁹ Frank, F.C. and Tosi, M. *Proc. R. Soc. London, Ser A.*, 1961, **263**, 323.
- ⁵⁰ Snyder, C.R. and Marand, H. *Macromolecules* 1997, **30**, 2759.
- ⁵¹ Snyder, C.R., Mansfield, M.L. and Marand, H. *Macromolecules* 1996, **29**, 7508.

-
- ⁵² DiMarzio, E.A., Guttman, C.M., Hoffman, J.D. Organization of the Macromolecules in the condensed Phase, *Faraday Discussions of the Royal Society of Chemistry*, n68, 1979, 210.
- ⁵³ Hoffman, J.D. and Lauritzen, J.I., Jr. *J. Appl. Phys.*, 1973, **44**, 4340.
- ⁵⁴ Xu, J., Srinivas, S. and Marand, H. *Macromolecules*, 1998, *in print*.
- ⁵⁵ Hoffman, J.D., Frolen, L.J., Ross, G.S. and Lauritzen, J.I., Jr. *J. Research NBS Sect. A* 1975, **79**, 671.
- ⁵⁶ Hoffman, J.D., Guttman, C.M. and Di Marzio, E.A. Organization of the Macromolecules in the condensed Phase, *Faraday Discussions of the Royal Society of Chemistry*, n68, 1979, 177.
- ⁵⁷ Hoffman, J.D., *Polymer* 1983, **24**, 3.
- ⁵⁸ Allen, R.C. and Mandelkern, L. *Polym. Bull.* 1987, **17**, 473.
- ⁵⁹ Fatou, J.G., Marco, C. and Mandelkern, L. *Polymer* 1990, **31**, 890.
- ⁶⁰ Heberer, D.P., Cheng, S.Z.D., Barley, J.S., Lien, S.H.S., Bryant, R.G. and Harris, F.W. *Macromolecules*, 1991, **24**, 1890.
- ⁶¹ Huang, J. and Marand, H. *Macromolecules*, 1997, **30**, 1069.
- ⁶² Huang, J., Prasad, A. and Marand, H. *Polymer*, 1994, **35**, 1896.
- ⁶³ Gibbs, J.W. in On the equilibrium of heterogeneous substances. *Trans. Conn. Acad.* **III**, 343. Also, “*The scientific works of J. Willard Gibbs*,” Vol. **I**, 1906, Longmans, Green, New York, pg. 219
- ⁶⁴ Blundell, D.J., Keller, A. and Kovacs, A.J. *J. Polym. Sci. Part B*, 1966, **4**, 481.
- ⁶⁵ Turnbull, D. and Fisher, J.C. *J. Chem. Phys.* 1949, **17**, 71.
- ⁶⁶ Keith, H.D. and Padden, F.J., Jr. *J. Appl. Phys.* 1964, **35**, 1270.
- ⁶⁷ Marentette, J.M. and Brown, G.R. *J. Chem. Edu.* 1993, **70**, 435.
- ⁶⁸ Lofgren, G. *J. Geophys. Res.* 1971, **76**, 5635.
- ⁶⁹ Price, F.P. *J. Polym. Sci.* 1959 **37**, 71.
- ⁷⁰ Keith, H.D., Padden, F.J., Jr. and Vadimisky, R.G. *J. Polym. Sci. Part A-2* 1966, **4**, 267.
- ⁷¹ Magill, J.H. in *Treatise on Materials Science and Technology* Ed. Schultz, J.M. 1977, **10**, 3.

-
- ⁷² Keith, H.D. and Padden, F.J. *J. Polym. Sci.* 1959, **39**, 101.
- ⁷³ Magill, J.H. *J. Poly. Sci. Part A* 1966, **4**, 243.
- ⁷⁴ Basett, D.C. and Turner, B. *Phil. Mag.* 1974, **29**, 285.
- ⁷⁵ Lane, J.E. *Brit. Plast.* 1966, **39**, 528.
- ⁷⁶ Sharples, A. *Introduction on Polymer Crystallization*, Arnold, London, 1966.
- ⁷⁷ Kargin, V.A., Sogolova, T.I. and Nadareishvili, L.I. *Polym. Sci. USSR* 1964, **6**, 1404.
- ⁷⁸ Way, J.L., Atkinson, J.R. and Nutting, J. *J. Mater. Sci.* 1974, **9**, 293.
- ⁷⁹ Reinshagen, J.H. and Dunlap, R.W. *J. Appl. Polym. Sci.* 1975, **17**, 3619.
- ⁸⁰ Avrami, M. *J. Chem. Phys.* 1939, **7**, 1103.
- ⁸¹ Poisson, S.D. “*Recherches sur la Probabilite des Jugements en matieres criminelle et en matiere civile*” Bachelier, Paris, pg. 206.
- ⁸² Hiemenz, P.C. *Polymer Chemistry: The Basic Concepts* Marcel Dekker, New York, 1984, pg. 219.
- ⁸³ Stefan, J. *Ann. Phys. Chem.* 1891, **42**, 269.
- ⁸⁴ Heberer, D.P., Cheng, S.Z.D., Barley, J.S., Lien, S.H.S., Bryant, R.G. and Harris, F.W. *Macromolecules* 1991, **24**, 1890.
- ⁸⁵ Price, F.P. *J. Appl. Phys.* 1965, **36**, 3014.
- ⁸⁶ Grenier, D. and Homme, R.E.P. *J. Poly. Sci. Part B* 1980, **18**, 1655.
- ⁸⁷ Tomka, J. *Eur. Poly. J.* 1968, **4**, 237.
- ⁸⁸ Hillier, I.H. *J. Poly. Sci. Part A* 1965, **3**, 3067.

Chapter 3

Semi-Flexible Semicrystalline Polyimides- Literature Review

3.1 Introduction

The prime objective of this research is to develop and characterize high temperature and high performance thermoplastic semicrystalline polyimides. Although strong arguments for such a research project would be presented in the proposal section of this report, this section will focus on the literature review of studies on this class of materials. The following section reviews the work in this area from the perspective of goals for this study. In this regard, this review will first focus on the crystallization ability of the various semicrystalline polyimides reported in literature. A special focus will be on the ability of these materials to crystallize from the melt. Thermal stability of various polyimides, with respect to the recrystallization from various melt conditions will be discussed. The review will also address the morphology of these systems and both microscopic and SAXS information will be reviewed. Crystallization kinetics of such melt processable polymers is extremely important from both a practical and fundamental standpoint and results in the literature will be discussed in this regard. Another important feature frequently exhibited by these polymers is the multiple melting behavior. The possible explanations of this phenomenon put forward in the literature will be highlighted. Lastly, results dealing with rheological and physical properties of this class of materials will be reviewed.

3.2 Crystallization behavior from the melt

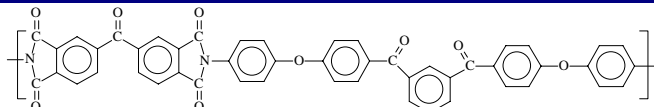
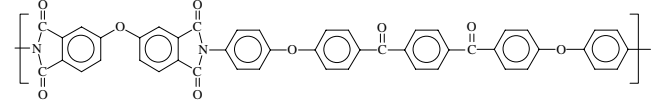
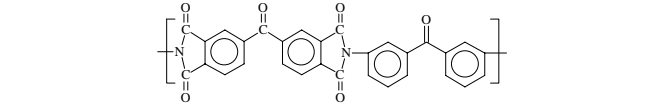
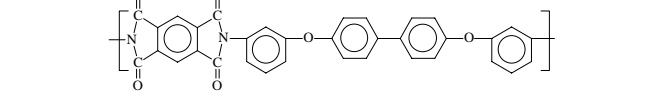
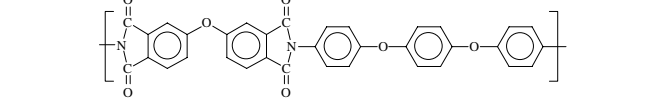
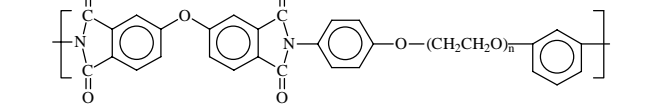
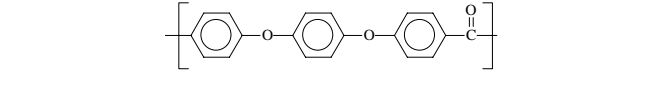
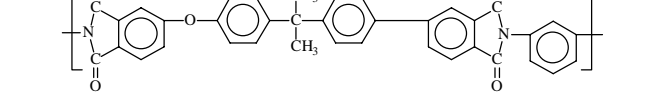
Although many crystalline polyimides have been reported in literature^{1,2,3,4,5,6}, the studies dealing with melt crystallization of these systems are scarce. As discussed in Chapter 1, polyimides with the appropriate chain structure will crystallize during the imidization process. It is however important to recognize that imidization of poly (amic acids) takes place in the presence of polar aprotic solvents and thus the initial processes of imidization and crystallization take place simultaneously. The initial crystallization is thus solvent aided and starts taking place before the chain attains its full rigidity. For crystallization from the melt however, the inherent crystallizability of the semi-flexible chain itself is important. Most initially semicrystalline polyimides lack this inherent crystallizability. The second important factor is the very high melting point ($>350^{\circ}\text{C}$) usually associated with such systems. At these temperatures, the possibility of degradation reactions leads to material being susceptible to crosslinking, chain scission and branching reactions. These degradation mechanisms, if they occur, will also lead to decreasing recrystallization ability. Of the several such systems discovered, New-TPI^{7,8,9} (New-Thermoplastic Polyimide) originally developed and licensed by Mitsui Toatsu Chemicals, has probably been the most popular system in attracting the attention of several research groups^{10,11,12,13}. Before New-TPI though, several other systems which showed varying degree of promise were developed by workers at NASA, many of them later being characterized in this laboratory. These were LaRC-CPI^{3,14,15} (Langley research center-crystalline polyimide), LaRC-CPI-2^{16,17} (second generation) and LaRC-TPI¹⁸. Another system investigated in this laboratory later was TPEQ-ODPA¹⁹. The structures of these polyimides and their glass transitions and melting points are shown in Table 3.1^{3,7,16,19,4}. It is important to mention that for each of these polyimides, there were several different grades that essentially differed in their molecular weight or sometimes the nature of the endcapping. The crystallizability of the different grades is different.

Most of these polyimides display the essential characteristics of T_g ($>200^{\circ}\text{C}$) and high T_m 's ($>350^{\circ}\text{C}$) and thus are candidates for high temperature and high performance applications from this standpoint. The desired recrystallization ability from the melt of these materials, however, is not like a typical thermoplastic. Figure 3.1 shows the

second heat DSC scans for different grades of LaRC-CPI³ after quenching from the melt. The lowest molecular weight 'A' is the only version showing the ability to crystallize after having been taken once to melt conditions. It is clear that the higher molecular grade labeled 'B' shows a much more sluggish crystallization behavior with the highest molecular weight versions (C&D) showing no crystallization ability. Similar behavior is also observed for LaRC-CPI-2¹⁶ in Figure 3.1 (first heat scans) which shows that higher molecular weight samples (lower offset) show significantly decreased ability to crystallize. LaRC-CPI-2¹⁶ also exhibits dual melting behavior with additional annealing being necessary to eliminate the lower melting form. While lower molecular weights increase the crystallization ability to some extent, they also lead to poorer mechanical properties (LaRC-CPI-2 films also show low elongation to break of less than 5%).

Figure 3.1 shows the first heat scans and subsequent heating scans at different heating rates for the TPEQ-ODPA¹⁹ polyimide. While the polymer exhibits crystallinity in the initial sample, the recrystallization ability decreases markedly once the polymer is taken to melt. Slower heating rates only seem to have a limited impact in improving the crystallinity and longer annealing times are required to induce crystallinity in the material. From the crystallization ability viewpoint, a superior behavior is exhibited by New-TPI⁹, probably the only semicrystalline polyimide successful in achieving wide attention from different academic and industrial research groups and also successfully commercial today. Figure 3.2 shows the second heat DSC scans for both a higher molecular weight (HV) and lower molecular weight (LV) versions⁹ after quenching from melt conditions. Both versions show stability of the melting point although the amount of crystallinity decreases substantially for the higher molecular weight version after the first heat. The lower molecular weight version seems to show slower crystallization kinetics from the melt with a significant crystallization occurring only during the heating scan from the room temperature. Also, for the lower viscosity samples it was found that isothermal crystallization at temperatures lower than 350°C was successful in inducing crystallinity and thus eliminated crystallization exotherms during heating.

Table 3.1 Chemical structures and T_g 's and T_m 's of various semicrystalline polyimides. The structures and values for ULTEM, an amorphous polyetherimide, and PEEK are also shown.

Chemical Structure	Name	$T_g(^{\circ}\text{C})$	$T_m(^{\circ}\text{C})$
	LaRC-CPI	220	360
	LaRC-CPI-2	217	334 & 364
	LaRC-TPI	240	330-350
	New-TPI	250	385
	TPEQ-OPDA	238	420
	Ethylene Glycol based diamine- ODPA	112 n=3 145 n=2 177 n=1	268 n=3 304 n=2 340 n=1
	PEEK	143	334
	Ultem®-PEI	215	ND

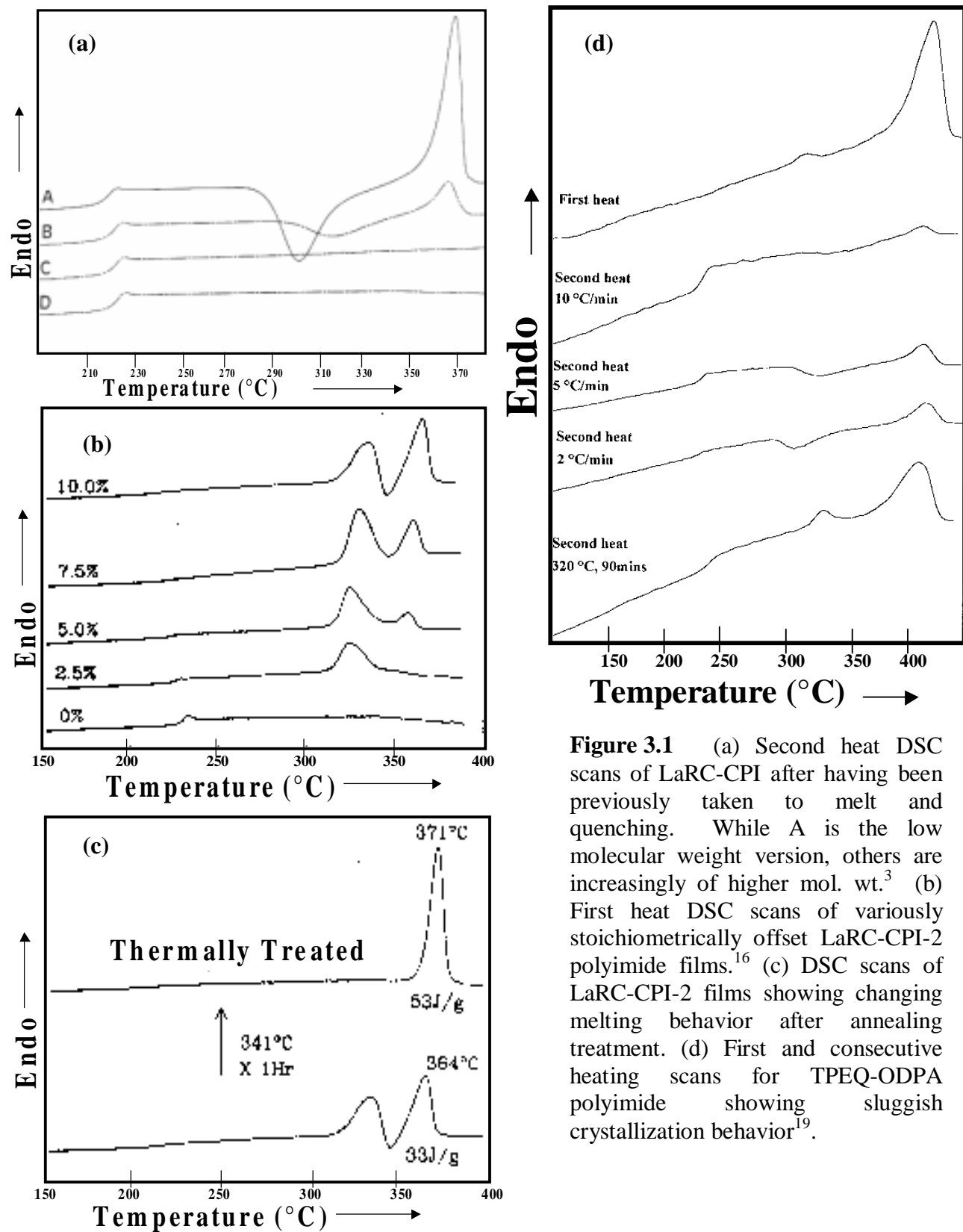


Figure 3.1 (a) Second heat DSC scans of LaRC-CPI after having been previously taken to melt and quenching. While A is the low molecular weight version, others are increasingly of higher mol. wt.³ (b) First heat DSC scans of variously stoichiometrically offset LaRC-CPI-2 polyimide films.¹⁶ (c) DSC scans of LaRC-CPI-2 films showing changing melting behavior after annealing treatment. (d) First and consecutive heating scans for TPEQ-ODPA polyimide showing sluggish crystallization behavior¹⁹.

While these results were promising, work conducted at different melt temperatures and times better characterized the window available in the melt from which the material could be crystallized without appreciable loss in degree of crystallinity. Unfortunately these results are not very exciting and show only a very limited thermal stability in the melt. Figure 3.3 illustrates the results for a range of melt times and temperatures with each point in the grid representing an individual DSC scan²⁰. Longer times and temperatures in the melt lead to a big drop in the crystallizability. The material seems to show significant drop in the heat of melting if melt residence times are longer than 10 minutes. From the practical standpoint, these results are disappointing and limit the range of melt operations that can be carried out.

3.3 Crystallization Kinetics

Fast crystallization kinetics from the melt becomes a crucial factor when these systems are processed from the melt. A faster crystallization response is obviously favorable from an economical perspective as it leads to decreased cycle times. A slower crystallization rate may force additional annealing times at certain temperatures and may in fact become a rate-determining step. In this regard, the traditional Avrami analysis has been utilized to quantify the bulk crystallization kinetics for some semicrystalline polyimides. Using this analysis for LaRC-CPI³, Muellerleile et al. found that the value of Avrami exponent was ca. 2 and surprisingly this value did not show much change with varying T_c . Morphological investigations revealed the existence of hedritic or sheaf-like structures, which gave additional credence to the values of Avrami exponent obtained. The value of bulk crystallization rate 'K' however could not be calculated reliably which therefore precludes any reliable comparisons with other systems. The thermal behavior for this polyimide indicated in Figure 3.3, and other DSC results presented by the authors, however, indicate only a sluggish crystallization response and limited thermal

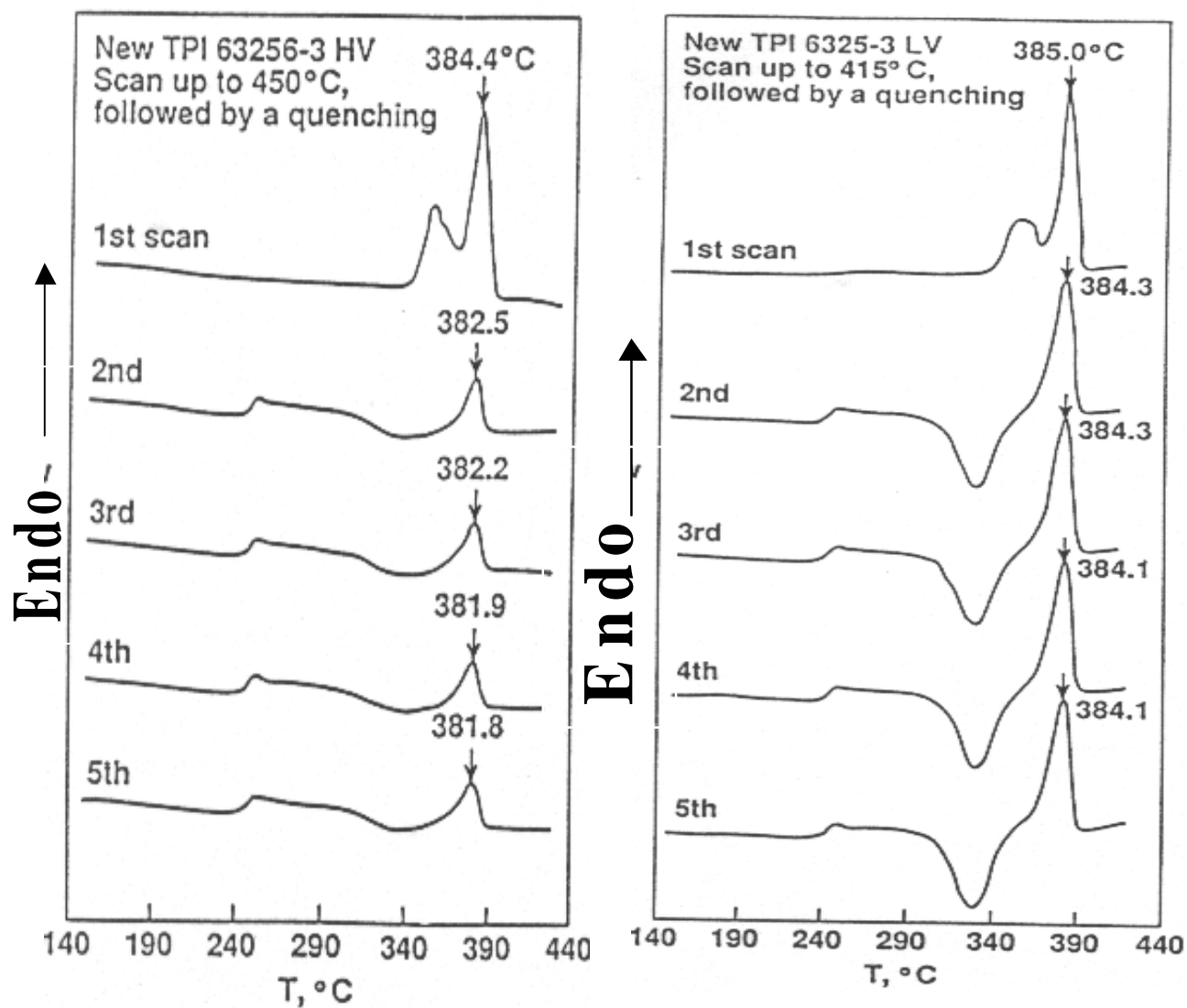
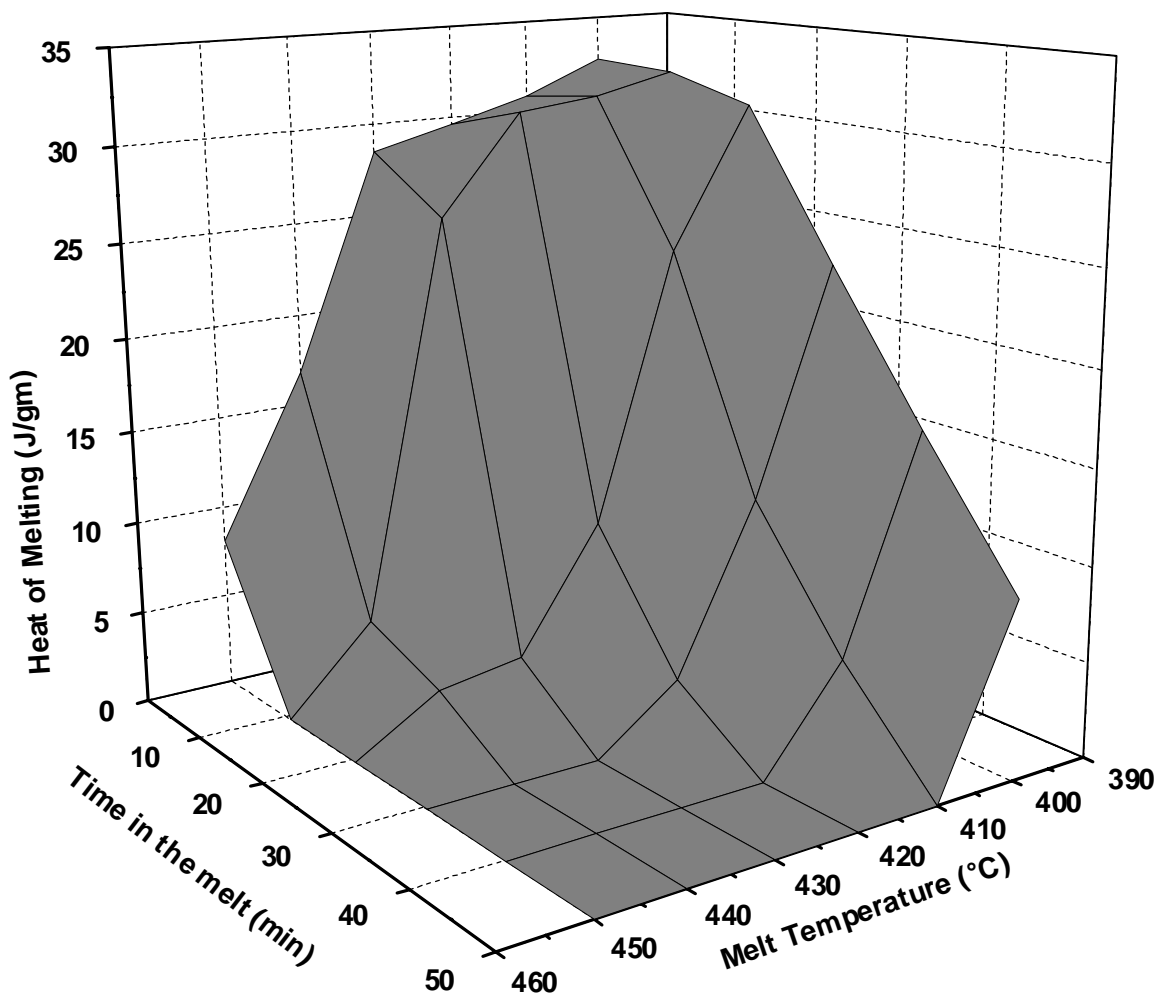
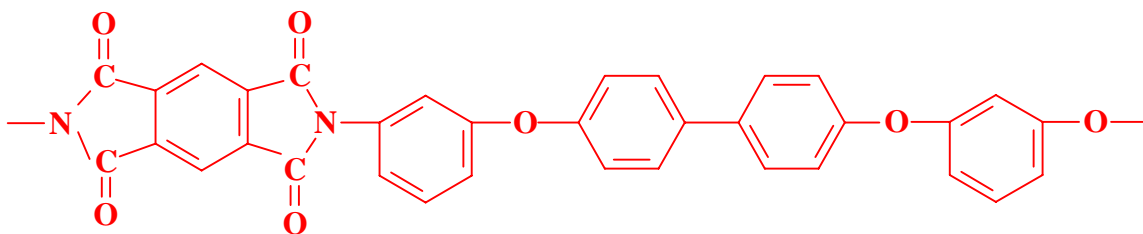


Figure 3.2 First heat and repeat heat DSC scans for the commercial New-TPI⁹. The scans are shown for two different grades (a) High Viscosity grade (b) Low viscosity grade.



Aurum New-TPI

Figure 3.3 Chemical structure and thermal stability of New-TPI polyimide. The 3-D plot illustrates the heat of melting after exposures to different melt temperatures and melt residence times²⁰.

stability in the melt. For LaRC-CPI-2, attempts by Brandom¹⁶ to perform Avrami analysis failed (by DSC) as a suitable exothermic signal could not be obtained for a range of melt conditions. While milder melt conditions led to a crystallization exotherm starting before the stabilization of the DSC signal, other more harsher conditions produced only a very weak exotherm. The authors thus observed faster response only in a narrow range of undercoolings and when using only very mild melt conditions. This behavior and other similar results presented in the study is due to incomplete melting (memory effect) and presence of large amounts residual nuclei, which then aid in subsequent crystallization. Once higher melt temperatures/times were utilized and these residual nuclei were destroyed, *the lack of inherent crystallizability* of the chain led to only a sluggish and weak crystallization response. Other attempts to quantify the crystallization behavior of LaRC-CPI-2 by Brandom²¹ involved using rheological measurements to perform Avrami analysis. The results indicated very high values of ‘n’ and ‘K’ and do not lend themselves to a conclusive interpretation. Additionally, the utilization of Avrami analysis (see Chapter 2) on rheological data, where the sensitivity is limited to the onset of crystallization, and the complete primary crystallization process cannot be followed reliably, is a very controversial proposition. For a different polyimide TPEQ-ODPA²², characterized in this laboratory by Srinivas et al.^{19,22}, the crystallization kinetics is again very slow. Three molecular weight versions were tried and only the low molecular weight version of $M_n=10,000$ Daltons resulted in any significant crystallizability. For this polyimide and others possessing similar structure, it has been observed that such low molecular weights result in very brittle films. However, M_n of 15,000 Daltons or more often leads to creasable films. It is thus likely that molecular weight of $M_n=10,000$ Daltons is either close to or below the critical molecular weight for entanglements and hence properties of the initial film are very poor. For TPEQ-ODPA, higher molecular weight versions showed a much reduced chain mobility and crystallized appreciably only in the presence of NMP. The very slow crystallization response and overall a languid crystallization behavior did not make any isothermal crystallization kinetics viable in this case. The story regarding the crystallization kinetics for another semicrystalline NASA polyimide LaRC-TPI, is yet again grim due to poor recrystallization stability from the melt²³. Two separate attempts at performing Avrami

analysis have been made by NASA workers¹⁸ and by Muellerleile²⁴ in this laboratory. NASA workers found the Avrami exponent to be '1' and ca. '2.5' for two different grades of LaRC-TPI. The value of the bulk crystallization rate parameter 'K' was found to be very low (at T_c of 280°C), the exact value being very unreliable and hence not being reported here. For New-TPI the crystallizability and crystallization rates are significantly better compared to the polyimides discussed above. Before presenting the absolute value of 'n & K' it is useful to recall from Chapter 2 that the value and units of K are dependent on value of n. Hence to make valid comparisons, values of $K^{1/n}$ should be compared. Secondly, the undercooling at which the crystallization is carried out will have a major influence. The values of 'n & $K^{1/n}$ ' that were found by Hsiao et al²⁵. are 4 and 0.04 min⁻¹ for thermal nucleation and the fastest rate observed. In this regard, it is useful to compare results with PEEK which, though not a polyimide, competes with polyimides in a variety of applications. Cebe and Hong²⁶ have reported a value of 0.22 min⁻¹ for $K^{1/n}$ at an undercooling of 87°C. Although the highest value of $K^{1/n}$ is reported here, it will be subsequently discussed in this research that value of $K^{1/n}$ is critically dependent on the previous melt conditions. Also, the results presented later for the polyimide researched in this work will show the rates of crystallization to be faster by more than a decade than the values shown above. It also needs to be mentioned that for many of these rigid polymer systems, equilibrium melting points are not known with certainty. Hoffman-Weeks analysis which has often been utilized for such a purpose is strictly inapplicable for estimating equilibrium melting points of these polymers. Thus there is some degree of inaccuracy when describing the exact undercooling at a given crystallization temperature. This could in turn sometimes lead to erroneous comparisons of crystallization kinetics for two polymers at the same stated undercooling.

3.4 Morphology of Semicrystalline Polyimides

Despite increased overall chain-rigidity and a highly aromatic backbone, these high temperature semicrystalline polyimides (at the proper conditions) often show a significant tendency to crystallize. The study of morphological behavior of these semi-

flexible polymers becomes especially interesting from a general polymer crystallization viewpoint. Most theories put forward to explain the observed morphologies in flexible polymers (like the L-H theory to explain and interpret the lamellar morphology) cannot be readily applied to these significantly more rigid chain systems. Several fundamental assumptions inherent in such theories will not hold for these materials. Yet for most of these semicrystalline polyimides similar morphological forms such as spherulites, linear growth rates of spherulites, lamellar morphology and SAXS evidence indicating the typical variation of long spacing with undercooling has been demonstrated^{21,22,24,27,28}. The following section examines the information on crystallization behavior of this different class of materials and illustrates the various similarities with the flexible chain systems.

For the commercially produced New-TPI, Hsiao²⁵ et al. have demonstrated the presence of negative spherulites that exhibit thermal nucleation. While the spherulites showed a smooth periphery at lower crystallization temperatures, the morphology at higher temperatures was coarse. The growth rates were found to be linear and could be measured across the growth rate maximum due to lower nucleation density and slower growth rate. Such general spherulitic morphology has also been observed for most other semicrystalline polyimides.

Muellerleile and Wilkes³ et al. demonstrated the presence of a sheaf like morphology for LaRC-CPI, with higher nucleation density and smaller structures observed on the glass side as compared to “air” side. The growth rates of these structures were found to be linear. To determine the growth rates, SEM was performed on samples quenched after varying amounts of crystallization time³. A specific etching cycle was developed to enhance the contrast¹⁵. Brandom and Wilkes^{16,17} observed a spherulitic structure for LaRC-CPI-2 using TEM. Interestingly, the development of the structure was non-uniform with the presence of an amorphous layer often observed for the “air” surface. For LaRC-TPI, Muellerleile²⁴ et al. observed that any morphological details of the crystalline superstructure could not be enhanced by any microscopic techniques. However, SAXS measurements revealed a long spacing value of ca. 200 Å. For New-TPI, Srinivas et al.²⁹ and others^{11,12,30,31,32} utilized SAXS to demonstrate the presence of long spacing. They also demonstrated the variation of lamellar thickness with

crystallization temperature, a typical behavior for flexible crystalline polymers. Surprisingly, ‘regime analysis’ has also been carried out for several of these polyimides and regime II→III transition has been reported²⁵. For New-TPI, the regime analysis was performed by Hsiao²⁵ et al. using the standard values of the constants and $T_m^\circ=406^\circ\text{C}$. The product of surface energies $\sigma\sigma_e$ was calculated to be $1176 \text{ erg}^2/\text{cm}^4$. It needs to be emphasized that such regime analysis is inherently erroneous for such rigid chain systems as it is based on the applicability of L-H theory to such rigid chain systems, an incorrect assumption. Secondly the equilibrium melting points are not known with any reasonable degree of certainty. Small variations in the value of equilibrium melting point can lead to artificial creation and disappearance of regimes. Thus such an analysis has little fundamental meaning.

Cheng⁴ et al. performed a regime analysis for a series of polyimides with varying amounts of ethylene glycol units. They observed that the product $\sigma\sigma_e$ was changed from $760 \text{ erg}^2/\text{cm}^4$ to $740 \text{ erg}^2/\text{cm}^4$ when the chain flexibility was increased by varying the number of ethylene glycol units from 1 to 3. The authors conjectured that as the lateral surface energy σ would be a constant, the decrease in $\sigma\sigma_e$ with increasing chain flexibility reflects a decreasing value of fold surface energy σ_e for the more flexible polymers. These conclusions although seemingly correct are based on very shaky experimental evidence. Firstly the linear spherulitic growth rates were not utilized but rather a $t_{0.05}$ (5% crystallinity) values were used instead. Secondly, and more importantly, the values of the T_m° were approximated to be 10°C above the DSC melting point. Slight changes in the value of T_m° can have a tremendous effect on the value of the product $\sigma\sigma_e$. Therefore putting any meaning to changes of less than 2% in $\sigma\sigma_e$ when using big assumptions to estimate the values of constants is dangerous.

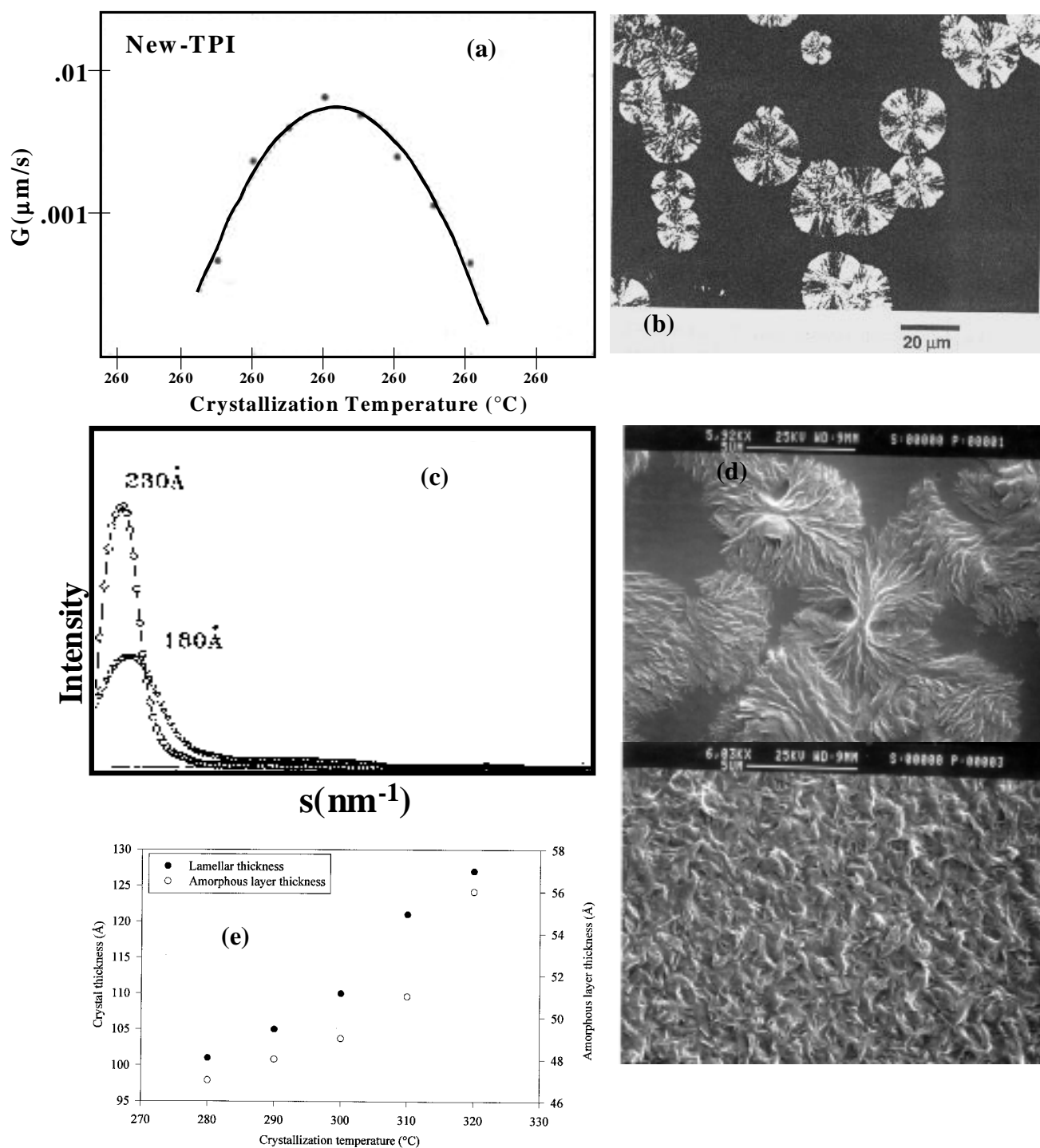


Figure 3.4 (a) Spherulitic growth rates for New-TPI²⁵. (b) Negatively birefringent spherulites observed for New-TPI. (c) SAXS for LaRC-CPI-2 samples indicating differently thick lamellae responsible for different endotherms²⁴. (d) The hedritic structure obtained for LaRC-CPI by Muellerleile et al.³. (e) The variation of lamellar thickness for New-TPI observed by Srinivas et al.²²

3.5 Melting Behavior of Semicrystalline Polyimides

Multiple melting behavior that is a characteristic of a large variety of semicrystalline polymers has also been observed for other more rigid chain materials like PEEK^{33,34,35,36} and the polyimides described earlier in this chapter^{4,11,17,20}. The presence of multiple melting endotherms can occur due to a variety of reasons like the presence of distinct lamellar populations, different crystal structures and continuous melting and recrystallization process. In this regard, the presence of a small endotherm 10-20°C above the crystallization temperature is a common occurrence and is usually explained on the basis of a secondary crystallization process. Muellerleile et al.³ observed such behavior for the LaRC-CPI samples. Bandom et al.¹⁷ observed double endotherms for LaRC-CPI-2 at 334°C and 364°C and explained it on the basis of dual lamellar populations. It was theorized that a thickening process was occurring which enabled the thinner lamellae to transform in to thicker ones by a recrystallization process, the kinetics of this being dependent upon the molecular weight of the polyimide. For New-TPI²⁵, only a main higher melting peak was observed after crystallization at different temperatures. The presence of a small endotherm at $T_c + 10^\circ\text{C}$ was attributed to the secondary crystallization process although sufficient evidence to prove this has not been presented. Kreuz et al.²⁸ synthesized a series of BPDA based copolyimides based on 134APB and 1,12-dodecanediamine and observed a triple melting behavior. The polyimide based on BPDA and 134 APB is also the subject of this study. The lowest melting endotherm was again attributed due to the secondary crystallization whereas the middle melting endotherms was explained on the basis of crystallites formed at the previous crystallization temperature²⁷. The highest melting endotherm was shown to be the result of melting and recrystallization process with its strength being heating rate dependent. Similar conclusions were later also reached for 134APB-based polyimide by Srinivas et al.²⁰.

Apart from the study by Srinivas et al. it seems that the attribution of different melting peaks (though seemingly correct) has been heavily influenced by evidence from PEEK. Although PEEK itself attracted extensive attention from different research groups

on the cause of multiple melting endotherms the conclusions reached for the various semicrystalline polyimides have been based on relatively smaller amount of experimental evidence. Detailed heating rate studies or Synchrotron SAXS analysis has been lacking in this area.

3.6 Melt Viscosity

Apart from a few handfuls of studies that deal with the rheological behavior of these materials, most research groups have largely ignored this very important aspect. This may be that most such polyimides have been introductory or only in initial stages of development. This is in small part also due to relatively high melting temperatures usually required by these materials and the lack of widespread availability of appropriate equipment for such experimental work. Some available examples of this work would be illustrated here.

Figure 3.5 depicts the shear loss modulus, shear storage modulus and the calculated complex viscosities for two grades of LaRC-TPI 1500 series polyimide¹⁸. The time sweep experiments (Figure 3.5) at 350°C show the behavior up to 3 hours and illustrate good stability at this relatively low melt temperature of 350°C. While the medium flow grade sample (MFG) remained unchanged, the high flow grade (HFG) sample showed an increase from 8000 to 45,000 dynes/cm² during the time frame of the experiment. Figure 3.5 illustrates the frequency sweep experiments at different melt temperatures and the calculated complex viscosity values are plotted. Apart from lower temperatures, a significant change in the viscosity-frequency profile or a clear shear-thinning behavior was not observed. These values were, however, utilized to construct a master plot (Figure 3.5) which enabled the predictions at a broader range of frequencies. The reference temperature was fixed at 320°C and the shift factors obtained did not show any dependence on the molecular weight. The authors thus concluded that the molecular weights were above the critical molecular weight for entanglement, M_c . It is also clear that the MFG grade was a higher molecular weight polymer. Additionally, the authors utilized the data to make predictions about the molecular weight distributions of the two samples. The ratio of the molecular weights was found to be ca. 1.6 and the molecular weight distribution was proposed to be approximately equal.

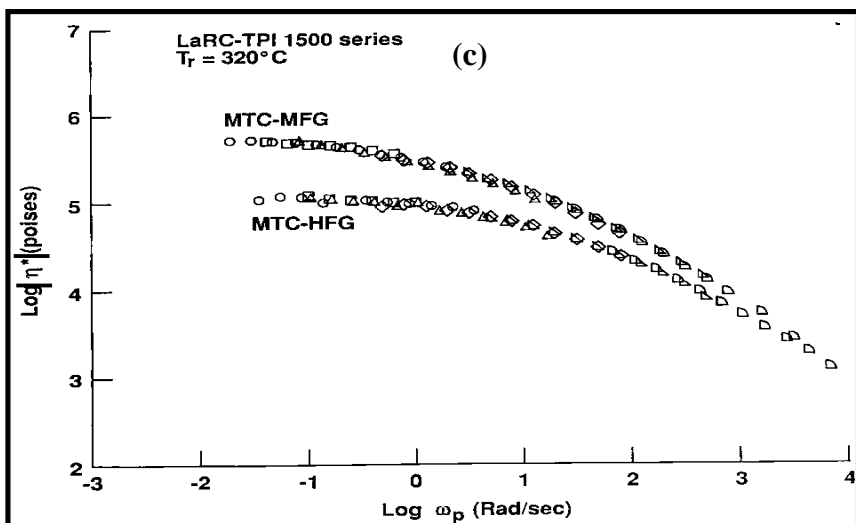
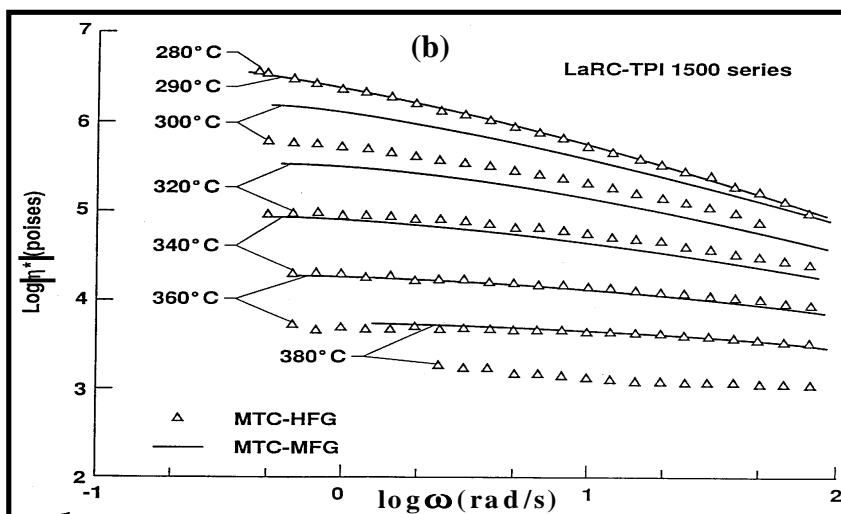
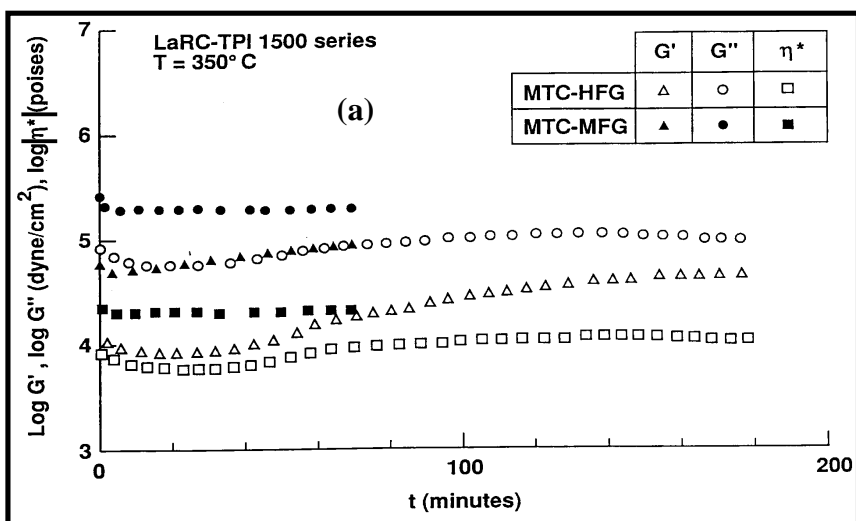


Figure 3.5 Rheological results for different grades of LaRC-TPI.¹⁸ (a) Loss modulus, storage modulus and complex viscosity at 350°C for up to 3 hrs. (b) Complex viscosity-frequency profiles at different melt temperatures for two grades of LaRC-TPI. (c) Master curves for the two grades constructed using the data in (b).

Figure 3.6 shows the viscosity frequencies profiles by Hergenrother et al.³⁷ for a polyimide adhesive. Also shown are two comparative scans of Ultem PEI and a polysulfone adhesive. It is, however, not clear as to what the authors were comparing because not only are the polymers of different molecular weights, but the scans are also run at different temperatures. Also, it is clear that for the polyimide, the complex viscosity values at 10 Hz (a common comparative frequency) are very high at ca. 10^6 poise (or 10^5 Pa.s). It is important to mention that regardless of the annealing treatments at various temperatures this polyimide did not crystallize after having been taken once above the melt temperature. Hence the polyimide serves no utility from the crystallization viewpoint.

Figure 3.6 however, shows viscosity results for a more promising polyimide, LaRC-8515³⁸, a polyimide which also has given excellent adhesion results³⁹. The polyimide chains are endcapped with phthalic anhydride and the dianhydride used is BPDA. The number 8515 in the name refers to the % of two different diamines used, 3,4'-ODA (85%) and 1,3-bis (3-APB) (15%). Consecutive time sweeps are illustrated at different melt temperatures, each being for a duration of 30 minutes. The polyimide displays significant thermal stability at all temperatures. The plot also illustrates the temperature dependence of the storage and loss moduli and depicts the crossover to a more solid-like behavior at 340°C (indicated by $G'' > G'$). The recrystallization ability of this interesting system is also indicated in Figure 3.6. Although the polyimide is not readily crystallizable, 1 hour annealing at 325°C is successful in reintroducing the crystallinity. Detailed DSC work to characterize the crystallization behavior has not been

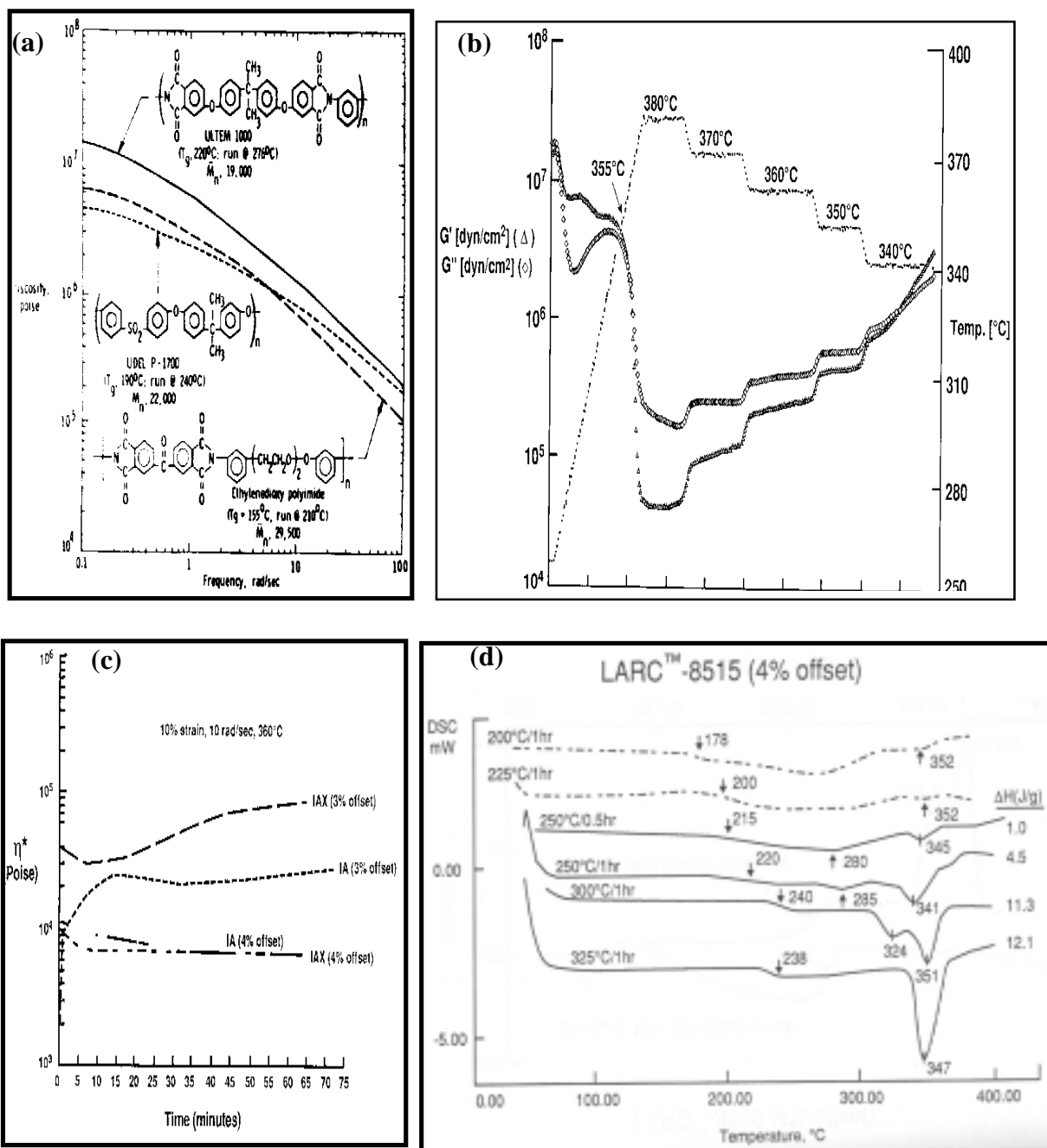
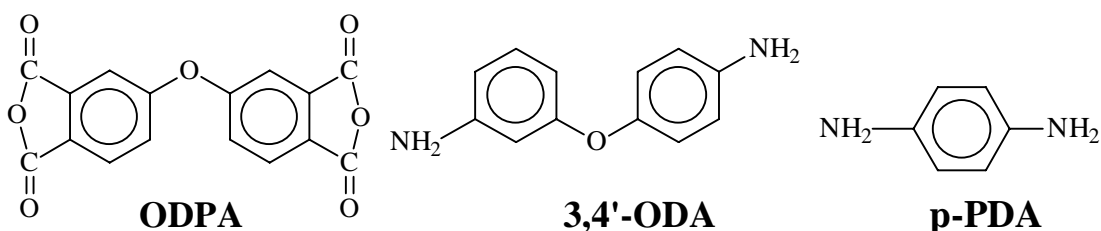


Figure 3.6 (a) Melt rheology of an amorphous polyimide by Hergenrother et al.³⁷ (b) Continuous loss and storage shear modulus for LaRC-8515 polyimide at different melt temperatures³⁸ (c) Melt viscosity vs. time at 360°C for LaRC-IA and -IAX⁴⁰ (d) Crystallization behavior of LaRC-8515 after annealing at different temperatures.

conducted on this polyimide so far. However, it is safe to say that the kinetics of crystallization of the polyimide would be poor due to narrow window of crystallization.

The results for two other NASA thermoplastic polyimides, LaRC-IA and LaRC-IAX are shown⁴⁰ in Figure 3.6. Significant thermal stability at a relatively low melt temperature of 360°C is shown for the polyimides. The chemical structure of the polyimides is based on ODPA dianhydrides with the chains endcapped with phthalic anhydride. The diamine utilized for LaRC-IA is 3,4'-ODA while for LaRC-IAX a mixture of 3,4'-ODA (90%) and p-PDA (10%) is used. The chemical structures of the monomers are shown below.



Scheme 3.1 Monomers used in LaRC-IAX synthesis⁴⁰.

Detailed crystallization work on this polyimide is however not available. Figure 3.7 shows the rheological behavior for New-TPI at different melt temperatures⁹. DSC results on the crystallization behavior of this polyimide have already been discussed earlier in this chapter. Thermal stability at such high melt temperatures is relatively poor with higher temperatures leading to a faster increase in viscosity. Substantial chain extension/crosslinking seem to be occurring at these temperatures leading to the viscosity increase⁹. It is useful to recall the earlier discussed results, which indicate that this polyimide loses its recrystallization ability catastrophically once exposed to these melt temperatures for even a short duration of time²⁰. Results are also presented in Figure 3.7 for the polyimide TPEQ-ODPA characterized in this laboratory^{19,22}. Although the chains were endcapped with phthalic anhydride the stability of the polyimide is poor with large increases in viscosity occurring in the melt. This is in large part due to the very high melting point associated with this polyimide thus requiring still higher melt temperatures.

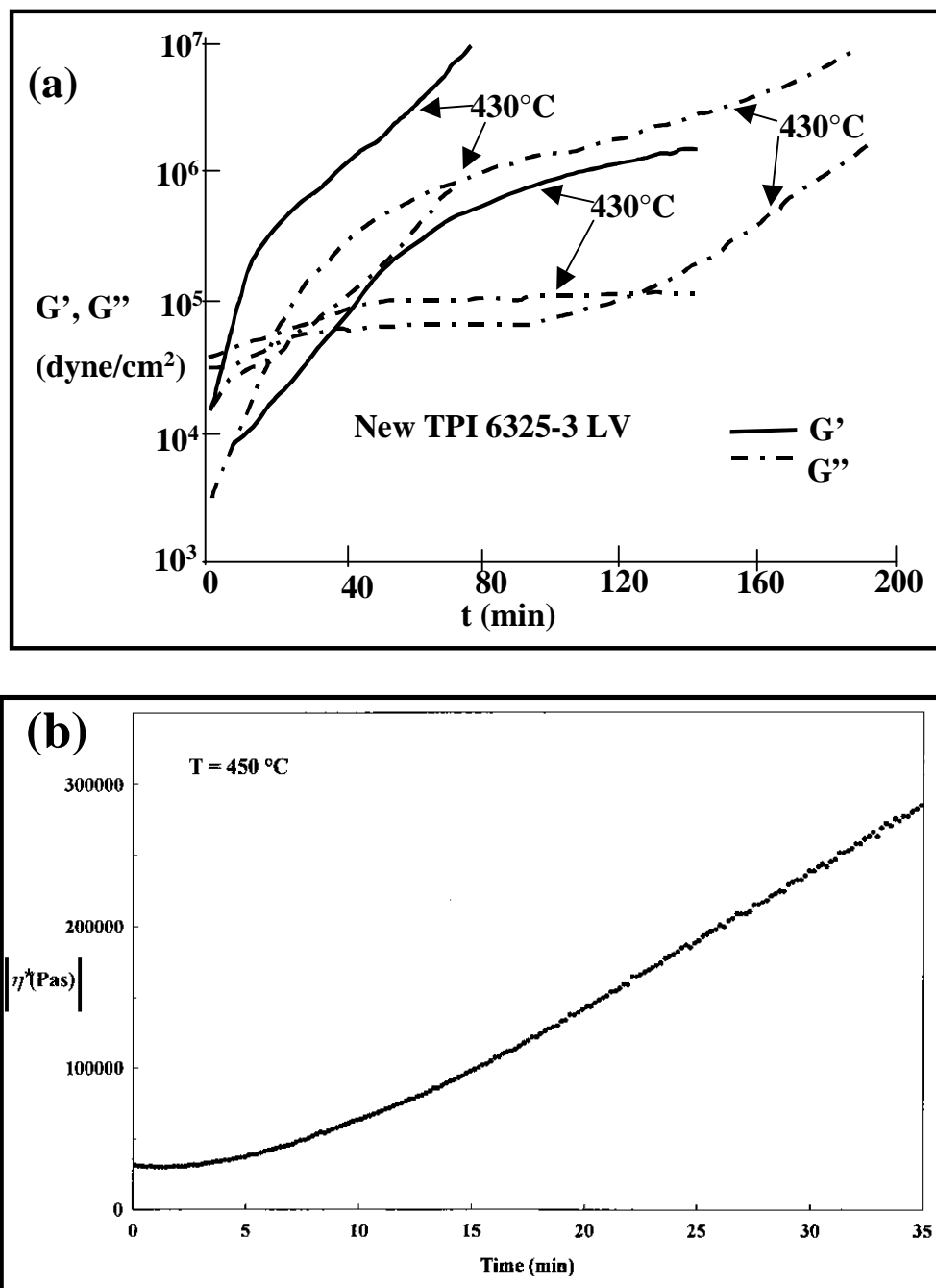


Figure 3.7 Rheological behavior of (a) New-TPI⁹ and (b) TPEQ-ODPA polyimides showing molecular weight changes for both polyimides¹⁹.

References:

-
- ¹ St, Clair, T.L. in *Polyimides* Eds. Wilson, D., Stenzenberger, H.D. and Hergenrother, P.M., 1990, Chapman and Hall, New York, pg. 58.
- ² Hergenrother, P.M. and Havens, S.J. in *Polyimides: Materials, Chemistry and Characterization* Eds. Ferger *et. al.* Elsevier, New York, 1989.
- ³ Muellerleile, J.T., Risch, B.G., Rodrigues, D.E., Jones, D.M. and Wilkes, G.L. *Polymer* 1992, **34**, 789.
- ⁴ Heberer, D.P., Cheng, S.Z.D., Barley, J.S., Lien, S.H., Bryant, R.G. and Harris, F.W. *Macromolecules* 1991, **24**, 1890.
- ⁵ Tamai, S., Yamaguchi, A. and Ohta, M. *Polymer*, 1996, **37**, 3683.
- ⁶ Tamai, S., Oikawa, H., Ohta, M. and Yamaguchi, A. *Polymer*, 1998, **39**, 1945.
- ⁷ Product Literature, “*New-TPP*” Mitsui Toatsu Chemicals, Inc.
- ⁸ Yamaguchi, A. and Ohta, M. Proceed. 18th Int. SAMPE Tech. Conf., Oct 1986, pg. 229.
- ⁹ Hou, T.H and Redy, R.M. *SAMPE quarterly*, Jan 1991, **22** (2), 38.
- ¹⁰ Hirade, T., hama, Y., Sasuga, T. and Seguchi, T. *Polymer*, 1991, **32** (14), 2499.
- ¹¹ Huo, P.P. and Cebe, P. *Polymer* 1993, **34** (4), 696.
- ¹² Friler, J.B. and Cebe, P. *Polym. Eng. Sci.* 1993, **33** (10), 587.
- ¹³ Okuyama, K., Sakaitani, H. and Arikawa, H. *Macromolecules* 1992, **25**, 7261.
- ¹⁴ Muellerleile, J.T., York, G.A. and Wilkes, G.L. *Polym. Commun.* 1991, **32**, 176.
- ¹⁵ Muellerleile, J.T. and Wilkes, G.L. *Polym. Prepr.* 1990, **31**, 637.
- ¹⁶ Bandom, D.K. and Wilkes, G.L. *Polymer* 1994, **35**, 5672.
- ¹⁷ Bandom, D.K. and Wilkes, G.L. *Polymer* 1995, **36**, 4083.
- ¹⁸ Hou. T.H. and Bai, J.M. *High Performance Polymers* 1990, vol. **2**.
- ¹⁹ Srinivas, S., Graham, M., Brink, M.H., Gardner, S., Davis, R.M., McGrath, J.E. and Wilkes, G.L. *Polym. Eng. Sci.* 1996, **36**, 1928.
- ²⁰ Srinivas, S, Caputo, F.E., Graham, M., Gardner, S., Davis, R.M., McGrath, J.E. and Wilkes, G.L. *Macromolecules* 1997, **30**, 1012.

-
- ²¹ Brandom, D.K. *Ph.D. Thesis*, Virginia tech. June 1996.
- ²² Srinivas, S. *Ph.D. Thesis*, Virginia Tech. June 1996.
- ²³ Product Literature, “High Performance Polyimide- LaRC-TPI” Mitsui Toatsu Chemicals, Inc.
- ²⁴ Muellerleile, D.K. *Ph.D. Thesis*, Virginia Tech. September 1991.
- ²⁵ Hsiao, B.S., Sauer, B.B. and Biswas, A. *J. Polym. Sci. Part B* 1994, **32**, 737.
- ²⁶ Cebe, P. and Hong, S.D. *Polymer* 1986, **27**, 1183.
- ²⁷ Hsiao, B.S., Kreuz, J.A. and Cheng, S.Z.D. *Macromolecules* 1996, **29**, 135.
- ²⁸ Kreuz, J.A., Hsiao, B.S., Renner, C.A. and Goff, D.L. *Macromolecules* 1995, **28**, 6926.
- ²⁹ Srinivas, S. and Wilkes, G.L. *Polymer* .
- ³⁰ Huo, P.P., Friler, J.B. and Cebe, P. *Polymer* 1993, **34**, 4387.
- ³¹ Brillhart, M.V. and Cebe, P. *J. Polym. Sci. Part B* 1995, **33**, 927.
- ³² Lu, S.X., Cebe, P. and Capel, M. *J. Appl. Polym. Sci.* 1995, **57**, 1359.
- ³³ Bassett, D.C., Olley, R.H. and Raheil, I.A.M.A. *Polymer* 1988, **29**, 1745.
- ³⁴ Blundell, D.J. and Osborn, B.N. *Polymer* 1983, **24**, 953.
- ³⁵ Blundell, D.J. *Polymer* 1987, 2248.
- ³⁶ Cheng, S.Z.D. Cao, M.Y., Wunderlich, B. *Macromolecules*, 1986, **19**, 1868.
- ³⁷ Harris, F.W., Beltz, M.W. and Hergenrother, P.M. *SAMPE Journal*, **Jan/Feb** 1987, 6.
- ³⁸ Hou, T.H., Wilkinson, S.P. and Jensen, B.J. *Polyimides: Trends in Materials and Applications, Proceedings of the Fifth International Conference on Polyimides*, 1994, 409.
- ³⁹ Hou, T.H., Wilkinson, S.P. and Jensen, B.J. *40th International SAMPE Symposium May*, 1995, 1072.
- ⁴⁰ Chang, A.C., Hou, T.H. and St. Clair, T.L. *Trends in Materials and Applications, Proceedings of the Fifth International Conference on Polyimides*, 1994, 3.

Chapter 4

Polyimides as Adhesives: -Literature review

4.1 Introduction

Much like the subject of polymer crystallization, the field of adhesion is vast and thus it is impossible to even remotely cover the area in a review of this size. The material presented therefore is intended to cover a few selected topics that are more relevant to the author's research. The selection of topics is therefore guided by the author's choice.

To quote R.C. Patrick¹, "adhesion is the phenomenon of causing two materials to be held together, while an adhesive is the material utilized in carrying out this phenomenon". This simple definition avoids much debate and confusion that has surrounded the exact meaning of the word adhesion. This fascinating field, however, has come a long way since man first realized that the blood caused his hair to cling together quite glutinously. Specifically, major strides have been made in the second half of this century, and these have enabled a more fundamental understanding of the subject. Notably, major interest has risen in the past decade or so regarding the use of various adhesives for military, aerospace and microelectronic and applications². In this regard, aromatic polyimides and related polymers have been of significant importance. Specifically, these materials possess a broad array of superior properties like excellent thermal stability, solvent resistance, good mechanical properties, radiation resistance, low thermal expansion, wear resistance, hydrolytic stability, low dielectric constant and high breakdown voltage³. This broad range of attractive properties in these high performance polymers has made them excellent candidates as adhesives.

4.2 Theories of adhesion

The definition of the word “adhesion” depends on whether the viewpoint is macroscopic or microscopic. However, it is important to realize an intimate contact between the adherend and the adhesive is necessary for the adhesion forces to be operative⁴. The various theories of adhesion essentially differ in qualifying the nature of these inherent adhesion forces. None of these widely prevalent theories, however, is successful in satisfactorily explaining the entire existing adhesion phenomenon. These theories are briefly addressed here to highlight the essential concepts on which they are based.

4.2.1 Mechanical interlocking

This theory postulates that the adhesion is achieved as a consequence of flowing of an adhesive into a rough surface and the resulting ‘interlocking’⁵. Thus this mechanical anchoring between the adhesive and the adherend prevents the removal of adhesive from the substrate. However, it is important to realize the degree of roughness that is being considered and the spreading of the adhesive that is achieved. It is meaningful to remember that the increase in roughness also results in availability of more area for intimate contact. The various surface treatments themselves have been divided by Venables et al^{6,7}. on the basis of roughness produced (i.e. pore size on the surface of the adherend) as:

- Group I: Surface treatments that produce no micro-roughness (pore size < 0.1 μm) or macro-roughness (pore size > 0.1 μm).
- Group II: Surface treatments that result in a large degree of macro-roughness.
- Group III: Surface treatments that result in a large degree of micro-roughness due to a porous oxide layer, with little or no macro-roughness produced.

4.2.2 Molecular interdiffusion

This theory proposed by Voyutskii⁸ and Vakula^{9,10} states that the polymer-polymer adhesion results from interdiffusion of polymer molecules across the interface.

This can be viewed as a molecular interlock enabled adhesion. The theory was proposed to account for the experimental results dealing with adhesion between dissimilar polymers when satisfactory explanations could not be reached by applying other existing theories. The theory accounted for effects of contact time, influence of time and temperature on bonding rate, and the influences of polymer molecular weight and polymer structure. Additionally, these models take into account the motion of the entire chain across the interface¹¹. While diffusion applies well for cases of self-adhesion or autohesion, its sole use to provide satisfactory explanation for polymer-polymer adhesion is questionable. High molecular weight thermoplastic polymers that often display very high melt viscosity may not diffuse easily within the time frame of most bonding operations.

4.2.3 Electronic theory

This theory is based on the argument that the electrostatic forces arising from the junction potentials between the contacting adhesive and substrate will contribute significantly towards the forces required to rupture the bonds. This theory was proposed by Derjaguin et al.^{12,13} who proposed the formation of an electrical double layer due to electron transfer during contact. This theory has invited some controversy as many workers have questioned the practical significance of the amount of forces involved¹⁴. While this concept may be useful to explain some specific instances of adhesion, substantial doubts have been cast regarding its overall utility. These include improved adhesion strengths with lowering of temperature for a large variety of systems (lower temperatures will favor smaller charge densities and hence poorer electrostatic forces) and negligible changes in adhesion performance with gross variations in the electronic character of the adhesives¹⁵.

4.2.4 Adsorption theory

This widely credited and much investigated theory is due to Sharpe and Schonhorn¹⁶. According to this theory, in the event of intimate contact between the adhesive and the adherend, the adhesive strength arises as a result of interatomic and

intermolecular forces at the interface. The forces between the adhesive and the adherend are usually grouped into two categories (1) primary forces and (2) secondary forces. Primary forces include ionic (600-1100 kJ/mole), covalent (60-700 kJ/mole) and metallic bonds (110-350 kJ/mole). Secondary bonds may include Van der Waals forces (0.02-40 kJ/mole), hydrogen bonds (10-40 kJ/mole), Lewis acid-base interactions (up to 80 kJ/mole), dipole-dipole and dipole-induced dipole (up to 20 kJ/mole) interactions. In this regard, introduction of chemical bonding between the adhesive and the adherend will obviously improve the adhesion strengths¹⁷. This can be done by in-situ reactions at the surface, by applying proper surface treatments, or by using various coupling agents.

4.3 Adhesion aspects of the present work

The study of adhesion can be broadly divided into the areas of “Surface Science”, “Mechanistic Studies” and “Material Properties”. Each of these aspects is extremely important and focuses on different but interrelated concepts in addressing the general phenomenon of adhesion. Without indulging in the task of describing details of the each of these sciences, the review will address the specific topics that are directly relevant to this research work. In this regard, the various features of the titanium adherend and the various surface treatments practiced for high performance adhesives will be discussed. Following this, the most widely used adhesion test, lap-shear test will be addressed with regards to the mechanics involved in this test. Some aspects of shear-lag approach due to Volkersen¹⁸ and effect of bending moments and peel stresses due to Goland and Reissner¹⁹ will also be discussed. The review of important material properties with respect to the semicrystalline adhesives will then be given with emphasis on crystalline morphology and bonding variables. Lastly, the techniques and the results from studies dealing with specifically the high performance and high temperature polyimide adhesives will be reviewed.

4.4 Titanium as an adherend

Titanium has a high strength to weight ratio, possesses excellent corrosion resistance and displays superb toughness relative to steel and aluminum and is able to retain its mechanical properties until very high temperatures²⁰. These properties have made titanium the metal of choice for applications like aerospace structural applications, landing gears, blades of gas turbines, nuclear power plants and prosthetic implants²¹. The high cost of this metal, however, limits its uses. Titanium possesses two different crystalline phases: the ' α -phase' which is hexagonal closed packed form and the ' β -phase' that is a body centered cubic form²². The β -phase is favored to form when temperatures exceed 882.5° and it shows lower strength to weight ratios and increased sensitivity to corrosion. On the positive side, β -phase metals show good hot and cold strength and are easily formed. ' α -Phase' alloys though showing poorer forming characteristics are stronger, tougher and resistant to environmental corrosion. Ti-6Al-4V is an α - β alloy having been developed to optimize the desirable properties of both phases^{23,24}. Aluminum stabilizes the α -phase and raises the $\alpha \rightarrow \beta$ conversion temperature while the vanadium stabilizes the β phase and raises the $\beta \rightarrow \alpha$ temperature. The comparison of Ti-6Al-4V with various other metals is illustrated in the Table 4.1 below²⁵.

Table 4.1 Some selected properties of different metals²⁵

Metal	E' [GPa]	σ_y [Mpa]	σ_{max} [Mpa]	K _{Ic} [Mpa m ^{1/2}]
Aluminum	70	40	200	100
Copper	120	60	400	To
Nickel	210	70	400	350
Ti-6Al-4V	110	900	1000	120
Al Alloys	70	100-380	250-480	23-40
Carbon Steel	210	250	420	140
Stainless Steel (304)	195	240	365	200

Surface treatment of the titanium-alloy is critical in improving the initial strength and long term durability of the adhesive joint. These surface treatments are utilized to remove the contaminants comprising the weak boundary layer and for creation of a stable adherend surface which may be *chemically* and *mechanically* compatible with the adhesive²³. For optimizing the durability of the adhesive joints, the surface treatments that enhance surface wettability and introduce macro- and to a greater degree micro-roughness are favored. In this regard, the chemical and morphological stability of the various surface treatments is especially important. The detailed procedures for various surface treatments have been extensively reviewed²³. Of the variety of surface treatments, three popular surface treatments utilized in this work are (1) grit blasting (2) TURCO 5578 and (3) chromic acid anodization (CAA). While grit blasting falls in the category of mechanical treatments, the TURCO 5578 treatment is chemical, and CAA falls under the category of anodization based treatments. The resulting surface morphology from these surface treatments differs in the nature of roughness and chemical composition of the oxide formed on the surface²⁶. The grit blasting involves high-speed alumina grit particles of micron level sizes hitting the surface at high speeds and thereby introducing macro-roughness (Group II) on the surface. The CAA treatment is perhaps the most popular of all surface treatments for titanium and it leads to the formation of a chemically durable and porous layer of amorphous TiO₂. The large degree of micro-roughness resulting from this treatment makes it a Group III type surface treatment. The increased surface area due to the micro-roughness and the generally observed durability of the oxide layer have been widely advocated to enhance both the physical and chemical bonding with the adhesive²⁷. The details of this involved surface treatment are described in several references and need to be followed very precisely in order to reproduce the experimental results^{26,28}. The morphology of the CAA treated surfaces is shown in Figure 4.1 and resembles a honeycomb-like structure with cell diameters of 30-40 nm and a wall thickness of 5-10 nm²⁶. The depth of the oxide layer depends on the concentration of the solution and the anodization voltage used and varies from 40 to 140 nm²³. The aqueous environment and high temperature durability of the CAA treatment is albeit a suspect. Regarding the effect of aqueous environments Clearfield et al.²³ have shown the

lack of stability of the oxide layer at temperatures approaching 300°C. Figure 4.1 shows the morphological transformation of the surface after a 3 hour moisture exposure at 300°C and shows that the originally present honeycomb structure has disappeared²⁶. These severe morphological changes that may occur on exposure to such conditions can destabilize the adhesive interface and thus have been advocated to cause a loss of bond strength or failure. With respect to the effect of dry and high temperature environments it has been observed that the treated surfaces maintained the honeycomb morphology even after exposure to air at 330°C for 1200 hours or vacuum at 400°C for 165 hours. However, bonds formed by these treatments failed under minimum force. The XPS studied revealed that the failure occurred in the oxide/metal interface. It has been proposed that development of microcracks takes place and leads to formation of an embrittled zone at the surface²³. While the exact causes of the failure of CAA treatment on exposures to high temperatures is not yet certain, it is important to state that similar results have been obtained in the present research work. Chromic acid anodization was briefly tried out in this research work as it is the most widely used treatment for titanium alloys. However, very weak adhesion and clear interfacial failures were obtained in this case (results are discussed in chapter 5). The bonding temperature utilized for the hot melt polyimide adhesive exceeded 400°C and thus could have been contributed to the failure of this surface treatment. Another important treatment for titanium adherends is TURCO 5578. The treatment is based on the sodium hydroxide etch and has been discussed in detail by Filbey²⁹. The treatment produces a micro-rough surface with formation of an oxide layer on the surface.

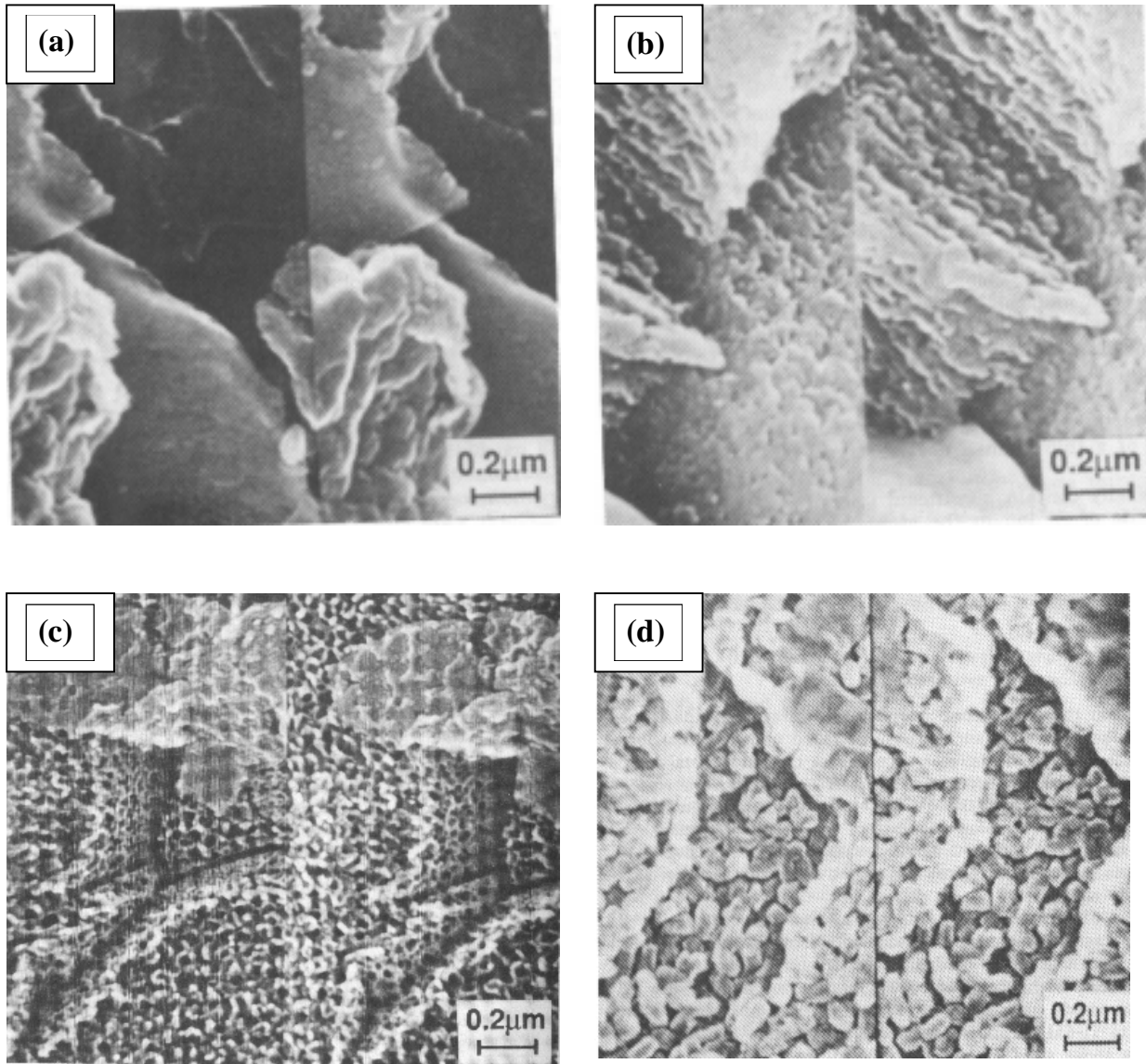


Figure 4.1 The surface morphology of the Ti-6Al-4V after various surface treatments²³ (a) gritblasting (b) TURCO 5578 sodium hydroxide etch (c) chromic acid treatment (d) chromic acid treated samples after exposure to water vapor at 300°C.

4.5 Some aspects of various adhesion tests

Before an adhesive is put into its final use, detailed analysis regarding design, testing and durability of the actual bonded structures needs to be conducted. This is especially true of structural adhesives where bond failures during actual use can have devastating consequences. However, during development of new adhesives such as the one attempted in the present work, standardized tests need to be conducted in order to compare and evaluate the various adhesion parameters. Probably the most important criteria for the new adhesive to be tested relate to (1) strength (2) fracture toughness and (3) solvent resistance of the bonded joints. The most widely used tests to characterize these phenomenon are the lap-shear test for strength comparisons, the double cantilever beam test to test the fracture toughness of the adhesive joints and the wedge test to evaluate the solvent resistance. Thus these three tests were conducted in the present study to characterize the polyimide used in this study as an adhesive. Once the material has been evaluated with these initial tests, subsequent testing methodology can be designed with respect to the proposed use. In the current section, the lap-shear test, which was the primary adhesion test used, is discussed.

4.6 Lap-shear test

This test is an ASTM standard (D1002) and is the most widely used adhesion test. The test gives the apparent average shear strength and is not intended for designing actual bonded structures or obtaining true shear strength of the adhesive. However, it is a sufficient comparative test and is especially useful due to its simple geometry³⁰. The average shear strength is given as:

$$\tau_m = P/bl \quad \{4.1\}$$

where τ_m is the apparent average shear strength, P is the applied load and b & l are the joint width and length respectively. While the geometry of the test is simple and a reason for its popularity, from a mechanistic viewpoint the lap-shear joint is a very complex loaded structure. The stress distributions within the sample are effected by several

factors such as (1) adherend modulus and thickness, (2) adhesive modulus and thickness, (3) bond overlap (4) other factors like presence of spew, shear moduli of adhesive etc^{31,32,33}. It is important to recognize these factors before testing as they can have a significant influence on the bond strengths obtained. Volkersen¹⁸ proposed a shear lag model to account for the non-uniform shear stress distribution along the bondline. The major assumptions of the model are that the adhesive deforms only in shear and the adherends only in tension. The equation that he derived for shear stress distribution along any point 'x' along the bondline is given by:

$$\tau(x) = \frac{P\omega}{2\sinh(\omega l/2)} \cosh(\omega x) + \frac{P\omega}{2\cosh(\omega l/2)} \sinh(\omega x) \left[\frac{E_2 t_2 - E_1 t_1}{E_2 t_2 + E_1 t_1} \right] \dots\dots\dots \{4.2\}$$

$$\text{where } \omega = \sqrt{\frac{G}{h} \left[\frac{E_2 t_2 + E_1 t_1}{E_2 t_2 E_1 t_1} \right]}$$

where:

h = Adhesive thickness

t = Adherend thickness

E = Young's modulus of the adherends

G = Shear modulus of the adhesive

l = Length of the overlap

P = Force per unit width

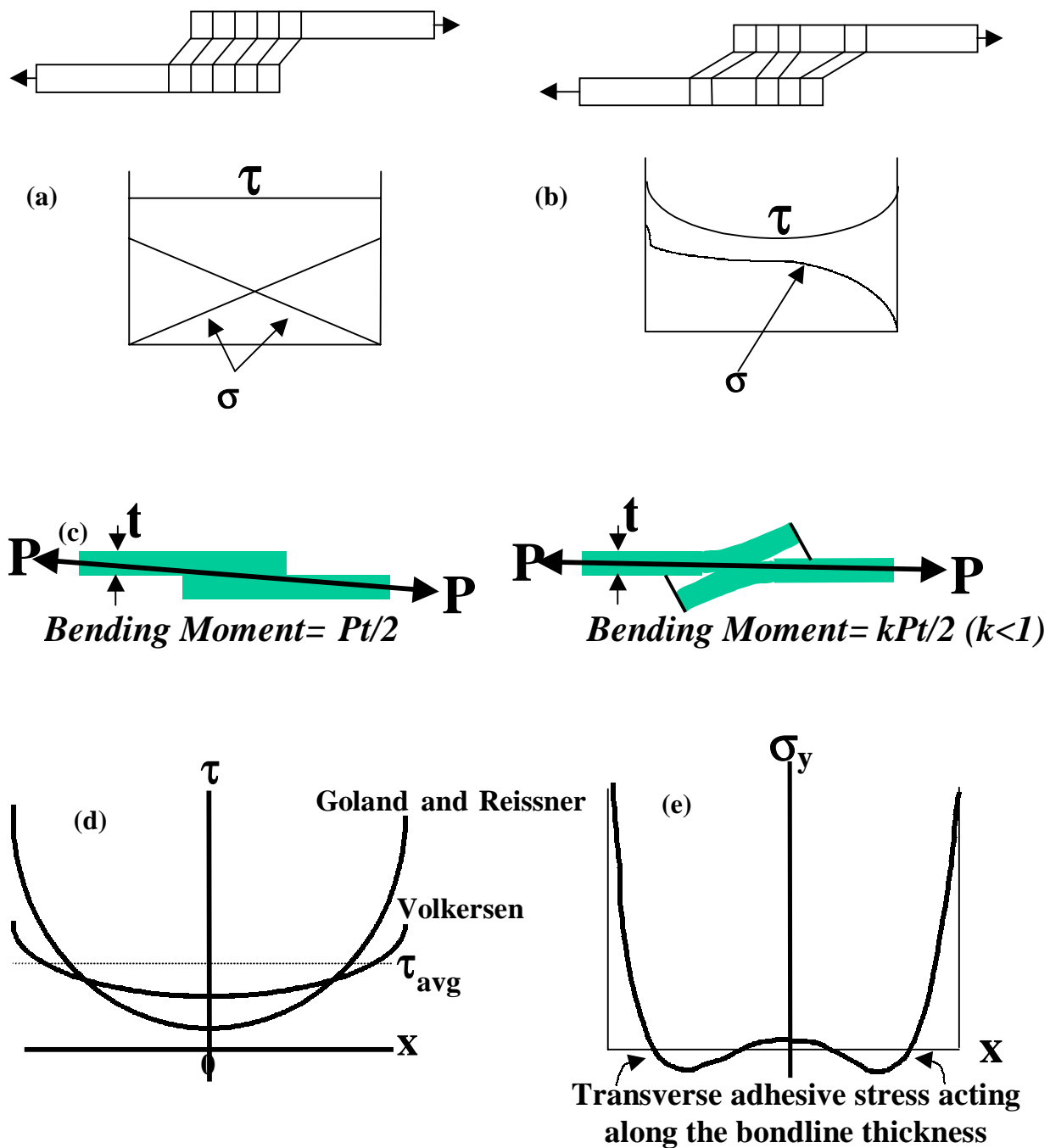


Figure 4.2 Shear strain (& shear stress) in the bond-line and tensile stress on the adherends as given (a) ideally & (b) predicted by Volkersen's analysis¹⁸. (c) effect of bending moment, which acts along the bondline to give a peel stress, thereby reducing joint strengths. (d) shear strength profile as given by various analysis (e) peel stresses along the bondline as calculated by Goland-Reissner analysis¹⁹.

Volkersen's shear lag approach also assumes that the adhesive and the adherend are *linearly elastic*. Figure 4.2 illustrates the shear stress profile for the adhesive and tensile stress profile for the adherend in the idealized case and with respect to Volkersen's approach. When proper account of the various joint parameters is taken, it is found that the adherend tensile stress decreases progressively from the loaded end to that on the unloaded end with the rate of change of the adherend stress being primarily dependent upon the adherend stiffness. The shear strain and shear stress in the adhesive are at the maximum at the ends and a minimum in the center. Also, dissimilar adherends will lead to a asymmetric shear stress distribution.

However, Volkersen ignored the bending moments in the sample due to non-linear load application. Any bending of the adherends changes the direction of the load line and in the adhesive deformation no longer is proportional to the applied load. Goland and Reissner¹⁹ took this fact into account and introduced a bending moment factor 'k' which relates the bending moment in the adherend end (M_0) to the applied load as:

$$M_0 = \frac{kPt}{2} \quad \{4.3\}$$

where 't' is the adherend thickness. While $k=1$ for no bending, it assumes a value less than one as the overlap area rotates and brings the load line closer to the center of the adherends. Goland and Reissner predicted a more non-uniform shear stress profile in the bondline than that predicted by Volkersen. One important aspect of Goland and Reissner analysis is that it predicts the excessive adhesive shear strains at the edges due to the elastic bending of the adherends. These excessive strains may lead to failure of the adhesive bond. In addition, the analysis predicts a 'peel stress' acting on the adhesive layer, σ_y which can be given as³⁴:

$$\sigma_y = \frac{\sigma^2}{C^2 R_3} \left[\left(R_2 \lambda^2 \frac{k}{2} - \lambda k' \cosh \lambda \cos \lambda \right) \cosh \frac{\lambda x}{C} \cos \frac{\lambda x}{C} + \left(R_1 \lambda^2 \frac{k}{2} - \lambda k' \sinh \lambda \sin \lambda \right) \sinh \frac{\lambda x}{C} \sin \frac{\lambda x}{C} \right] \quad \{4.4\}$$

where:

σ = mean tensile stress in the adherends

t = adherend thickness

x = position along the glue line

$$C=l/2$$

$$\lambda=C/t(6E_3t/Et_3)^{1/4}$$

$$k'=k(C/t)[3(1-\nu^2)\sigma/E]^{1/2}$$

$$R_1=\sinh\lambda \cos\lambda + \cosh\lambda \sin\lambda$$

$$R_2=\sinh\lambda \cos\lambda - \cosh\lambda \sin\lambda$$

$$R_3=(\sinh 2\lambda + \sin 2\lambda)/2$$

ν = Poisson's ratio

The shear and peel stresses are assumed to be constant along the bond thickness. The peel test itself is non-uniform and varies along the bond overlap, the maximum being at the edges. As predicted by Goland and Reissner, the value of the bending moment factor 'k' does not go to zero but approaches 0.2 towards the middle of the bondline. The analysis by Hart-Smith, however, predicts this value will fall to zero, implying negligible peel stress towards the middle^{31,35}. It is thus important to recognize that peel forces affect the bond strength values critically in lap-shear joints and often the failure can be attributed to these effects. Secondly, increasing the length of the overlap or increasing the shear modulus of the adhesive increases the non-uniformity of the shear stress profile. Increasing the modulus of the adherend, thickness of the adherends and the bondline thickness increase the uniformity of the shear stress distribution. These factors need to be kept in mind before any direct comparisons of the lap-shear strengths are made of results from different laboratories.

While most of the above quantitative relationships are based on elastic deformation of adhesive, an elastic-plastic model is often more appropriate in describing the fracture behavior of many viscoelastic adhesives. The large magnitude of fracture energy for some materials is attributed to their ability to undergo localized deformation in a relatively large region around the crack tip. The stress concentration is therefore reduced and the crack is blunted. The reduction in stress concentration can be related to the radius of the deformation zone. In this regard, the bond thickness if too small can limit the radius of the deformation zone and thus limit the toughness³⁶. The crack tip deformation process is viscoelastic in nature and the usual loading rate dependence and temperature dependence are thus introduced. Increasing the temperature or decreasing the loading rate increases the size of the deformation zone and thus the optimum bond thickness³⁷.

4.7 Crystallization aspects in adhesion

While crystalline polymers like polyethylene and polypropylene are widely used as hot melt adhesives, the amount of research work studying the effect of polymer crystallization on adhesion is surprisingly scarce. Only a few authors have looked at the effect of crystallinity and crystalline morphology on the adhesive performance (this may be in large part due to the widely prevalent misconception that crystallinity always promotes brittleness and loss of toughness). In fact, despite extensive literature search, this author was not able to come across a single study that addresses the effect of crystallinity on the solvent resistance of the adhesive interfaces.

With respect to the effect of crystallinity on adhesion, two features become important, (1) the effect due to strengthening/weakening of the bulk of the adhesive and (2) the effect on the adhesive interface. With regards to the first factor, Packham et al.³⁸ studied polyethylene adhesion to copper using the peel test. It was found that quenched samples gave higher peel strengths and a rougher fracture surface morphology than the samples that were slow cooled. Earlier Fan³⁹ and Tordella⁴⁰ had achieved similar results where they found extensively drawn polymer at the substrate for quenched samples. However, the failure was cohesive for all cases and thus it was proposed that the higher fracture energy values obtained for quenched samples were not due to the inhibition of weak boundary layer at the surface. Although the spherulitic sizes were not obtained the results may in part be due to smaller spherulitic sizes and reduced percentage crystallinity. Love et al.⁴¹ showed that faster cooling rates gave stronger adhesion between PCTFE and glass due to greater ductility and higher fracture energy of the adhesive. The peel test specimens showed that slower cooling rates gave more percentage crystallinity as more time was available for the polymer to crystallize. However, this increase in crystallinity resulted in lower adhesion strengths and an interfacial mode of failure (as observed visually).

The second factor deals with the effect of crystalline morphology on the adhesive interface. In this regard, the effect of transcrystallinity at the substrate becomes

important in effecting the adhesion strength. Schonhorn^{42,43} has shown that the critical surface tension of wetting increases with transcrystallinity for polyethylene from 31mJ/m² to 69.6mJ/m². The increase in wettability will improve adhesion and thus will lead to higher joint strengths. Additionally, the presence of low molecular weight chains and impurities at the spherulitic boundaries has been widely documented. These regions will generally possess lower strength and have been proposed to constitute a weak boundary layer at the surface⁴⁴. The elimination of this weak boundary layer in theory can be achieved by introducing transcrystallinity or decreasing spherulitic sizes. However, Tordella⁴⁵ and Nakao⁴⁶ using peel tests on aluminum-polyethylene joints have shown that the peel strengths were unaffected by the presence or absence of transcrystalline regions. Nakao obtained similar results⁴⁷ for Nylon 12-steel joints where adhesive failures were obtained regardless of the presence or absence of transcrystallinity. Detailed systematic studies on these aspects for different adhesives and different bond types, however, have not been conducted to make firm conclusions. This may be area of potential research for workers dealing with semicrystalline hot-melt adhesives.

4.8 Polyimides as high performance adhesives

The bulk of the adhesive work dealing with high performance polyimides has come from workers at NASA^{48,49,50}. The method of choice has been the lap shear test on which the effect of the following variables has been studied:

- (1) effect of conditions utilized during tape making
- (2) effect of bonding time, bonding temperature and bonding pressure⁵¹
- (3) effect of aging time and aging temperature on room temperature lap-shear strengths⁵²
- (4) some results studying the effect of high testing temperature on lap-shear strengths
- (5) few results studying the effect of a limited number of solvents & boiling water on lap-shear strengths⁵³.
- (6) effect of surface treatments.

All the studies to date dealing with polyimide adhesion studies involve the preparation of an adhesive tape and subsequent bonding steps. While many polyimide systems have been thermosetting in origin, the use of this process for thermoplastic polyimides is due to unavailability of melt processable resins and the lack of thermal stability of the polymers above their high melting points. Secondly, as discussed before, the crystallization ability of the past polyimides rapidly deteriorates once taken to melt temperatures. Hence in order to preserve crystallinity which often occurs in the thermoplastic systems during the imidization process, the solvent route is preferred. The adhesive tape serves as:

- (1) a carrier of adhesive
- (2) for bondline control
- (3) the escape channel for solvent and volatile reaction products
- (4) may serve as additional reinforcement

The adhesive tape preparation is laborious and a procedure is presented from a study of Progar et al.⁴⁹ to illustrate the various steps usually involved:

- (a) brush coating of 0.1 mm thick 112 E-glass cloth with 7.5 wt.% DMAc poly (amic acid) solution
- (b) drying of glass cloth in forced air oven at 100°C for 0.5 hour
- (c) priming the scrim cloth with A-1110 finish (γ -aminopropylsilane) and drying for 0.5 hour.
- (d) second coating of 7.5-wt.% DMAc solution is applied.
- (e) placing the tape in forced air oven and conducting the thermal imidization cycle (in their case 1 hour each at 100, 150 and 175°C.
- (f) subsequent applications of 15 wt.% DMAc solution and repeating the thermal imidization cycle.
- (g) repeating step (f) till the desired tape thickness is achieved.

It is obvious that the adhesive tape preparation procedure is very involved, takes a long time and involves repeated handling of dangerous solvents. The repeat imidization steps are necessary due to the thickness effects on imidization discussed in Chapter I.

Various polyimides, which were described earlier in Chapter 3, were tested in accordance with the steps described earlier and using the lap-shear geometry. Jensen et al.⁵⁴ while evaluating LaRC-8515 found that higher bonding pressures produced thinner bondlines and higher strengths. While the strengths were in the range of ca. 6400 psi for bonding pressures of 150 psi (1h at 371°C), they dropped to 5000-5500 psi when the pressure was lowered to 75psi and 5700psi for bond pressure of 84 psi. For samples bonded at 84psi, the strengths decreased with testing temperature with the value of 4310 psi obtained at 177°C. For samples exposed to a variety of solvents for period as long as 2 days, the strengths were found to be in the range of 3380-4700 psi. Progar et al.⁵² found that for different copolymer grades of LaRC-TPI and pasajell treated surfaces, the lap-shear strengths were 4680-4860 psi at RT and dropped to 4180-4450 psi at 177°C. Progar and St. Clair et al.⁵⁰ conducted studies on amorphous grades of LaRC-TPI and found that bonding pressures could be decreased significantly (to 15 psi) by increasing the bonding temperature. Bonding temperatures 20°C in excess of the glass transition only required a 100psi bond pressure while at 350°C (90°C above the glass transition) only very low bonding pressures of 15psi were needed. Average lap-shear strengths as high as 5780psi were obtained at room temperature while at 204°C, various samples were in the range of ca. 3000-4000psi. Solvent resistance of these systems was not reported in this paper. In 1994, St. Clair et al.⁵² again conducted adhesive evaluations on newly developed grades of LaRC-TPI manufactured by Mitsui Toatsu Chemicals, Inc. While the materials could be bonded at temperatures in the range of 343-371°C at low pressures of 15 psi, the materials were amorphous in character. The optimized strengths at room temperature were in the range of 3000-6000 psi and 2000-3000 psi at elevated temperatures. While the strengths were reported to decrease by about 2000 psi after a 72 hour water boil, resistance to solvents was not reported in that paper. Hergenrother et al.⁵³ reported average lap shear strengths for an amorphous polyimide as high as 7850 psi with cohesive failure (the polyimide was based on BTDA dianhydride and 1,3-bis(2,3-aminophenoxy) ethyl ether). The strengths dropped to ca. 4100 psi when tested at 121°C (no aging). The water 72-hour water boil strengths were in the range of 3000-3600 psi. In 1991, Progar and St.Clair⁵⁰ reported the effect of bisimide additives on the strengths of LaRC-TPI bonds. The additives were added to lower the melt viscosity without lowering

the T_g . While some lowering of the bonding pressures was achieved, the elevated temperature strengths dropped. It was found that the additives were not effective in lowering the melt viscosity of LaRC-TPI.

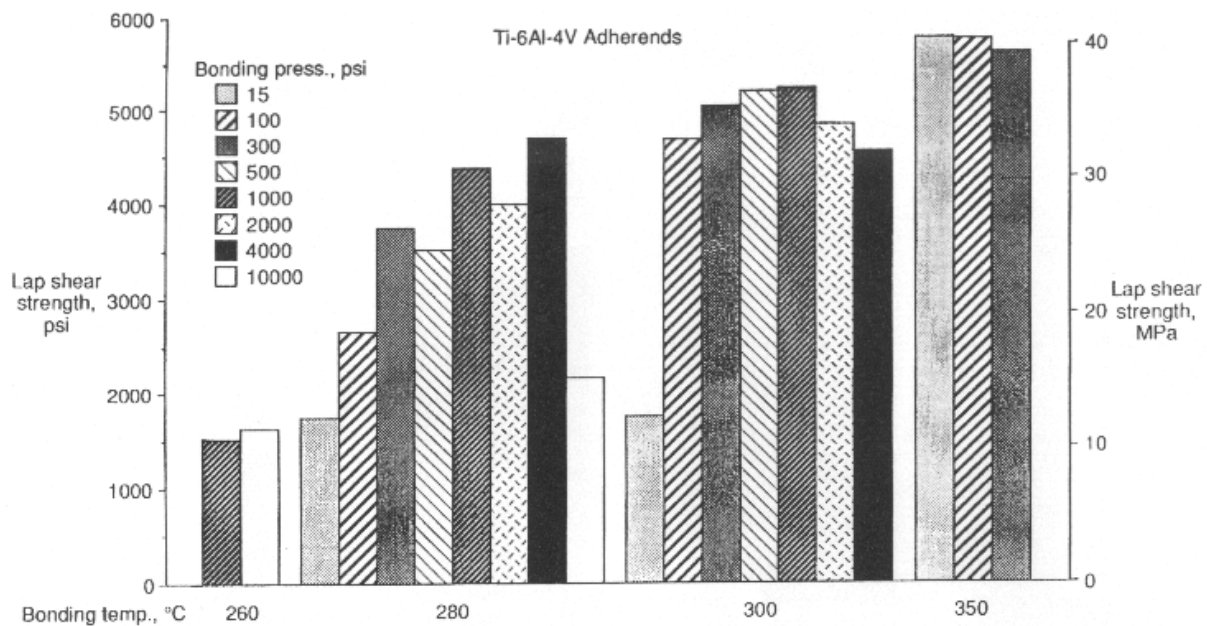


Figure 4.3 Room temperature lap-shear strength of the LaRC-TPI-am adhesive for various bonding temperatures and pressures⁴⁹.

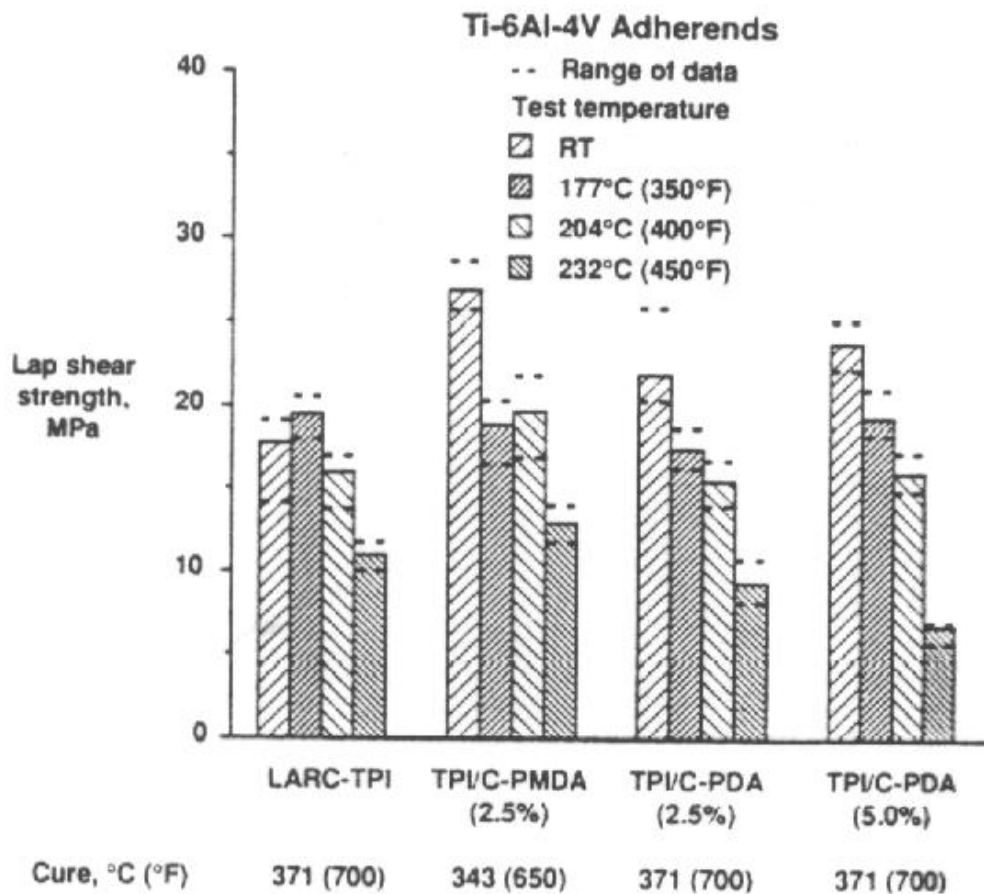


Figure 4.4 Lap-shear strengths for LaRC-TPI and effect of adding various additives (to change the melt viscosity) when bonded at 50 psi⁵⁰.

References:

- ¹ Patrick, R.C., in *Treatise on Adhesion and Adhesives*, **Vol. 2** 1969, Marcel Dekker, New York, V.
- ² Wilson, D., Stenzenberger, H.D. and Hergenrother, P.M. *Polyimides* 1990, Chapman and Hall, New York.

-
- ³ Ghosh, M.K. and Mittal, K.L. in *Polyimides: Fundamentals and Applications*, 1996, Marcel Dekker, New York.
- ⁴ Kinloch, A.J. in *Adhesion and Adhesives-Science and Technology*, 1987, Chapman and hall, London, 311.
- ⁵ McBain, J.W. and Hopkins, D.G. *J. Phys. Chem.*, 1925, **29**, 188.
- ⁶ Venables, J.D., McNamara, D.K., Chen, J.M., Sun, T.S., Hopping, R.L. *Appl. Surf. Sci.* 1979, **3**, 88.
- ⁷ Davis, G.D., Sun T.S., Ahearn, J.S. and Venables, J.D. *J. Mater. Sci.*, 1982, **17**, 1807.
- ⁸ Voyutskii, S.S. *Autohesion and Adhesion of High Polymers*, Wiley Interscience, New York 1963, pg. 127.
- ⁹ Voyutskii, S.S. and Vakula, V.L. *J. Appl. Polym. Sci.* 1963, **7**, 475.
- ¹⁰ Voyutskii, S.S., Vakula, V.L., Smelaya, N.I. and Tutorskii, I.A. *Vysokomolekul. Soedin.* 1960, **2**, 1671.
- ¹¹ Wool, R.P., *Polymer Interfaces, Structure and Strength*, pg. 48, Hanser Publications, Inc., Cincinnati, 1995.
- ¹² Derjaguin B.V., Krotova, N.A., Karssev, V.V., Kirillova, Y.M. and Aleinikova, I.N. *Proc. Int. Congr. Surface Activity*, 2nd, London, III, 1957, 417.
- ¹³ Derjaguin, B.V. and Smilga, V.P. *Proc. Int. Congr. Surface Activity*, 3rd, London, IIB, 1960, 349.
- ¹⁴ Zisman, W.A. *Ind. Eng. Chem.* 1963, **55**, 18.
- ¹⁵ Huntsberger, J.R. in *Treatise on Adhesion and Adhesives* Ed. Patrick, R.L. Vol. 1, Marcel Dekker, New York, 1967, 119.
- ¹⁶ Sharpe, L.H. and Schonhorn, H. *Adv. Chem. Ser.* 1964, **43**, 189.
- ¹⁷ Kinloch, A.J. *J. Mater. Sci.*, 1980, **15**, 2141.
- ¹⁸ Volkersen, O. *Luftfahrtforsch* 1938, **15**, 41.
- ¹⁹ Goland, M. and Reissner, E. *J. Appl. Mech.* 1944, **2**, A-17.
- ²⁰ Sanders, L.R., Baxter, R.S. and Jurgens, R.J. in *Titanium Science and Technology*, Eds. Jaffe, R.I. and Burte, H.M., Vol. 1, Plenum Press, New York, 1973, 105.
- ²¹ Donachie, M.J., Jr., ed., *Titanium and Titanium Alloys: Source Book*, ASTM, Ohio, 1983, 3.

-
- ²² Cotton, F.A. and Wilkinson, G. *Basic Inorganic Chemistry* John Wiley and Sons, New York, 1976.
- ²³ Shaffer, D.K., and Clearfield, H.M. and Ahearn J.S. *Treatise on Adhesion and Adhesives* Ed. Minford, J.D., Vol. **7**, Marcel Dekker, New York, 1991, 437.
- ²⁴ Critchlow, G.W. and Brewis, D.M. *Int. J. Adhesion and Adhesives* 1995, **15**, 161.
- ²⁵ Chawla, K.K. *Composite Materials* Springer-Verlag, New York, 1987.
- ²⁶ Clearfield, H.M., Shaffer, D.K., Ahearn, J.S. and Venables, J.D. *J. Adhesion* 1987, **23**, 83.
- ²⁷ Venables, J.D. *J. Mater. Sci.* 1984, **19**, 2431.
- ²⁸ Moji, Y. and Marceau, J.A. *Method of Anodizing Titanium to Promote Adhesion*, US Patent 3,959,091, The Boeing Company, 1976.
- ²⁹ Filbey, J.A. *Ph.D. Thesis*, Virginia Polytechnic Institute and State University, Blacksburg, VA, 1987.
- ³⁰ Kinloch, A.J. *J. Mater. Sci.* 1982, **17**, 617.
- ³¹ Hart-Smith, L.J. in *Developments in Adhesives-2* Ed. Kinloch, A.J., Applied Science, London, 1981, 1.
- ³² Adams, R.D. . in *Developments in Adhesives-2* Ed. Kinloch, A.J., Applied Science, London, 1981, 45.
- ³³ Harrison, N.L. and Harrison, W.J. *J. Adhesion* 1972, **3**, 195.
- ³⁴ Adams, R.D. *Engineered materials handbook: Adhesives and Sealants* Vol. **3**, Materials park, OH: ASM International, 1995, 325.
- ³⁵ Hart-Smith, L.J. *NASA report*, Washington D.C., Report no. CR-2218, 1974.
- ³⁶ Bascom, W.D. and Cottingham, R.L., *J. Adhesion*, 1976, **7**, 333.
- ³⁷ Hunston, D.L., Bitner, J.L., Rushford, J.L., Oroshnik, J. and Rose W.S., *J. Elastomers & Plastics*, **12**, 1980.
- ³⁸ Packham, D.E. and Evans, J.R.G. *Int. J. Adhesion and Adhesives*, 1981, **1**, 149.
- ³⁹ Fan, Y.L. *J. Adhesion*. 1972, **4**, 261.
- ⁴⁰ Tordella, J.P. *J. Appl. Polym. Sci.* 1970, **14**, 1627.
- ⁴¹ Longhenry, J.L., Murthy, N.S. and Love, B.J. *J. Mater. Sci.* 1997, **32**, 2283.
- ⁴² Schonhorn, H.J. *J. Polym. Sci. Part B*, 1967, **5**, 919.

-
- ⁴³ Schonhorn, H.J. *Macromolecules* 1968, **1**, 145.
- ⁴⁴ Ritchie, P.J.A. and Cherry, B.W. in *Adhesion Vol. 1* Ed. Allen, K.W. Applied Science, London, 1977, 235.
- ⁴⁵ Tordella, J.P. *J. Appl. Polym. Sci.* 1970, **14**, 1627.
- ⁴⁶ Nakao, K. *J. Adhesion Soc. (Japan)*, 1970, **6**, 291.
- ⁴⁷ Nakao, K. *J. Adhesion*, 1972, **4**, 95.
- ⁴⁸ Progar, D.J. and Dezern, J.F. *J. Adhesion Sci. Tech.* 1989, **4**, 305.
- ⁴⁹ Progar, D.J. and St. Clair, T.L. *J. Adhesion. Sci. Tech.* 1994, **8**, 67.
- ⁵⁰ Progar, D.J. and St. Clair, T.L. *J. Adhesion. Sci. Tech.* 1991, **5**, 711.
- ⁵¹ Cano, R.J. and Jensen, B.J. *J. Adhesion* 1997, **60**, 113.
- ⁵² Progar, D.J. and St. Clair, T.L. *J. Adhesion* 1994, **47**, 67.
- ⁵³ Harris, F.W., Beltz, M.W. and Hergenrother, P.M. *SAMPE J.* **Jan/Feb** 1987, 6.
- ⁵⁴ Jensen, B.J., Hou, T.H. and Wilkinson, S.P. *40th Int. SAMPE symposium* **May**, 1995, 1072.

Chapter 5

A Melt Processable Semicrystalline Polyimide Structural Adhesive based on 1,3-bis (4-aminophenoxy) benzene and 3,3', 4,4'-biphenyltetracarboxylic dianhydride.

Abstract:

Introducing crystallinity in polyimides offers the advantage of increased solvent resistance and retention of mechanical properties above the glass transition temperature (T_g). This work examines the thermal stability, semicrystalline morphology and adhesive properties of a new polyimide based on 1,3-bis (4-aminophenoxy) benzene (TPER diamine) and 3,3', 4,4'-biphenyltetracarboxylic dianhydride (BPDA). The polymer has a T_g of ca. 210°C and a T_m of 395°C. Polarized light microscopy was used to evaluate the morphology and spherulitic growth rates from the melt for $M_n=15,000$ daltons and $M_n=30,000$ daltons molecular weight polymer. Lap-shear specimens were made using Ti-6Al-4V alloy coupons using a melt process. Three surface treatments: gritblasting, chromic acid anodization and sodium hydroxide etch were evaluated and it was found that macroroughness provided by gritblasting was sufficient in providing a strong interface. The bonding conditions were optimized with respect to bonding temperature, bonding time and pressure and adhesive bonds made using the optimized conditions displayed a bondline thickness of ca. 2-3 mils. High room temperature lap-shear strengths of more than 6000psi were obtained and the fracture surface investigation using the SEM revealed a very rough and plastically deformed surface. Durability studies on lap-shear specimens were conducted for aging and testing temperatures of ambient, 177°C and 232°C. Significant stability was observed for all these aging and testing temperatures for a period up to seven weeks. The bond strengths were affected by testing temperatures rather than the aging conditions for the duration of the study. The influence of various solvents on

the lap-shear strengths was investigated by immersing the specimens in these solvents for 9 days. None of the solvents had any major effect on the strength of lap-shear specimens.

5.1 Introduction

Aromatic polyimides exhibit good thermal stability, chemical and radiation resistance and have been shown to be promising as high temperature structural adhesives^{1-2,9-10,17-18}. Polyimides are reaction products of diamines and dianhydrides and the final properties such as tensile strength, toughness, modulus and upper use temperature are dependent on the selection of the starting monomers. These aromatic based polyimide materials generally display high glass transition temperatures in the range of 200°C to 400°C or higher, which greatly depends on the stiffness of the backbone chain. However, most polyimides are amorphous in nature and this often leaves them susceptible to attack by different solvents. Thus, introduction of crystallinity in polyimides offers the advantage of increased resistance to solvents and enhanced radiation resistance. The presence of crystallinity can also lead to partial retention of properties much above the glass transition temperature thus effectively increasing the upper use temperature substantially. This makes semicrystalline polyimides very attractive and efforts have continued to develop such materials in various laboratories²⁻⁶. One successful way of introducing crystallinity in the polyimides has been the introduction of flexible aliphatic units in the chain backbone⁷. Although this introduces the crystallinity, it can greatly lower the glass transition temperature thereby often limiting the upper use temperature. Other attempts utilizing a change in the backbone structure have yielded semicrystalline polyimides with glass transitions in excess of 200°C and melting temperatures in the range of 400°C² respectively. However, to process such polyimides, it involves utilizing temperatures in excess of 400°C that often leads to the degradation of the material. Hence, most of the structural polyimide adhesives suffer from the drawback that they are often processed by casting the polyamic acid precursor onto a glass scrim cloth before use in the bonding process. This often involves elaborate adhesive tape/scrim cloth preparation, with the

imidization reaction taking place during this step⁸⁻¹⁰. Sometimes, successive coatings of polyamic acid are applied and the imidization step repeated several times to obtain the desired thickness⁸⁻¹⁰. Also, this often leads to the entrapment of reaction volatiles in the adhesive tape which are finally released during the bonding step. In order to reduce the high financial and environmental costs of such a process, there has been considerable interest in thermoplastic polyimides which are amenable to melt processing^{2, 3,5-7}. Melt processing is advantageous from both the economical and environmental standpoint and offers considerable savings on processing time which makes it very attractive for large scale industrial processes.

The high temperature stability of these materials is usually examined by dynamic or isothermal thermogravimetric analysis which detects the weight loss as either a function of increasing temperature or as a function of time at a given temperature. It has been shown that melt processing of even thermogravimetrically stable polyimides has an adverse effect on the recrystallization ability of these materials². Recrystallization has been shown to decrease substantially with increased temperature and time in the melt; while in most cases it was not possible to attain any crystallinity in the polyimide once it was taken to melt temperatures. Thus, efforts have continued to develop such semicrystalline polyimides that display sufficient thermal and recrystallization stability. Out of the relatively few such polyimides investigated in the literature, many have been characterized in laboratories at Virginia Tech². One such new polyimide developed here is based on 1,3-bis (4-aminophenoxy) benzene (TPER diamine or 1,3(4) APB) and 3,3', 4,4'-biphenyltetracarboxylic dianhydride (BPDA). The polymer has a T_g of ca. 210°C and a T_m of 395°C. This material has shown excellent thermal and recrystallization stability and very fast crystallization kinetics². The polyimide maintained its recrystallization ability after exposure to melt temperatures of 430°C and melt times of 30 minutes, with essentially no changes in the melting temperature and the heat of melting. These characteristics have made this polyimide an attractive candidate for melt processing.

This paper deals with the adhesive properties of this melt processable semicrystalline polyimide with surface treated Ti-6Al-4V alloy coupons using lap-shear test geometry. Although the lap-shear geometry suffers from various drawbacks such as

presence of a bending moment, peel stresses and non-uniform shear stresses along the adhesive layer²⁶, this test serves as a useful tool for evaluating the ultimate strengths of various adhesives and also affords easy comparison with other similar studies in the literature. This test was thus selected for evaluating the adhesive properties of TPER-BPDA-PA. The first steps in the adhesion study were the selection of an appropriate molecular weight polyimide to be bonded and the evaluation of several common surface treatments. Polyimides inherently show a very high melt viscosity due to their rigid aromatic backbone. This has been one of their major drawbacks and efforts have continued to lower the viscosity to improve processability. Wetting of the substrate and good interfacial contact is critical in obtaining a strong and durable interface. The earlier characterization studies with this polyimide involved primarily the use of $M_n = 30,000$ daltons (30K) material. This molecular weight version displayed very high viscosity of the order of 10,000 Pa.s and hence there was a need to lower the viscosity. It was found that lowering the number average molecular weight to 15,000-daltons (15K) decreased the viscosity substantially while still producing films that were creasable. This lower molecular weight allowed the use of lower bonding pressure of ca.100 psi that is in the range of traditional processing equipment, e.g. autoclaves.

Suitable surface preparation is essential in any adhesive work and the presence of a robust interface is necessary for making a strong and durable bond. In this regard much work has been presented in literature with the applicability of various surface treatments for Ti-6Al-4V alloy substrates. The surface treatments generally involve the removal of weak boundary layers and the creation of new surfaces that are chemically and mechanically compatible with the adhesive. Traditional processes like chromic acid anodization (CAA), sodium hydroxide anodization (SHA) and silane coupling agents have been used to form a stable oxide layer on the surface¹¹⁻¹³. Some studies have dealt with the effect of the surface morphology of this oxide layer on bond strength and durability. In this regard the surface treatments have been generally divided into three groups by Venables et al^{14,15}.

These are :

Group I: surface treatments which result in no microroughness ($<0.1\ \mu\text{m}$) or macroroughness ($>1\ \mu\text{m}$)

Group II: surface treatments that result in a large degree of macroroughness. Sandblasting used in this work falls in this category.

Group III: surface treatments that produce a microporous oxide with little or no macroroughness. The chromic acid anodization and sodium hydroxide etch fall in this category although the latter also results in some amount of macroroughness. The presence of microroughness has been advocated for attaining better bonds and much of these arguments are based on increased mechanical interlocking that this microroughness may provide^{13, 14}. Although these oxides have been shown to be effective for moderately harsh environments like 60°C and 95% relative humidity, they result in very low bond strengths if exposed to temperatures higher than 300°C ¹⁴⁻¹⁶. In the present work three such common treatments were selected and evaluated.

The presence of a suitable and strong interface is often indicated by the mode of failure of the adhesive specimen. In this regard, a cohesive failure, i.e. failure in the adhesive, is the desired objective and is a sign of a strong interface. However, once such an interface has been obtained, the strength of the adhesive bond is primarily dependent on the properties of the polymeric adhesive. For a semicrystalline polymer such as the one used in this work, the polymer properties like modulus, yield strength and toughness may significantly depend on the degree of crystallinity and the crystalline morphology. The way the crystalline content is arranged is affected by factors like thermal history, strain in the melt at the time of crystallization, presence of nucleating agents and the molecular weight of the polymer. Crystallization of an unstrained melt, however, typically promotes a crystalline morphology that is usually spherulitic, the spherulites themselves being composed of outward radiating lamellae originating from a centralized nucleation point. The degree of crystallinity within a spherulite may vary significantly for different polymers and also the size and the number of such spherulitic moieties may vary considerably. These factors influence the morphology and the overall degree of crystallinity and are strongly dependent on the structure of the polymer chain, molecular weight and the thermal history. In the present work the semicrystalline morphology was investigated by

optical microscopy as a function of various crystallization temperatures. The effect of crystallization temperature on the subsequent morphology will be discussed. The information gained from this portion of the study was utilized in the development of an optimum thermal cycle for forming the adhesive bonds. The other factors considered in the optimization procedure were bonding temperature, time and pressure.

After optimizing the bonding conditions, the next step was to study the durability of these lap-shear bonds when exposed to high temperatures. High temperature structural adhesives are often required to sustain temperatures of ca. 177°C for a long duration of time^{17, 18}. In addition, the studies dealing with high temperature adhesives often have utilized testing temperatures of ambient, 204°C and 232°C⁸⁻¹⁰. For this study, aging temperatures of ambient, 177°C and 232°C and aging times of 1, 3 and 7 weeks (~1200 hours) were selected. While the material in any such high temperature environment may repeatedly encounter these high temperatures, the failure may be initiated at some different temperature due to various reasons. Thus in this study, all the samples which were aged at room temperature, 177°C and 232°C were also tested at each of these aforementioned temperatures. Finally, the effect of various common solvents on the lap-shear strength will also be presented.

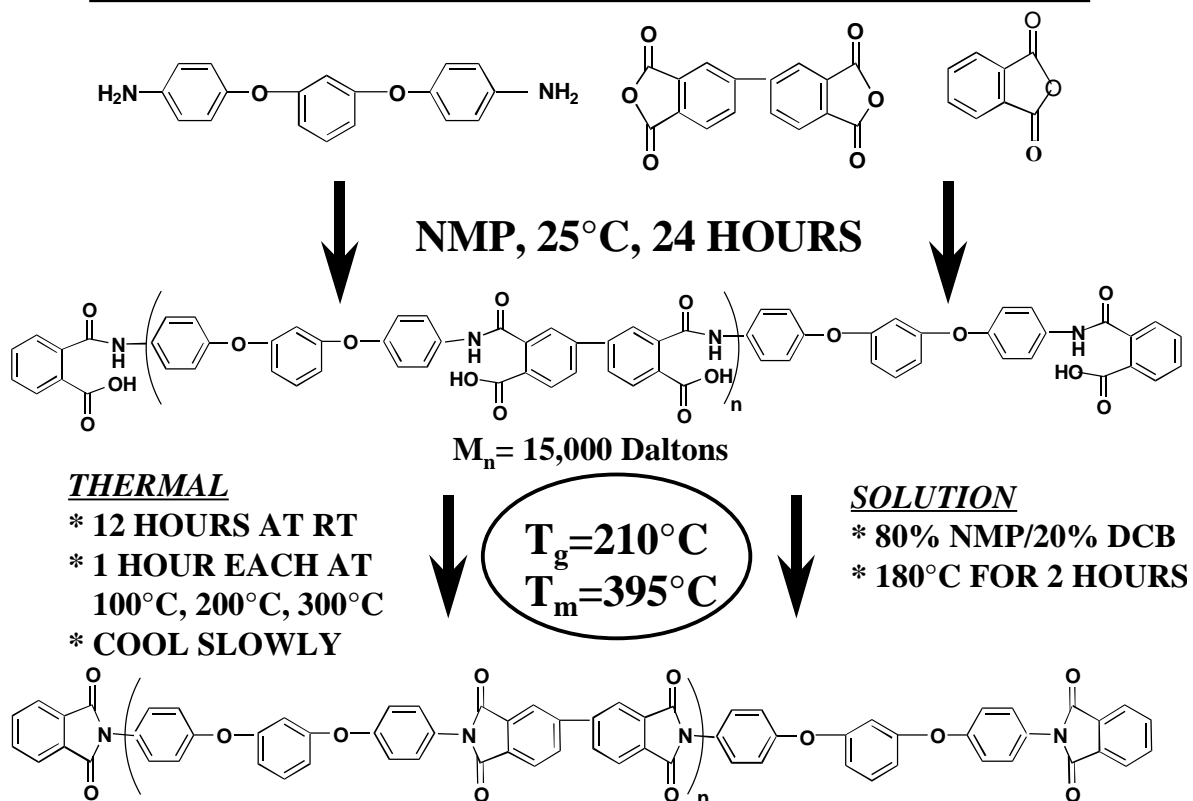
5.2 Experimental

5.2.1 Synthesis

1,3-bis (4-aminophenoxy) benzene (TPER diamine) was supplied by Ken-Seika and was recrystallized from toluene before use. 3,3', 4,4'-biphenyltetracarboxylic dianhydride (BPDA) was supplied by the Occidental Chemical Corporation and was dried at 120°C prior to use. The endcapper phthalic anhydride (PA) was obtained from Aldrich and sublimed prior to use. N-methylpyrrolidinone (NMP) and 1,2-dichlorobenzene (DCB) were obtained from Fisher and vacuum distilled after drying over P₂O₅ before use.

Polymer samples were synthesized with a number average molecular weights 15,000 (15K) and 30,000-(30K) daltons by controlling monomer and endcapper concentration. The monomer concentration was calculated using the Carothers equation. The reaction vessel was a three neck round bottom flask equipped with a mechanical stirrer, nitrogen inlet and a drying tube. Sufficient NMP was added to achieve a 10% solids concentration and the solution was allowed to stir for 24 hours, to afford a homogenous poly(amic acid) solution as shown in Scheme I. A stepwise thermal imidization procedure was utilized which has been used successfully in the past². The first step was the casting of the poly(amic acid) precursor on the pyrex glass plates. It was important in this work to obtain films with uniform thickness as the initial film thickness and the bonding pressure served as the controlling factors in obtaining the desired final bondline thickness. To achieve the desired uniform thickness of the final films (~2mils for 15K and ~3mils for the 30K) and also to prevent any resin flow out of the glass plates, careful control was exercised on leveling the glass plates. This was done by using aluminum base plates equipped with three screws at the corners. The problem of resin overflow was particularly encountered for the 15K resin as the temperature was raised due to the decreased poly(amic acid) viscosity. These plates were placed in the vacuum oven overnight until smooth non tacky films were obtained. Thermal imidization was achieved by raising the temperature to 100°C, 200°C and 300°C and holding at each of these temperatures for 1 hour. The time to go from one temperature to the next was ca. one hour each at the fastest heating rate available with the oven. After the completion of the cycle, the plates were allowed to cool down to room temperature before being removed from the oven. The films were carefully stripped off the glass plates in hot water and stored in a dessicator before use. For preparing the lap-shear specimens the film was carefully cut into pieces having the dimension of 2.54 cm × 1.27 cm and the thickness of was measured using the micrometer before use.

Synthesis of TPER-BPDA-PA



Scheme 5.1 Scheme followed for the synthesis of TPER-BPDA-PA.

5.2.2 Characterization:

Thermogravimetric (TGA) studies utilized a Seiko TG/DTA and all experiments were carried in either a nitrogen or air atmosphere. The temperature was calibrated using indium and zinc standards and the dynamic experiments utilized a heating rate of 10°C/min. The isothermal experiments were performed for a duration of 1000 minutes and the final weight loss reported.

The DSC experiments were conducted with a Seiko DSC 220C on 6-8 mg of sample under a nitrogen purge and a heating rate of 10°C/min unless otherwise specified. Indium, tin and zinc were used to calibrate the temperature and the heat flow. The DSC curves shown in the paper have been normalized to a 1mg-sample mass.

Rheological experiments were carried out on a Bohlin VOR Rheometer using a 12mm diameter parallel plate fixture. The temperature was controlled with a Bohlin HTC using nitrogen as the heating gas. The samples for this test were prepared by pressing together several of the imidized films at room temperature. The fluids torque measuring head was used with a 96 g-cm torque bar. Testing was done using the oscillation mode with a frequency of 0.1 Hz and a strain of 2%. The data was collected from 395°C and the rate of heating was approximately 3°C/min.

Polarized optical microscopy was carried out on a Zeiss optical microscope equipped with a Linkam 600 hot stage and 35mm camera. The hot stage was calibrated using indium, tin and zinc. The same imidized film, which was used for the adhesive work, was also utilized for doing the optical microscopy. The film (~2 mils) was sandwiched between two glass slides and a nitrogen purge was maintained inside the hot stage. The sample was taken to 430°C and kept there for 20 minutes before being quenched to a specific crystallization temperature or cooled to room temperature. The quenching was achieved by using a separate nitrogen source.

For fracture surface analysis of the lap-shear specimens, the overlap area was cut and sputter coated with a layer of gold of ca. 100Å using a Bio-Rad E5400 high resolution

sputter coater. A Cambridge instrument stereoscan model 200SEM was used to analyze the surface structure.

Lap-shear tests were conducted in accordance with ASTM D1002. Ti-6Al-4V alloy was purchased from 'President Titanium Inc.' in the form of $2.54\text{ cm} \times 10.16\text{ cm} \times 0.3175\text{-cm}$ coupons. The strips of the polyimide film were cut into $2.54\text{ cm} \times 1.27\text{ cm}$ pieces after which these were stacked up and carefully placed between the two titanium adherends. For all the bonding purposes the total thickness of the film utilized was 6 mils. Because of this relatively thin bondline thickness, it was important to match the titanium coupons very carefully. Five to six lap-shear specimens were made in a single run of the hot press. The thickness of all the titanium coupons was measured using calipers and the coupons were matched to less than 0.01mm before use. The hot press used was equipped with four thermocouples in the platens. The necessary rate of cooling could be achieved by utilizing water as a coolant. An Instron universal testing machine equipped with a 25,000 lbf. (11,325 kgf) load cell was utilized for breaking the lap-shear specimens.

5.2.3 Surface treatment:

In order to make a strong interface, three different surface treatments were initially evaluated. These were standard sandblasting, chromic acid anodization (CAA) and a sodium hydroxide etch. The coupons utilizing the standard sandblasting were washed in water, dried in an oven and subsequently wiped with acetone. The chromic acid anodization consisted of scrubbing with a crocus cloth to promote a mirror like finish and a water break free surface. The coupons were subsequently soaked in a Isoprep 177 solution (75 g/l) supplied by Boeing for 10 minutes at room temperature with stirring. The coupons were rinsed in de-ionized water and soaked in an acid solution consisting of fuming nitric acid (151 ml), de-ionized water (114 ml) and HF (10.9 ml) for 1.5 minutes. The coupons were rinsed again with de-ionized water and checked for water break free surface. If water did not spread on the surface then the coupons were soaked again in the

acid solution. The anodization was carried out at room temperature in a solution consisting of 45-g/l chromic acid solution for 20 minutes using 5 volts and 1.25 amp/ft². The desired current density was achieved using 48-52% HF solution. The coupons were rinsed with de-ionized water and dried at 50°C for 1 hour. These coupons were stored in a desiccator and bonded within 72 hours of anodization. For the sodium hydroxide etch, the solution was prepared by dissolving Turco 5578 (supplied by Boeing) in deionized water. The coupons were abraded and washed with acetone; subsequently the coupons were immersed in Turco 5578 solution (37.6 g/l) at 70-80°C for 5 minutes. The coupons were rinsed in de-ionized water for 5 minutes at room temperature and immersed in a second Turco solution (360g/l) at 80-100°C for 10 minutes. The coupons were then soaked in deionized water at 60-70°C for 5 minutes and subsequently dried in an oven.

5.3 Results and Discussion

5.3.1 Thermal Stability:

Thermogravimetric analysis has been the traditional method to evaluate the thermal stability of most high temperature polyimides. This technique relies on detecting the loss in sample weight due to emission of volatiles and degradation products as a function of varying temperature or time. Figure 5.1 shows the temperature scans of TPER-BPDA-PA (15K) in air and in nitrogen. The 5% weight loss temperatures in air and nitrogen are 572°C and 564°C respectively. Also, isothermal scans of 15K material at 430°C in air and nitrogen for a duration of more than 16 hours were performed to assess the weight loss characteristics at this melt processing temperature. The 5% weight loss time in air was 372 minutes while there was only 2.4% weight loss in nitrogen after 1000 minutes. These values compare well with other semicrystalline polyimides like New-TPI². However, earlier studies in this laboratory have shown that a thermogravimetric experiment is not the best means to evaluate all the facets of thermal stability of these semicrystalline thermoplastic polyimides if they are to be candidates as melt processable materials. Crosslinking and chain-branching reactions may occur above the melting temperature of the polymer without any significant weight loss. These reactions can adversely affect the recrystallization ability of the polyimide and indeed this seems to be the case for most semicrystalline polyimides investigated in the literature and in this laboratory¹.

Figure 5.2 shows the DSC rescans of TPER-BPDA-PA (15K) after heating the polymer to melt temperatures of 430°C for 1 min, cooling to below the glass transition at a rate of 200°C/min, and then again heating to 430°C at 10°C/min. This was repeated several times although only the initial and the subsequent four rescans are reported here. It is observed that the DSC melting point and $\Delta H_{\text{melting}}$ remain relatively unaffected after repeated exposures to a melt temperature of 430°C. Also, as shown earlier², this polyimide crystallizes during the cooling scan as is indicated by the absence of any

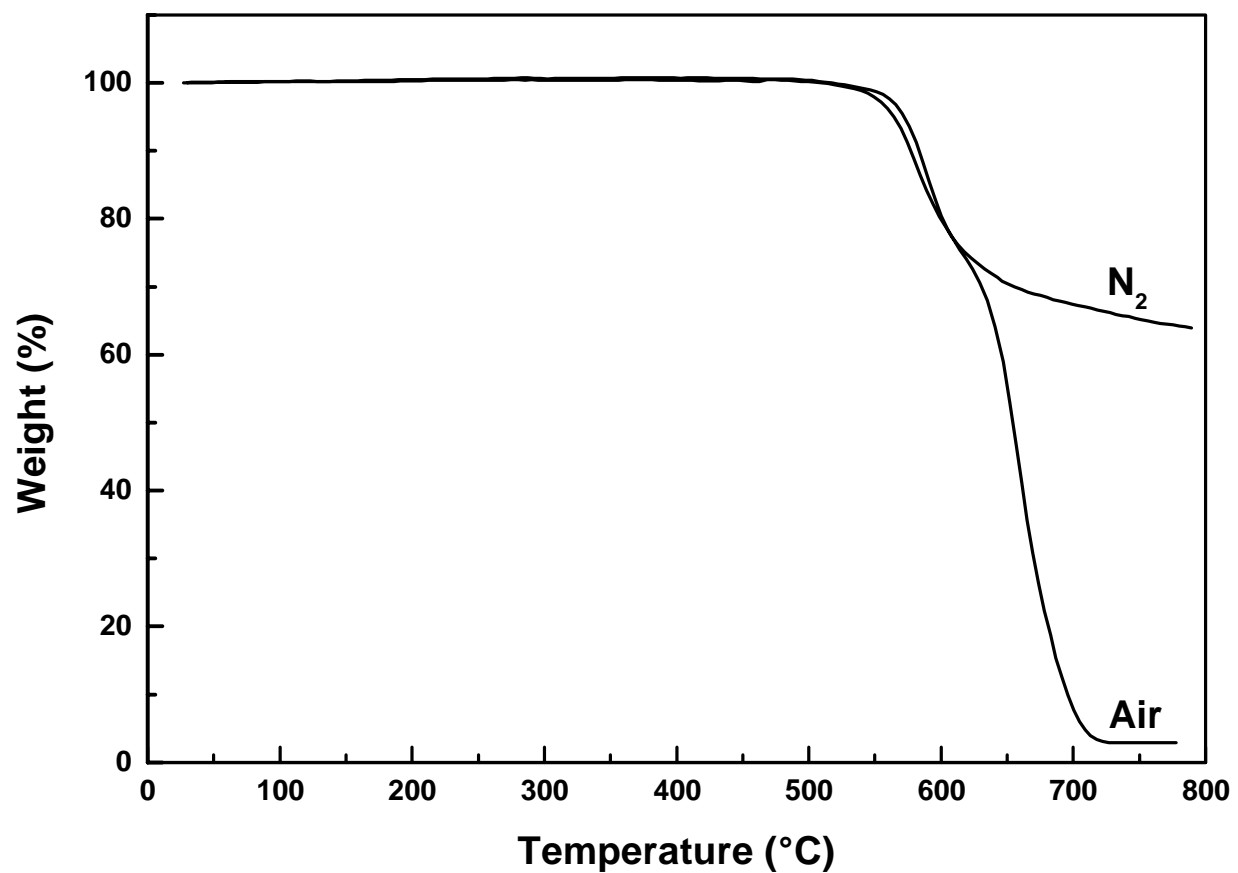


Figure 5.1 Percentage weight loss as a function of increasing temperature in nitrogen and air for TPER-BPDA-PA (15K) when heated at 10°C/minute.

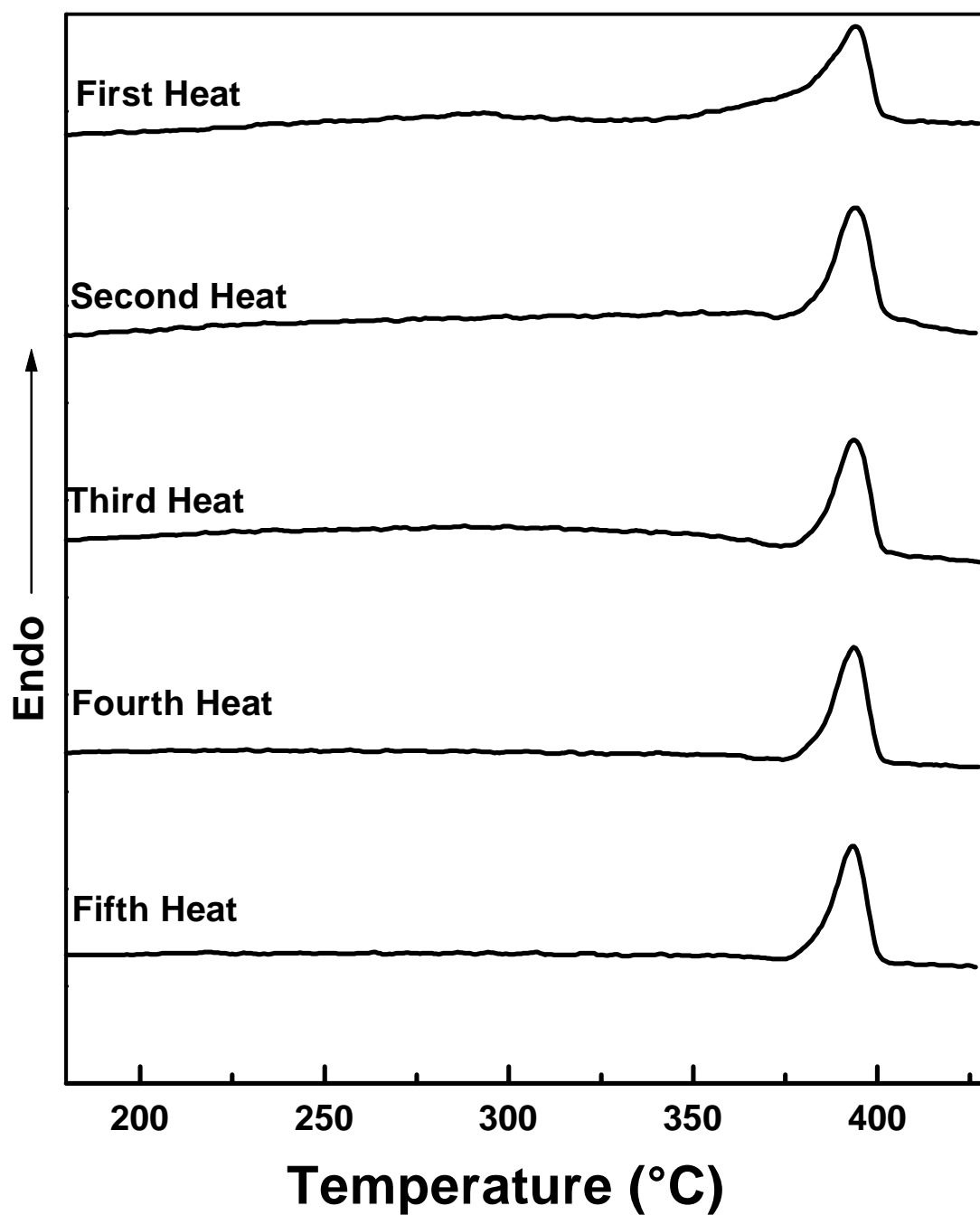


Figure 5.2 Consecutive DSC heating scans for TPER-BPDA-PA ($M_n=15,000$ daltons) after heating to 430°C at 10°C/min, holding for 1 min, quenching to 150°C and reheating at 10°C/min.

significant crystallization exotherm during the heating scan. This indicates the fast crystallization kinetics of the system even after repeated exposures to relatively harsh melt conditions in excess of 400°C. Also, at 430°C this behavior is maintained for 30 min, though for longer duration some effect on the recrystallizability of the material from melt conditions begin to be noted². The reduction in molecular weight from $M_n=30,000$ to $M_n=15,000$ does not affect the recrystallization stability of the material. The $\Delta H_{\text{melting}}$ for the 15K material is 39.6 J/g and for 30K material is 24.5 J/g which indicates the higher amount of crystallinity present in the lower molecular weight sample as might be expected.

5.3.2 Melt Rheology

Melt viscosity is an important property for any hot-melt thermoplastic adhesive application. Lower viscosity is required of the adhesive for enhancing the spreadability and for ease of applicability¹⁹. Often, this requires using the lower molecular weight versions of the polymer or the use of suitable diluents¹⁹. It is well known, however, that molecular weight also affects the mechanical properties of the polymer. At molecular weights below the entanglement molecular weight (M_e) the mechanical properties are generally poor but there is a substantial improvement in the properties as the molecular weight is increased beyond this critical value. The viscosity on the other hand increases with an increase in the molecular weight ($\eta \propto MW^1$ below M_e and $\eta \propto MW^{3.4}$ above M_e). In this regard, most hot-melt adhesives like ethylene-vinyl acetate copolymers, polyvinyl acetates, polyethylene and polyesters can be used above their entanglement molecular weight and yet afford low viscosity. However, this problem is especially significant for rigid chain polymers like aromatic polyimides (like the one used in this work) which often show very high melt viscosity above their entanglement molecular weights. Figure 5.3 shows the viscosity of $M_n=30,000$ daltons TPER-BPDA-PA as a function of increasing temperature. Although the material shows significant thermal stability with the viscosity essentially constant up to 450°C, the viscosity is too high to allow easy spreading at pressures of 100-200 psi, which are common for many structural adhesives. Bonding pressures lower than 300 psi are necessary in order to use the polymer as a structural

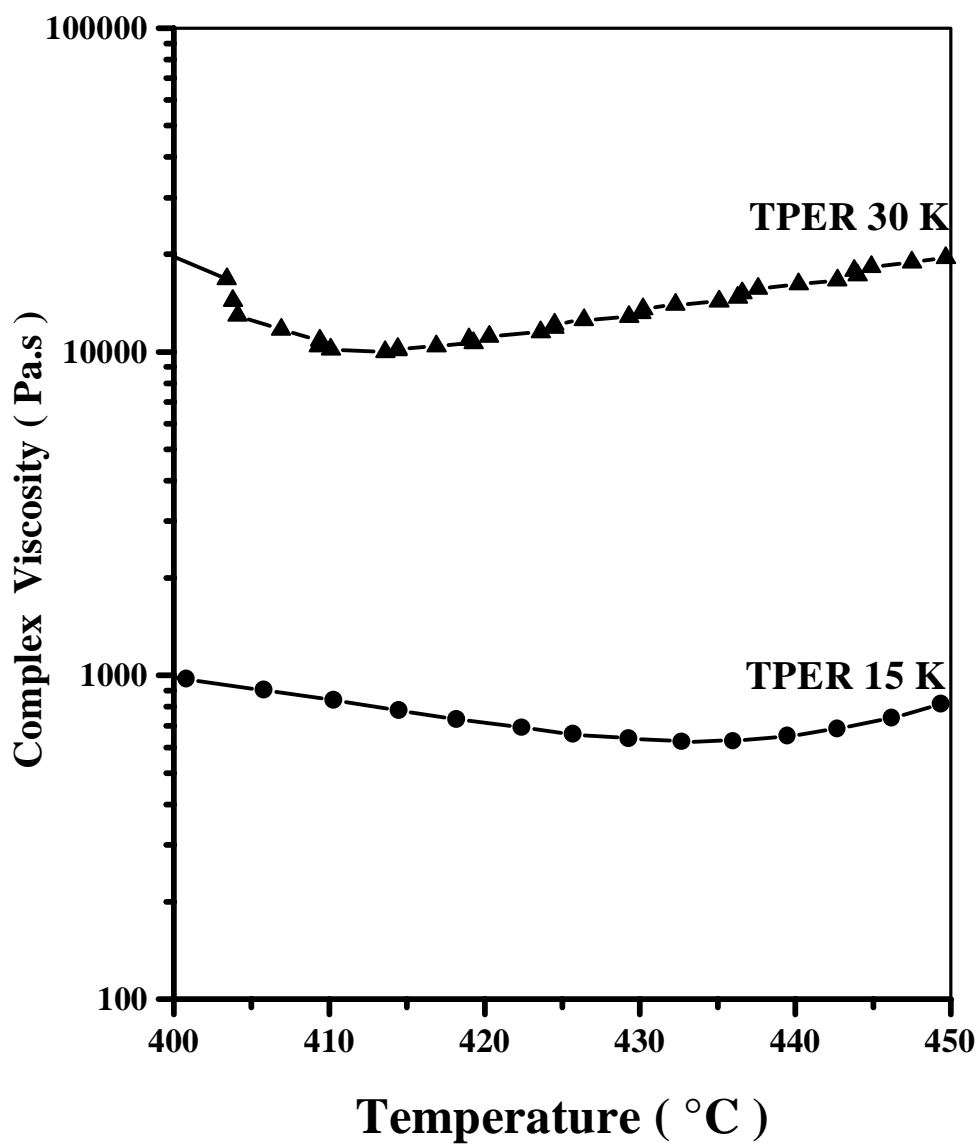


Figure 5.3 Complex viscosity as a function of increasing temperature for TPER-BPDA-PA (30K) and TPER-BPDA-PA (15K).

adhesive in large scale industrial processes^{9, 10}. Hence, the molecular weight was decreased to $M_n=15,000$ daltons (15K) which resulted in a large drop in viscosity by almost an order of magnitude. As stated earlier, the film with this molecular weight was still creasable although the elongation at break in a tensile test was reduced from ca. 140% for the 30K film to ca. 22% for the 15K film at the same strain rate for testing. The polymer with lower molecular weight of 12K and 10K was also prepared but was extremely brittle and lacked any structural integrity for a tensile test. It is clear from Figure 5.3 that the 15K version of the polymer also displayed very good thermal stability with much lower viscosity at temperatures almost 55°C above the DSC melting temperature. The reason for this thermal stability is use of full endcapping of the polymer chains by phthalic anhydride as discussed elsewhere². Hence, the 15K material was selected and the data presented in this paper will focus on the use of only this molecular weight polymer.

5.3.3 Morphology of TPER-BPDA-PA:

The initial cast and thermally imidized film was semicrystalline and showed a fine grainy morphology indicating very small superstructure (Figure 5.4). Recall that this initial film undergoes a complex thermal history where the polyamic acid is converted to polyimide when exposed to temperatures of 100°C, 200°C and 300°C for one hour each. The solvent present during these imidization steps influences the formation of the observed spherulites that melt at approximately 400°C. With respect to the melt crystallization, the two important parameters controlling the final amount of crystallization and morphology are the nucleation density and the spherulitic growth rate. Both these factors are highly dependent on the amount of undercooling and the crystallization temperature. The nucleation density generally increases with increasing amount of undercooling when cooling from the melt²¹. Also, it is well known that for melt

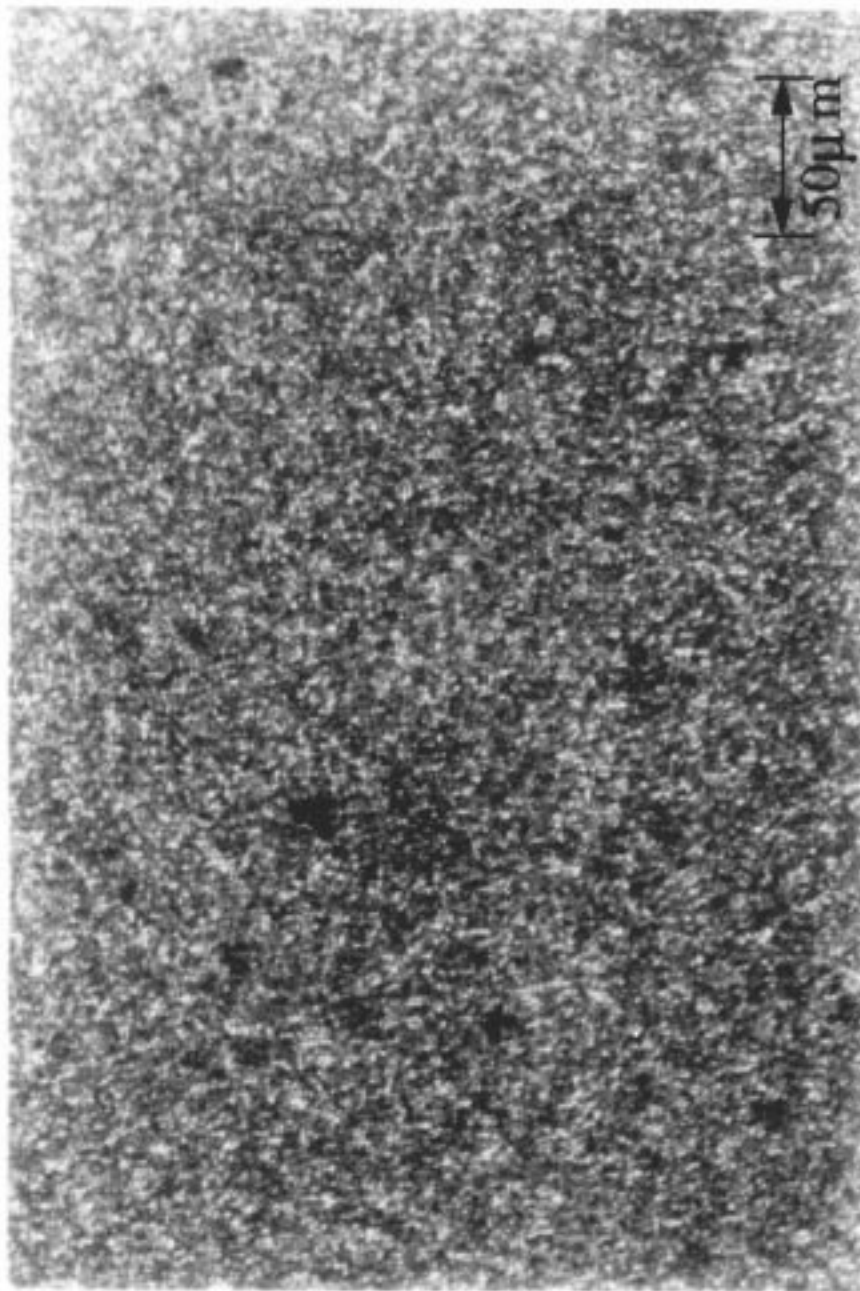


Figure 5.4 Polarized optical micrograph of the initial TPER-BPDA-PA film.

crystallization, a number of nuclei may survive above the DSC melting point²⁰ and influence the final crystallization morphology during the cooling step. For the rigid chain polyimide studied here, the melt temperature and melt times are important parameters influencing the number of nuclei surviving the melt conditions. For these rigid chain polyimides, sufficient nuclei may be present well above the DSC melting temperature that then may aid in the subsequent crystallization on cooling. However, for the results presented here, the samples were exposed for 20 minutes at melt temperatures of 420°C or 430°C. These melt conditions used for the microscopy study corresponded with the conditions used for bonding the lap-shear specimens as will be discussed later. These melt conditions should be sufficient to remove the effect of previous thermal history to a large extent though some nuclei may still survive.

For any semicrystalline polymer, the growth rate of spherulites increases with increasing amount of undercooling till a certain temperature at which these spherulitic moieties show a maximum in growth rate. Below the peak growth rate temperature, the rate of diffusive transport of the chain molecules determines the growth rate and above this peak temperature, the rate of surface nucleation at the growth front of a spherulite (nucleation control) is more important in determining the growth rate. The higher molecular weight sample obviously has much more entanglements for a given polymer chain and thus higher viscosity. Hence the growth rate for higher molecular weight species are significantly lower at any crystallization temperature. Figure 5.5 shows the spherulitic morphologies (15K) observed at different crystallization temperatures after being in the melt for 20 minutes at 430°C. The time at the isothermal crystallization temperature at which these micrographs were taken is also indicated. It is evident that the resulting morphology is very sensitive to the crystallization temperature. At an isothermal crystallization temperature of 355°C, large spherulites are observed which is due to a low nucleation density at this temperature. Also the radial growth rate of the spherulites is quite low as is illustrated in Figure 5.6 which shows the growth rates of spherulites as a function of crystallization temperature. As the crystallization temperature is decreased to 345°C, the nucleation density increases significantly and there is substantial increase in the spherulitic growth rate. In Figure 5.5, the third micrograph shows the semicrystalline

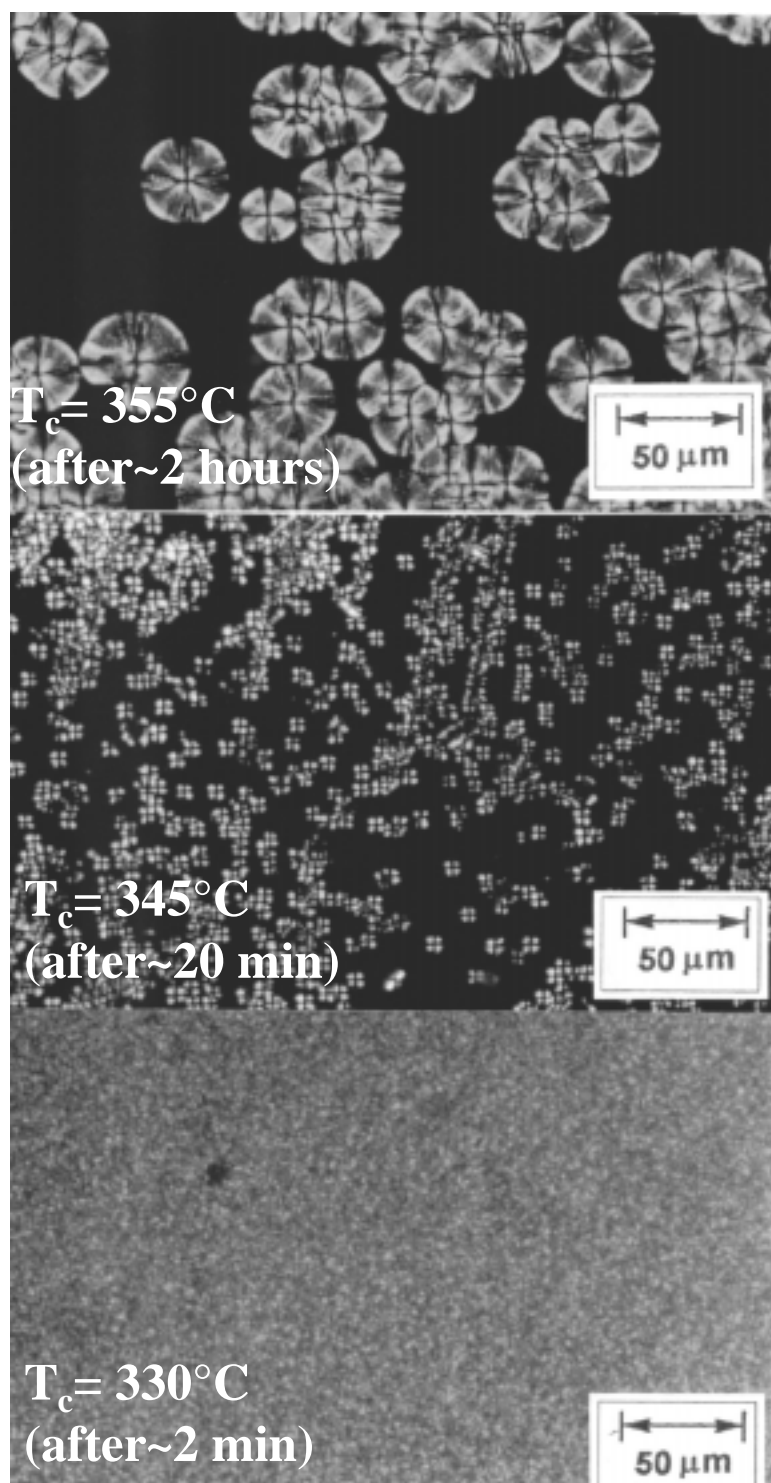


Figure 5.5 Polarized optical micrograph of TPER-BPDA-PA (15K) after heating at 430°C for 20 minutes and subsequent quenching to various crystallization temperatures.

morphology observed for a crystallization temperature of 330°C. In this case there is a large increase in the nucleation density as is indicated by the fine grainy pattern obtained. The size of the crystalline moieties is too small to observe by optical microscopy. The space filling times shown with the respective micrographs are an indication of the difference in the crystallization kinetics with various crystallization temperatures. While it takes only 2 minutes at 330°C to totally fill the volume with small spherulites, it takes ca. 2 hours at 355°C! The induction time at which the first crystallites are observed also decreases from ca. 90 seconds at 330°C to ca. 12 minutes at 355°C. Similar behavior is observed for the 30K TPER-BPDA-PA, although in this case the fine morphology appears at 340°C, also within 2 minutes. The effect of crystallization temperature on the kinetics of crystallization is even more pronounced for the 30K polymer as it shows significantly lower radial growth rates at higher crystallization temperatures as shown in Figure 5.6. The growth rates observed for both the molecular weights are not high compared to growth rates observed for other semicrystalline polymers²¹. Thus it is clear that the increase in nucleation density at temperatures below 340°C is responsible for the fast crystallization kinetics of the system. Also, it was not possible to quench the sample to an amorphous state even after taking it out directly from the hot stage after 430°C, 20 minutes into liquid nitrogen or dry ice and acetone. The fine morphology was obtained regardless of how fast the sample was cooled. For the same reason growth rates could not be observed on the lower temperature side of the crystallization window, where they may be expected to decrease with increasing undercooling.

Few semicrystalline polymers are processed at these high melt temperatures of 420°C and 430°C and thus any crosslinking that may take place at these conditions is of concern. However, if any such reactions are occurring at these conditions then the relative amount of these reactions will be greater at 430°C than at 420°C. Figure 5.6 also shows the growth rates for two different melt treatments of 430°C and 420°C for 20 minutes. Any significant amount of crosslinking or chain branching taking place by raising the temperature to 430°C will reflect in lower growth rates observed at the same crystallization temperature. It is clear that for the melt time utilized, this increase in melt temperature does not influence the spherulitic growth rates for either 30K or the 15K

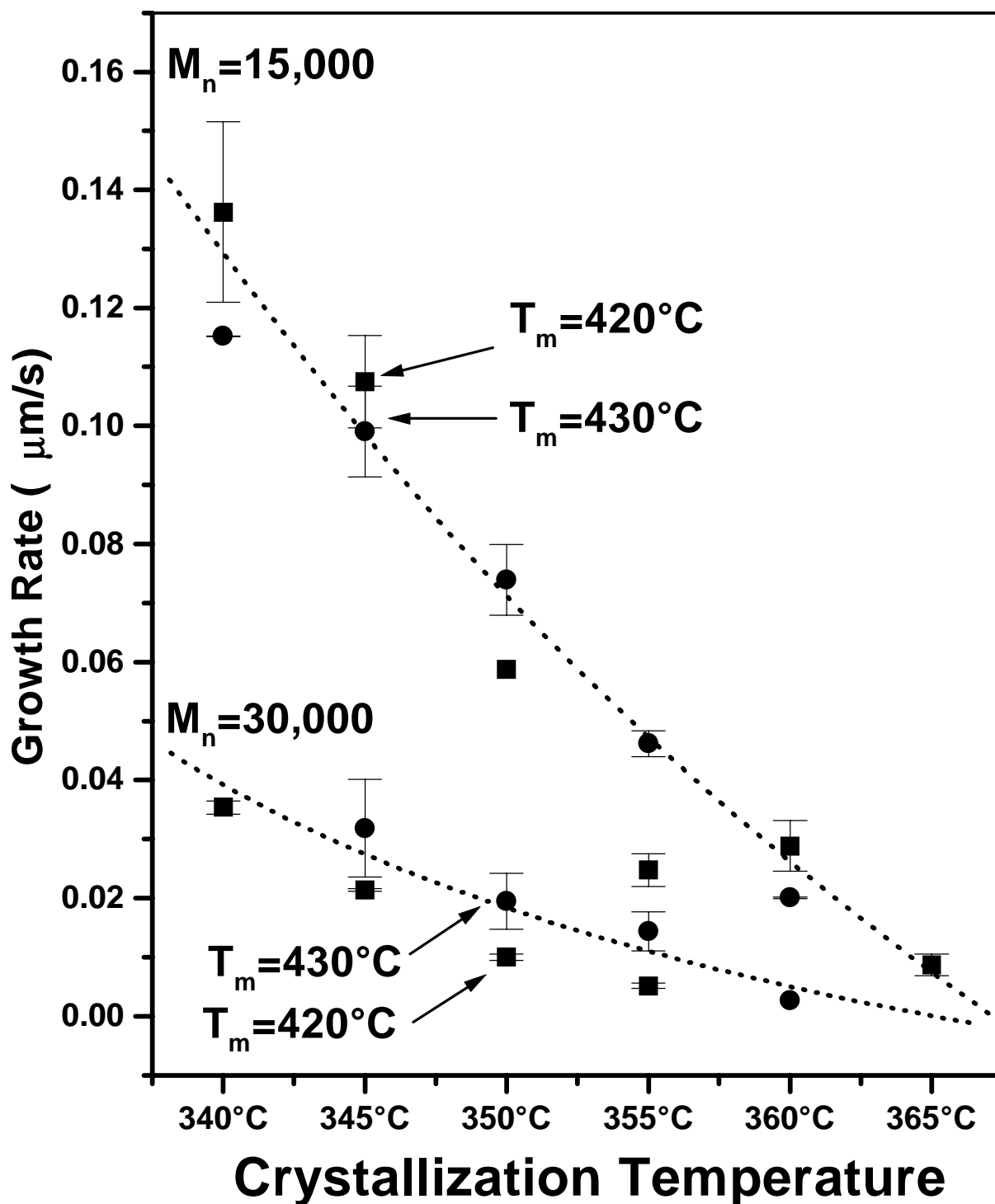


Figure 5.6 Growth rate of spherulites as a function of crystallization temperature for TPER-BPDA-PA (both 15K and 30K molecular weights) after 20 minutes in melt at (■) 420°C and (●) 430°C .

molecular weight. These results thus reinforce the earlier conclusions based on the DSC study about the thermal stability of TPER-BPDA-PA.

It is well known that smaller spherulites result in significantly better mechanical properties than larger spherulites²¹ (other factors like molecular weight, degree of crystallinity etc being constant). Sharples et al.²² showed that the yield stress of a specific nylon 66 increases from 72 MPa to 98 MPa as the average spherulite size was varied from 50 μ m to 3 μ m. Friedrich et al.²³ studied the fracture stress and fracture strain of semicrystalline polypropylene at -40°C for samples with coarse and fine spherulitic morphology. The fracture stress was found to increase from 34 MPa to 64 MPa while the fracture strain increased from 1.5% to 6.5% as the morphology varied from coarse to fine spherulitic. This is not surprising, as the fracture path for a fine spherulitic will be much more tortuous than for the sample with coarse spherulites. Also, depending upon the molecular weight of the polymer, the fine spherulitic microstructure will possess much larger amounts of interspherulitic linkages than the sample with coarse spherulitic microstructure thus providing increased toughness. In fact, specimens displaying large spherulitic structure often show brittle fracture. Thus it is clear that for the polymer used in this study, fine spherulitic superstructure observed at 330°C and at lower temperatures needs to be promoted to attain higher lap-shear strengths. The thermal cycle for preparing the adhesive specimens thus was designed in such a way that the rapid cooling to temperatures in the vicinity of 330° took place. In this regard some adhesive specimens were intentionally made with thin films and unmatched adherends so that it became possible to study the unbonded film with the optical microscope. For any adhesive specimens using slow cooling rates, some coarse spherulites may form although much of the polymer did still consist of the fine structure. Although, any such coarse structure was not observed in any of the samples prepared in such a way, the effect of these few large spherulites will be relatively small as compared to the presence of solely large spherulites.

Also, sometimes transcrystallinity is observed in many polymer samples in the presence of a foreign surface such as a metal like titanium alloy used in this work. This morphology can develop due to the presence of small amounts of strain at the polymer-metal interface leading to high nucleation density. Another explanation for such an effect

results from the heat transfer difference between a surface layer and the bulk polymer resulting in the cooling of the surface layer, thereby resulting in increased nucleation density. This results in the formation of large amounts of outwardly radiating crystalline lamellae from the foreign surface. Such an effect, if present, may alter the properties of the interface significantly. In this regard several experiments were conducted using the titanium alloy coil which was grit blasted in a fashion similar to that used for adhesive specimens and the 15K TPER-BPDA-PA film. Various optical microscopy experiments conducted at different isothermal crystallization temperatures and at various cooling rates from the melt gave no evidence of any transcrystallization on the metal surface. Thus transcrystallization was ruled out for any of the adhesive specimens presented in this work.

5.3.4 Surface Preparation:

Much work has been done evaluating the durability and strength provided by chromic acid anodization (CAA) and sodium hydroxide etching (SH) as surface treatments¹¹⁻¹⁵ for Ti-6Al-4V alloy. Venables^{14, 15} and coworkers found excellent results with CAA and SH surface treatments with respect to the durability of adhesive joints when using liquid resins and attributed this to penetration of the microporous oxide layers by the liquid resin. Other workers^{11, 13} have also advocated the use of surface treatments producing large amounts of microroughness to improve the durability of adhesive joints although most work in this regard has been done with liquid resins, thermosets or low viscosity amorphous polymers. In this work, three such common surface treatments-CAA, SH and sandblasting were evaluated for bonding the Ti-6Al-4V alloy coupons with TPER-BPDA-PA. For evaluating these surface treatments, the titanium alloy coupons were bonded at conditions of 420°C, 20 minutes and a pressure of 300 psi. The highest lap-shear strength was obtained for the sandblasted specimens (2500-psi) whereas the chromic acid anodization gave the lowest values (500-psi). The lap-shear strengths of bonds using the sodium hydroxide etch as surface treatment fell between the two values

(1500-psi). Also, perhaps more important than the absolute values of these lap-shear strengths obtained was the fact that chromic acid anodization and sodium hydroxide etch always gave 100% adhesive failure (by visual inspection) whereas sandblasting gave cohesive failures. These results were not surprising and support the earlier studies done with regards to the high temperature instability of the chromic acid and sodium hydroxide treatments. Clearfield et al.^{11, 12} have showed the lack of stability of the oxide metal interface at temperatures approaching 300°C. They found that dissociation of oxide followed by the dissolution of oxygen into the alloy led to the formation of an embrittled zone on the surface. It is clear, that in the present case, macroroughness provided by the sandblasting technique was sufficient in giving a strong interface. However, for the CAA and SH surface treatments, significant degradation of the oxide layer will already take place before the adhesive melts at ca. 400°C. Also, it is unlikely that microroughness present in the chromic acid and sodium hydroxide treatments will provide a significant amount of interlocking as the bonding pressure used in this work (100 psi) will be insufficient to force the high viscosity polymer melt into the nanometer sized pores provided by these treatments. The slightly higher values obtained by the SH treatment may be due to the presence of a substantial amount of macroroughness often present for this treatment.

Hence, sandblasting was selected as the surface treatment for this adhesive study. The lap-shear strengths obtained on bonds exposed to 232°C for 7 weeks (presented later in the paper) and cohesive failures of specimens in these cases show the long term high temperature stability of these treatments. Also, the high strengths and cohesive failures of samples exposed to various solvents (for up to 9 days) point to the durability of this surface treatment in the present case.

5.3.5 Optimization of Bonding Process:

It is well known that for any hot melt adhesive application there are at least three important parameters that will affect the degree of spreading and thus these need to be properly controlled in order to attain good adhesion¹⁹. These are the melt temperature, the bonding pressure and the bonding time. These conditions were optimized in this study to obtain high lap-shear strengths. Lower molecular weights and higher temperatures have been proven to increase the ease of spreading significantly by lowering the viscosity of the polymer melt. Wightman et al.²⁴ showed that the wetting of the metal by polystyrene increased significantly as the temperature was increased. Figure 5.7 shows the lap-shear strengths when the bonding temperature was varied from 420°C to 430°C while the bonding time and pressure were kept constant at 20 minutes and 300 psi respectively. Temperatures higher than 430°C were not selected as recrystallizability of the material begins to decrease at 440°C. The lap-shear strength improved significantly over this range from 4000 psi to ca. 6600 psi and thus 430°C was selected as the bonding temperature. The next step was to vary the bonding time keeping the bonding temperature and bonding pressure constant. It was found that the average lap-shear strengths increased from 6000 to 6600 psi when bonding time was increased from 10 to 20 minutes (Figure 5.8) though the average values are well within the range of error for the two cases. However, the specimens bonded for 30 minutes showed reduced strengths (3500 psi). Thus 20 minutes was selected as the bonding time which is relatively low compared to times required for bonding with other high temperature adhesives. Also, for hot melt adhesives, the high viscosity results in low interfacial contact area due to the presence of voids and air at the substrate surface. Thus increasing the bonding pressure helps in increasing the interfacial contact area. In this regard, bonding pressures of 100-300 psi are common when using high temperature polymeric adhesives^{8, 9, 10}. Four different bonding pressures were tried for this study: 100, 200, 300, 500 psi. As shown in Figure 5.9, the average bond strengths obtained were within the error bars associated with the lap-shear tests. Thus it was found

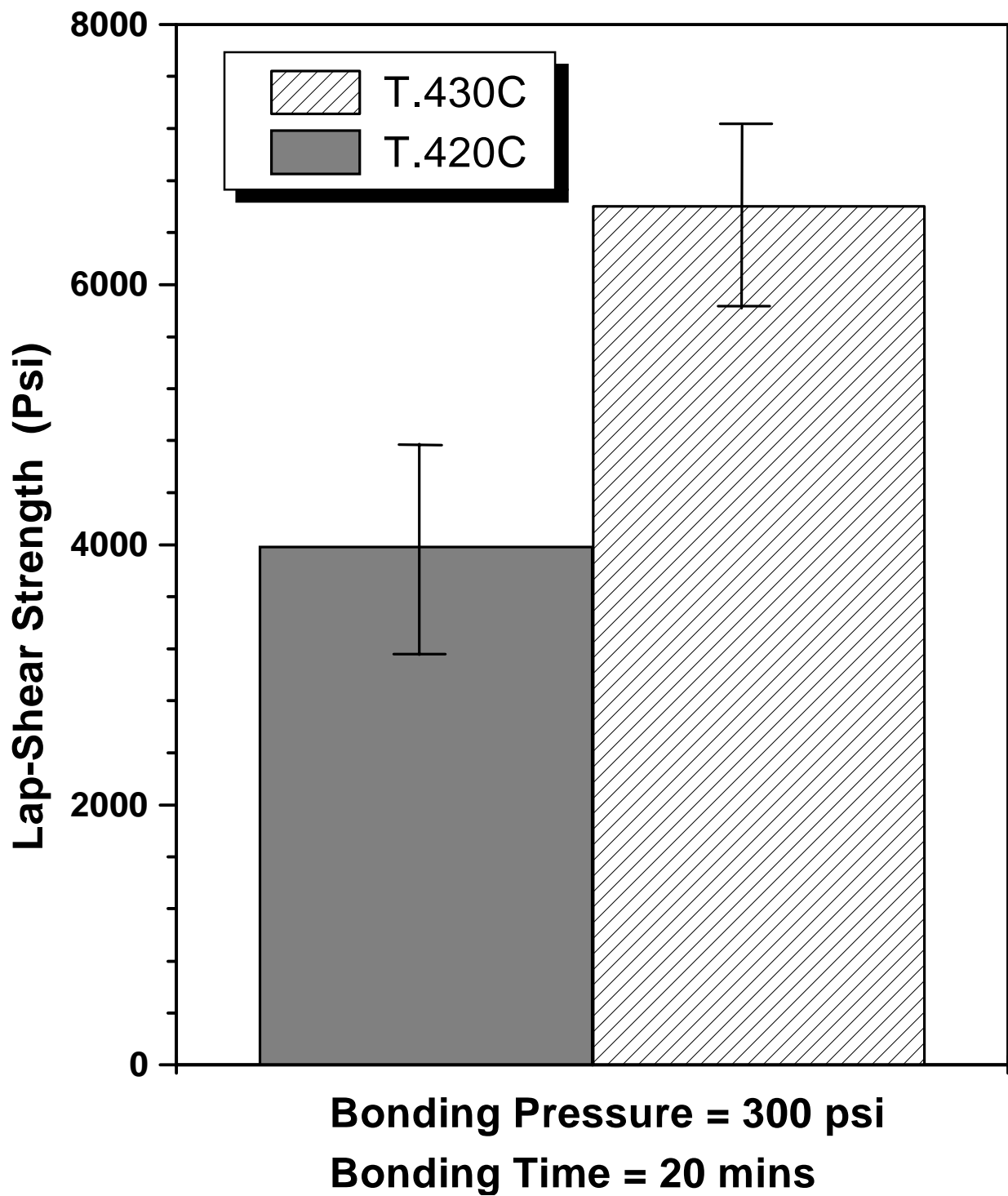


Figure 5.7 Lap-shear strengths as a function of bonding temperature (420°C and 430°C). Bonding pressure and bonding time were kept constant at 300 psi and 20 minutes respectively.

that a pressure of 100 psi, which is also within the range of traditional autoclaves was sufficient to attain good bond strengths. Pressures lower than 100 psi were not tried due to the limitations of the hot press. Also as discussed earlier, the cooling step was designed such that the fine spherulitic superstructure was developed. This was accomplished by cooling at $\sim 20^{\circ}\text{C}/\text{min}$ to 340°C , holding at that temperature for 5 minutes followed by slow cooling. This cooling cycle was followed for all the results presented in this paper. The overall thermal cycle thus is shown in Figure 5.10 whereas Figure 5.11 lists the bonding conditions that were tried and those that were finally selected.

The average lap-shear strengths obtained at the optimized conditions are of the order of 8400 psi (which compare favorably with the highest values reported for other polyimide adhesives) while some individual specimens showed lap-shear strengths as high as 9800 psi. In fact, significant bending of the 3.175-mm thick titanium alloy coupons was observed for some of these specimens. This makes this material a strong candidate as a structural adhesive for areas demanding high strengths at high temperatures. The fracture surface of the broken lap-shear samples was analyzed using SEM and a representative micrograph is shown in Figure 5.12. It is evident that the polymer provides a very rough and plastically deformed fracture surface. Similar features were observed on both sides of the fractured lap-shear specimens. This kind of rough fracture surface is uncommon for most high performance thermosetting adhesives and likely is responsible for the high strengths obtained for this material.

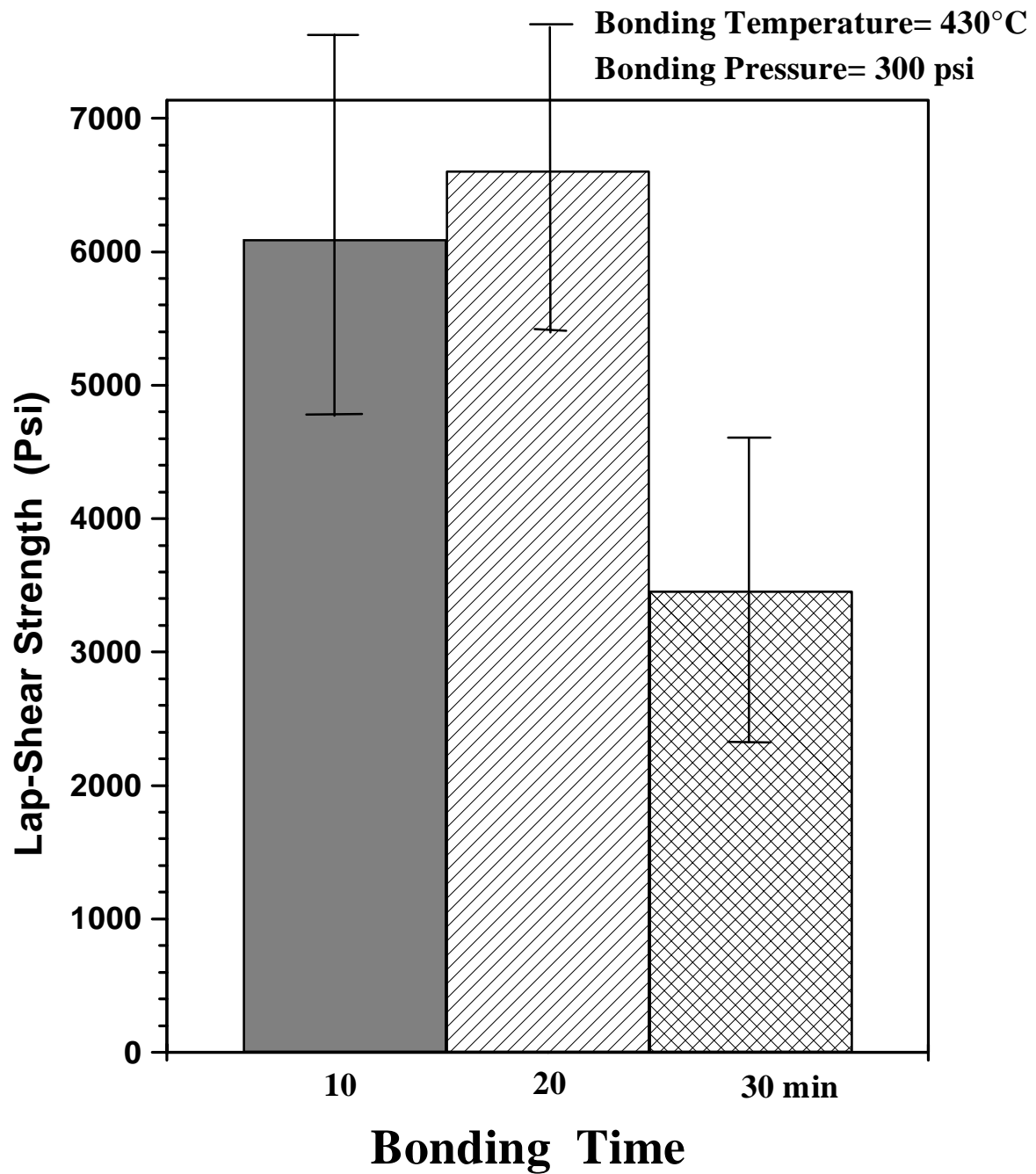


Figure 5.8 Lap-shear strengths as a function of bonding time (10, 20 and 30 minutes). Bonding pressure and bonding temperature were kept constant at 300 psi and 430°C respectively.

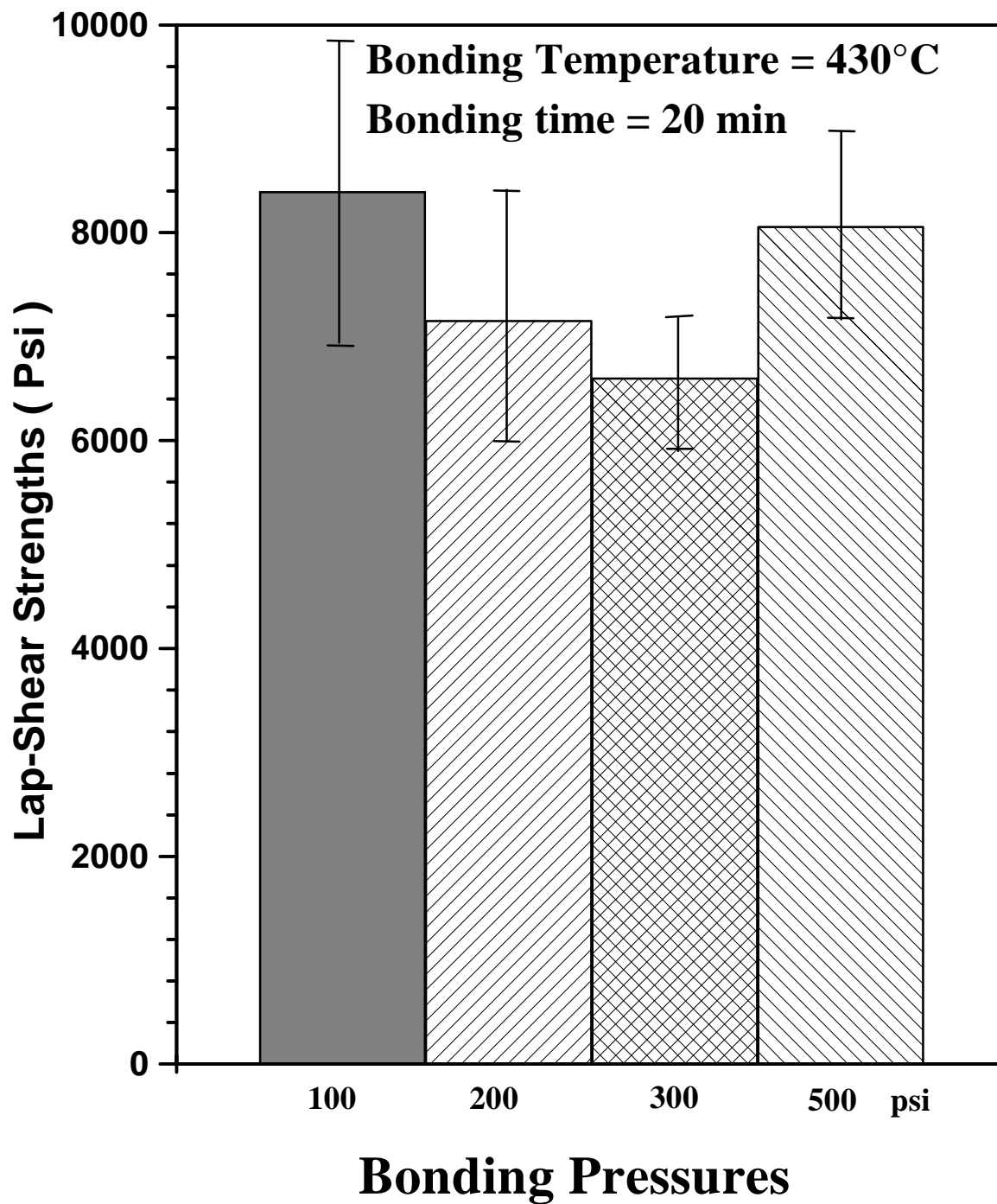
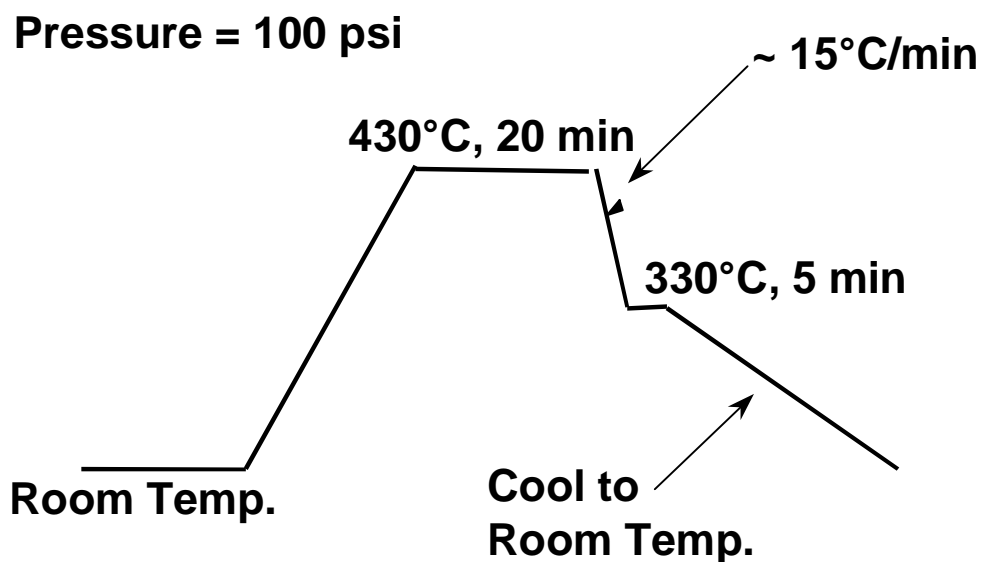


Figure 5.9 Lap-shear strengths as a function of bonding pressure (100, 200, 300 and 500 psi). Bonding temperature and bonding time were kept constant at 430°C and 20 minutes respectively.



Thermal Cycle for TPER-BPDA-PA Lap-Shear Specimen Preparation

Figure 5.10 Thermal cycle followed for preparing lap-shear specimens.

Optimization of the Bonding Process

1. Surface Preparation:

Chromic Acid Anodization

Gritblasting

Turco 5578

2. Bonding Temperature:

420°C

430°C

3. Bonding Pressure:

100 psi

200 psi

300 psi

500 psi

4. Bonding Time:

10 min

20 min

30 min

Figure 5.11 Scheme illustrating the conditions tried and finally selected for optimization of the bonding process.

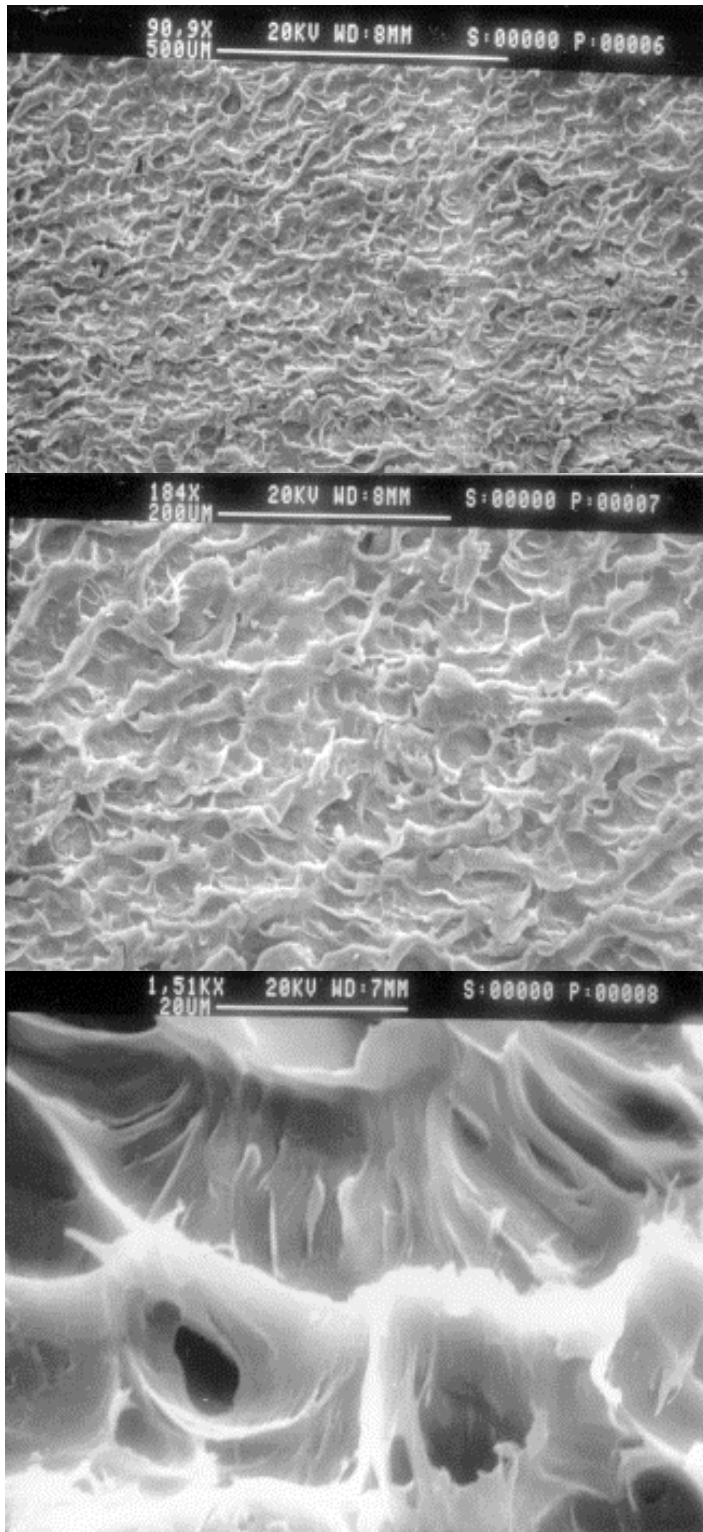


Figure 5.12 SEM micrographs of the fracture surface of the lap-shear specimens.

5.3.6 Durability Studies on Lap-Shear Bonds

Considerable work has been done by workers at NASA^{8-10, 17,18} with respect to durability of lap-shear bonds when exposed to high temperatures for extended periods of times. In this regard, testing of bonds exposed for long times at 177°C, 204°C and 232°C has been done while in a few studies lap-shears have been tested at these temperatures after extended periods of aging. Nonetheless, it is sufficient to say that for any material being used in such high temperature environments, degradation of the polymeric adhesive or the interface may lead to failure at the use temperature or some other higher or lower temperatures that the adhesive may experience. Also, thermal stresses may build up due to difference in the thermal expansion coefficient between the adhesive and the adherend leading to failure of the adhesive bond. Thus while aging temperature and time are important variables of interest, the importance of testing temperature cannot be ignored. In this study results are presented for specimens aged at temperatures of ambient, 177°C and 232°C for a period of 1, 3 and 7 weeks. In addition all the specimens aged at these conditions were also tested at temperatures of ambient, 177°C and 232°C. Figure 5.13 shows the overall aging and testing scheme followed in this study. For each test, 4-5 specimens were used. It is important to point out that while 177°C is 33°C below the glass transition, the aging and testing temperature of 232°C is 22°C above the glass transition of the polymeric adhesive. In this regard the presence of crystallinity and the nature of crystalline morphology becomes important in maintaining sufficient strength above the glass transition. Figure 5.14, 5.15 and 5.16 present the results obtained for different aging temperatures as a function of aging time and three testing temperatures. It is clear that for any given aging and testing temperature the specimens maintain their strengths (within the range of error) with varying aging times. Also it is evident that the

Aging Study of Lap-Shear Bonds

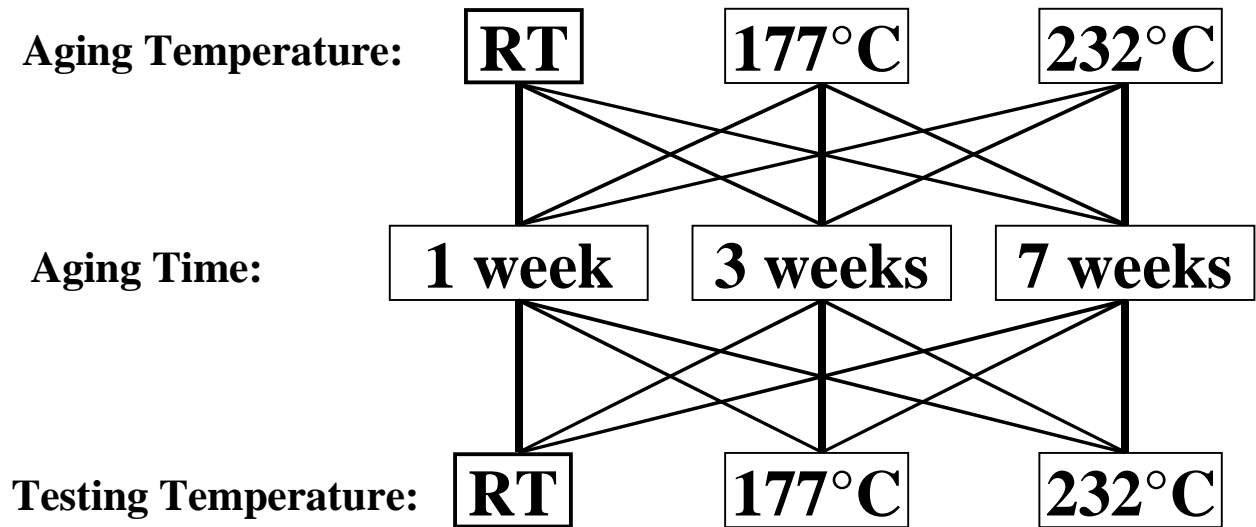


Figure 5.13 Scheme followed in the aging study of the lap-shear bonds.

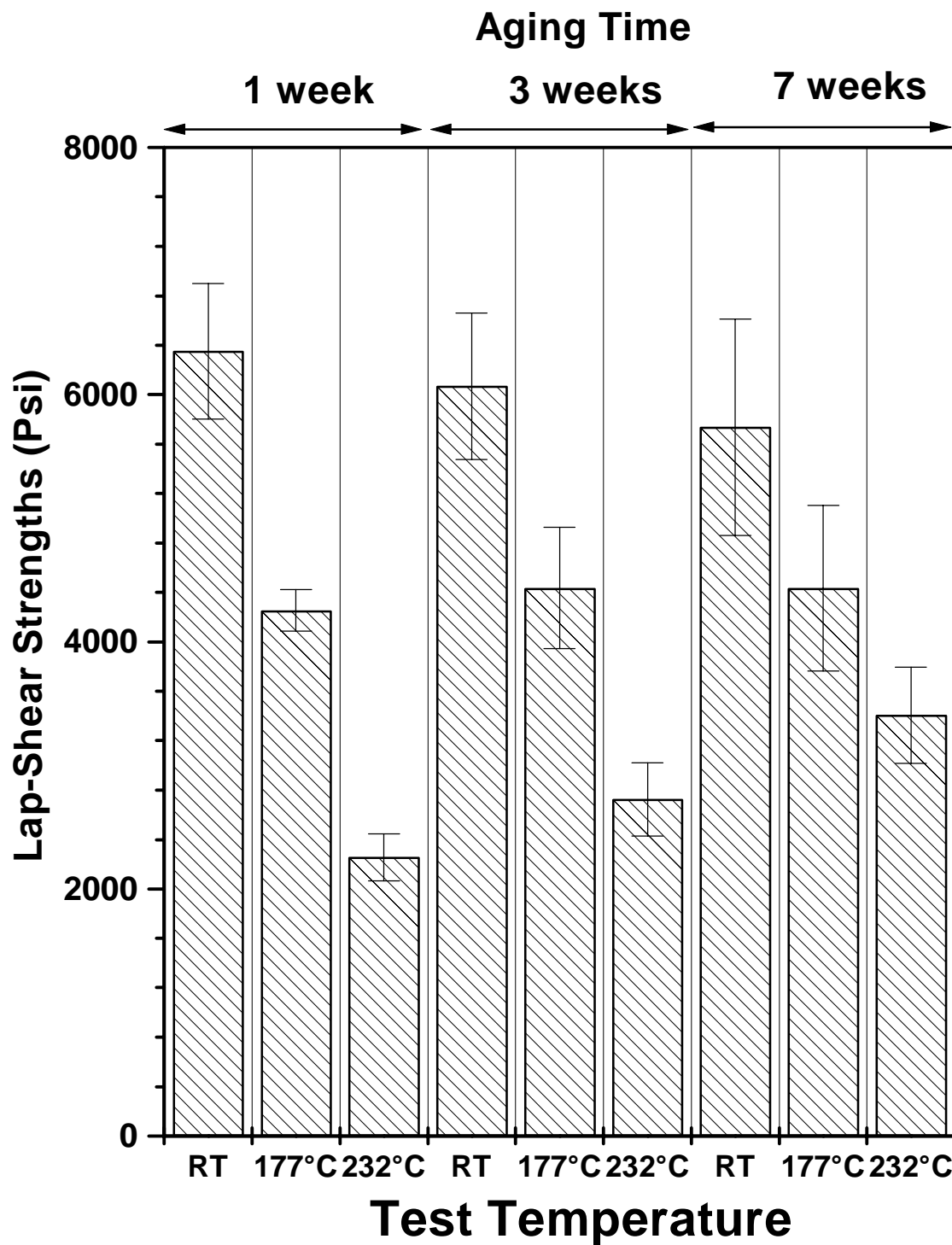


Figure 5.14 Lap-shear strengths after aging at room temperature for a period of 1,3 and 7 weeks and testing at ambient, 177°C and 232°C.

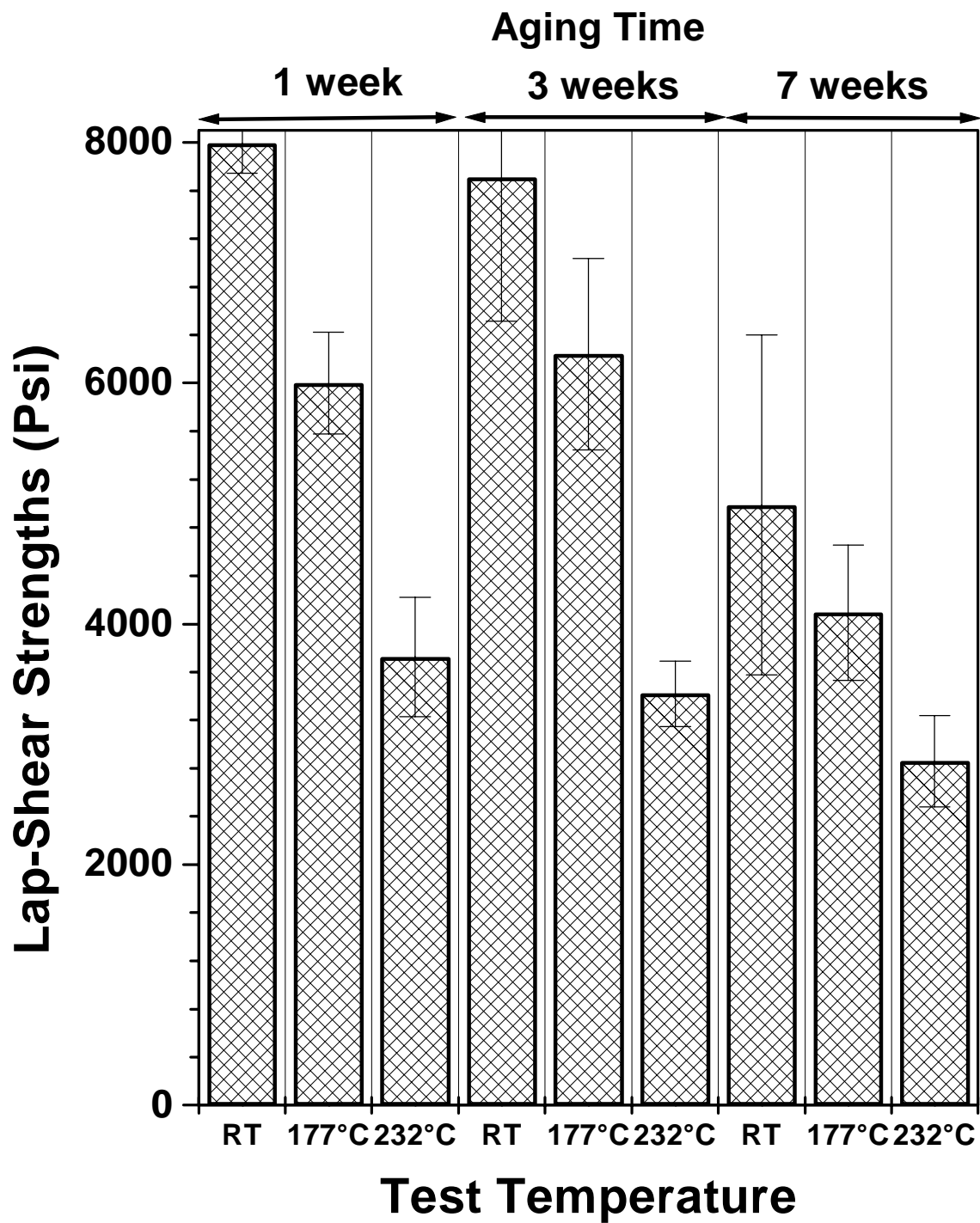


Figure 5.15 Lap-shear strengths after aging at 177°C for a period of 1,3 and 7 weeks and testing at ambient, 177°C and 232°C.

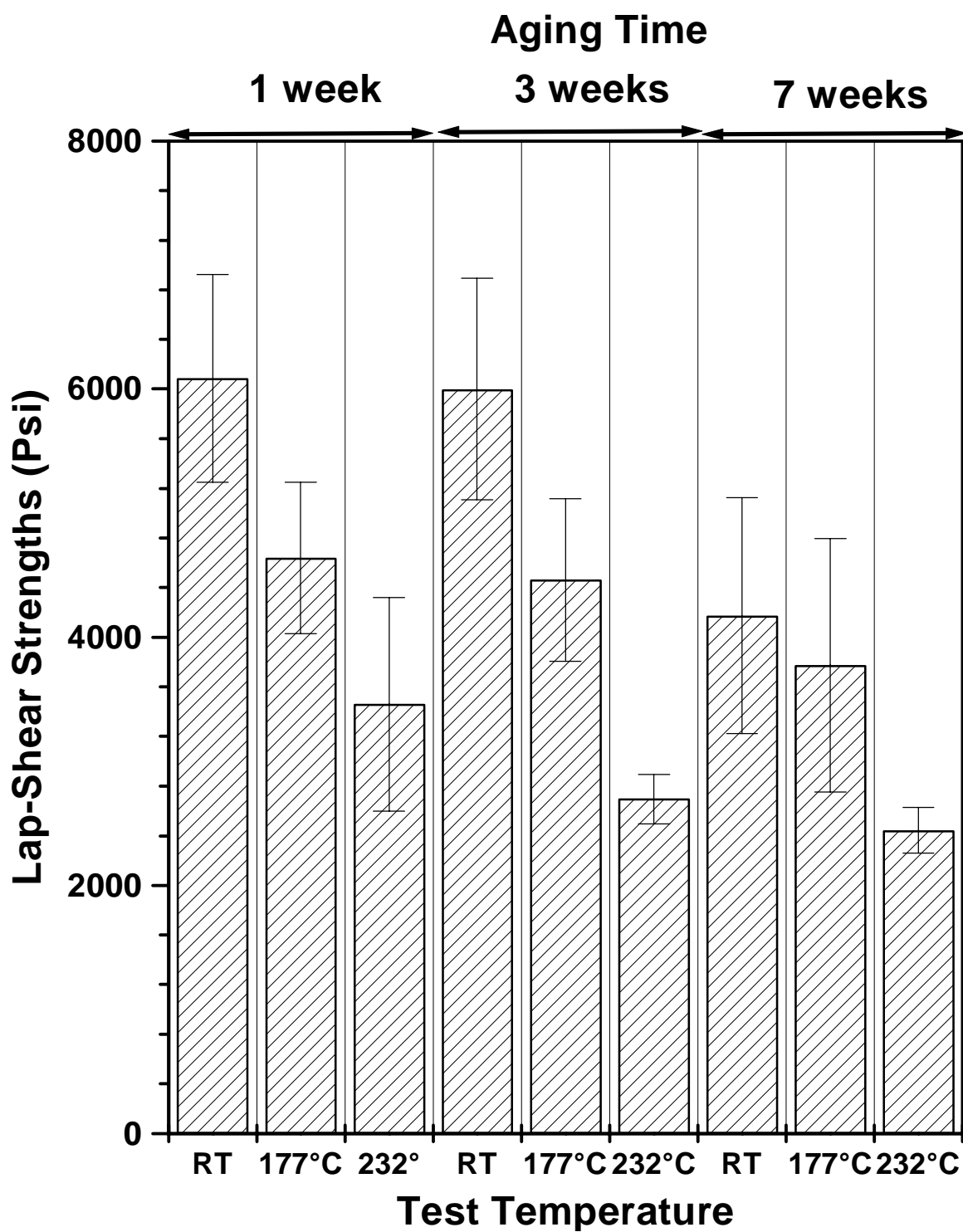


Figure 5.16 Lap-shear strengths after aging at 232°C for a period of 1,3 and 7 weeks and testing at ambient, 177°C and 232°C.

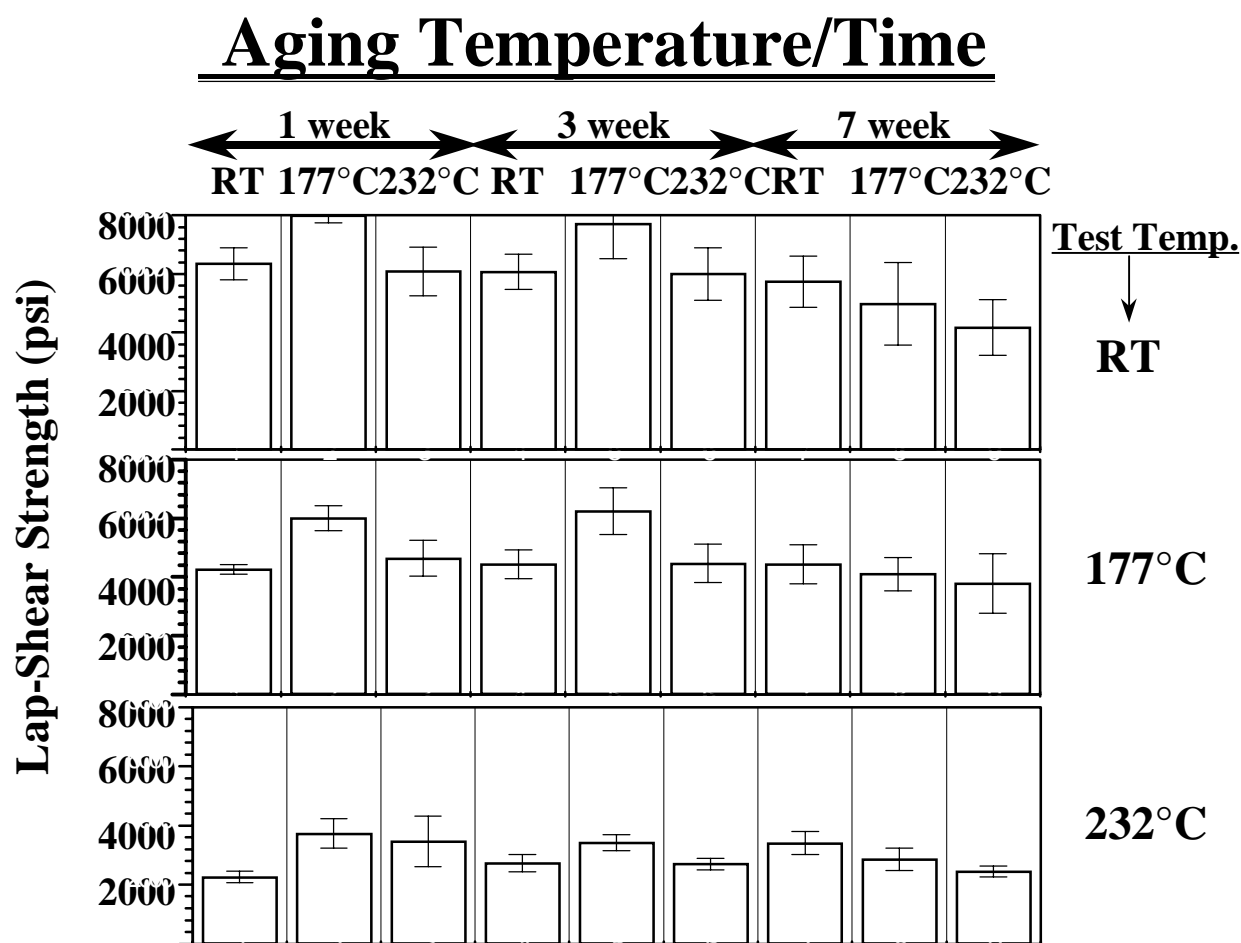


Figure 5.17 Lap-shear strengths shown as function of test temperature for various aging times and aging temperatures.

testing temperature and not the aging temperature affects the lap-shear strengths obtained. The strengths always decrease with increasing test temperature as would be expected. Figure 5.17 presents all the data in a slightly different form which makes it clear that the bond strengths are a function of test temperature and remain relatively unaffected by aging temperature or time for up to seven weeks. While the strengths vary between 6000-8000psi for an ambient test, they are between 4000-6000 psi for at 177°C. Also, interestingly the material shows good bond strengths of 2500-4000 psi for test temperatures of 232°C. These values compare favorably with some of the highest values reported at these temperatures for some other polyimides by workers at NASA⁸⁻¹⁰. The semicrystalline nature of the polymer is thus clearly advantageous in this regard. These results make this material a strong candidate for any high temperature and high service environment needed for advanced aerospace applications and further long-term aging studies are continuing.

5.3.7 Effect of various solvents:

The lap-shears were tested against various solvents which the adhesive may encounter when used as a structural adhesive. These solvents were selected on the basis of similar studies done by others^{8-10, 17,18} so as to compare the performance of this adhesive with other such studies. Figure 5.18 shows the effect of methyl ethyl ketone, toluene, hydraulic fluid, jet fuel, antifreeze and acetone on adhesive bonds made with TPER-BPDA-PA. Values after the 72-hour water boil tests are also presented. Some of the best results in the literature using similar solvents are presented for comparison though the duration of testing for these specimens was significantly shorter than that used in this study. It is evident that the common solvents do not seem to have any effect on the lap-shear strengths of TPER-BPDA-PA while similar solvents had a significant effect on the thermoplastics LARC-8515²⁵ and LARC-TPI¹⁰. The failure mode was 100% cohesive for TPER-BPDA-PA indicating the stability of interface when exposed to these various

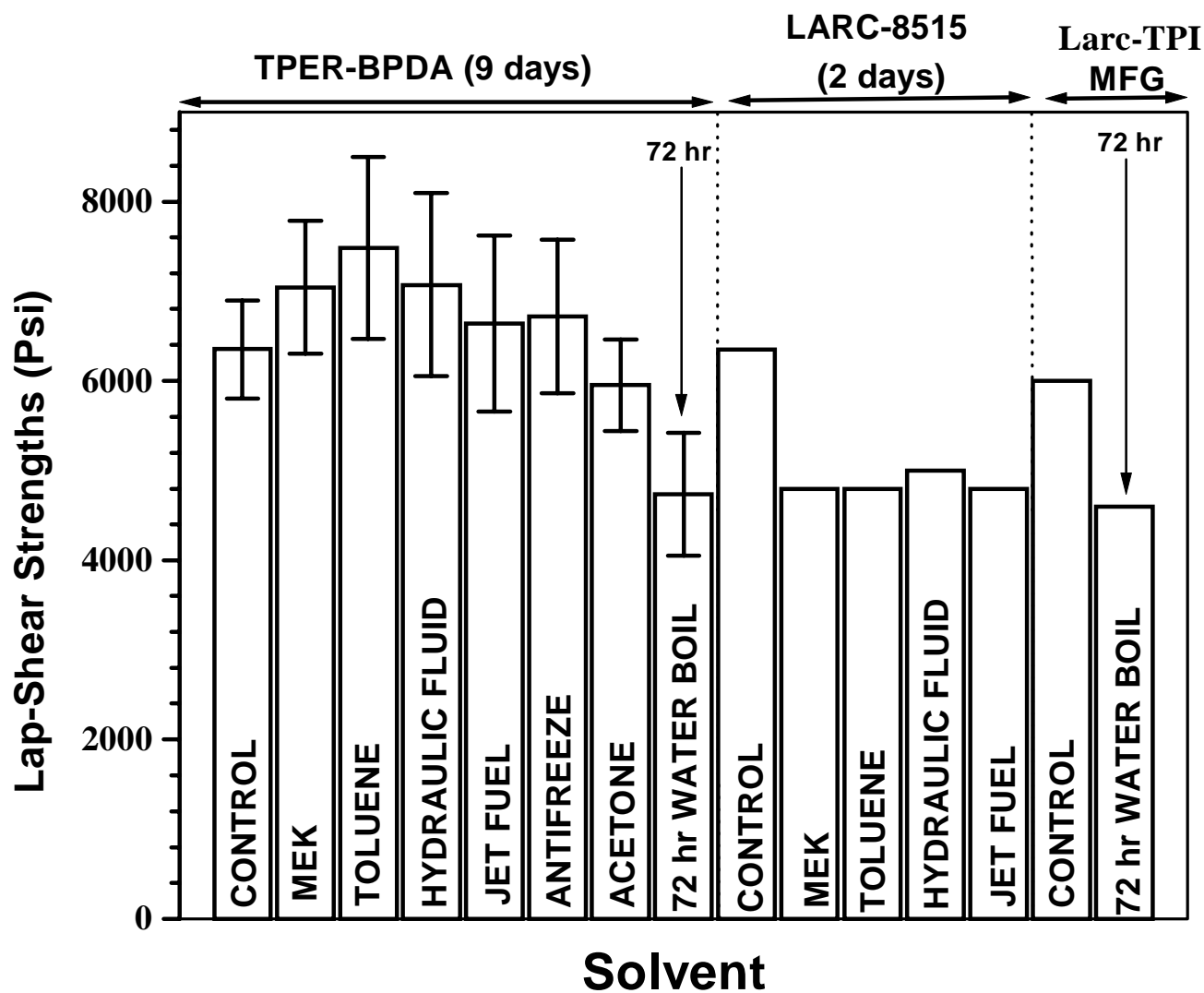


Figure 5.18 Lap-shear strengths of TPER-BPDA-PA (15K) after exposure to different solvents for a period of nine days. Values from other similar studies in literature are also shown for comparison.

solvents. It is important to point out that both LARC-8515 and LARC-TPI were completely amorphous and thus susceptible to some degree of solvent attack. The presence of crystallinity thus seems to greatly aid the solvent resistance of TPER-BPDA-PA significantly. It is likely that sometimes the effect of solvents on the interface may not become evident in lap-shear test geometry while a wedge test geometry may give contrasting results. Thus, wedge tests were also conducted for these solvents and the results are presented in chapter 7.

5.4 Conclusions

The crystalline morphology was studied for a new semicrystalline polyimide, TPER-BPDA-PA-PA and it was found that the final morphology was very sensitive to the crystallization temperature. The nucleation density increased at ca.330°C leading to the formation of fine grainy spherulitic morphology. Also, the spherulitic growth rates were significantly higher for the 15K material compared to the 30K system although the increase in nucleation density also occurred for the latter at ca.340°C. The melt conditions did not affect the spherulitic growth rates for either molecular weight reinforcing the results from the earlier studies indicating the exceptional thermal stability of this polymer.

Three surface treatments were evaluated with simple sandblasting giving the best results. The chromic acid anodization and sodium hydroxide etch gave interfacial failures while sandblasting always gave cohesive failures. The lap-shear strengths were greatly affected by the bonding conditions with a temperature of 430°C for 20 minutes at a pressure of 100psi giving the best results. The fracture surface was rough and showed large amounts of plastic deformation. The overall cycle time for preparing the adhesive specimen was considerably lower due to the melt processability, simple surface treatment needed and reduced bonding time.

The high temperature durability studies were conducted at three different temperatures of ambient, 177°C and 232°C and it was found that the strengths remained relatively unaffected for up to 7 weeks for a given test temperature. For any given set of aging conditions the strengths decreased as the testing temperature was increased from ambient to 177°C to 232°C. Lap-shear strengths in the range of 6000-8400 psi were obtained for ambient testing while strengths were in the range of 4000-6000 psi for test temperature of 177°C. Also, testing above the glass transition at 232°C gave reasonable strengths of approximately 2500-4000 psi owing to the presence of crystallinity. Finally, common solvents did not seem to affect the lap-shear strengths of TPER-BPDA-PA lap-shear adhesive specimens.

5.5 Acknowledgments

The author would like to acknowledge the NSF Science and Technology Center for High Performance Polymeric Adhesives and Composites for full support of this study under contract number DMR 912004.

References:

1. Hergenrother, P.M., Stenzenberger, H.D. and Wilson, D. 'Polyimides', Blackie & Son Ltd, London, 1990.
2. Srinivas, S., Caputo, F.E., Graham, M., Gardner, S., Davis, R.M., McGrath, J.E. and Wilkes, G.L. *Macromolecules*, 1997, **30**, 1012.
3. Kreuz, J.A., Hsiao, B.S., Renner, C.A. and Goff, D.L. *Macromolecules* 1995, **28**, 6926.
4. Wang, Y.D., Cakmak, M. and Harris, F.W. *J. Appl. Polym. Sc.* 1995, **56**, 837.
5. Bandom, D.K. and Wilkes, G.L. *Polymer* 1994, **35**, 5672.
6. Hsiao, B.S., Kreuz, J.A. and Cheng, S.Z.D. *Macromolecules* 1996, **29**, 135.

7. Heberer, D.P., Cheng, S.Z.D., Barley, J.S., Lien, S.H.S., Bryant, R.G. and Harris, F.W. *Macromolecules* 1991, **24**, 1890.
8. Progar, D.J. and Dezern, J.F. *J. Adhes. Sci. Technol.* 1989, **3**, 305.
9. Progar, D.J. and Clair, T.L. *St. J. Adhesion* 1989, **30**, 185.
10. Progar, D.J. and Clair, T.L. *St. J. Adhes. Sci. Technol* 1994, **8**, 67.
11. Clearfield, H.M., Shaffer, D.K., Vandoren, S.L. and Ahearn, J.S. *J. Adhesion* 1989, **29**, 81.
12. Clearfield, H.M., Cote, G.O., Olver, K.A., Shaffer, D.K. and Ahearn, J.S. *Surface and Interface analysis* 1988, **11**, 34.
13. Dezfuly, M. A., Vlachos, C. and Andrews, E.H. *J. Mater. Sci.* 1984, **19**, 3626.
14. Venables, J.D., McNamara, D.K., Chen, J.M. and Sun, T.S. *Appl. Surf. Sci.* 1979, **3**, 88.
15. Davis, G.D., Sun, T.S., Ahearn, J.S. and Venables, J.D. *J. Mater. Sci.* 1982, **17**, 1807.
16. Kennedy, A.C., Kohler, R. and Poole, P. *Int. J. Adhes. And Adhesives* 1983, **3**, 133.
17. Progar, D.J. and Clair, T.L. *St. J. Adhesion* 1987, **21**, 35.
18. Progar, D.J. *J. Adhes. Sci. Technol.* 1987, **1**, 135.
19. Gauthier, M.M. pg. 80, Vol 3, 'Engineered Materials Handbook, Adhesives and Sealants' ASM International, 1995, Materials Park, Ohio.
20. Lee, Y. and Porter, R.S. *Macromolecules* 1988, **21**, 2770.
21. Krevelen, V. in Ch 19, Crystallization and Recrystallization, in the book 'Physical Properties of Polymers', Elsevier, 1990, London.
22. Sharples, A. 'Introduction to polymer crystallization', Edw. Arnold, 1966, London.
23. Friedrich, K. and Karsch, U.A. 'The influence of Molecular Weight on Crazing and Fracture in Polypropylene', in Proc. 27th Int. Symp. on Macromolecules, Vol 2, 1981, 1035.
24. Wightman J.P., Department of Chemistry, Virginia Tech, (private communication).
25. Jensen, B.J., Hou, T.H. and Wilkinson, S.P. 40th Int. SAMPE Symp., May 8-11, 1995, 1072.
26. Adams, R.D. pg 325, Vol 3, 'Engineered Materials Handbook, Adhesives and Sealants', ASM International, 1995, Materials Park, Ohio.

Chapter 6

Thermal Stability, Crystallization Kinetics and Morphology of a New Semicrystalline Polyimide based on 1,3-bis (4-aminophenoxy) benzene (TPER) and 3,3', 4,4'-biphenyltetracarboxylic dianhydride (BPDA).

Abstract

This work investigates the crystallization kinetics and thermal stability of a new melt processable semicrystalline polyimide (T_g = ca. 210°C, T_m = ca. 395°C) based on 1,3-bis(4-aminophenoxy) benzene (TPER) and 3,3',4,4'-biphenyltetracarboxylic dianhydride (BPDA), and endcapped with phthalic anhydride (PA). Earlier studies have demonstrated that this polymer is a strong candidate as a structural adhesive for high temperature and high performance applications. This study deals with the thermal stability, the effect on crystallization kinetics, and the crystalline morphology of the polymer when exposed to melt temperatures in excess of 410°C for various residence times. In the present study, an Avrami analysis was utilized to study the overall bulk crystallization kinetics after a specific thermal history. The Avrami exponent (n) slightly increased and the parameter 'K' decreased with increasing supercooling. Also, Avrami analysis (at 355°C) was utilized to evaluate the effect of melt temperature (from 410°C to 450°C) and effect of melt residence time (2 min to 30 min at 430°C) on the crystallization kinetics. The increase in melt temperature led to an increase in the value of Avrami exponent while the value of parameter 'K' dropped significantly. Although the melt residence time did not have much effect on the Avrami exponent, a significant drop in the value of parameter 'K' was observed with increasing residence time in the melt. To evaluate the thermal stability, melt viscosity was followed at 430°C as a function of frequency. The melt displayed shear-thinning behavior with a significant drop in viscosity with increasing frequency. Also, the isothermal viscosity at lower frequencies increased by nearly an order of magnitude after ca. 20 minutes at 430°C. Isothermal time sweeps of the melt viscosity were carried out at

different melt temperatures (410°C-450°C) for up to 20 minutes. By increasing the melt temperature, the viscosity increased at faster rates with time, the rate of increase being significantly more above 430°C. Crystallization was investigated by rheological experiments when cooled from the above harsh thermal histories at 10°C/min. With increasing isothermal melt temperature, the onset of crystallization occurred at higher supercoolings. Optical microscopy was utilized to follow the growth rates of the spherulites from the melt at 345°C after quenching from the different melt temperatures. The growth rates decreased significantly as the melt temperature was increased beyond 430°C. Non-isothermal experiments using a DSC were carried out from different melt temperatures. Both optical microscopy and DSC analysis gave evidence of a distinct 'catastrophic nucleation' process at temperatures in vicinity of 330°C.

6.1 Introduction

Aromatic based polyimides are an important subset of high performance and high temperature polymers which, due to their outstanding properties, are finding increasing use in applications such as high temperature adhesives, composites, electronics packaging, fibers, foams and as membranes for gas separation^{1,2}. Semicrystallinity in polyimides further improves certain mechanical properties³, thermal stability^{4,5}, radiation⁶ and chemical resistance⁷. However, of the relatively few semicrystalline polyimides available, most rapidly lose their crystallization ability once taken to the required melt temperature, which is often in excess of 380°C. Melt relative to solution processing of these high performance polymers is thought desirable both from an environmental standpoint (to avoid toxic solvents) and also for ease of processing. Recently, a new polyimide was developed in this laboratory that has displayed excellent characteristics from this standpoint. This polyimide (T_g =ca.210°C, T_m = ca. 395°C) is based on 1,3-bis(4-aminophenoxy) benzene (TPER diamine or 1,3(4)APB) and 3,3',4,4'-biphenyltetracarboxylic dianhydride (BPDA)^{4,5,8}. It was also very important to fully endcap the chains with phthalic anhydride (PA) to maximize thermal stability⁵. Earlier

DSC melting studies in this laboratory have demonstrated the excellent thermal stability of this polyimide by showing that very little change in the melting behavior occurred, even after 20 min at 430°C^{4,5}. Subsequent studies have also shown the outstanding adhesion properties of this polyimide to titanium alloy, e.g. average lap-shear strengths of 6600-8400psi at ambient temperatures. The adhesive bonds were also stable to a variety of solvents, high temperature aging and elevated test temperatures of 177°C and 232°C⁴.

However, for such high temperature thermoplastic polymers processed from the melt, melt time and temperature become important variables from processing and thermal stability viewpoints. Side reactions like crosslinking, branching or chain scission, that may occur at these high melt temperatures usually lead to build up in the molecular weight, and will not only change the rheological behavior but may also result in reduced crystallinity and slower crystallization kinetics. On the positive side, the rise in the molecular weight usually leads to improvement of certain mechanical properties, like higher elongation to break and increased toughness. Thus if the rise in molecular weight can be limited to an extent, such that the crystallization kinetics and the amount of crystallinity are not affected much, than a synergistic effect can be produced. In order to obtain this synergism however, it is important to evaluate the rheological behavior at these melt temperatures and the crystallization response when the polyimide is cooled from these harsh melt conditions. The effect of various melt conditions on the subsequent crystallization response also serves as a direct tool in evaluating the thermal stability of the system.

This work examines some of these later issues in detail such as the effect of melt holding conditions on isothermal crystallization kinetics and on the related morphology. Avrami analysis using the DSC and corresponding polarized optical microscopy (POM) experiments were utilized to individually understand the effect of 1) crystallization temperature, 2) melt time and 3) melt temperature on the crystallization kinetics and the resulting morphology of the system.

Melt viscosity studies were conducted at various temperatures to detect the presence of any chemical changes and to ascertain the effect on subsequent crystallization. Non-isothermal studies were also performed using the DSC and hot stage POM to

understand the effect of previous melt holding conditions on the subsequent crystallization behavior and semicrystalline morphology of the polyimide.

6.2 Experimental

The details specifying the synthesis of this polymer has been described elsewhere^{3,4}. This study, however, will only utilize $M_n=15,000$ daltons ($M_w=30,000$ daltons) molecular weight version of this polymer which facilitates a low melt viscosity. However, the molecular weight is sufficiently so as to high to demonstrate good physical behavior (creasable films).

Polarized optical microscopy was performed on a Zeiss optical microscope equipped with a Linkam 600 hot stage, a 35mm camera and a video camera. The hot stage was calibrated using melting point standards and all experiments were conducted under a nitrogen purge. The spherulitic growth rate measurements were performed on thin films (ca. 2 mils) sandwiched between two microscope cover slips. The samples were rapidly heated (ca. 90°C/min) to various melt temperatures and quenched to the desired crystallization temperature (within 15 seconds) using separate nitrogen source. The growth of spherulites was measured as function of time using a Boeckeler Video measurement system. Measurements were performed on 4-6 spherulites in a given sample and the average is reported.

DSC experiments for both isothermal and non-isothermal crystallization were performed on a Perkin Elmer DSC-7. The amount of polymer utilized in a given thermal scan was kept between 6-8 mg. The DSC was calibrated with indium and zinc standards. All experiments were conducted under a nitrogen purge and a DSC baseline was determined by running empty pans. For isothermal crystallization experiments, the samples were kept at room temperature and purged with nitrogen for 5 minutes to remove air from the DSC cell. The samples were then rapidly heated to the desired melt temperatures and kept at that temperature for the desired amount of time. Cooling from

these melt temperatures to specific crystallization temperatures was conducted at 200°C/min. In this regard, data collection at high supercoolings was hampered by the initial instability of the DSC signal. This initial instability occurs on cooling to the crystallization temperature at fast cooling rates and may persist for ca. one minute on Perkin Elmer DSC 7 utilized in this study. At higher supercooling, the induction times are short and crystallization is so fast that it is nearly over before the DSC signal has equilibrated. To obtain the initial portion of the exotherm at these temperatures, the straight line from the beginning of the exotherm was extended to the horizontal baseline drawn from the end of the exotherm. The intersection of these two lines was taken as the start of the crystallization exotherm. Such a procedure was attempted for higher degrees of supercooling only when a sufficient straight-line portion of the initial exotherm was available.

Rheological measurements were performed using a Rheometrics RMS-800 rheometer equipped with a 25 mm parallel plate tooling. The experiments were conducted using a percent strain of 5% and the gap between the plates was set at 1.6 mm. All the experiments were carried out in a nitrogen environment. To prepare the specimens, 1.5 grams of the polymer film was compacted at 300°C under a pressure of more than 20 MPa to yield circular discs. These discs were inserted between the circular plates of the rheometer, which were already preheated to 10-15°C above the designated temperature. Although the temperature usually decreased 20-30°C while inserting the samples, the predetermined temperature was again quickly attained by fast heating. The sample was compacted and the polymer that had squeezed out of the ends was scraped off. The data was collected from the time the material again reached the desired temperature and these time sweep experiments were conducted at temperatures of 410, 420, 430, 440 and 450°C for a period of 20 minutes at a frequency of 1 radian/second. To observe the rheology of supercooled melts, all the samples used for time sweep experiments were cooled at a rate of 10°C/ minute while the percent strain and frequency were unchanged. These tests were stopped after crystallization of the sample was observed and the torque had exceeded 500 g.cm. Tests were also conducted to examine the change in complex viscosity when the angular frequency was varied from 0.1 to 100 radians/sec while keeping the strain

amplitude constant at 5% and the temperature held at 430°C. Viscosity at the highest frequency was measured first while the lowest frequency was determined last. It took ca. 8 minutes for one such isothermal ‘frequency sweep’ while four such consecutive sweeps were carried out on the same sample.

6.3 Results and discussion

Although the various experimental⁹ and theoretical complications^{10,11,12,13} associated with the traditional isothermal Avrami analysis are well recognized, it continues to be the most widely used means of describing the overall bulk isothermal crystallization of polymers. Also, its use together with direct morphological information using microscopy yields important information about the crystallization mechanism and kinetics of a given polymer. In this regard, the Avrami equation is generally written as:

$$X_c(t) = 1 - \exp(-Kt^n) \quad \{6.1\}$$

In this equation, $X_c(t)$ is the normalized crystalline content at time t . ‘ K ’ and ‘ n ’ are Avrami constants and are indicative of crystallization mechanisms that are involved. The exponent ‘ n ’ in the Avrami equation can provide information on nucleation type and crystal growth geometry. ‘ K ’ is dependent upon the shape of the growing crystalline entities (for e.g., whether they are spheres, discs or rods), as well as the type and amount of nucleation (sporadic or predetermined) and the linear growth rate ‘ G ’ of the growing crystalline moieties. For example, in case of three-dimensional predetermined spherulitic crystallization ‘ K ’ can be expressed as:

$$K = (4\pi/3) N_0 G^3 \quad \{6.2\}$$

Here N_0 is the nucleation density whereas the exponent of 3 on the growth rate term indicates the Avrami exponent for such a process. The parameters in Eq (1) are usually determined by taking the double logarithm and expressing in the form:

$$\text{Log} [-\ln(1-X_c(t))] = \log K + n \log t \quad \{6.3\}$$

Isothermal DSC analysis is the primary means of performing such an analysis where the normalized crystal fraction $X_c(t)$ is written as :

$$X_c(t) = \Delta H(t) / \Delta H(\infty) \quad \{6.4\}$$

where $\Delta H(t)$ is the fractional heat of crystallization after time 't' and $\Delta H(\infty)$ being the total heat of crystallization observed at that isothermal crystallization temperature.

An alternate method¹⁴ often used to determine the two Avrami constants utilizes the data for crystallization half time along with Eq (1). However, this method was not used here because of deviations from Avrami behavior at normalized conversions approaching 50%.

Figure 6.1 shows the crystallization exotherms for TPER-BPDA-PA ($M_n=15,000$ daltons) after quenching from the melt to various crystallization temperatures. As is clearly evident, the overall bulk crystallization is very temperature sensitive in the narrow 20°C range of 340°C to 360°C. Although the rate of crystallization at 360°C is slow as evidenced by a broad crystallization exotherm, an increase in the degree of supercooling by 20°C leads to a large increase in the rate of crystallization. This change in rate of bulk crystallization is reflected in crystallization half-time ($t_{1/2}$), the time to complete 50% of the total crystallization, which decreases from ca. 20 minutes at 360°C to 1.38 minutes at 340°C! At crystallization temperatures higher than 360°C, the crystallization is very slow and the exothermic signal approaches the sensitivity of DSC making collection of reliable data difficult. Collection of isothermal data below 340°C was not possible as the crystallization half time at those temperatures is less than the time it takes for the DSC signal to become stable (ca. one minute). Crystallization of this polyimide ($M_n=11,500$ daltons) has also been studied by Cheng, Hsiao and Kreuz¹⁵ who suggest a $t_{1/2}$ time of 12 sec at 350°C after cooling at 320°C/min from a less stringent initial melt condition of 420°C for 10 minutes. Although the effects of initial melt history on $t_{1/2}$ are discussed later in this work, it is important to point out that these conclusions by Cheng and coworkers are believed to be inaccurate. While it is not clear how they measured such a short $t_{1/2}$ (the initial instability in the DSC signal itself always lasts for much more than 12 sec), it is also surprising that they indicate three $t_{1/2}$ data points below the glass transition temperature (T_g of 220°C as indicated in their paper).

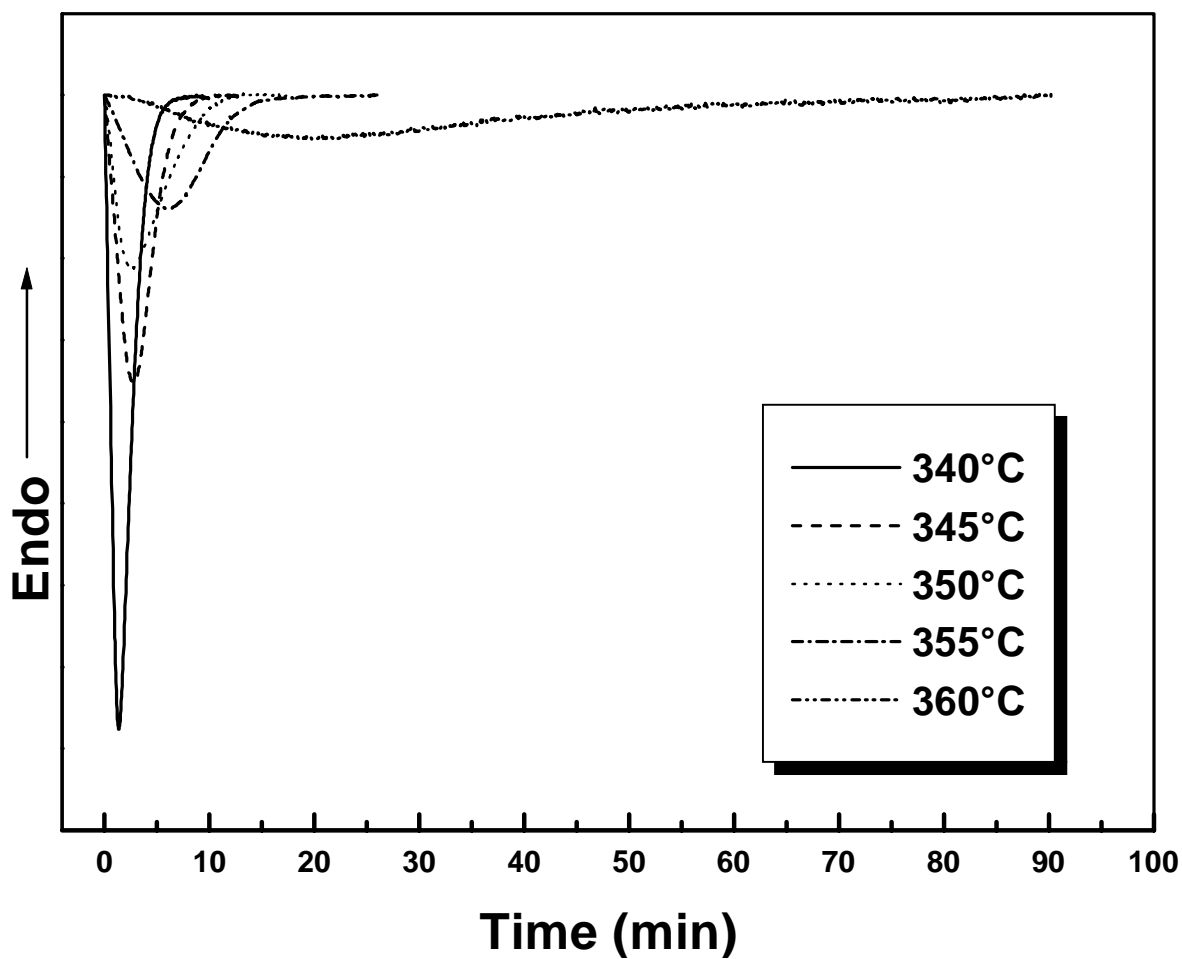


Figure 6.1 Crystallization exotherms at various crystallization temperatures for TPER-BPDA-PA after 20min residence time at 430°C.

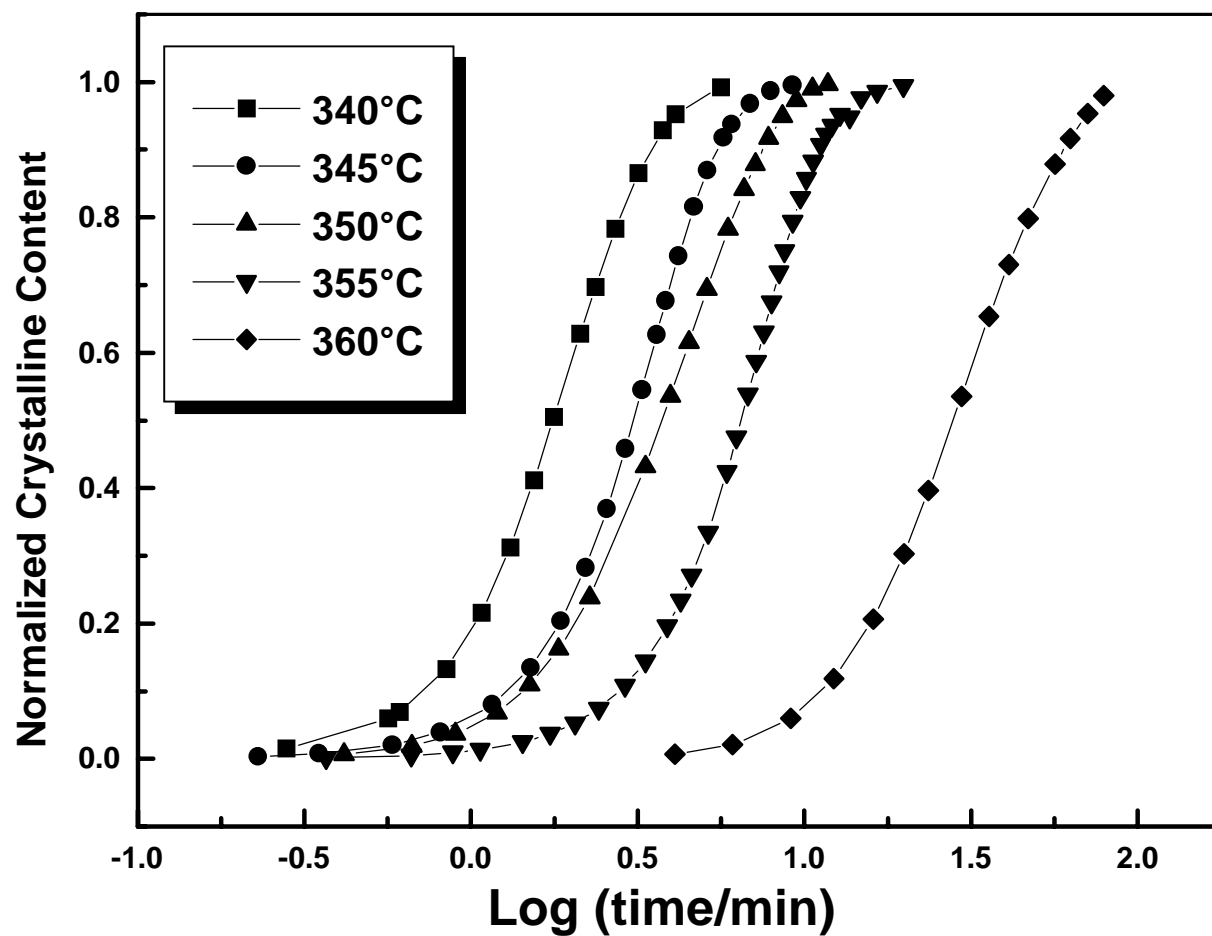


Figure 6.2(a) Normalized crystalline content as a function of Log (time) at various crystallization temperatures.

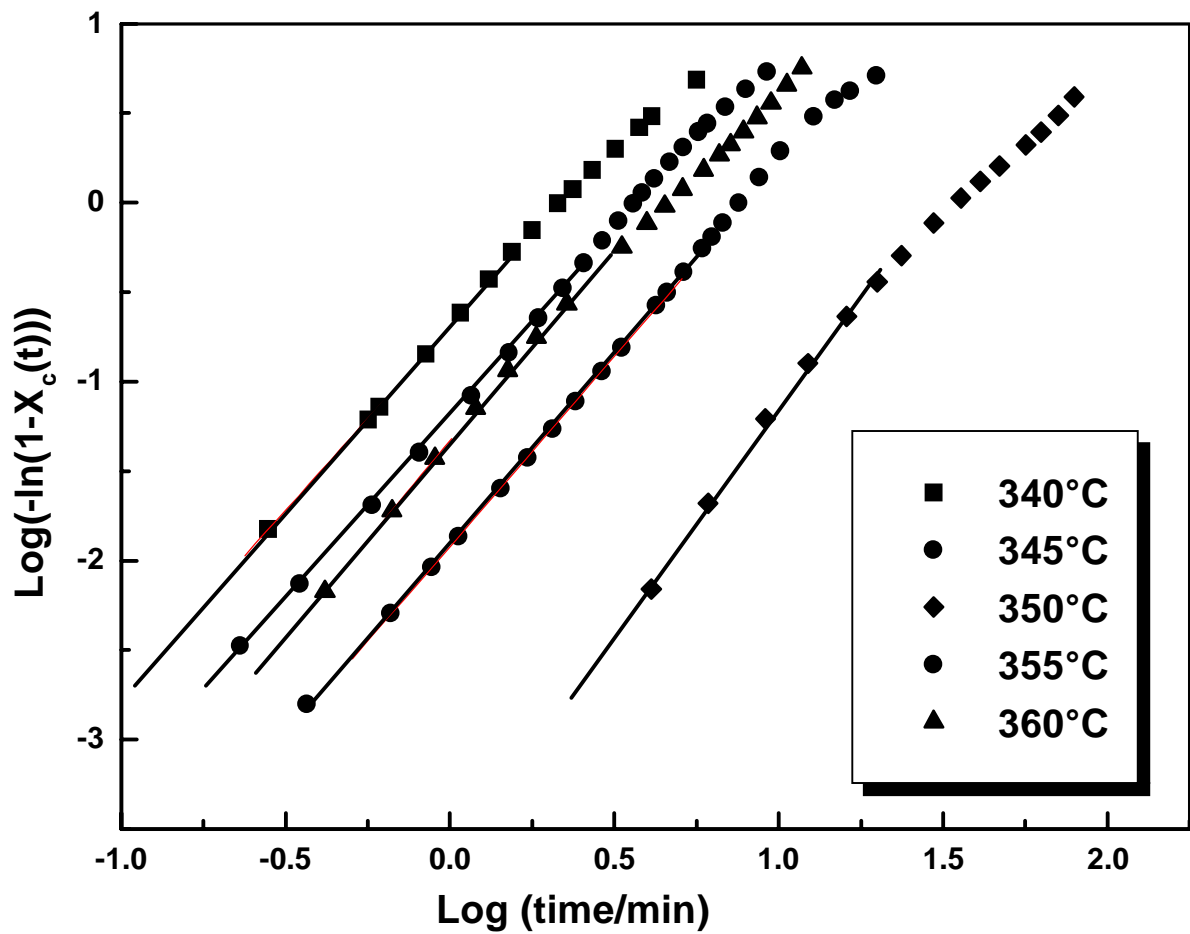


Figure 6.2(b) Plot of $\log [-\ln (1-X_c (t))]$ versus $\log (\text{time})$ at various crystallization temperatures.

Figure 6.2(a) shows the normalized crystalline content as a function of log (time) for the crystallization temperatures examined in this study. It is observed that crystallization shifts to longer times with every 5°C increase in the crystallization temperature. However, this shift to longer times is most noticeable between crystallization temperatures of 355°C and 360°C. Figure 6.2(b) shows the corresponding Avrami plots for the various crystallization temperatures. The curves show an initial linear section but a change in the slope is observed at longer times. The straight lines fit through the initial section of the curves, however, yield the two important Avrami parameters, 'K' and 'n'. The variation of bulk transformation rate 'K' with crystallization temperature is shown in Figure 6.3. The figure also shows the corresponding changes in crystallization half-time ' $t_{1/2}$ '. A strong correlation between the value of parameter 'K' and crystallization half time is observed as expected. Crystallization half time, which is a measure of the rate of crystallization, decreases with increasing values of 'K'. Figure 6.4 shows the optical micrographs taken at various crystallization temperatures, the initial melt conditions being identical to the DSC experiments described above. While the nucleation density is low at 355°C, it increases sharply with small increases in the degree of supercooling. Thus it is evident that the final spherulitic size decreases greatly with relatively small changes in the crystallization temperature. In fact, no optically resolvable spherulites were observed at and below 330°C due to a catastrophic increase in the nucleation density. This phenomenon will be addressed later in the paper. A small but noticeable change in the Avrami exponent is also observed with varying crystallization temperature. The Avrami exponent is 2.7 at 360°C whereas it decreases to 2.0 at 345°C and 340°C. However, for spherulitic crystallization and a somewhat mixed mode of nucleation observed, the value of the Avrami exponent is expected to be slightly above 3. Although optical microscopy clearly reveals a spherulitic morphology at the discussed crystallization temperatures, the initial growth of such a spherulitic structure may not be truly three-dimensional. Figure 6.5 shows the schematic development of a fully-grown spherulite from an initial single lamella. The presence of an intermediate sheaf like structures would tend to decrease the Avrami exponent from 3 as has also been suggested previously^{16, 17}. Also, the Avrami exponent is calculated using the earlier stages of crystallization where the presence of such

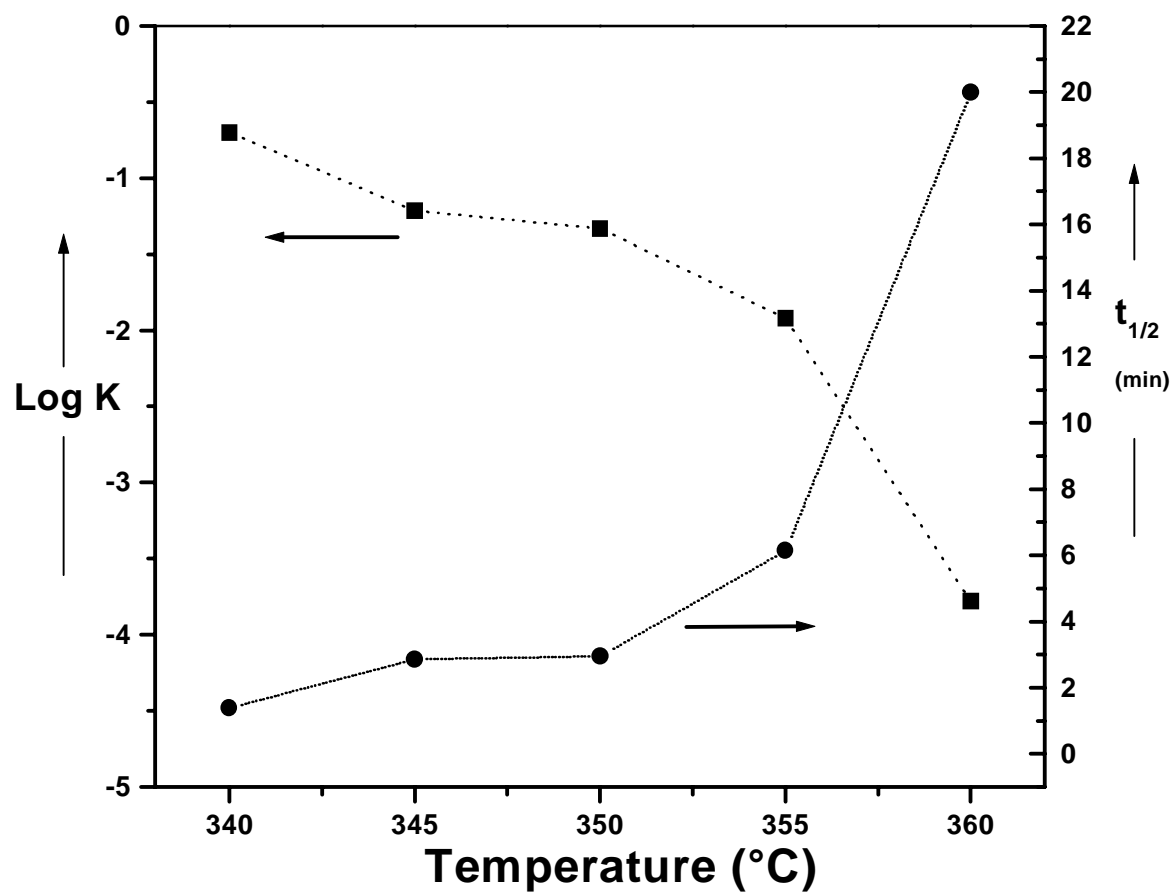


Figure 6.3 Variation of logarithm of transformation rate 'K', and crystallization half time ' $t_{1/2}$ ', as a function of crystallization time after melt holding conditions of 430°C for 20 minutes.

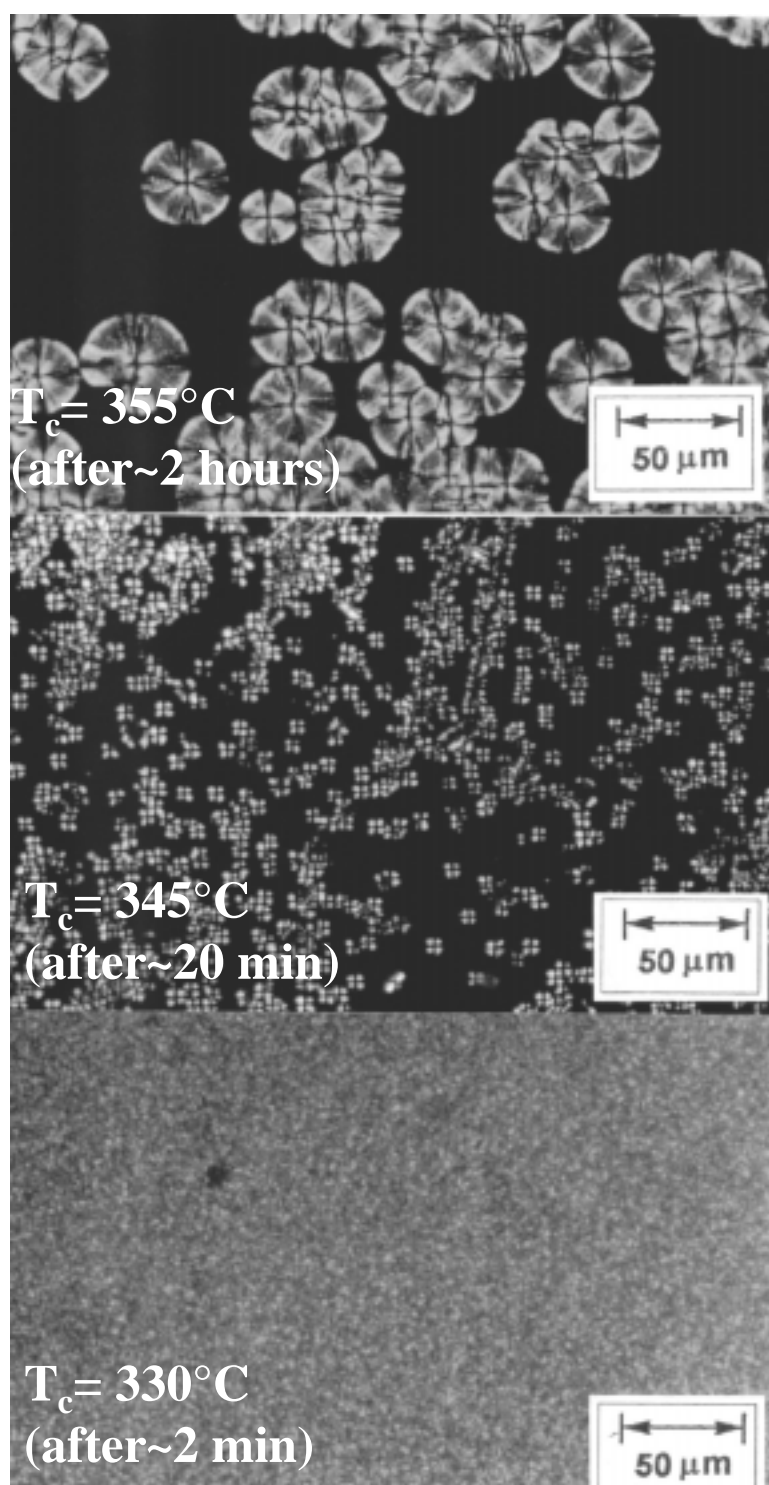


Figure 6.4 Polarized optical micrographs at the indicated crystallization temperatures after being at a melt temperature of 430°C for 20 minutes.

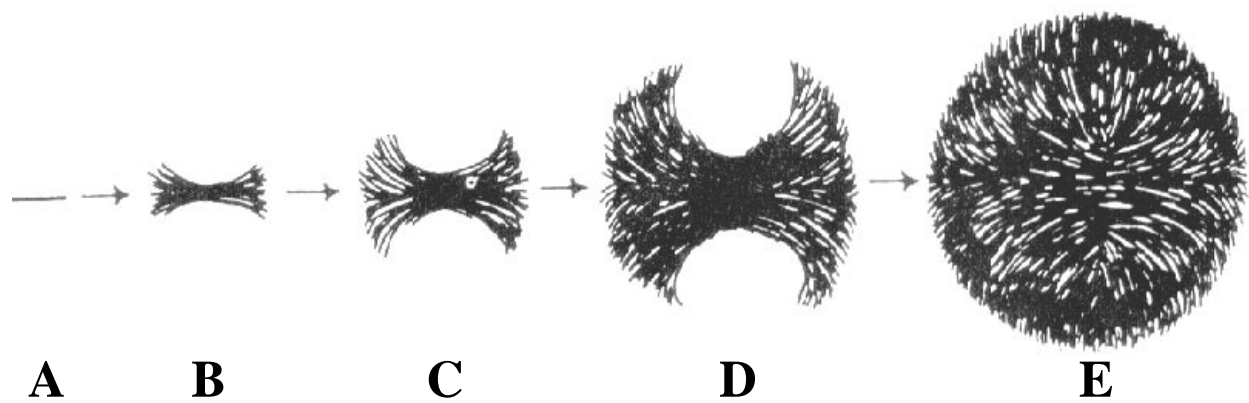


Figure 6.5 Evolution of spherulitic growth ranging from a folded-chain single crystal to a fully developed spherulite²¹.

intermediate structures is more likely and thus would contribute to a decreased Avrami exponent. Such an effect may become even more important as the crystallization temperature is lowered and the nucleation density increases. This increase in nucleation density could result in a large number of only partially developed spherulites colliding with each other at an early stage thus giving rise to sheaf-like structures and/or truncated spherulites. This type of geometry would again lower the Avrami exponent.

It is of interest to compare the bulk crystallization rate 'K' obtained for this polyimide with similar results obtained for other high performance polymers. However, before making any such comparison it is important to recognize that the units of K depend on the value of the Avrami exponent 'n'. Thus, in order to make such comparisons, it is more useful to compare the values of $K^{1/n}$. Secondly, the supercooling at which these comparisons are made need to be similar. Also, the initial melt conditions can substantially affect the crystallization rate at a given undercooling. The initial melt temperature, if below the equilibrium melting point, can often result in self-seeding nucleation and thus lead to a higher value of the transformation rate 'K'. Thus in order to assess the differences in crystallization kinetics and make valid comparisons, it is essential that the initial melt temperatures for the two polymers are above their respective equilibrium melting points. In this regard, Lee and Porter¹⁷ obtained a value of 0.17min^{-1} for $K^{1/n}$ in the case of PEEK at a supercooling of 80°C when cooled from a melt temperature of 370°C ($T_m^0=395^\circ\text{C}$). However the value of $K^{1/n}$ dropped to 0.06min^{-1} at the same undercooling when the melt temperature was increased to 410°C (due to possible crosslinking at that temperature). Cebe and Hong¹⁸ noted a value of 0.05min^{-1} for PEEK at the ΔT_c of 80°C and 0.22min^{-1} at ΔT_c of 87°C when cooling from 400°C . Cheng¹⁹ et al. obtained a value of 0.01min^{-1} at a ΔT_c of 96°C for a polyimide with flexible ethylene glycol sequence (inherent viscosity 0.68 dL/g) when cooled from above the equilibrium melting point of that polymer. Hsiao²⁰ et al. obtained a value of 0.04 min^{-1} at a supercooling of 121°C for a commercial semicrystalline polyimide, New-TPI, when cooled from melt at 410°C ($T_m^0=406^\circ\text{C}$). Lopez and Wilkes²¹ achieved a value of ca. of 0.71min^{-1} for poly (p-phenylene sulfide) at a ΔT_c of 70°C when cooled from 320°C ($T_m^0=312^\circ\text{C}$). For the semicrystalline polyimide used in this study, the author has obtained a value of 0.45min^{-1}

for $K^{1/n}$ at ΔT_c of ca. 70°C (based on T_m^o of 410°C). However, it is important to state here that this value was obtained after residence times of 20 minutes at 430°C. Smaller residence times at the same temperature would result in even higher value of 'K' as will be discussed later. These results thus clearly illustrate the very fast crystallization kinetics demonstrated by this polymer. The bulk crystallization rate 'K' depends upon the nucleation mode, nucleation density and the growth rate of the individual crystalline moieties²². In this regard, the overall crystallization therefore depends on two factors: (1) the growth rates of the individual spherulites and (2) the number of such spherulites growing (nucleation density).

Figure 6.6 shows the spherulitic growth rates at the various crystallization temperatures discussed earlier. Also, the melt temperature and time of 430°C and 20 minutes used for this study were the same as the melt conditions utilized for the bulk crystallization DSC studies. At a particular crystallization temperature, the radial growth rates were constant with time. The increased growth rates at larger supercooling contribute to a faster crystallization response and this would be reflected in the higher values of 'K' obtained at 345°C. The second important contribution to the increase in crystallization rate with increasing supercooling is due to the increase in nucleation density. While the nucleation mode is primarily athermal at 360°C, new spherulites also appear with time at lower crystallization temperatures, indicating some degree of thermal nucleation. This mixed mode of nucleation does not allow for a convenient calculation of a numerical value of the nucleation density using a simple expression like Eq (2) from classical Avrami theory. The contribution of nucleation density to overall crystallization kinetics, however, is clearly revealed by optical microscopy. This large increase in nucleation density obviously greatly increases the overall bulk crystallization rate 'K'.

Although both faster growth rates and increase in nucleation density contribute to a large increase in the bulk transformation rate, it is important to visualize which of these two factors is more responsible in determining the observed crystallization response. Nucleation mode and value of the Avrami exponent 'n' decide the exact form of relationship between the growth rate 'G' and the parameter 'K' (the growth rate is raised to power n). In this regard, it is meaningful to recognize that although the optical

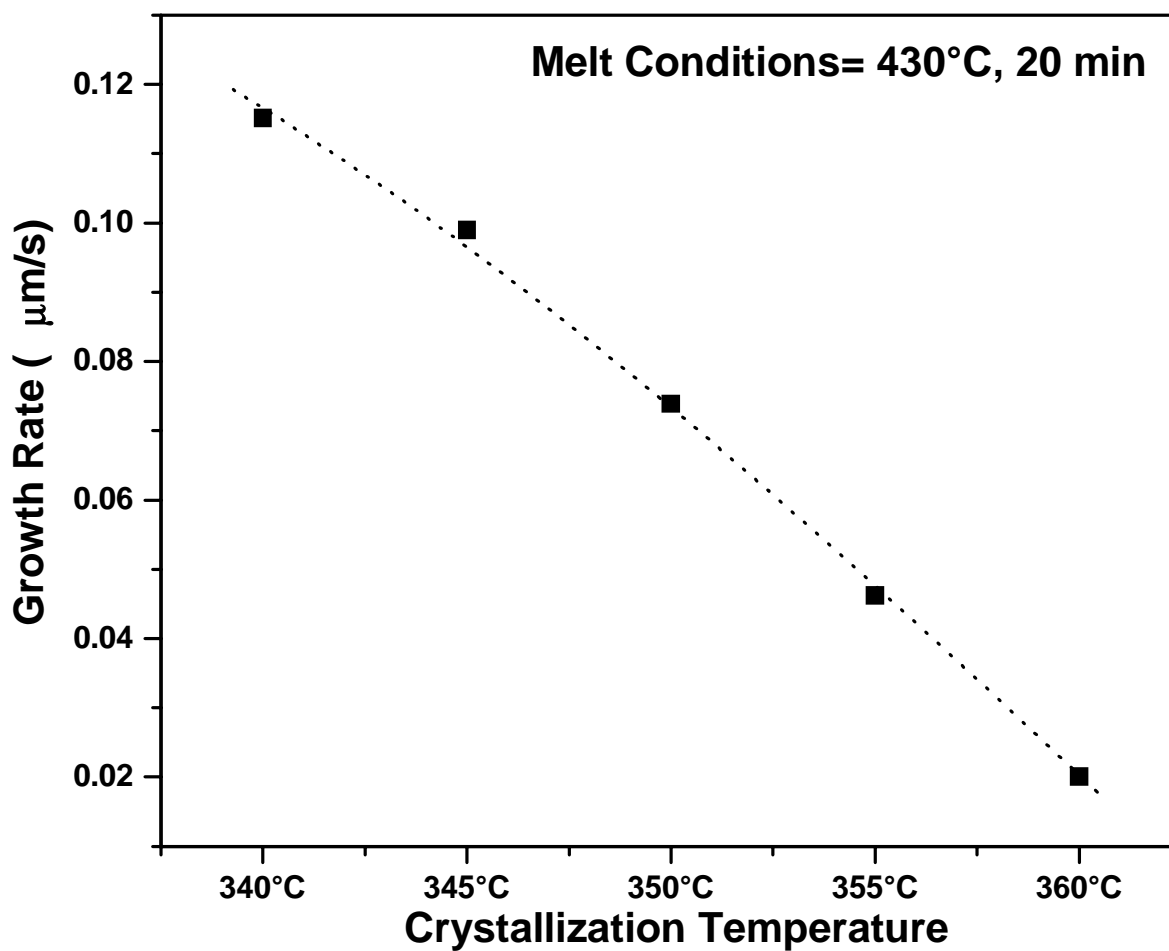


Figure 6.6 Radial growth rates of spherulites at various crystallization temperatures after melt temperature of 430°C for 20 minutes. ($M_n=15,000$ daltons, $M_w=30,000$ daltons)

micrographs shown here suggest increasing nucleation density to be more important, small changes in growth rate alone may significantly affect the bulk transformation rate. However, if effects due to nucleation density were absent, then the transformation rate $K^{1/n}$ would scale proportionally with changes in growth rate 'G'. An estimate of the two competing processes can thus be obtained by comparing the relative changes in ' $K^{1/n}$ ' and 'G' at two typical crystallization temperatures of 340°C and 345°C (the value of the Avrami exponent 'n' is ca. 2 in both cases). While it is found that the value of $K^{1/n}$ is ca. 82% more at 340°C than at 345°C, the growth rate of the spherulites 'G' is only increased by 14% at 340°C. This clearly suggests a strong contribution of nucleation density to increasing the bulk transformation rate. This deduction is also in accordance with the trend observed in the optical micrographs (Figure 6.4).

It is often observed that the overall crystallization consists of two separate parts: the initial stages being indicative of a primary crystallization process while, at later times, a change to a lower slope is often ascribed to secondary crystallization. Secondary crystallization further tends to lower the Avrami exponent by one or more. In this case, these changes in slope of the Avrami curve are prominently observed for higher crystallization temperatures while for lower crystallization temperatures the change in slope is less prominent. Also, this change in slope occurs after ca. 60-70% of the total crystallization. The change in slope at these conversions is also the reason for not using the crystallization half-time method to calculate the two Avrami constants. Also in this case, the deviations in the slope always occur after the peak of the crystallization exotherm. It is often assumed that the likelihood of spherulitic impingement in the bulk of the sample increases in the vicinity of the peak of the crystallization exotherm. Thus it is very likely that the most spherulitic impingement's take place at times where these changes in slope are observed. These spherulitic impingement's would further tend to lower the slope. Additionally, the process of secondary crystallization (which also lowers the slope) is expected to be more pronounced once these spherulitic impingement's have taken place (and the primary crystallization largely stopped). The effects of secondary crystallization on the overall bulk crystallization kinetics have also been observed for numerous other

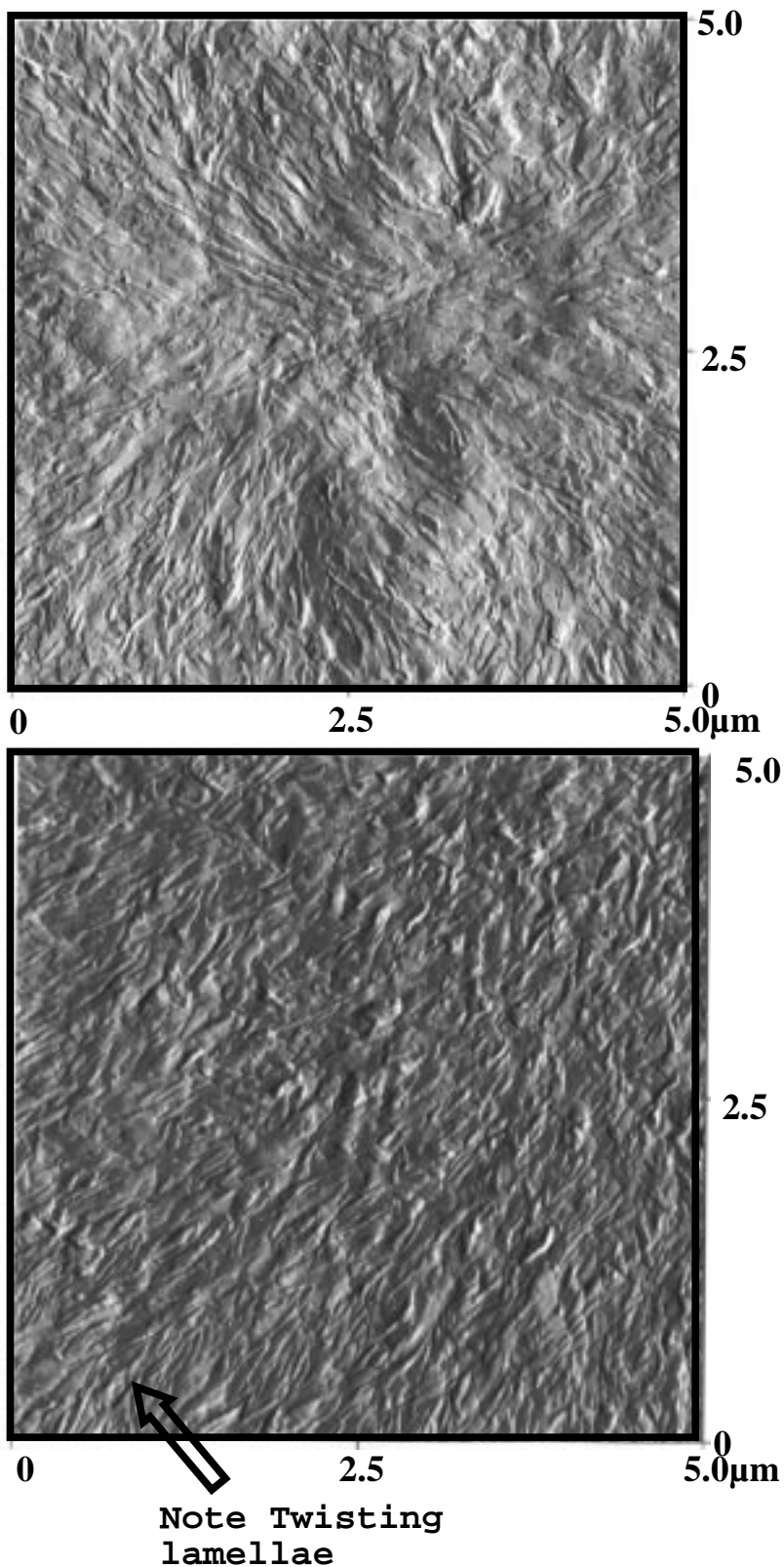


Figure 6.7 (a) AFM height image of a central part of a spherulite for a sample crystallized at 360°C after a melt temperature of 430°C for 20 minutes. **(b)** AFM height image of a outward region of a spherulite for a sample crystallized at 360°C after a melt temperature of 430°C for 20 minutes. The center of the spherulite lies toward the upper-right of the micrograph.

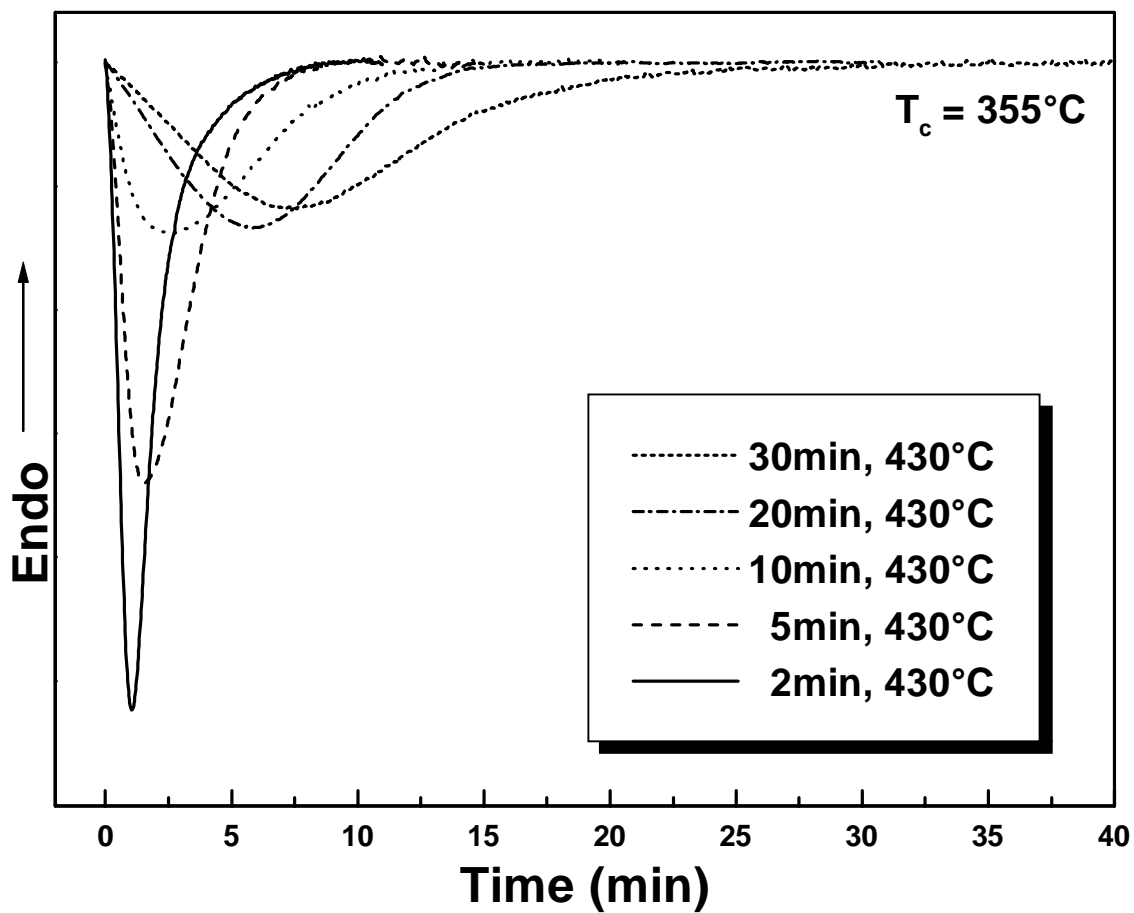


Figure 6.8 Crystallization exotherms at 355°C after various melt residence times at 430°C .

polymers²³ including polyethylene^{24,25}, PEEK^{11, 12,26} and other semicrystalline polyimides^{13, 14}.

Although, the bulk morphology as revealed by optical microscopy is spherulitic, the underlying lamellar substructure responsible for such final spherulitic development is distinctly discernible by atomic force microscopy. Figure 6.7(a) shows the AFM micrograph of a sheaf like structure present at initial stages of development of a spherulite. Considerable branching of the lamellae in regions away from the center is observed which is finally responsible for a three-dimensional spherulitic structure. Figure 6.7(b) shows the AFM micrograph of a region away from the center of a fully developed spherulite. Outwardly radiating lamellae from the center of the spherulite (the center of the spherulite is towards the bottom-right of the micrograph) are clearly revealed. It is particularly interesting that the fundamental crystalline structure of this polymer is lamellar although the polymer has a rather large repeat unit size ($M_u=536$ daltons). Also, earlier SAXS studies³ in this laboratory have yielded average Bragg spacing of ca. 163 Å for this polymer. Considerable twisting of the lamellae (“banding”) could also be observed, some of which is visible in Figure 6.7 (b). For POM experiments, banding was observed for the higher crystallization temperatures of 360°C or more (not shown here).

6.3.1 Effect of melt residence time and melt temperature on crystallization kinetics:

Nucleation of macromolecular melts when cooled is critically dependent upon the previous melt temperature and time in the melt. Generally, it is found that the supercooling required to achieve crystallization in a given time, over a certain temperature range, depends strongly on the superheating above the bulk melting temperature of the material. This trend continues till a given degree of heating above the melting temperature after which the crystallization behavior is independent of the melt temperature¹⁶. Such a behavior is explicable on the basis of thermal history sensitive nucleation proposed by

Turnbull²⁷. According to this, the crystalline material present in the crevices and cracks of heterogeneity may wet the surface and thus may require a temperature above the melting point of the material to destroy these sites. *In fact, depending upon the size and the shape of the cracks, and the interfacial surface energy, the dissolution temperature for these sites may considerably exceed the bulk melting temperature*^{16, 19, 28}. These sites if not destroyed can serve as possible nucleation sites (heterogeneous nucleation due to residual nuclei) on subsequent cooling. The second type of nucleation that may affect the crystallization behavior is the self-seeding nucleation by crystals surviving the nominal melting point of the polymer¹⁶. To completely erase the effect due to this type of nucleation, it is often necessary to raise the temperature above the equilibrium melting temperature. The resulting nucleation density on cooling can thus be significantly dependent on the previous melt temperature and position of melt temperature vis a vis the true equilibrium melting point of the polymer. Time in the melt is another important factor that might influence the subsequent crystallization. If exposed for very short amounts of time above the melting temperature, the crystals often reappear at exactly the same place (memory effect)²⁹. Also, when the melt temperatures are in excess of 400°C, it becomes important to evaluate the effect of possible degradation reactions on the crystallization kinetics. Chemical changes leading to crosslinking, molecular weight increase, or chain branching may severely inhibit the ability of the system to crystallize. The effect of such severe melt conditions on the crystallization kinetics thus serves as a direct tool in evaluating the thermal stability of the polymer.

Thus Avrami analysis was utilized to examine the effect of melt residence time on isothermal crystallization kinetics at a given crystallization temperature and for a typical melt temperature of 430°C. This melt temperature is in the vicinity of possible melt processing temperatures that this polyimide may experience and was in fact found to be the optimum processing temperature for attaining the best adhesive strengths in an earlier work on the same material⁴. The melt residence times selected were varied between 2 to 30 minutes and are representative of the processing times that may be required for different applications. Figure 6.8 illustrates the crystallization exotherms obtained after cooling to 355°C, the polymer being in the melt at 430°C for the melt residence times

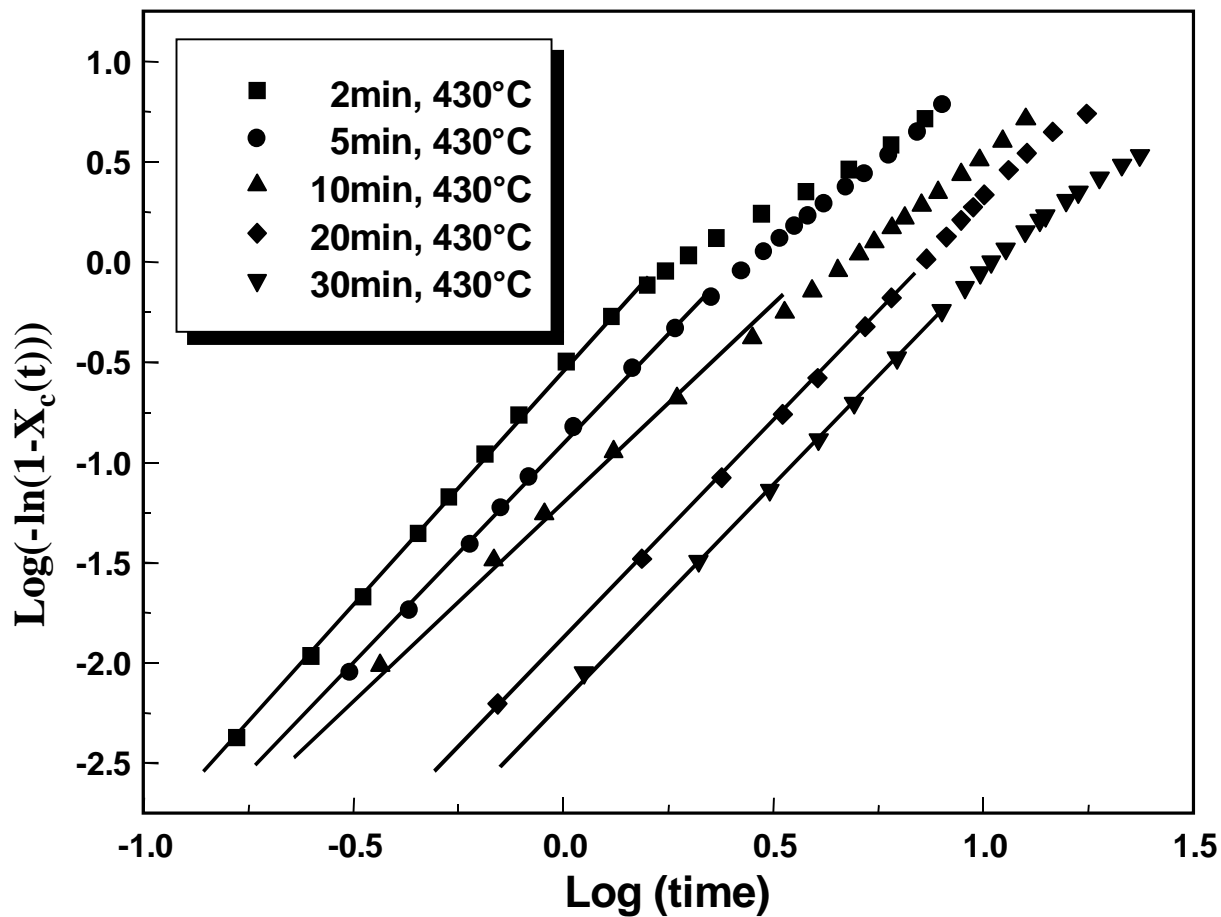


Figure 6.9 Plot of $\log [-\ln (1-X_c (t))]$ versus $\log (\text{time})$ at 355°C after various melt residence times at 430°C.

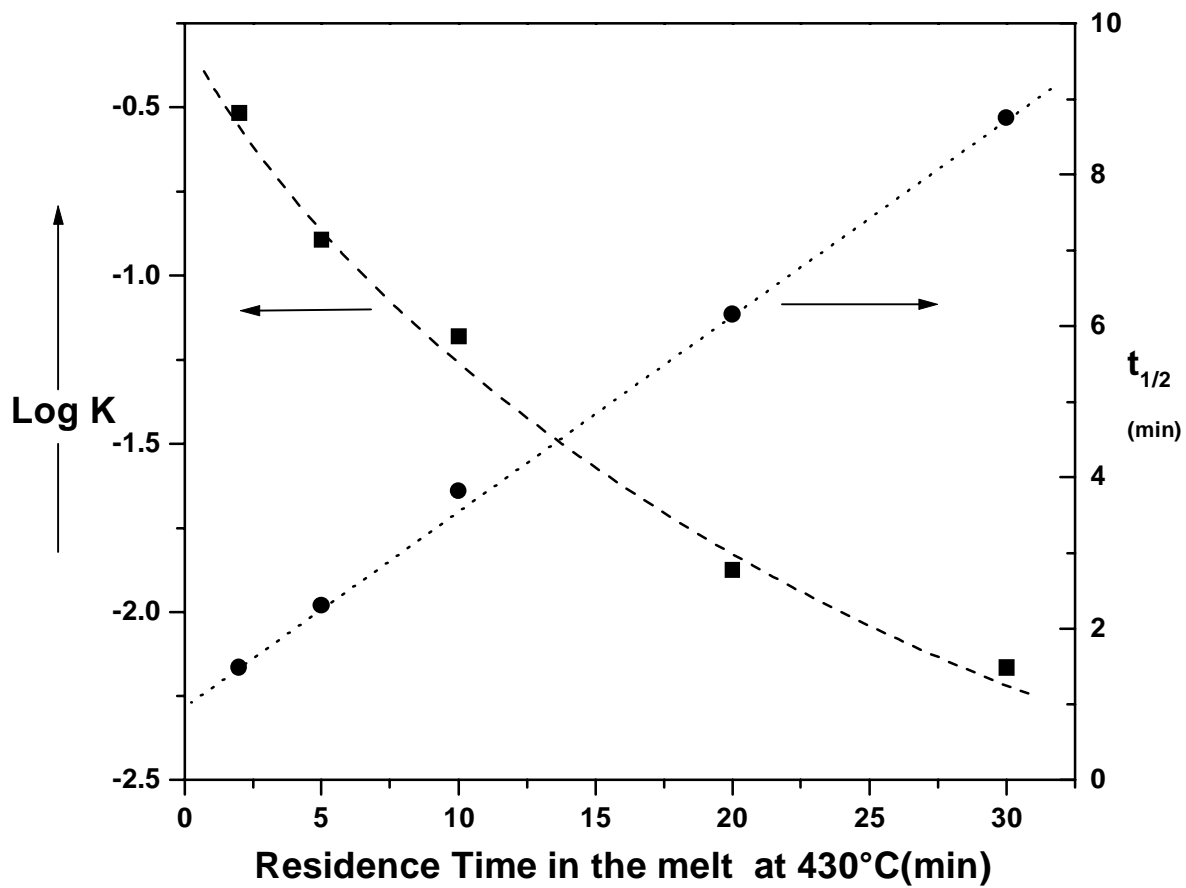


Figure 6.10 Variation of logarithm of transformation rate 'K', and crystallization half time ' $t_{1/2}$ ' at the crystallization temperature of 355°C, as a function of residence time at 430°C.

shown. It is clear that melt residence time has a major effect on the crystallization behavior of TPER-BPDA-PA. Short residence times of only 2 or 5 min result in a relatively faster crystallization response, while an increase in the melt residence times to 10 or 20 min leads to significant slowing down of the crystallization kinetics. For longer residence time of 30 min, the decrease in crystallization rate is also accompanied by significant broadening of the crystallization exotherm. Figure 6.9 shows the corresponding Avrami plot for the exotherms shown in Figure 6.8. It is clear that the crystallization behavior shifts continuously to longer times with increasing residence times in the melt. However, the value of the Avrami exponent did not show much change ($n=2.1-2.4$) with change in melt residence time. Figure 6.10 depicts the change in the value of the bulk crystallization rate 'K' and the crystallization half-time ($t_{1/2}$) as the residence time in the melt was increased at 430°C. The value of 'K' decreased progressively with increasing residence times in the melt, while $t_{1/2}$ showed a corresponding increase indicating again a slower rate of crystallization. The lower crystallization rate with increasing melt residence times can be due to the slower spherulitic growth and/or lower nucleation density. To examine this aspect, independent optical microscopy measurements were also conducted at the same crystallization temperature and the micrographs are shown in Figure 6.11. The optical micrographs reveal a significant drop in nucleation density with increased residence times in the melt at 430°C. For short residence times, the melt has not become truly homogenous and previous thermal history affects the subsequent crystallization. It is clear that a number of residual nuclei survive these short melt exposure times and serve as nucleation sites on cooling. However, with increasing melt exposure times, the melt becomes more homogenous and reduction in the number of surviving nuclei takes place. This leads to a lower nucleation density as revealed by optical microscopy. Any chemical changes occurring in the melt would also tend to slow down the rates of crystallization if these reactions lead to increases in the molecular weight through chain extension, branching and cross-linking. Later results presented in this paper show evidence of noticeable chemical changes occurring at and above 430°C for longer melt residence times (20min). The cross-linking and branching reactions influence the crystallization kinetics and the amount

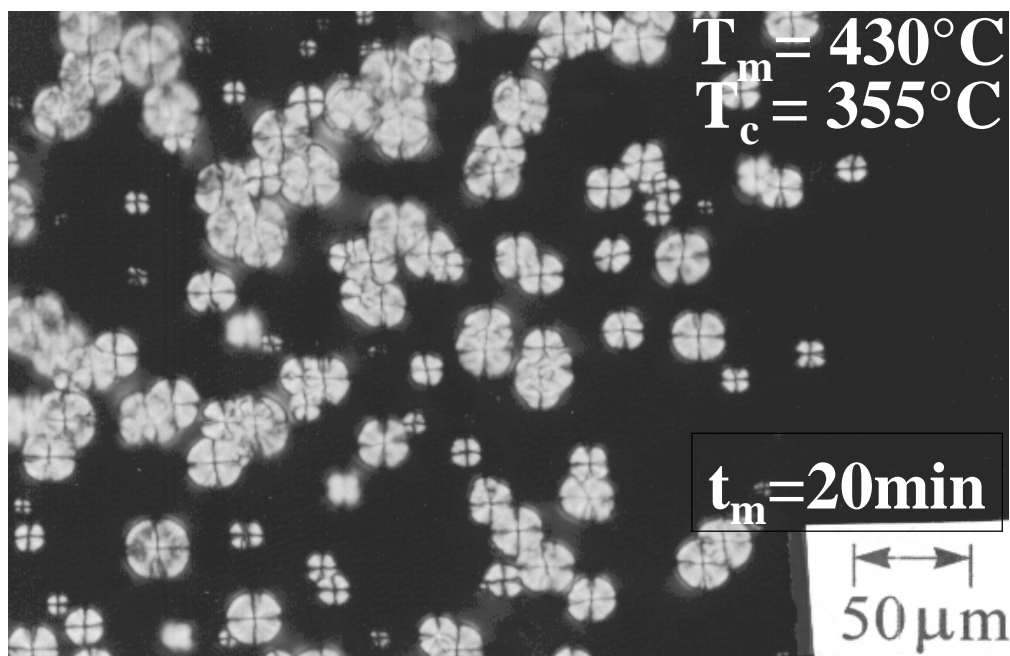
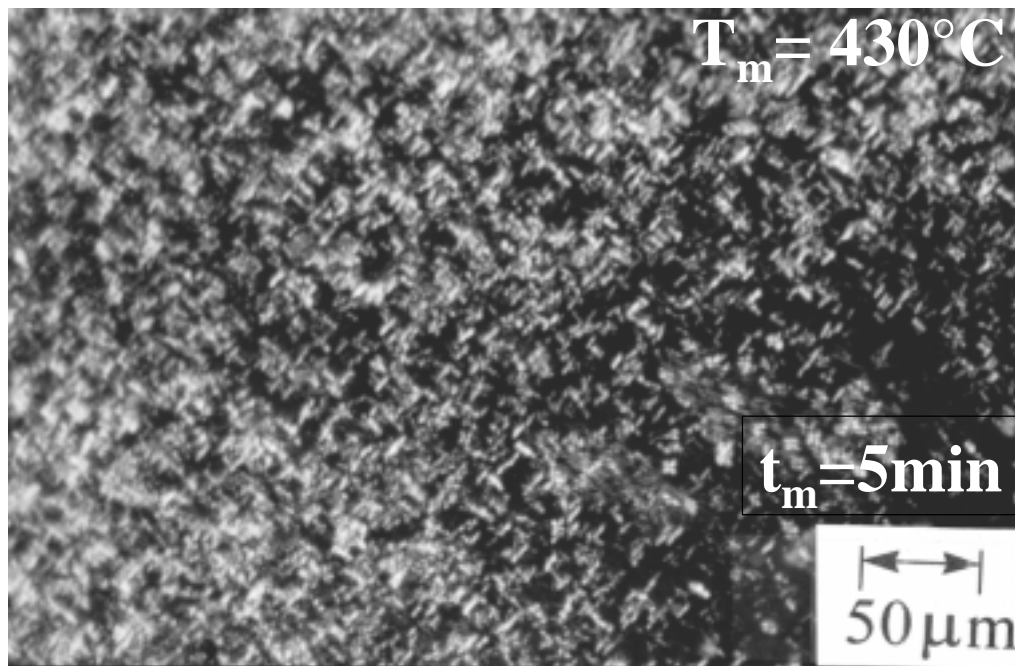


Figure 6.11 Polarized optical micrographs at 355°C after the indicated melt residence times at 430°C .

of these chemical reactions increases with longer melt residence times. The molecular weight increase due to these reactions would also decrease the spherulitic growth rate. However, for the shorter residence times of 2min and 5min, the degradation processes are minimal and thus spherulitic growth rates are not expected to vary much. Yet there is a large difference in the crystallization kinetics as evidenced by the respective crystallization exotherms and values of $K^{1/n}$ obtained from Avrami analysis. While the value of $K^{1/n}$ is 0.61min^{-1} after a residence time of 2min, it decreases to 0.40min^{-1} by increasing the residence time to 5 minutes. This difference is due to decreasing the nucleation density with higher '5 min' residence time. For still higher melt residence times, the degradation reactions which occur result in decreasing the spherulitic growth rates (shown later), which also contribute in slower crystallization kinetics. Thus, while $K^{1/n}$ decreases from 0.40min^{-1} to 0.13min^{-1} as the residence time is increased from 5min to 20min (i.e. by a factor of more than 3), growth rates also decrease by a factor of 2. Therefore, although variations in nucleation density are influencing the crystallization kinetics at shorter residence times, reduced spherulitic growth rates at longer residence times also contribute to decreasing the transformation rates.

Similar effects of the melt residence times on the crystallization behavior would generally be expected for other melt temperatures. Temperatures greater than 430°C lead to a decrease in the isothermal crystallization kinetics while this effect becomes markedly less pronounced for lower melt temperatures. In fact for a melt residence temperature of 410°C , which is close to the bulk melting point, considerable residual nuclei survive much longer residence times, the residual nuclei resulting in an increased rate of crystallization.

Next the influence of melt temperatures on the crystallization kinetics is examined while keeping the melt residence time and the isothermal crystallization temperature constant. Figure 6.12 shows the crystallization exotherms at 355°C after cooling from melt temperatures ranging from 410°C to 430°C for 20 minutes. As can be noted, the melt temperature strongly affects the isothermal crystallization behavior. As the melt temperature is increased, the peak of the crystallization exotherm shifts to longer times. While no considerable broadening is observed, the shapes of the crystallization exotherms change with increasing melt temperatures. As the initial melt temperature is varied from

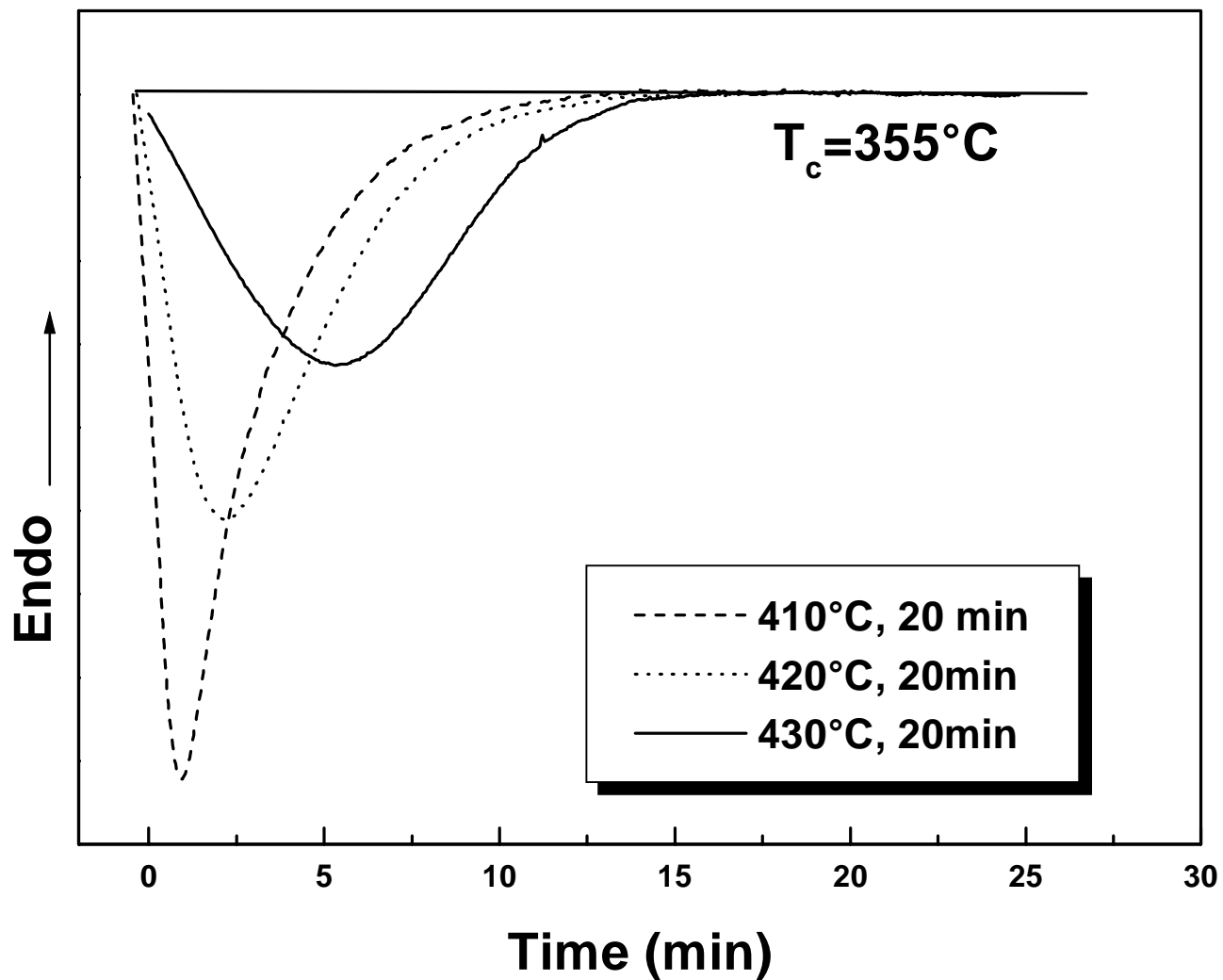


Figure 6.12 Crystallization exotherms at 355°C after a 20 minutes residence time at various melt temperatures.

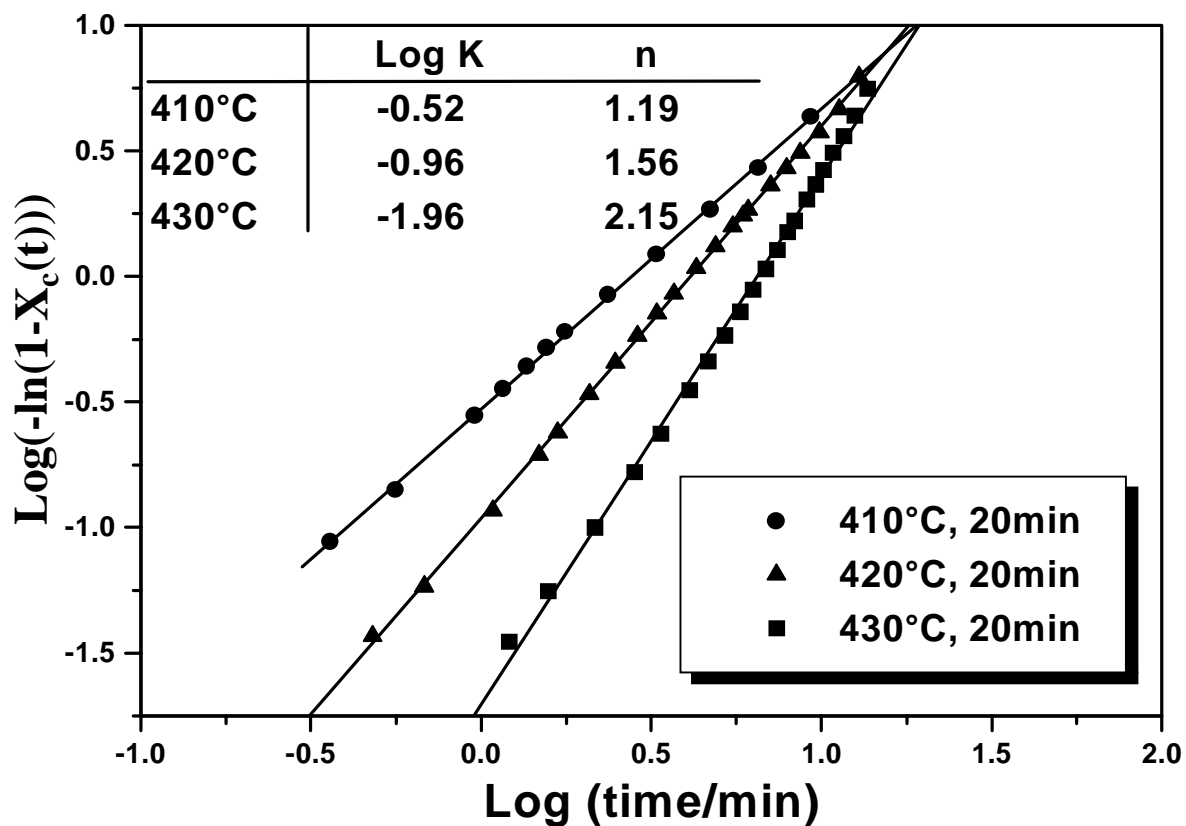


Figure 6.13 Plot of $\log [-\ln (1-X_c (t))]$ versus $\log (\text{time})$ at 355°C after various melt temperatures and a 20 minutes residence time.

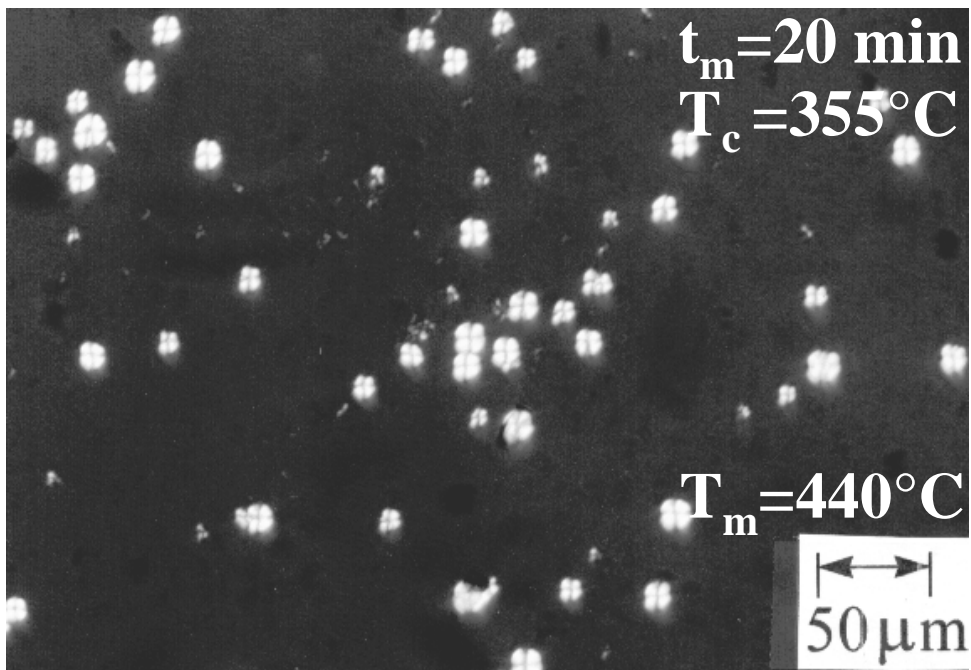
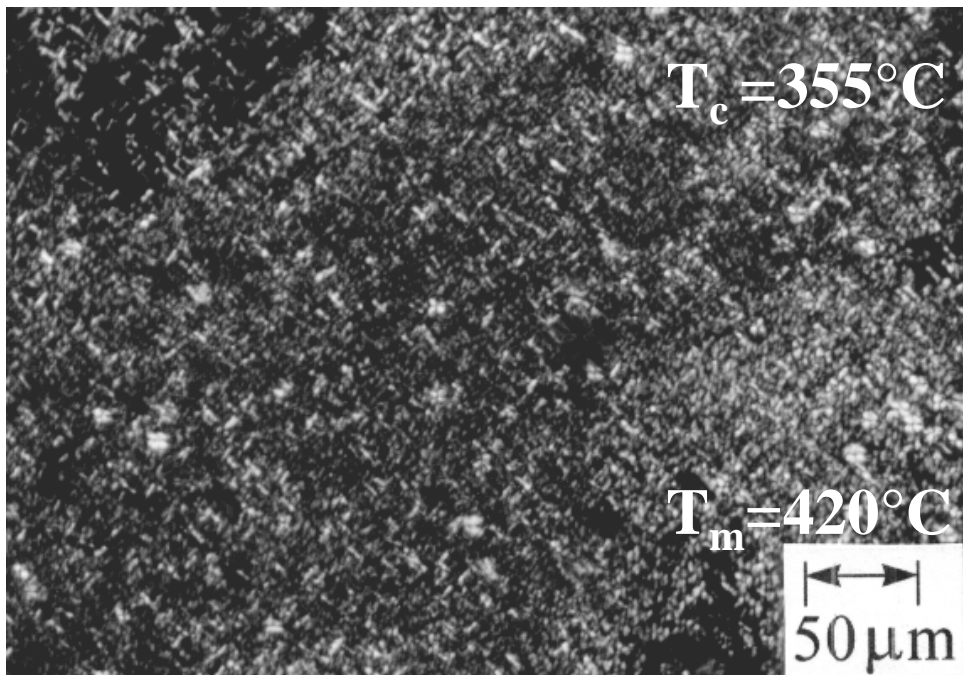


Figure 6.14 Polarized optical micrographs at 355°C after the indicated melt temperatures and a 20 minutes residence time.

410°C to 430°C, the initial crystallization response markedly slows. Interestingly, however, completion times for the overall crystallization do not show much change for the above range of melt temperatures. The corresponding Avrami plot (Figure 6.13) shows the effect of increased melt temperatures on the Avrami constants 'K' and 'n'. The significantly increased value of 'K' with decreasing melt temperature is clearly reflective of a much higher nucleation density for lower melt temperatures. This is in fact confirmed by microscopy studies. Figure 6.14 shows the optical micrographs after 20 minutes at the melt temperatures of 420°C and 440°C. The change in nucleation density with a 20°C increase in melt temperature is strongly evident. The higher nucleation density thus contributes significantly towards the values of the bulk crystallization rate 'K'. The decrease in the growth rates with increasing melt temperatures would also affect the bulk crystallization rates. This feature will be discussed later in the paper. It is clear however, that for isothermal crystallization experiments, melt temperatures have a tremendous effect on the subsequent morphology with regards to the final spherulitic size obtained. Also, an increase in nucleation density leads to the development of more sheaf-like structures and thus a lower Avrami exponent.

Although most flexible chain polymers provide a sufficient temperature range above the melting point where such effects due to residual nuclei or self-seeding nucleation are greatly suppressed, similar results have been obtained for other high melting polymers like PEEK^{13, 14,22}. Although higher melt residence times and higher melt temperatures may be utilized to decrease the effect of previous thermal history, such conditions may also result in chemical reactions taking place. The ensuing discussion addresses this phenomenon.

6.3.2 Rheological studies

6.3.2.1 Isothermal frequency sweeps at 430°C

Semi-rigid chain polyimides like the one utilized in this study do not lend themselves to dissolution in any solvent and thus GPC analysis to quantify initial molecular weight or changes after various melt treatments is not possible. However, melt viscosity determination at various times and temperature serves as a good qualitative tool to detect changes in the molecular weight due to chemical changes at the desired melt temperature. Also, any changes in viscosity are important from a melt-processing viewpoint. Figure 6.15 shows the isothermal complex viscosity of TPER-BPDA-PA (15K) at 430°C as a function of frequency. The melt viscosity displays typical non-Newtonian behavior with the viscosity decreasing with increasing shear rates. At lower shear rates, the viscosity appears to be equilibrating towards a constant value (zero shear viscosity). The experiments were not performed at frequencies lower than 0.1 rad/s as the amount of time needed for these measurements is large and thus the polymer could undergo substantial changes in rheological response during the test at a given frequency. Also, in Figure 6.15, owing to the times needed for data collection at various frequencies, the complex viscosity ($|\eta^*|$) at 0.1Hz represents the values obtained after 8, 16, 24 and 32 minutes. It is very clear that the polymer is undergoing molecular weight changes at 430°C with the viscosity at the lower frequencies increasing by an order of magnitude within the time frame of the experiment. It is well known that η_0 often scales with $M_w^{3.4}$ for many linear thermoplastic polymers above the entanglement molecular weight. Thus assuming the initial M_w of ca. 30,000 daltons (as determined by GPC analysis of the poly (amic acid)) to be above the entanglement M_w , this enables correlating the initial zero shear rate viscosity with M_w (once it is also assumed that the polyimide chains are largely linear).

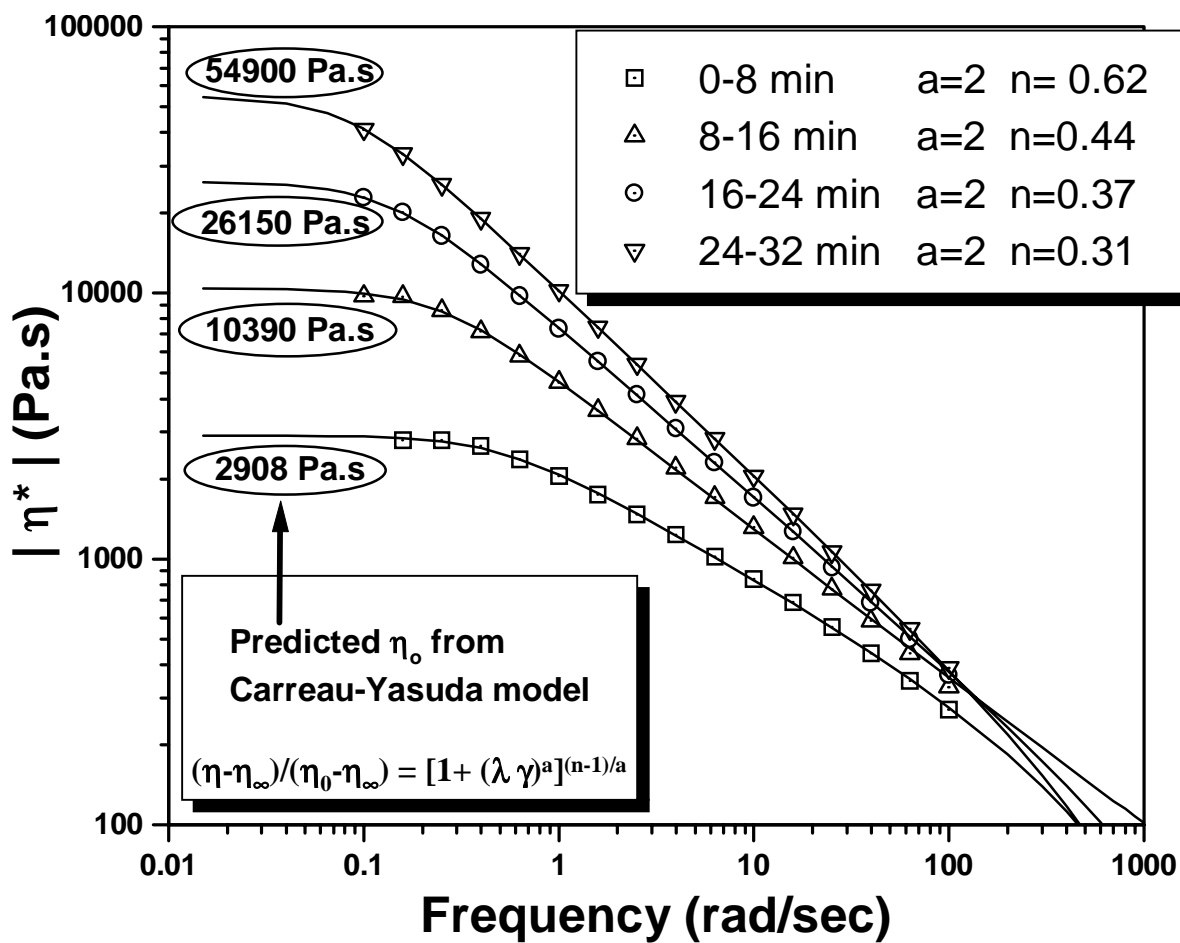


Figure 6.15 Non-Newtonian viscosity-frequency profile of TPER-BPDA-PA (initial $M_n=15,000$ daltons, $M_w=30,000$ daltons) at 430°C . The plot also indicates the data collection times for consecutive scans at the same temperature.

In order to obtain a ‘qualitative’ evaluation of molecular weight changes occurring in the material with time at 430°C, calculation of η_0 is thus required for the different curves. To estimate these variations in η_0 , the Carreau-Yasuda model was utilized to fit the experimental data. This five parameter empirical model has proven very useful in the case of numerous polymer melts for providing analytical expressions for the non-Newtonian viscosity behavior. It has also been widely utilized to extrapolate the value of η_0 from available data that otherwise is often limited to experimentally attainable window of deformation rates. The model is given by the equation:

$$(\eta - \eta_\infty) / (\eta_0 - \eta_\infty) = [1 + (\lambda \dot{\gamma})^a]^{(n-1)/a} \quad \{6.5\}$$

Here λ is a characteristic “time constant”, ‘n’ is the power-law exponent and ‘a’ is a dimension less parameter that describes the transition breadth from the zero shear rate region to the power law region³⁰. ‘ η_0 ’ and ‘ η_∞ ’ represent the zero-shear rate and infinite-shear rate viscosity respectively. Also for higher shear rates (100 rad/s); $\eta_\infty \ll \eta_0$ and thus η_∞ can be set equal to zero without introducing any significant error, though resulting in a simpler equation for fitting the data. While various values of ‘a’ were tried, good fits of the data were obtained for a=2. The calculated values of η_0 are indicated in Figure 6.15. While the estimated value of η_0 is ca.2900 Pa.s. after 8 minutes, it increases to ca. 55,000 Pa.s. after 32 minutes in the melt at 430°C! In this regard, if the $\eta_0 \propto M_w^{3.4}$ relationship is assumed and Carreau-Yasuda model is utilized to approximate η_0 , a coarse estimate of the molecular weight changes occurring in the material can be obtained. *This rough analysis leads to the conclusion, that the initial weight average molecular weight (M_w) of ca. 30K, reaches ca. 44K after 16 minutes, ca.57K after 24 minutes and ca. 71K after 32 minutes!* These crudely estimated values indicate a more than two-fold increase in M_w after 32 minutes at 430°C. It is thus evident that relatively longer residence times of ca. 32 min at 430°C lead to significant occurrence of chemical reactions resulting in build up of molecular weight or crosslinking/branching reactions.

6.3.2.2 Isothermal time sweeps at various melt temperatures

Figure 6.16 shows the magnitude of the isothermal complex viscosity $|\eta^*|$ at temperatures ranging from 410°C to 450°C while keeping the frequency fixed at 1 rad/s. It is observed that the initial viscosity of the material is very sensitive to melt temperature. While the initial viscosity is ca. 2500 Pa.s at 410°C, it decreases to ca. 650 Pa.s when measured at 450°C. Although, higher temperatures would be expected to lead to a lower viscosity, destruction of residual nuclei at higher temperatures, leading to a more homogenous melt, could also contribute in lowering the viscosity. Earlier, optical microscopy experiments have shown that while the number of residual nuclei decrease with increasing melt temperatures and residence times in the melt, a large number of these nuclei do survive short exposure times at melt temperatures as high as 430°C. However, even short residence times at higher temperatures of 440°C and 450°C reduce the population of residual nuclei by a large amount. The effect of residual nuclei on melt viscosity is believed to be prominent at a melt temperature of 410°C. Although, earlier studies have indicated that the equilibrium melting point of this polymer is close to this temperature, the exact value of this temperature is not known with certainty. In this regard, if 410°C is below the true equilibrium melting point, a larger number of initial crystals may survive and could also contribute to a higher melt viscosity. This may lead to crystallization at lower supercoolings due to self-seeding nucleation. While the decreasing number of residual nuclei with time at any melt temperature would lead to a decrease in viscosity, molecular weight increases due to cross-linking reactions lead to an increasing viscosity with time in the melt.

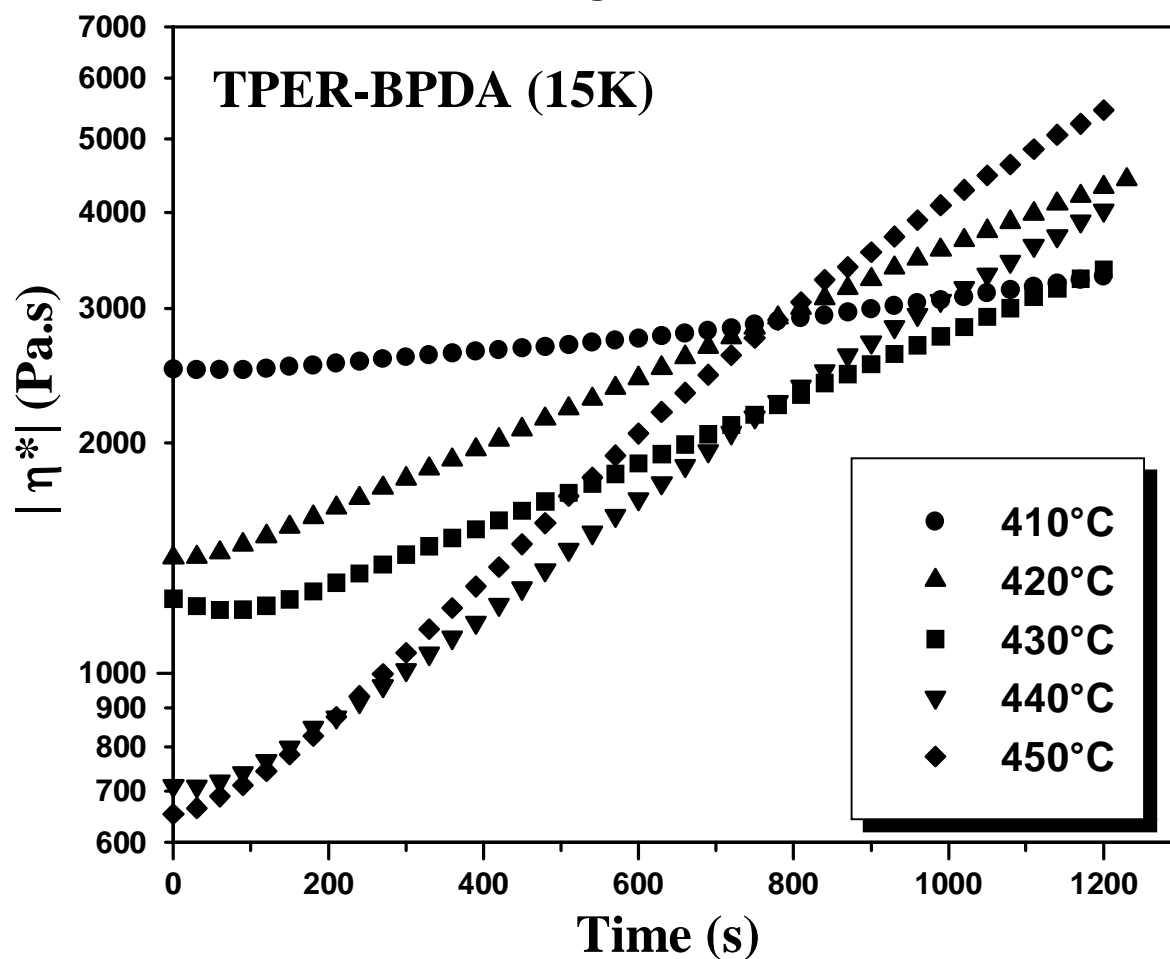


Figure 6.16 Isothermal complex viscosity (1 radian/s) as a function of residence time in the melt at various melt temperatures.

There is some indication that these chemical reactions are of some significance even at 410°C, after 15 minutes. At melt temperatures of 420°C and 430°C, the initial viscosity is much lower which is conjectured to be due to the destruction of residual nuclei (a more homogenous melt) and increased temperatures. However, it is clear that chemical (degradation) reactions (leading to molecular weight increase due to branching/crosslinking) begin at temperatures of 420°C and 430°C since the viscosity begins to rise soon after the melting of the polymer. The difference in severity of these reactions at 420°C and 430°C, however, is not great, as can be seen by the nearly parallel slope of viscosity vs. time curves for the two temperatures. The small difference in viscosity curves at these temperatures may be attributed to both the differences in temperatures and in the difference in the population of residual nuclei. At 430°C, the viscosity (at 1 rad/s) increases from ca. 1200 Pa.s to above 3000 Pa.s within 20 minutes, which, as shown earlier, is indicative of branching/crosslinking (degradation). Interestingly, however, earlier DSC studies^{3, 4} from this laboratory has shown that the melting behavior after similar melt treatment remains unaffected, with no changes in the peak melting point, heat of melting or broadness of the melting endotherm! Hence it is clear that although these changes in the magnitude of complex viscosity indicate some chemical changes, the overall crystallizability and melting behavior of the polymer show little change. Increasing the temperature to 440°C or 450°C leads to a further initial drop in the melt viscosity due to the reasons discussed above. However, there is not much difference in the viscosity at 440°C and 450°C although there is a significant drop in the viscosity on increasing the melt temperature from 430°C to 440°C. This large decrease in initial viscosity is believed in large part due to a decrease in the population of residual nuclei. This would also lead to lower nucleation density on crystallization, this helping to confirm the earlier optical microscopy data in Figure 6.14.

The degradation reactions at 440°C and 450°C are significantly greater and lead to a faster increase in viscosity than at 420°C and 430°C. Interestingly, for melt temperatures of 420°C and 440°C, the final viscosity after a period of 20 minutes is nearly the same although the condition or structure of the melt is very different! While there is significantly less chemical reactions at 420°C, lower temperature and existing order in the

melt is responsible for a higher viscosity. For a melt temperature of 440°C, however, the melt has an increased molecular weight due to crosslinking/ chain branching while most of the residual order is completely destroyed. The slope of complex viscosity vs. time can be approximately taken as the measure of the rate of degradation reactions at various temperatures. It is clear that the rate of chemical changes, although very similar at 420°C and 430°C, is largely increased when the melt temperature is increased to 440°C and 450°C. In fact the viscosity increases by nearly an order of magnitude in 20 minutes at 450°C. Also, although the time frame of 20 minutes was selected on the basis of earlier work, it is noticed that the state of the melt would be very different for shorter holding times. While holding times shorter than 3 minutes induce relatively little branching/crosslinking even at 450°C, successively higher melt temperatures also lead to a decreased viscosity. This lower viscosity would affect the melt processing as well as the final crystallization behavior on cooling.

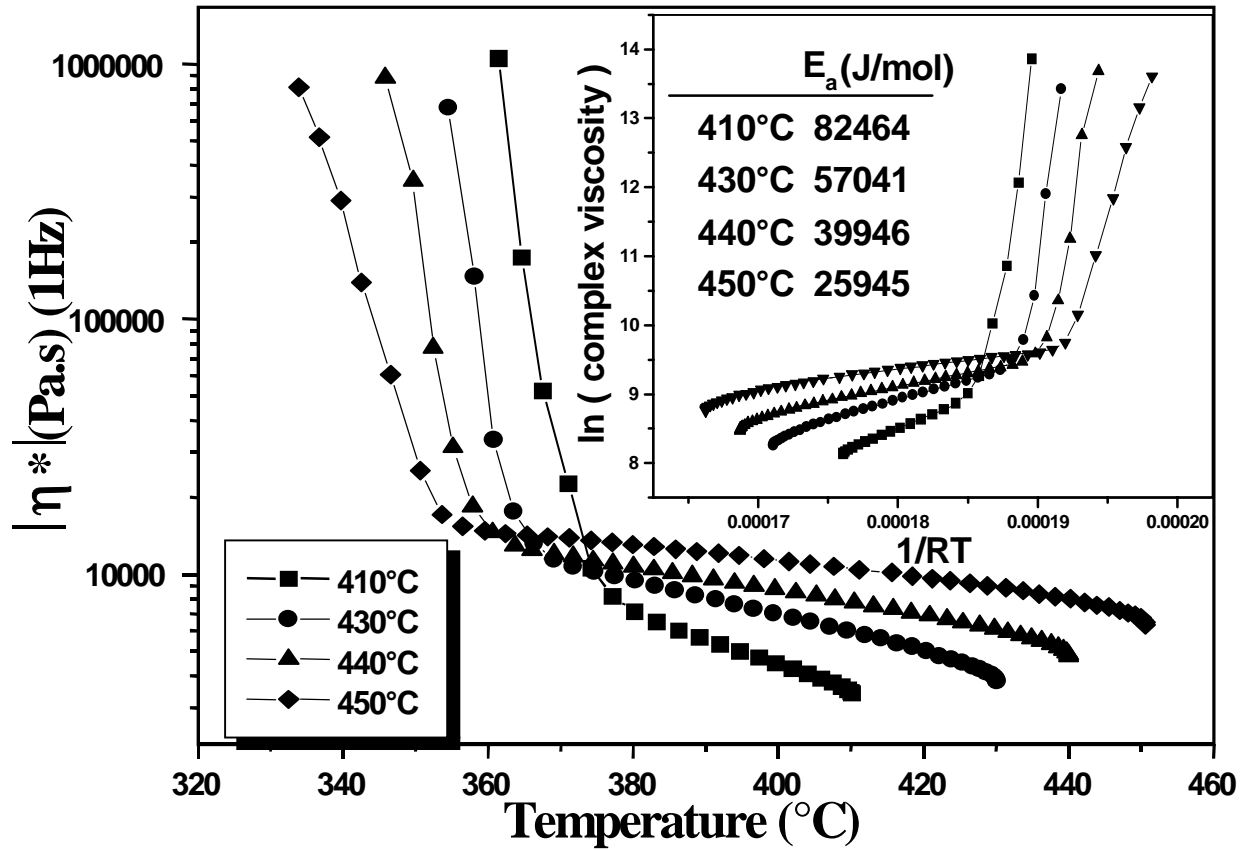


Figure 6.17 Non-isothermal complex viscosity (1 radians/s) when cooled at 10°C/min from various melt temperatures after 20 minutes residence time. *Inset:* Corresponding Arrhenius plots for the non-isothermal viscosity profiles when cooled from various melt temperatures. The initial regions prior to crystallization were utilized for estimating the value of activation energy using the Andrade-Eyring equation.

6.3.2.3 Complex viscosity on cooling from various melt temperatures

For processing operations it is important to know the variation of melt viscosity with cooling and also the temperatures at which solidification of the melt due to the crystallization may occur. The effect of thermal history on solidification temperatures is thus examined when the polymer melt was cooled at $10^{\circ}\text{C}/\text{min}$ after 20 minutes at various melt temperatures and the results shown in Figure 6.17. The onset of crystallization was observed for all samples with the viscosity increasing sharply at various degrees of supercoolings. *A strong dependence, however, of the prior melt temperature on the crystallization is observed with the degree of supercooling necessary for crystallization increasing with higher melt temperatures.* Lower melt temperatures hasten the onset of crystallization with the onset temperature shifting from 377°C to 356°C when the melt temperature was changed from 410°C to 450°C . Crystallization at such low supercooling, when cooling from 410°C , clearly shows the strong effect of residual nuclei on crystallization behavior. Also, the supercooling required for crystallization was ca. $7\text{--}8^{\circ}\text{C}$ more for a sample cooled from 450°C in comparison to a sample cooled from 440°C . This difference cannot be explained due to residual nuclei, as there is expected to be little difference in their population at these two temperatures (i.e. most of the residual nuclei are expected to be destroyed once the temperature is raised to 440°C , and thus no substantial decrement in their population is further expected by raising the temperature to 450°C). However, the higher molecular weight of samples caused by higher melt temperature leads to slower crystallization. Both the decreasing population of residual nuclei with increasing melt temperatures as well as the increased molecular weight of samples exposed to higher melt temperatures contribute to the onset temperature of crystallization. However, it should be clear that there is a strong frequency dependence in the above analysis and thus only qualitative trends can be made. For the same reason these results cannot be quantitatively compared with traditional DSC experiments, which are less sensitive in detecting the onset of crystallization.

6.3.2.4 Activation energy (E_a) values on cooling from various melt temperatures

It was also noted that the viscosity profiles before the onset of crystallization were also dependent upon the previous thermal history. It is well established that, the viscosity dependence on temperature can generally be described by the Andrade-Eyring equation³¹:

$$\eta = B \exp (E_a/RT) \quad \{6.6\}$$

This equation was derived initially for small molecules and is generally valid at temperatures in excess of 100 K above T_g for polymers. Here E_a is the flow activation energy of viscous flow and is representative of the energy barrier for successive segmental jumps into unoccupied sites or ‘holes’. The value of E_a thus depends on the ease with which the polymer segments can “jump” into the available holes through conformational changes³². The higher value of E_a is indicative of a lower “jump frequency” and/or decreased availability of these holes. The lower “jump frequency” (higher E_a) can also be viewed as the result of a higher degree of co-operativity needed to create the required ‘holes’. The general range of value of E_a varies between 20 KJ/mol to well over 120 KJ/mol for various polymers. The inset in Figure 6.17 also shows the corresponding Arrhenius plots based on this relationship. The regions of the curve before the onset of crystallization were used to *estimate* the activation energy for different curves. While the temperature range utilized to fit the data to the Andrade-Eyring equation was largest for crystallization from 450°C, sufficient data points were still available for a reasonable fit when following crystallization from 410°C. The activation energy was found to depend strongly on the initial thermal history. While the value of activation energy obtained was 82 KJ/mol when cooled from 410°C, it was only 26 KJ/mol when cooled from a melt temperature of 450°C!

It is well recognized that ‘local segmental character’ and not the molecular weight determines the value of activation energy. The value of activation energy, although

dependent upon the chemistry, can also differ with changes in chain topology. Long chain branched polymer would be expected to show a higher value of activation energy than its linear homologue, the difference being dependent upon the amount and nature of the branching³³. In this regard, the increase in molecular weight for a higher melt temperature would not explain to the lower values of activation energy obtained. However, the branching reactions that occur at these higher temperatures, would only serve to increase the translational/rotational restrictions along the chain backbone and thus should lead to a higher value of activation energy. However, an opposite trend is observed here! This result can be explained on the basis of residual order (residual nuclei) that still exists at lower melt temperatures. Increasing melt temperatures lead to destruction of this previous order and a more homogenous melt. The destruction of this residual order has already been confirmed on the basis of the earlier discussed optical microscopy results. The large differences observed in the value of activation energy are thus believed to be indicative of a more homogenous melt at higher temperatures. However, this homogeneity is accompanied with increased viscosity at these higher temperatures and is thus associated with increases in molecular weight.

It should be mentioned that evaluation of E_a would show some frequency dependence of such an analysis if carried out in the shear-thinning region. In this case however, results are based on viscosity at 1 rad/s, the lowest frequency experimentally feasible for such a study. *The values of E_a thus obtained serve more as a comparison between various experimental conditions rather than suggesting some truly absolute value for the polymer.*

6.3.3 Growth rates as a function of melt histories and non-isothermal behavior:

It was earlier demonstrated that harsher melt conditions lead to slower crystallization kinetics, which is in part due to the reduction in residual nuclei. Another important reason for slower crystallization response may be the decreased spherulitic

growth rates due to increased melt viscosity caused by enhanced molecular weight/branching reactions following harsher melt conditions. To evaluate this effect, thin polymer films sandwiched between two glass slides were quenched to 345°C after 20 min residence times at 420°C-460°C. These melt conditions are similar to the experiments discussed earlier and adhesion experiments described elsewhere⁴. A spherulitic morphology was observed for all melt temperatures with no microscopically observable changes in the morphological character of the spherulites. *Interestingly, a spherulitic morphology was observed even after 20 minutes in the melt at 460°C!* This perhaps is the highest melt temperature from which organic polymer spherulites have been observed on cooling after such a long residence time in the melt. However, melt temperature and melt residence time have a strong effect on the subsequent spherulitic growth rate (Figure 6.18). The degradation (branching) associated with higher melt temperature/longer residence times results in significantly reduced growth rates. The growth rate studies also show a close correlation with earlier rheological results. For a residence time of 20 min, the growth rates show a sharp decrease if the melt temperatures are raised above 430°C. However, there is relatively a smaller drop in growth rate if the temperature is raised from 420°C to 430°C. This indicates that the extent of branching/cross-linking reactions, though somewhat similar at 420°C and 430°C, is largely increased if the melt temperatures are taken above 430°C. A similar conclusion was also reached after the previous rheological study and in earlier studies^{3, 4}. Growth rate data was also collected after a 5 minute residence at 420°C and 430°C although the high nucleation density encountered due to these less stringent melt conditions necessitated several repetitions of this experiment. The growth rate after 5 min and 20 min residence times at 420°C were found to be 0.21 μm/s and 0.107 μm/s respectively. Similar results are obtained for a melt temperature of 430°C. The significant reduction in growth rate with increased residence times is also in agreement with previous rheological results which indicate a corresponding two-fold increase in melt viscosity. Thus both techniques indicate the presence

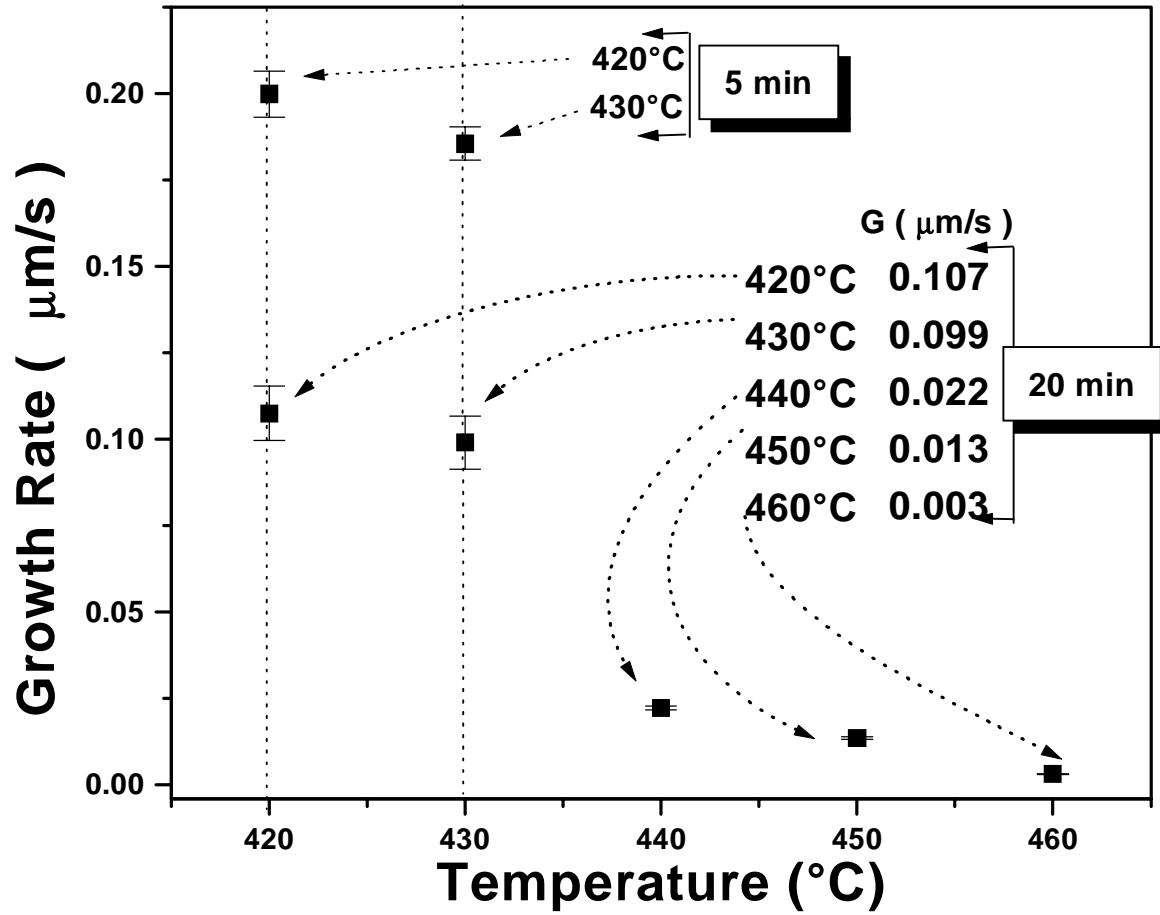


Figure 6.18 Spherulitic growth rates at 345°C after 20 minutes at various initial melt temperatures.

of some chemical reactions even at 420°C which is only 25°C above the bulk melting point of the polymer. These conclusions also highlight the importance of melt conditions for studies dealing with other high melting polymers. Proper selection of initial melt conditions is vitally important before any fundamental studies are attempted to model the crystallization behavior. However, for many such polymers including the one utilized in this study, such ideal conditions may not exist.

While the above spherulitic growth rate study helps in gauging the degradation effect of melt conditions, it also has important ramifications with regards to more conventional non-isothermal crystallization behavior. These results indicate that for a given cooling rate, as the initial melt temperature is increased, the crystallization would occur at larger supercooling. In fact, for harsher melt conditions, for e.g. 460°C for 20 min, the growth rates are significantly reduced and thus it should be possible to quench the polymer to a state with little or no crystallinity present. However, a significant amount of crystallinity was found to be present by DSC and a very fine grainy morphology was revealed by optical microscopy for such a quenched sample. Non-isothermal studies were thus attempted to interpret this behavior.

DSC was utilized to observe the non-isothermal crystallization behavior from different initial melt temperatures. Figure 6.19 shows the cooling scans at 10°C/min after 10 minutes in the melt at temperatures varying from 400°C to 450°C. As the temperature is increased beyond 400°C, the crystallization exotherm shifts to higher undercoolings, the amount of shift increasing with increasing melt temperatures. While the scans from 400°C and 450°C give a characteristic single crystallization peak, the intermediate scans lead to a double peak in the crystallization exotherm! A melt temperature of 400°C, which is above the bulk melting point of 395°C (but below the expected equilibrium melting point), does not erase the previous thermal history and thus the crystallization occurs at much smaller undercoolings. The sharper (and higher) crystallization exotherm (from 400°C) is believed to result from the recrystallization of previously unmelted residual crystals. However it is interesting to note that a second crystallization peak appears for intermediate melt

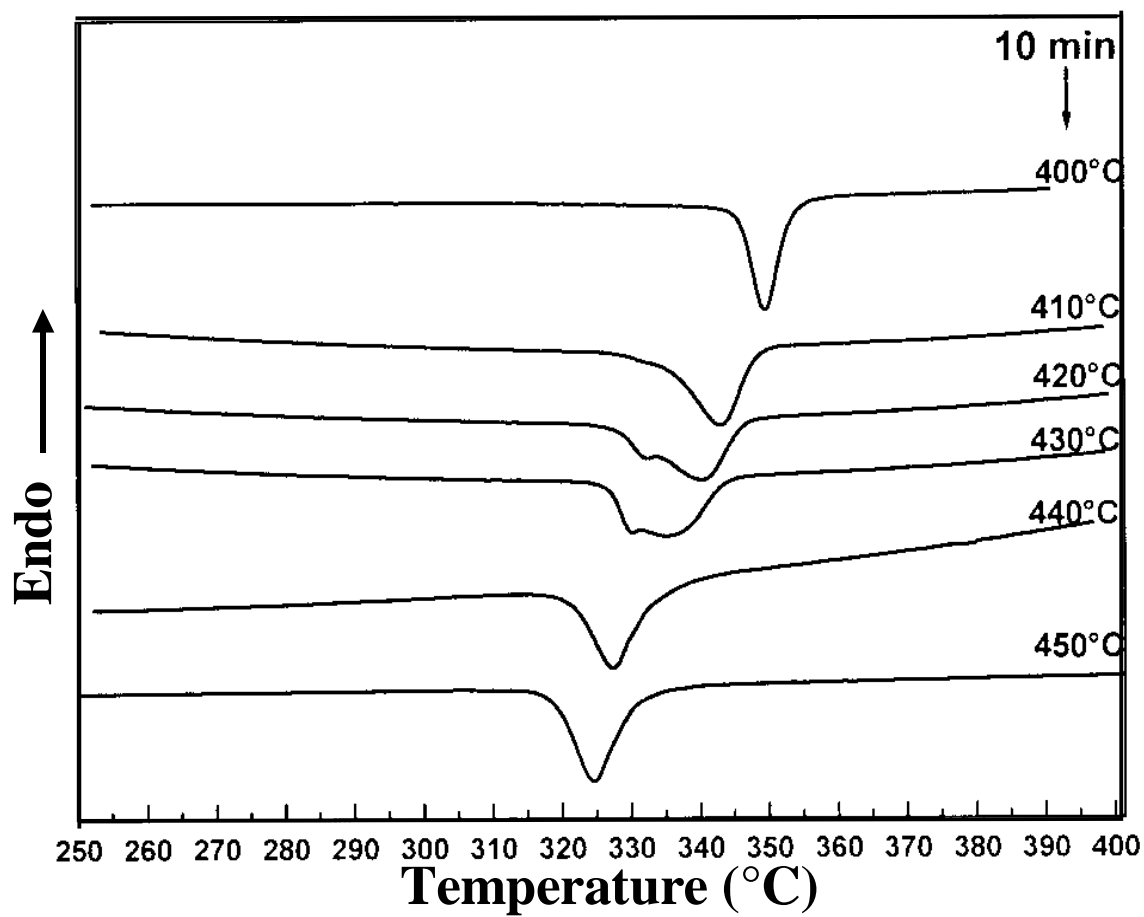


Figure 6.19 DSC cooling scans at 10°C/min after 10 minutes at various melt temperatures.

temperatures. This second peak appears first as a shoulder on the low temperature side of the exotherm when cooling from 410°C, but becomes a separate peak as the melt temperature is increased. It is clear that the double exothermic behavior is indicative of two separate crystallization phenomenon. The occurrence of these crystallization exotherms, however, is dependent on previous melt history. Also, earlier studies^{4,5} have not indicated any evidence of polymorphism in this polymer.

Isothermal crystallization experiments were performed at temperatures in the vicinity of the double exothermic behavior (at 335°C) using a hot-stage on an optical microscope between crossed polars. It was found that the initial spherulitic crystallization was followed by a sudden ‘catastrophic nucleation’ leading to the development of a fine grainy background! The details of the superstructure that developed due to this catastrophic nucleation were not optically resolvable and caused the initially observable larger spherulites to become totally enveloped in the subsequent overall fine pattern. The double exothermic behavior on non-isothermal crystallization from the melt is easily explained due to this catastrophic nucleation process. When cooling from 420°C, the initial exotherm is indicative of spherulitic development, while the onset of ‘catastrophic nucleation’ at lower temperatures leads to a second exothermic peak. As shown earlier, increasing the melt temperature to 440°C and 450°C leads to a significant reduction in the nucleation density (Figure 6.14) and much decreased spherulitic growth rates (Figure 6.18). *Thus, a lesser number of heterogeneous sites available for spherulitic development and reduced spherulitic growth rates decrease the chances of any spherulitic crystallization at lower supercooling (i.e. at $T_c > 340^\circ\text{C}$) during a non-isothermal cooling scan in a DSC.* This is distinctly observed in DSC cooling scans (Figure 6.19) as the melt temperatures are increased to 440°C and 450°C. While at temperatures lower than 430°C, initial spherulitic crystallization contributes significantly to the overall crystallization, the second ‘catastrophic nucleation’ process is mainly responsible for crystallization from 440°C and 450°C. The crystallization peak, however, shifts to 324°C from 327°C as the melt temperature is increased from 440°C to 450°C, thus indicating a small dependence of ‘catastrophic nucleation’ on the initial melt temperature.

To study the crystalline morphology when crystallization occurs under nonisothermal conditions, a typical experiment was performed from the melt at a cooling rate of 20°C/min. The melt conditions observed for this experiment were 430°C and 20 minutes respectively. While spherulitic development begins early, a subsequent decrease in the temperature in the vicinity of 330°C leads to a catastrophic increase in nucleation density as shown in the last micrograph of Figure 6.20. As observed in isothermal experiments, this rapid increase in nucleation density leads to development of a fine pattern, which envelops the initially growing spherulites. However when cooled from higher melt temperatures (eg. 450°C), at the same cooling rate, no spherulites were observed and only the ‘catastrophic nucleation’ was responsible for the crystallization. The initial melt conditions and cooling rate thus are critical in deciding the final morphology of this polymer.

6.4 Conclusions

Isothermal crystallization of semicrystalline polyimide, TPER-BPDA-PA was characterized as a function of crystallization temperature and thermal history in the melt. It was found that isothermal crystallization was very sensitive to crystallization temperature thereby limiting the thermal window of study. The holding time in the melt also had a strong affect on crystallization behavior. At a given supercooling, increased holding time in the melt at 430°C substantially broadened the crystallization exotherm. While the Avrami exponent did not show a significant change, the value of the Avrami parameter ‘K’ decreased considerably with residence time in the melt. Melt temperatures also affected the crystallization behavior substantially with the Avrami analysis showing strong changes in both the exponent ‘n’ and the parameter ‘K’. A substantial decrease in the nucleation density with harsher melt conditions was revealed by optical microscopy and was primarily responsible for slowing the crystallization kinetics at 355°C.

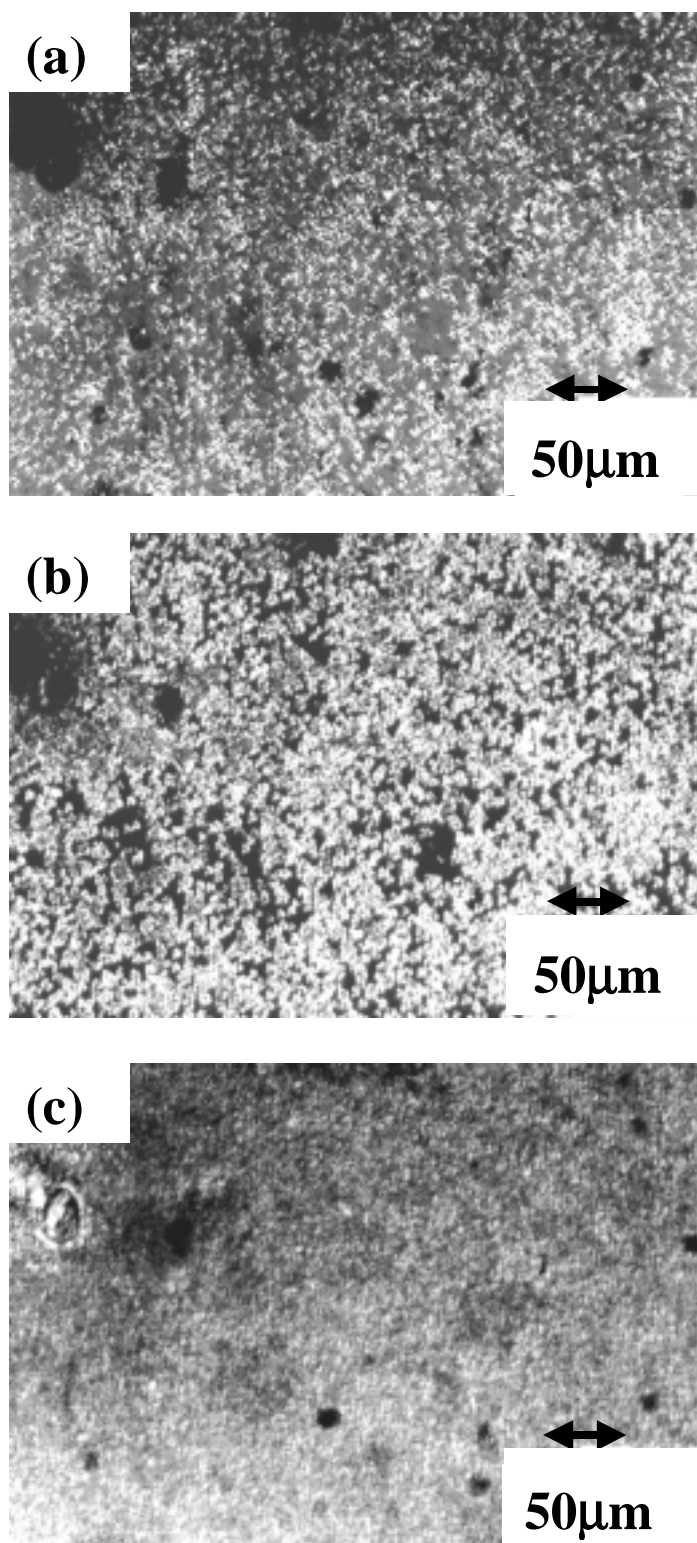


Figure 6.20 Polarized optical micrographs illustrating the morphological development when cooled at 20°C/min from the melt at 430°C for 20 minutes. Micrographs taken at (a) 340°C (b) 332°C (c) 323°C.

Melt viscosity experiments conducted at 430°C showed that chemical reactions (branching/cross-linking) were indeed present at these temperatures. The rate of these reactions however, increased substantially above 440°C. At lower melt temperatures of 410°C, however, little evidence of any major chemical changes was evidenced. However, although higher temperatures lead to build up of molecular weight, they also succeed in removing the previous thermal history to a large extent. Crystallization experiments performed using a rheometer showed that the onset of crystallization shifts to higher undercoolings with increasing melt temperatures. The temperature dependence of the complex viscosity as a function of previous melt temperature was evaluated using the Andrade-Eyring equation. The estimated activation energies found by such an analysis decreased strongly with increasing melt temperatures. This was due to the decreasing constraints of the residual nuclei, whose population decreased with increasing melt temperature.

Isothermal experiments at 345°C showed that growth rates were also dependent upon the previous melt temperature, with large decreases in growth rates observed when the initial melt temperature was raised above 430°C. The growth rates did not show any significant change when the initial melt temperature was changed from 420°C to 430°C. However, experiments carried out for shorter residence times at 420°C and 430°C showed higher growth rates due to lesser degradation. Interestingly, spherulites (with no observable change in the overall superstructure) were even obtained from melt temperatures as high as 460°C after residence times as long as 20 minutes.

Non-isothermal DSC experiments revealed double peaks in the crystallization exotherms. A ‘catastrophic nucleation’ process was found to explain the presence of the second peak as revealed by both isothermal and nonisothermal POM studies. This second crystallization process dominated the overall crystallization as the melt temperatures were raised. The crystalline morphology resulting from this ‘catastrophic nucleation’ process could not be resolved by optical microscopy.

6.5 Acknowledgments

The author wishes to thank the NSF Science and Technology Center for High Performance Polymeric Adhesives and Composites for full support of this study under contract number DMR 9120004. Generous support from the GenCorp Foundation is also acknowledged.

References:

-
- ¹ Hergenrother, P.M., Stenzenberger, H.D. and Wilson D., *Polyimides*, Blackie & Son Ltd., London, 1990.
 - ² Mittal, K.L. and Ghosh, M.K., *Polyimides: Fundamentals and Applications*, Marcel Dekker, Inc., 1996.
 - ³ Wilkes, G.L. *Ency. Phy. Sci. Tech.* 1987, Vol. **11**, 61.
 - ⁴ Ratta, V., Stancik, E.J., Ayambem, A., Parvatareddy, H., McGrath, J.E. and Wilkes, G.L. *Submitted to Polymer*.
 - ⁵ Srinivas, S., Caputo, F.E., Graham, M., Gardner, S., Davis, R.M., McGrath, J.E. and Wilkes, G.L. *Macromolecules*, 1997, **30**, 1012.
 - ⁶ Sasuga, T. *Polymer*, 1991, **32**, 1539.
 - ⁷ Chang, A.C., Hou, T.H., St. Clair, T.L. in *Polyimides: Trends in Materials and Applications, Proc. Fifth Int. Conf. on Polyimides*, 1994, 3.
 - ⁸ Graham, M.J., Srinivas, S., Ayambem, A., Ratta, V., Wilkes, G.L. and McGrath, J.E. *Polymer Preprints*, April, 1997, **38(1)**, 306.
 - ⁹ Grenier, D. and Homme, R.E.P. *Journal of Polymer Science: Polymer Physics Edition*, 1980, **18**, 1655.
 - ¹⁰ Price, F.P. *Journal of Applied Physics* 1965, **36**, 3014.
 - ¹¹ Tomka, J. *European Polymer Journal*, 1968, **4**, 237.
 - ¹² Hillier, I.H. *Journal of Polymer Science: Part A*, 1965, **3**, 3067.

-
- ¹³ Banks, W., Hay, J.N., Sharples, A., and Thompson, G. *Polymer*, 1964, **5**, 163.
- ¹⁴ Risch, B.G., Warakowski, J.M. and Wilkes, G.L. *Polymer*, 1993, **34**, 2330.
- ¹⁵ Hsiao, B.S., Kreuz, J.A., and Cheng, S.Z.D., *Macromolecules* 1996, **29**, 135.
- ¹⁶ Muellerleile, J.T., Risch, B.G., Rodrigues, D.E., and Wilkes, G.L., *Polymer* 1993, **34**, 789.
- ¹⁷ Lee, Y. and Porter, R.S. *Macromolecules* 1988, **21**, 2770.
- ¹⁸ Cebe, P. and Hong, S. *Polymer* 1986, **27**, 1183.
- ¹⁹ Heberer, D.P., Cheng, S.Z.D., Barley, J.S., Lien, S.H.S., Bryant, R.G. and Harris, F.W. *Macromolecules* **24**, 1890.
- ²⁰ Hsiao, B.S., Sauer, B.B. and Biswas, A. *Journal of Polymer Science: Part B: Polymer Physics*, 1994, **32**, 737.
- ²¹ Lopez, L.C. and Wilkes, G.L. *Polymer* 1988, **29**, 106.
- ²² Wunderlich, B. 'Macromolecular Physics: Crystal Nucleation, Growth and Annealing', Vol. 2, Academic Press, New York, 1976.
- ²³ Fatou, J.G. "Crystallization Kinetics", *Encyclopedia of Polymer Science and Engineering*, (Suppl. Vol.), John Wiley and Sons, New York, 1989, 231.
- ²⁴ Hoffman, J.D., Davis, G.T. and Lauritzen, J.I., Jr., 'Treatise in Solid-State Chemistry', (ed. Hannay, H.B.), Vol. 3, Plenum Press, New York, 1976, 497.
- ²⁵ Ergoz, E., Fatou, J.G. and Mandelkern, L. *Macromolecules* 1972, **5**, 147.
- ²⁶ Jonas, A. and Legras, R. *Polymer* 1991, **32**, 2691.
- ²⁷ Turnbull, D. *J. Chem. Phys.* 1950, **18**, 198.
- ²⁸ Morgan, L.B. *J. Appl. Chem.*, 1954, **4**, 160.
- ²⁹ Jorda, R., and Wilkes, G.L. *Polymer Bulletin* 1988, **19**, 409.
- ³⁰ Bird, R.B., Armstrong, R.C., Hassager, O. in "Dynamics of Polymeric Liquids" John Wiley and Sons, New York, Vol. 1, Fluid Mechanics, 1987, 171.
- ³¹ Mendelson, R. *Polymer Engineering Science* 1968, **8**, 235.
- ³² Cowie, J.M.G., in "Polymers: Chemistry and Physics of Modern Materials", 2nd edition, Blackie A & P, 1997, 255.
- ³³ Wilkes, G.L. *Journal of Chemical Education* 1981, **58**, 880.

Chapter 7

Wedge and Double Cantilever Beam Tests on a High Temperature Melt Processable Polyimide Adhesive, TPER-BPDA-PA

7.1 Introduction

This work focuses on with the wedge and double cantilever beam tests on a novel high temperature polyimide that is based on 1, 3-bis (4-aminophenoxy) benzene (TPER or 1,3 (4) APB) and 3, 3', 4, 4'-biphenyltetracarboxylic dianhydride (BPDA). The chain ends are endcapped with phthalic anhydride (PA). This semicrystalline polyimide henceforth referred to as TPER-BPDA has already been discussed in earlier chapters and demonstrates a high T_g of ca. 210°C and a peak DSC melting point of 395°C. In chapter 5 and in chapter 6 the crystallization kinetics, thermal stability, crystalline morphology, melting behavior and rheology of this polyimide has been discussed. Additionally, the excellent adhesive properties of this polyimide have been demonstrated using the lap-shear test geometry.

Several promising features of this polyimide when used as a high temperature adhesive and relevant with respect to the present work are:

- The polyimide demonstrates exceptional thermal stability with little change in its crystallization behavior after 30 minutes in the melt at 430°C.
- Very fast crystallization kinetics from the melt is demonstrated and no additional annealing steps are required to introduce crystallinity (even when the polyimide has been quenched from the melt).
- A simple and solvent free '*Grit Blasting*' as the surface treatment is sufficient in providing a strong and durable interface as determined by cohesive failures at room temperature, after aging and testing at higher temperatures of 177°C and 232°C, and after exposure in various solvents (as revealed by the presence of polymer on both

faces of the fractured coupons. SEM was utilized to examine the lap-shear fracture surfaces after various tests).

- High lap-shear strengths ranging from 6600-8400 psi were obtained at room temperature after various aging times at aging temperatures of 177°C, 232°C and ambient. The strengths remained still high at ca. 4400 psi when tested at 177°C and ca. 2500-3500 psi when tested at 232°C. These values also demonstrate the excellent adhesive strengths at high temperatures and good durability of the adhesive after elongated exposures at high aging temperatures.
- The adhesive bonding procedure is simple as it is solvent free, involves no adhesive tape preparation using the scrim cloth and relatively short cycle times.

In light of these results, it was decided to further evaluate this polyimide as an adhesive by using the wedge and double cantilever beam (DCB) test geometry's.

7.2 Wedge test (experimental methodology):

The Boeing wedge test is a commonly utilized method to test the durability of fractured and stressed adhesive joints when exposed to different environments¹. This fracture test is an ASTM standard (ASTM D 3762) and utilizes a mode I specimen configuration (see Figure 7.1). The test consists of creating an initial crack by inserting a wedge, and then following the propagation of the crack with time. The driving force for the propagation of crack comes primarily from the stiffness of the beams separated by the wedge and this driving force decreases as the crack propagates. It is important to note that in this test the cracked specimen also experiences simultaneous environmental attack at the crack site (when the specimens are placed in that environment). Upon introduction of the wedge, the crack propagates to length 'a'. This results in creation of two new surfaces (each of area A), and release of elastic energy stored in the beams. If this released elastic energy by the beams is given by U_E and the energy to create the two new surfaces is given by U_S , then:

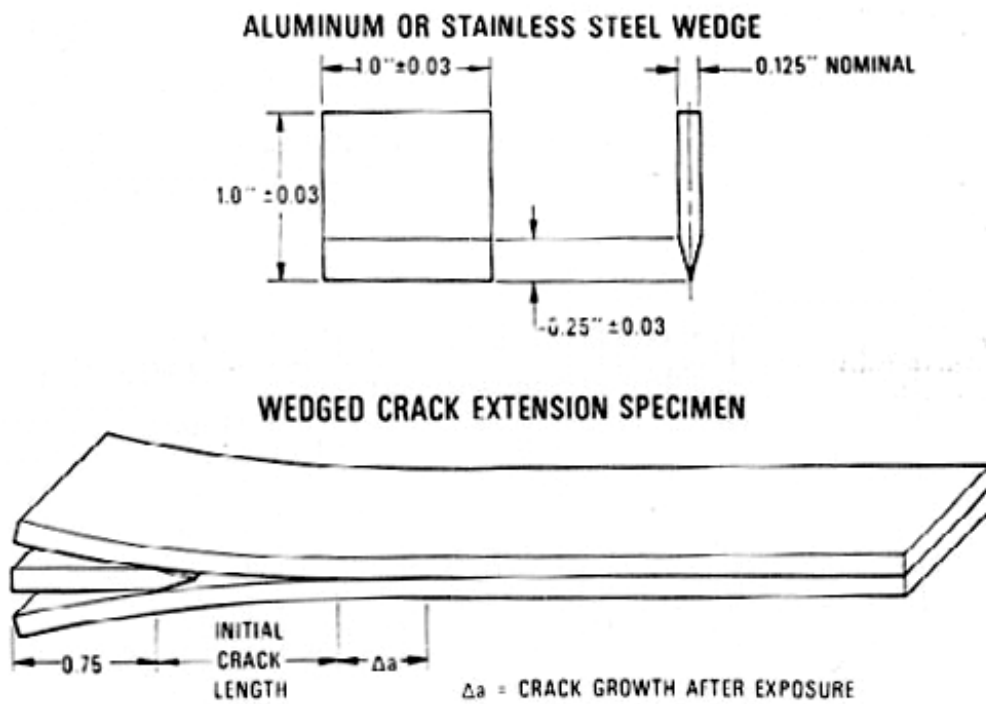


Figure 7.1 Specimen configuration for the wedge test.

Release rate of elastic energy is given by, $G = \partial U_E / \partial A$ {7.1}

Energy needed to create a unit surface² is, $W_s = \partial U_s / \partial A$ {7.2}

The crack propagation stops when $G=W_s$ (this is also known as Griffith's criterion)¹. Till 'G' is higher than W_s , the crack continues to propagate. The value of G, also known as the strain energy release rate (the 'rate' refers to 'release of energy per unit *area*' and not 'release of energy per unit *time*') is calculated to be,

$$G = \frac{3Et^3h^2}{16a^4} \quad \{7.3\}$$

where, E = young's modulus of the beam

t = thickness of the beam

h = wedge thickness

a = crack length

An important assumption in this test is that adherends should not deform plastically. This is usually not a problem when using thick and stiff adherends like the ones utilized in the present study. The decreasing effective cleavage load results in the crack stopping at some equilibrium value, the value itself dependent upon the system conditions. Any contributions due to the viscoelastic properties of the adhesive are not taken into account in the above calculations³. One of the disadvantages of the wedge test is that it is often necessary to remove the specimens from the test environment to make crack length measurements. Also, the cracks may not be easy to view or may propagate unevenly across the specimen width.

The wedge test may test the adhesive strength or cohesive strength depending upon whether the crack propagates on the adhesive interface or purely in the polymer itself (cohesive failure). This test is widely utilized when comparing different surface treatments, especially when the mode of failure is interfacial.

7.3 Double cantilever beam (DCB) test (experimental methodology):

This popular test (ASTM 3433) is used to obtain the mode I fracture energy of the adhesive bonds, which is a measure of the fracture toughness of the adhesive in the presence of flaws. Similar to a wedge test, a crack is initiated first by inserting a wedge. The specimen is then loaded by pulling apart the two beams at a certain rate, this increasing load resulting in increased deflection of two beams. At a certain critical load, the crack begins to propagate resulting in a slight drop in the load (due to the increased compliance). At this point, the beams are stopped from moving apart, thus keeping the deflection constant. The drop in load (due to increasing crack length) and the crack length are carefully followed. Following the equilibration of the crack, the specimen is consecutively unloaded and then loaded. Ideally, the compliance of the fixture should remain the same during these two cycles if there is no further propagation of the crack. This overall procedure is repeated several times leading to total cleavage of the specimen. The data finally collected at various times consists of load, deflection, crack length and the compliance. This data can then be analyzed using several different approaches, two of which are discussed next.

ASTM method:

The ASTM method calculates the fracture toughness, G_{1c} (from load to start of crack), in joules per square meter as:

$$G_{1c} = \frac{(4L^2(\max))(3a^2 + h^2)}{EB^2h^3} \quad \{7.4\}$$

and the fracture toughness, G_{1a} (from arrest load), as follows:

$$G_{1a} = \frac{(4L^2(\min))(3a^2 + h^2)}{EB^2h^3} \quad \{7.5\}$$

where:

L(max) = load to start crack, N

L(min) = load at which crack stops growing, N

E = tensile modulus of adherend, MPa

B = specimen width, mm

a = crack length, mm (distance from crack tip to pin hole centers)

h = thickness of the adherend, normal to plane of bonding, mm

These equations have been established on the basis of elastic stress analysis, and hold for a sharp-crack condition under severe tensile constraint. It is assumed that the crack-tip plastic region is small compared with the size of the crack^{4,5} (an assumption that may not strictly hold for tough adhesive systems). Thus systems of similar toughness should only be compared when using these equations. Also, the analysis can be used to understand the effect of various environments on a particular type of bonded system.

Compliance Method

In the case of compliant adhesives, the adhesive properties become important, as there may be crack tip deflections and rotations. To account for these adhesive properties, bond thickness and other system dependent factors, the compliance method is used which calculates the fracture energy as⁶:

$$G = \frac{9\Delta^2(EI_{eff})}{4B(a+x)^4} \quad \{7.6\}$$

where:

B = specimen width

C = compliance (C = Δ/P)

a = crack length

x = apparent crack length offset

EI_{eff} = effective flexural rigidity

Δ = specimen's opening displacement at point of load application

The parameters EI_{eff} and ' x ' are determined as:

$EI_{\text{eff}} = 2/(3m^3)$ and $x = b/m$

The factors ' b ' and ' m ' are calculated as the slope and y-intercept of $C^{1/3}$ vs. ' a ' curve, the two factors being often related linearly.

7.4 Experimental:

Surface Preparation of Ti-6Al-4V

Surface preparation of titanium alloys often plays a dominant and critical role in obtaining good adhesion strengths and in deciding the long-term durability of the adhesive joints. Based on the earlier work⁷, grit blasting was chosen as the surface treatment for this study. The titanium coupons were first carefully selected so that their thickness' matched closely and that the thickness was constant across the area of the coupons. A special carbide drill was used to carefully drill the holes in titanium specimens used for the DCB tests. Titanium coupons were grit blasted (using alumina particles) just prior to bonding. The coupons were washed with water, dried and then wiped with acetone. The wedges (for the wedge test) were made out of standard stainless steel.

Preparation of Polyimide Strips for the Adhesive Bonding

One of the problems with the present polyimide was its unavailability in films of sufficient size (the problem is related to film casting process during the imidization). In

order to circumvent this problem and obtain a large number of strips of size 7" X 1" needed for the adhesive joints, strips were made from the powder. For this purpose, the available film was first ground to fine powder. A mold of size 7" X 1" was constructed for making films of the exact size needed for bonding. The powder (four grams) was evenly spread between two Kapton sheets, placed in the mold, and consolidated in a hot press. A force of 20,000 pounds and a temperature of 700°F for 12 minutes were used. The initial thickness of the polyimide films obtained was ca. 0.9 mm.

Bonding Conditions for the Wedge tests

The conditions optimized earlier for the lap-shear study were again utilized. These are:

Bonding Pressure = 100 psi	Bonding Temperature = 430°C
Bonding time = 20 min	Cooling rate = 21°C/min

Bonding Conditions for the DCB tests

While the bonding pressure and temperature were kept the same as above, bonding time and cooling rate were varied for this study to understand the effect on the fracture energy. The bonding times tried were 2 min, 20 min and 30 min respectively. For the cooling cycle, in addition to cooling at 21°C/min, some specimens were quenched directly to room temperature while some specimens were held at 365°C for 2.5 hours and then cooled to room temperature. While all the above experiments utilized a $M_n = 15,000$ daltons polymer, some specimens were evaluated for a $M_n = 30,000$ daltons polyimide (while keeping the bonded conditions same) to understand the effect of molecular weight on the fracture energy. A higher molecular weight polymer is expected to demonstrate increased toughness though it often requires higher bonding pressures to make a good bond. In this regard, it was to be seen whether a low bonding pressure of 100 psi was sufficient in adequately bonding the higher molecular weight ($M_n = 30,000$ daltons) polyimide. Additionally, some specimens were made using both the molecular weight versions (with the surface consisting of 15K polymer and the bulk core of 30K

polyimide) to see if improvements in fracture energies could be obtained. In this case, the lower molecular weight polyimide was kept closer to the metal surface whereas the higher molecular weight polyimide constituted the bulk of the polymer adhesive. The reasoning behind such a design was that the lower molecular weight version would facilitate adequate spreading to ensure a good adhesive interface while the bulk of the adhesive would show increased toughness as it was constituted of the higher molecular weight polyimide. However, it remained to be seen whether the low bonding pressure of 100 psi was sufficient in adequately mixing the two different molecular weight versions of the polyimide.

7.5 Results and discussion

One of the most desirable characteristics often required of the adhesive is the resistance to attack from a variety of solvents. To this end, the presence of crystallinity in the polymer (like in the polyimide under discussion) is especially useful as it generally leads to improved solvent resistance. From this viewpoint, in a previous study⁷, TPER-BPDA lap-shear adhesive specimens were exposed to a variety of solvents typically used in aerospace applications. The results achieved in that study were very promising, as there did not seem to be any effect by any of the solvents even after a period of nine days. For specimens exposed to boiling water for as long as 72 hours, the lap-shear strengths were still high at above 4300 psi. These results also compared favorably with other similar studies reported in the literature⁸⁻¹³.

7.5.1 Wedge Tests

While such an initial lap-shear study provided some qualitative idea about the degree of solvent resistance, it was realized that a ‘lap-shear’ specimen geometry is not best suited for testing the solvent resistance of adhesive bonds. This is because any environmental

attack may be limited to the edges of the bond and not over the total specimen. The effect due to different solvents then depends upon the diffusion of the solvent into the central regions of the bond and towards the adhesive interface. Also, any degradation due to the solvent attack is non-uniform across the bonded area. Such conditions are thus not ideally suited for testing the effect of environment on the adhesive.

A wedge test provides a better and a more severe way of testing the effect of various solvents on the bond performance. In this test, the solvent attacks closer to bondline and directly at the site of the initiated crack. It is thus not surprising that wedge tests often lead to interfacial fracture surfaces. This feature has also made the 'wedge test' a method of choice when testing the efficacy of various surface pretreatments.

For the present study the same solvents as the ones used in the previous lap-shear testing were utilized. This also included the 72-hour water boil test, which is usually one of the most severe conditions utilized in such measurements. Due to the experimental nature of the present polyimide, a large amount of this polymer was unavailable. As the amount of polymer required per sample is relatively large for such tests, the testing was restricted in that only two samples were utilized for each solvent exposure. Although, this sometimes resulted in significant differences between the results for the two samples, it is believed that it still provided sufficient understanding of the adhesive performance on exposure to different solvents.

For the wedge tests, the bonding conditions utilized were the ones optimized in an earlier lap-shear study⁷. As the mode of fracture and testing method is different for the wedge test, these conditions may not represent the best possible conditions for a wedge test geometry. For this preliminary study, the objective was to gain a better understanding of the fracture behavior in different solvents. It was also important to see if the 'grit blasting' surface treatment, found sufficient in an earlier lap-shear study, was still effective in providing cohesive failures and not clean interfacial failures instead. The bond thickness was kept similar for all the bonds and averaged at ca. 0.20 ± 0.05 mm with only minor variations (always less than 0.05 mm) along the bonded area for any particular bond.

The results for the wedge tests are shown in Figure 7.2(a) and 7.2(b), with the results for the two samples plotted separately (in no particular fashion). It is clear that for

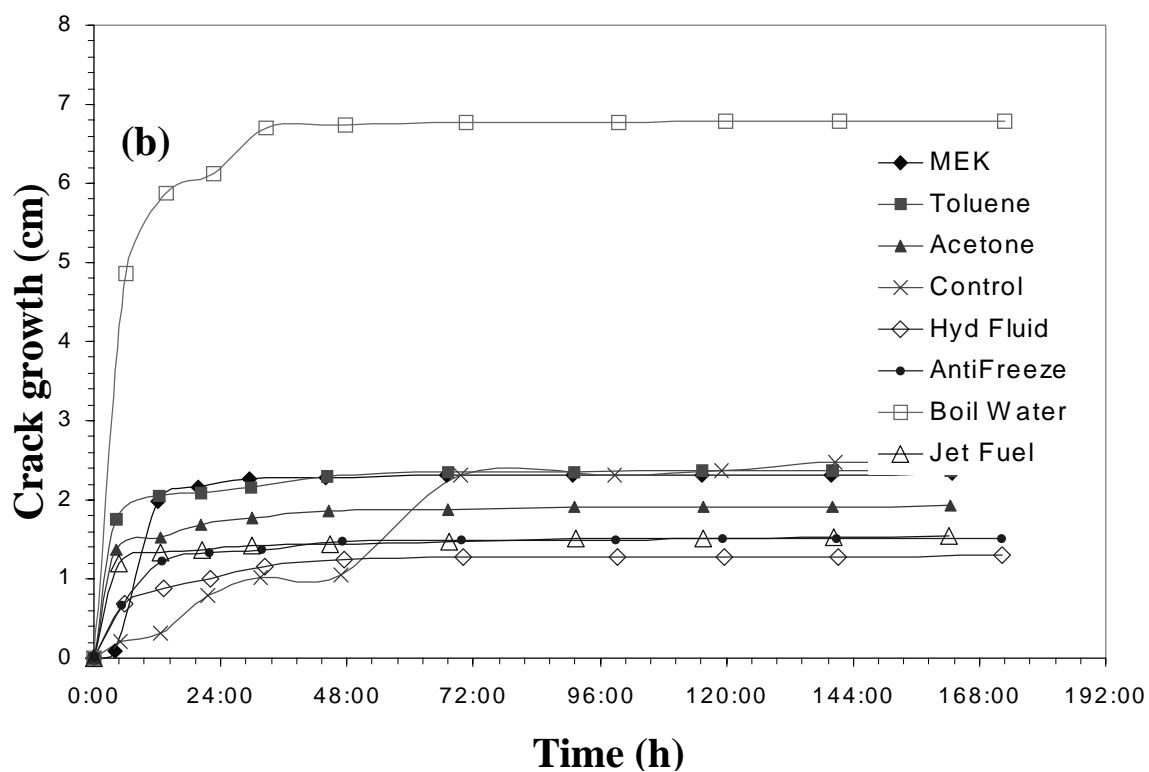
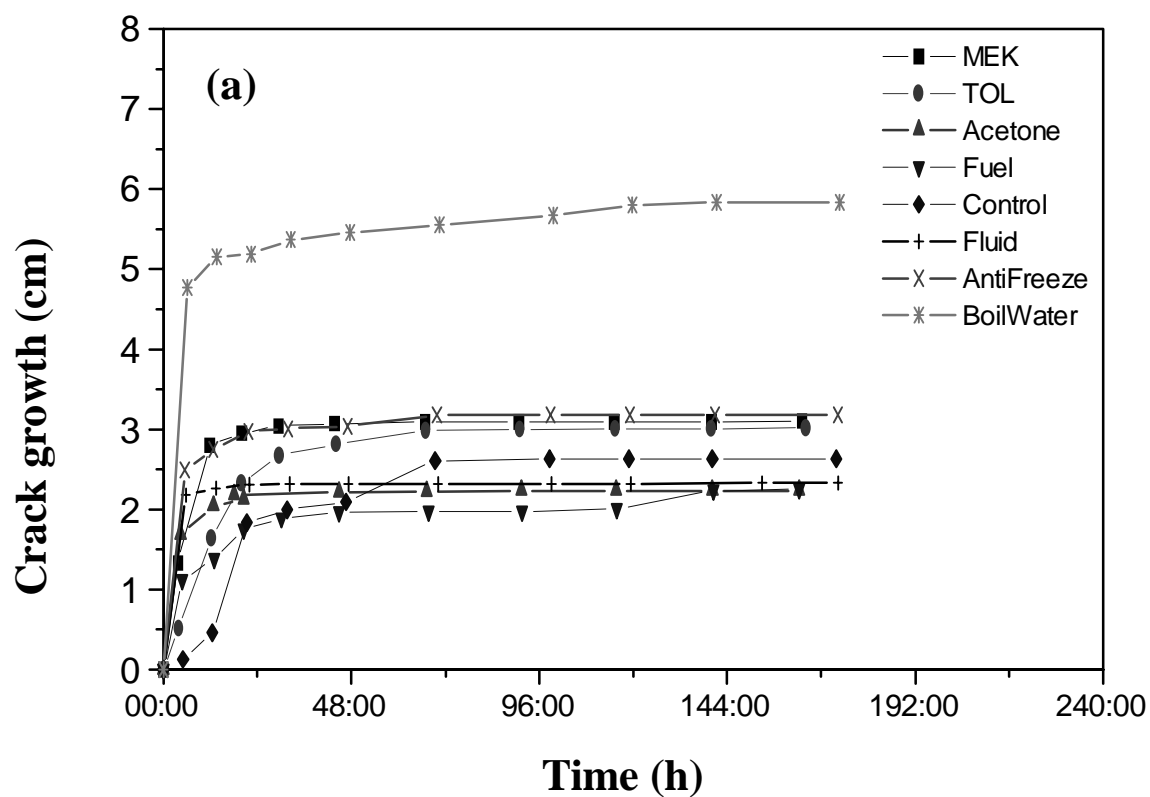


Figure 7.2 Crack growth vs. time in various solvents. (a) and (b) represent the data for each of the two samples.

most of the samples, a significant percentage of the total crack growth takes place in the first 24 hours of the experiment, where the driving force for the crack is at a maximum. The crack growth then tends to stabilize towards a particular value. The total crack growth value, however, depends upon the solvent being used. From the results it is clear that boiling water results in maximum crack growth (ca. 5-7 cm) whereas the rest of the solvents lead to only a modest crack growth of ca. 1.05 to ca. 3.00 cm. It is, however, observed that due to the nature of the test, subtle differences exist in the results obtained for the two samples for any particular solvent. Thus it can only be argued that 'boiling water' stands out as clearly the most severe environment whereas the rest of the solvents are similar in the effect they cause on the adhesive. Furthermore, it is noted that there are no clear differences in the crack propagation between the control specimen (placed in a dessicator) and that for samples placed in various environments. This suggests that the various solvents (except the boiling water) are no more effective in propagating the crack than the control environment itself. This then clearly indicates the relative stability of the adhesive bonds on exposure to various solvents.

The arrest strain energy release rate for various solvents is calculated by using the stabilized value of the crack growth in the equation presented earlier. This results in strain energy release rates of ca. 100-200 J/m² for bonds in boiling water and 900-1000 J/m² in other solvents. Figure 7.3 shows the photomicrographs of samples that were dipped in acetone and boiling water and were later completely fractured after the completion of the test. The fracture surfaces clearly reveal polymer on both sides of the specimen thus indicating a cohesive failure. In fact, an interfacial failure was not observed for any of the wedge samples. This clearly demonstrates the effectiveness of the grit blasting surface treatment and the utilized bonding conditions in providing a suitably strong interface. These results thus reinforce the previously derived conclusions from the lap-shear study about the efficacy of the simple 'grit-blasting' surface treatment.

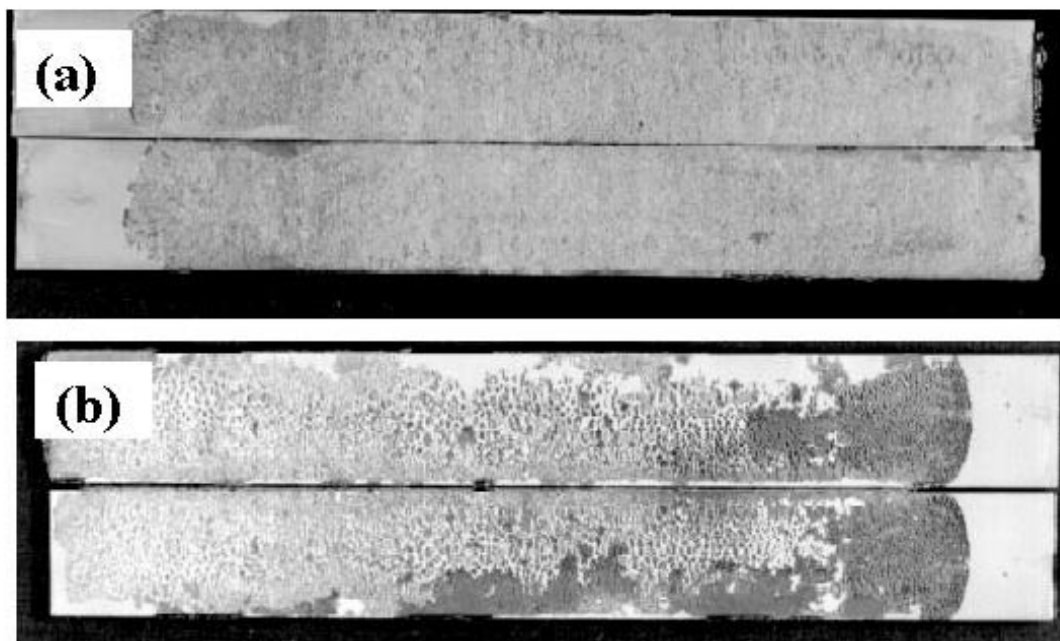


Figure 7.3 Fractured wedge test samples in environment (a) acetone (b) boiling water.

7.5.2 Double cantilever beam tests

The bond thickness for the various specimens was similar to the wedge test specimens and averaged at 0.20 ± 0.05 mm. The first set of specimens consisted of samples that used the bonding conditions utilized earlier in the lap-shear and the wedge test study. The load vs. displacement curves for one of the samples is shown in Figure 7.4(a). Figure 7.4(b) also shows the corresponding plot for the cube root of compliance vs. crack length that was utilized to calculate the fracture toughness using the compliance method. Good results were obtained for both of these samples and are plotted in Figure 7.5. The maximum strain energy release rate G_{\max} was found to be ca. 1600-2000 J/m² for the two samples. The arrest strain energy release rate was found to be ca. 1200-1600 J/m². While the calculated values for the strain energy release rates were similar, it was found that the standard deviation and the differences between the two samples were much less when the compliance method was utilized. The mode of the failure for both these samples was purely cohesive as is clearly visible in the photomicrograph of one of the samples (Figure 7.6). For closer examination of the fracture surface, small sections of the fractured specimen from both sides were cut and observed using the scanning electron microscope. Figure 7.7(a), which is a lower magnification micrograph, shows the fracture surface representative of the total area on both sides of the specimen. The fracture surface shows considerable roughness with the polymer being pulled apart in long striations running parallel to the width of the specimen. A higher magnification micrograph in Figure 7.7(b) better illustrates the considerable ductility exhibited by the polymer. These observations suggest considerable toughness exhibited by the adhesive and go along with the results achieved.

Additionally some samples were bonded for only 2 min (instead of 20 min for the standard conditions) in order to see whether such a short bonding time could be sufficient in attaining good fracture strengths. The results shown in Figure 7.8, reveal a considerable drop in fracture toughness with G_{\max} decreasing to 1000 J/m² and ca. 500 J/m² for the two samples. The arrest strain energy release rate also shows a considerable decrease and falls to ca. 800 J/m² and 375 J/m² for the two samples. The

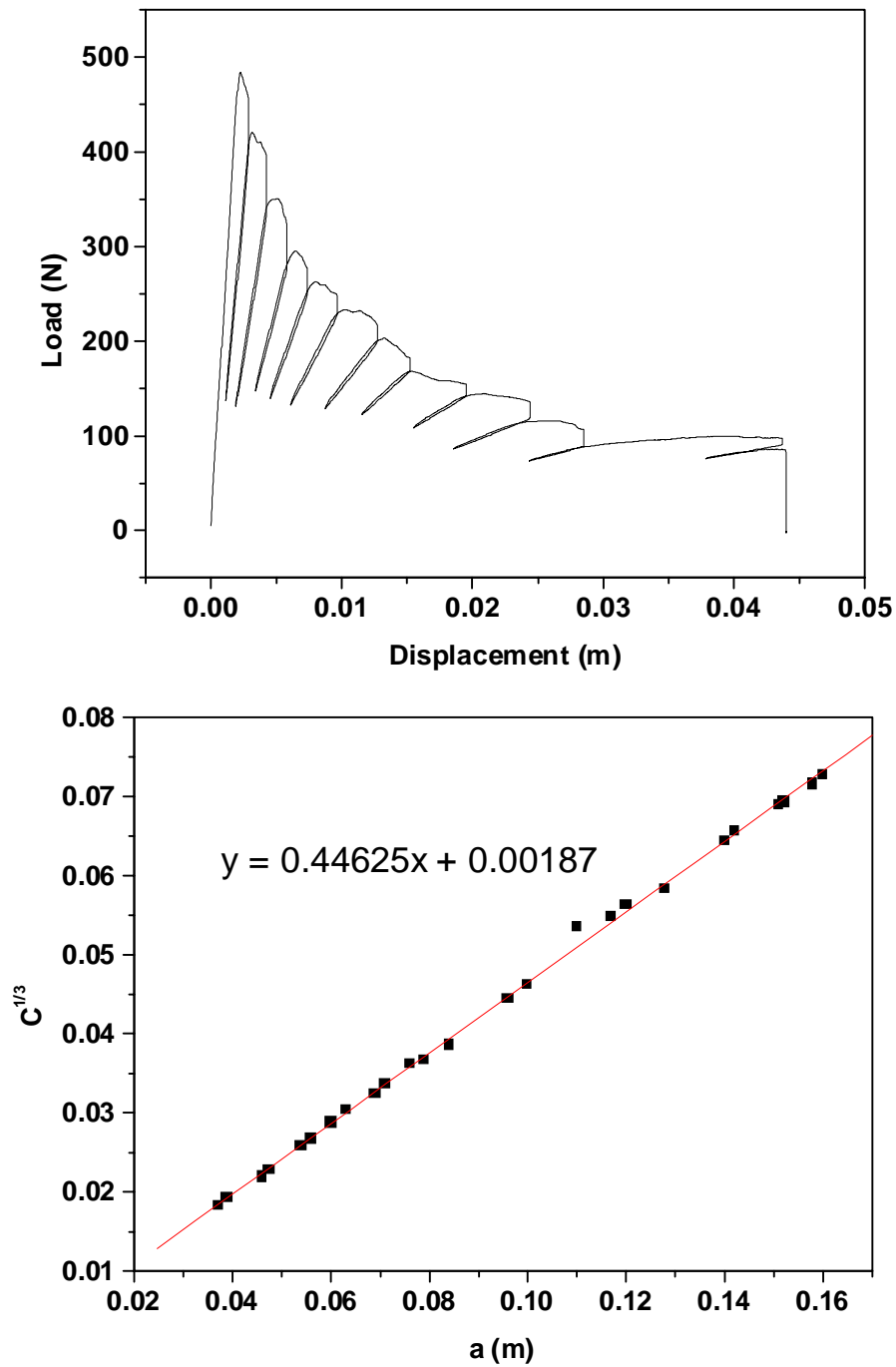


Figure 7.4 (a) Collected data for the DCB sample for the standard bonding condition (b) Calculation using the compliance method.

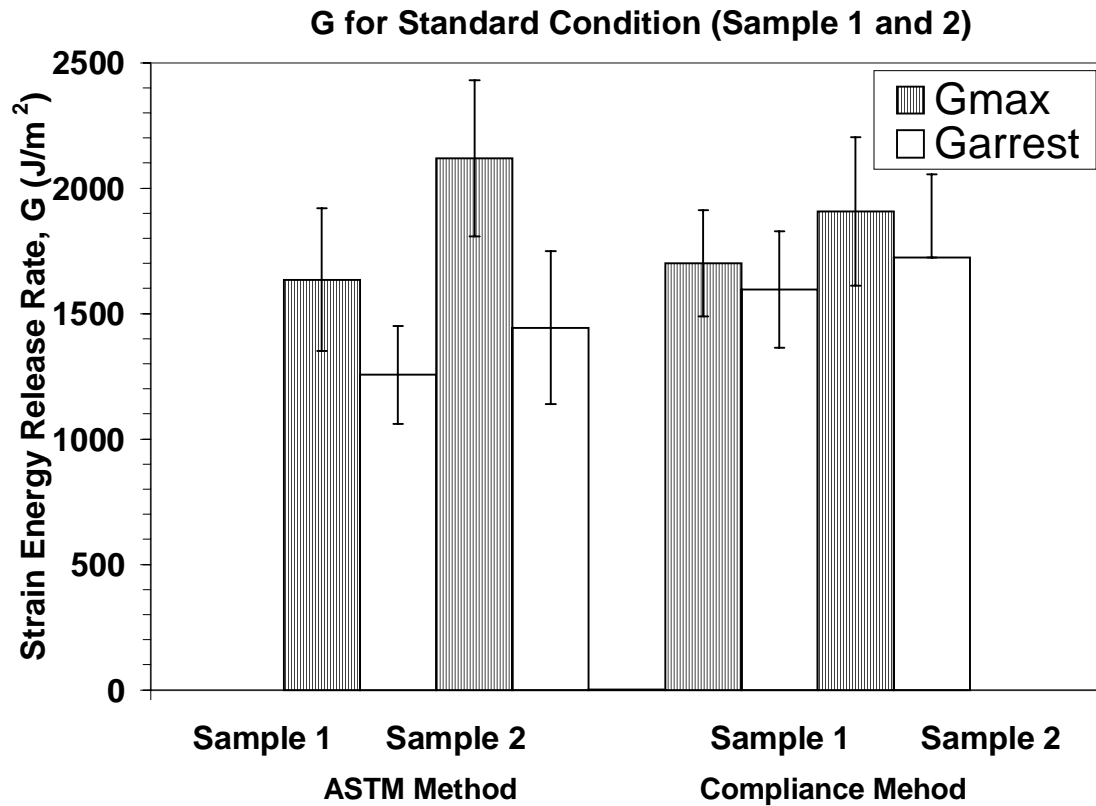


Figure 7.5 Maximum and Arrest strain energy release rates for samples bonded under the standard bonding conditions. Both ASTM and Compliance method are used to calculate the results.

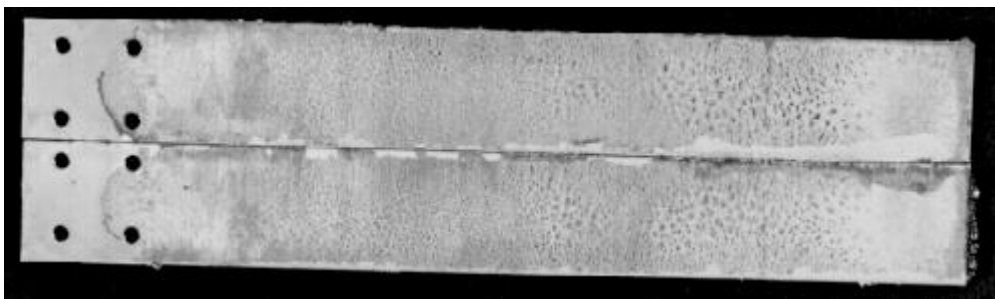


Figure 7.6 Photomicrograph of the fractured DCB specimen that was bonded under the standard bonding conditions.

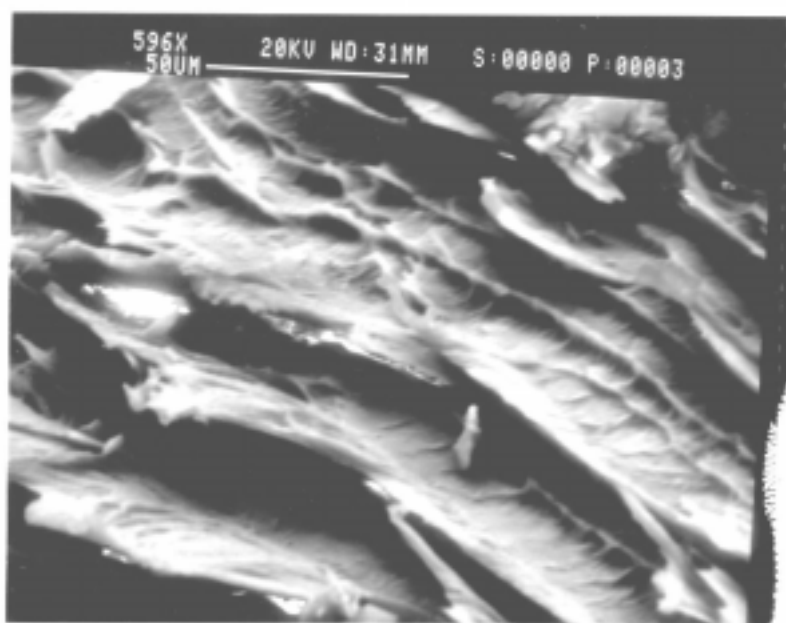
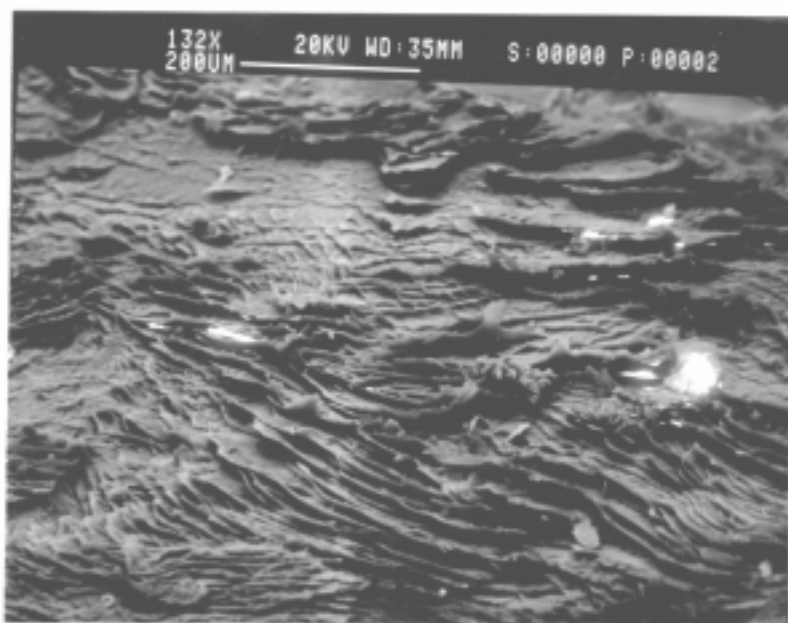


Figure 7.7 Scanning electron micrographs of the fractured DCB specimen that was bonded under the standard bonding conditions. (a) Lower magnification (b) Higher magnification

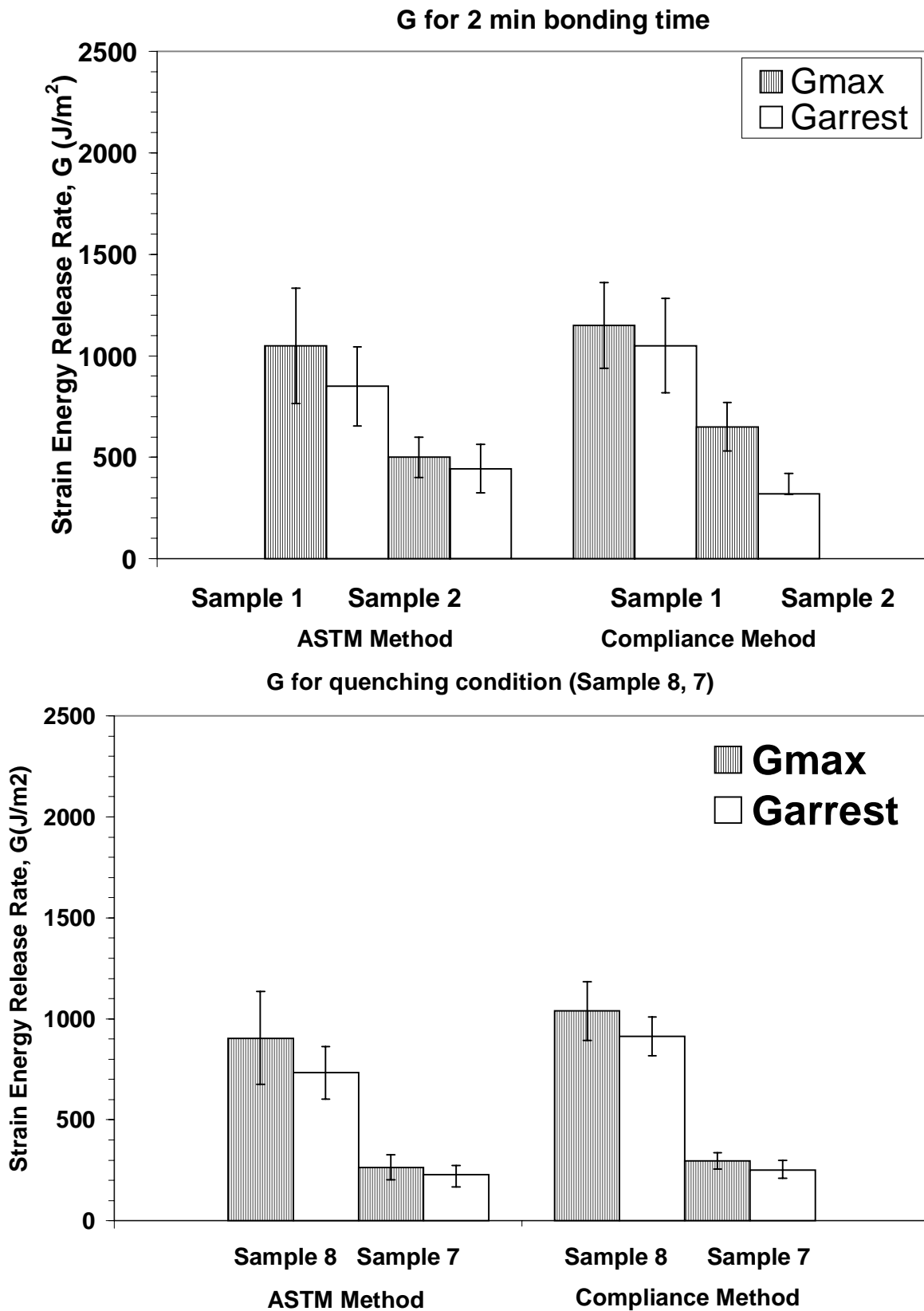


Figure 7.8 Results for the samples (a) that were only bonded for 2 min and (b) that were quenched to room temperature from the standard bonding conditions.

photomicrographs for the better sample is shown in Figure 7.9 and seems to exhibit considerable interfacial failure (visual observation only). This indicates the poor wetting of the surface achieved in such a short bonding time.

Another variation tried in the bonding conditions was quenching the bonded samples to room temperature instead of cooling at ca. 20°C/min. Though the photomicrographs suggest cohesive failure (not shown here), the obtained fracture energy values are much lower at ca. 900 and 200 J/m². This indicates relatively poorer consolidation of the sample at such fast cooling rates. Some samples were also held at 365°C for 2 hours from the melt before being cooled to room temperature. Based on earlier studies, these conditions should promote large sized spherulites instead of the fine grainy morphology promoted by the standard bonding conditions. These samples were thus expected to show lower toughness that is associated with such a coarse spherulitic morphology. *Interestingly, both samples that were bonded at these conditions exhibited ‘catastrophic failures’ along the complete length of the specimen when the wedges were inserted!* This brittle fracture was purely cohesive (Figure 7.10) and is thereby representative of the poor adhesive mechanical properties that result due to such conditions.

7.6 Conclusions

It is clear that TPER-BPDA-PA adhesive exhibits excellent solvent resistance even when the fracture surface is exposed to variety of solvents in a wedge-opening mode. While none of the common solvents seems to have any major effect on the fracture toughness of the adhesive, ‘boiling water’ results in significant drop in ‘arrest strain energy release rate’. Most of the crack growth for any environment occurs in the first 24 hours after which the crack growth seems to slow down significantly. Also it is clear that ‘grit-blasting’, as surface treatment is effective in providing a strong interface, as indicated by mostly cohesive failure for most of the samples.

The double cantilever beam tests yield the best results for the bonding conditions utilized for the wedge test study and the previous lap-shear study, thus re-emphasizing the effectiveness of these bonding conditions in making a strong, tough and durable adhesive bond. The photomicrographs reveal a clear cohesive fracture surface whereas the SEM investigations indicate considerable ductility in the fractured polymer and a rough fracture surface, which go along with the high strain energy release rates for the specimens. Reducing the bonding time or quenching the bonds quickly to room temperature results in a lowering of the fracture toughness. The prior conditions also promote interfacial failures possibly due to incomplete wetting of the substrate. Interestingly, promoting a coarse spherulitic morphology by changing the bonding condition results in very brittle bonds that fail catastrophically along the complete length of the specimen on insertion of the wedge.



Figure 7.9 Photomicrograph of the fractured DCB specimen that was bonded for only two minutes.

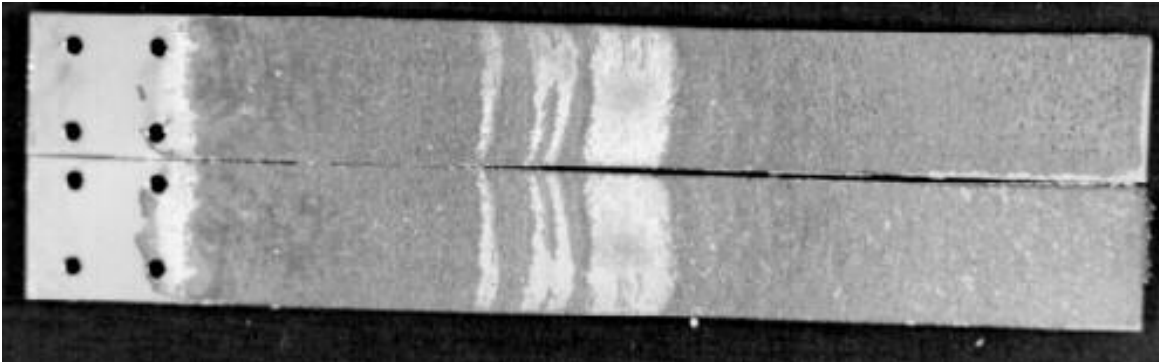


Figure 7.10 Photomicrograph of the fractured DCB specimen that was held at 365°C for 2 hours before cooling to room temperature.

References:

-
- ¹ Ed. Adams R.D., Engineered Materials Handbook, Adhesives and Sealants, Vol. 3, Materials Park, OH: ASM International, 1995:325.
- ² Cognard, J., *J. Adhesion*, 1986, **20**, 1.
- ³ Cognard, J., *J. Adhesion*, 1987, **22**, 97.
- ⁴ Ripling, E.J., Mostovoy, S. and Parick, R.L., *Mat. Res. Stand.*, 1964, **4**, 129.
- ⁵ Mostovoy, S., Crosley, P.B. and Ripling E.J., *J. Mater.*, **2**, 1967, 661.
- ⁶ Dillard, D.A., Rakestraw, M.D., Taylor, M.W. and Chang, T., *J. Adhesion*, **55**, 1995, 123.
- ⁷ Ratta, V., Stancik, E.J., Ayaambem, A, Parvattareddy, H., McGrath, J.E. and Wilkes, G.L., *Polymer*, **40**, 1999, 1889.
- ⁸ Progar, D.J. and Clair, T.L.St. *J. Adhesion* 1987, **21**, 35.
- ⁹ Progar, D.J. *J. Adhes. Sci. Technol.* 1987, **1**, 135.
- ¹⁰ Progar, D.J. and Clair, T.L.St. *J. Adhes. Sci. Technol* 1994, **8**, 67.
- ¹¹ Progar, D.J. and Clair, T.L.St. *J. Adhesion* 1989, **30**, 185.
- ¹² Progar, D.J. and Dezern, J.F. *J. Adhes. Sci. Technol.* 1989, **3**, 305.
- ¹³ Hergenrother, P.M., Stenzenberger, H.D.and Wilson, D. 'Polyimides', Blackie & Son Ltd, London, 1990.

CHAPTER 8

Crystallization and Multiple Melting Behavior of a New Semicrystalline Polyimide based on 1,3-bis (4-aminophenoxy) benzene (TPER) and 3,3', 4,4'-benzophenonetetracarboxylic dianhydride (BTDA)

Abstract

This study addresses the crystallization and multiple melting behavior of a new high temperature semicrystalline polyimide, which is based on an ether diamine (TPER or 1,3 (4) APB) and BTDA dianhydride, both of which are commercially available. It also uses phthalic anhydride to endcap the chains thus improving thermal stability. The polyimide displays a T_g at ca. 230°C and two prominent melting endotherms at 360°C and 416°C respectively, with a sharp recrystallization exotherm immediately after the lower melting endotherm. The polyimide is able to crystallize even after exposure to high melt temperatures of 450°C (for 1 min) and displays fast crystallization kinetics with cooling rates larger than 200°C/min necessary to quench the polymer into an amorphous state. Additionally, the melting behavior is tremendously influenced by small variations in the melt crystallization temperature. A small melting shoulder appears ca. 10-15°C above the crystallization temperature (for $T_c \leq 345^\circ\text{C}$), while only one prominent higher melting endotherm is observed for $T_c \geq 350^\circ\text{C}$. DSC, hot stage polarized optical microscopy and WAXD experiments are utilized to interpret the melting behavior. Indirect evidence suggests that the two prominent melting endotherms are due to different crystal unit cell structures. The prominent multiple melting endotherms represent the melting of primary crystals formed at the crystallization temperature and are not a consequence of a 'continuous' melting and recrystallization process. For temperatures

higher than 350°C, an isothermal thickening phenomenon occurs with significant increases in the peak melting point (10-14°C) observed for longer crystallization times.

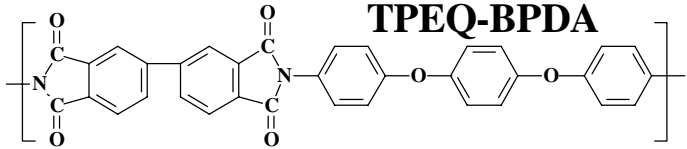
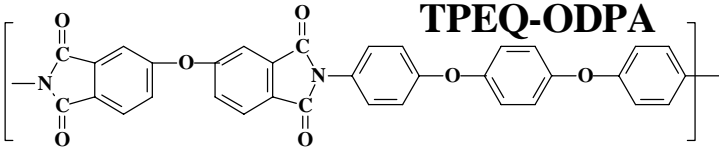
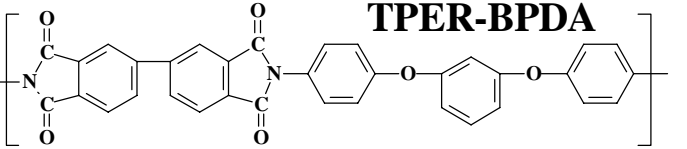
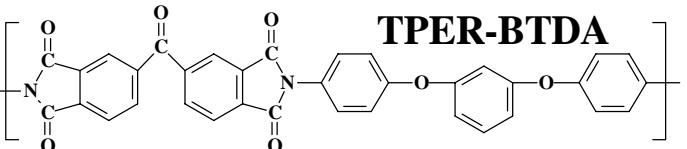
8.1 Introduction

Polyimides are a class of thermally stable and high performance polymers that continue to gain increasing importance in a wide variety of applications like high performance and high temperature adhesives and composites, microelectronics, membranes and as photosensitive materials¹⁻³. These wide ranging applications are due to many desirable characteristics generally exhibited by polyimides like excellent mechanical properties, good radiation and chemical resistance, good adhesion properties and low dielectric constant. Presence of crystallinity in these materials can further substantially improve the thermal stability⁴⁻⁶, solvent resistance⁷, radiation resistance⁸ and partial retention of mechanical properties above the glass transition temperature. In this regard, while many polyimides in the literature have been reported to exhibit crystallinity in the initial material^{9,10}, most do not recrystallize once taken to the melt^{4-6,11}. The initial crystallinity is in large part due to the solvent aided crystallization which usually accompanies the imidization process, while the usually slow crystallization kinetics prevents the polyimide chain from crystallizing from the melt. Among the few polyimides that do show some evidence of crystallization from the melt, the recrystallization ability decreases rapidly with increasing times and temperatures in the melt. The glass transition temperature of these high temperature polymers is usually in excess of 200°C and the melting points are in the range of 400°C. The melt processing temperatures can thus often exceed 400°C and the poor melt recrystallization behavior can, in part, be explained due to the degradation reactions that can occur at these very high temperatures. Thus it is no surprise that polyimides are almost exclusively processed from the solvent route, which necessitates use of toxic solvents such as N-methyl pyrrolidinone (NMP), N,N- dimethyl formamide (DMF) and dimethyl acetamide (DMAc) among others. Additionally, these solvent aided processes are more time consuming and expensive than the traditional melt processing operations. It is therefore obvious that development of melt processable thermoplastic polyimides can be beneficial

from both an environmental and processing standpoint. With this aim in mind, several semicrystalline polyimides have been synthesized and characterized^{4-6,11}, some of which are shown in Table 1. Additionally, all these polyimides are based on commonly available dianhydrides and ether diamines and thus no separate synthesis step is required to prepare the monomers. Each of these polyimides show crystallinity in the initial material, a high glass transition and a high melting temperature. However, depending upon small differences in their structure, the success in terms of their melt crystallization behavior varies. Incorporating flexible ether or carbonyl linkages in the dianhydride and changing the nature of isomeric attachment in the diamines influences the melt crystallization behavior significantly. In earlier work from this laboratory, it has been shown that TPEQ-ODPA shows limited recrystallizability from the melt¹². It was also found that the polyimide TPEQ-BPDA demonstrated a very high DSC peak melting point of 471°C and did not recrystallize once taken to the melt¹¹. The third polyimide TPER-BPDA, however, has provided excellent results from the viewpoint of melt recrystallization. Earlier works have shown the excellent thermal stability and melting characteristics^{4,5}, crystallization and morphological behavior⁴⁻⁶, fast crystallization kinetics⁶, rheological behavior⁶ and very promising adhesive strengths and durability of this polyimide⁴. The work reported in this chapter introduces another new semicrystalline polyimide (polyimide (d) in Table 1) based on 1,3-bis (4-aminophenoxy) benzene (TPER or 1,3(4) APB) and 3,3', 4,4'-benzophenonetetracarboxylic dianhydride (BTDA). The polyimide henceforth referred to as TPER-BTDA displays a T_g of ca. 230°C and two prominent melting endotherms with peak melting points of ca. 350°C and 410°C. Additionally, the chains are endcapped with phthalic anhydride that serves to control the molecular weight and tremendously improves the thermal stability of the polyimide.

Several reasons for synthesizing the present polyimide exist. Traditionally BTDA based polyimides have been found to be promising with respect to their crystallization behavior. Also, an earlier study dealing with this polyimide seemed to indicate that this material may crystallize from the high melt temperatures¹³. Changing the dianhydride structure to BTDA also helps in better understanding the structure property behavior in these ether diamine based semicrystalline polyimides. Additionally BTDA

Table 8.1 Previously developed semicrystalline polyimides developed at Virginia Tech.

	M.W. (daltons)	T _g (°C)	T _m (°C)
 <p>TPEQ-BPDA</p>	550	259	471
 <p>TPEQ-ODPA</p>	550	238	420
 <p>TPER-BPDA</p>	566	210	395
 <p>TPER-BTDA</p>	578	230	416

based polyimides are more attractive from the commercial viewpoint due to the lower cost of BTDA vis a vis other dianhydrides. The present study deals with the crystallization from the melt and the multiple melting behavior of TPER-BTDA polyimide. A subsequent study will also address the thermal stability, morphology and dynamic mechanical behavior of this polyimide.

The DSC melting behavior of this semicrystalline polyimide is particularly interesting in that it demonstrates two very distinct and widely spaced melting endotherms at ca. 350°C and at ca. 410°C. Also, as will be subsequently shown, additionally endotherms develop depending upon the temperatures at which the polymer is crystallized. It is very important from both a fundamental and practical standpoint to understand the causes of this multiple melting behavior and how it may depend upon the previous thermal history of the polyimide. While such widely spaced distinct melting endotherms with a prominent intermediate crystallization exotherm have not commonly been observed, the problem of multiple melting behavior in semicrystalline polymers itself is not new. Multiple melting behavior has been observed in polyethylene¹⁴⁻¹⁷, polypropylene¹⁸⁻²⁰, poly(ethylene terephthalate) (PET)²¹⁻²⁷, poly(butylene terephthalate) (PBT)²⁸⁻³³, poly(phenylene sulfide)^{34,35}, poly(ether ether ketone) (PEEK)³⁶⁻⁵⁵ semicrystalline polyimides^{5,56-61} and other polymers. The multiple melting behavior itself can occur due to a wide variety of reasons like different crystal unit cell structures, presence of two or more distinct morphological forms or due to a continuous melting and recrystallization process. Other reasons presented in literature include molecular weight fractionation¹⁷, dependence on the heating rate in the DSC⁶² and ascribing the lower endotherm to some sort of a physical aging process⁴⁵⁻⁴⁷. In recent years, considerable debate has re-arisen over the reasons for dual melting behavior observed in PEEK and other polymers. The two widely advocated models for explaining the melting behavior differ in that one proposes a melting-recrystallization process while the other explains it on the basis of two different lamellar populations. For the melting recrystallization process, the lower endotherm has been argued to be due to melting of the lamellae that form at the crystallization temperature, while a continuous recrystallization and melting process ensues simultaneously with the higher endotherm occurring when melting rate

sufficiently exceeds the recrystallization rate. One of the several forms of evidence that is cited to support this description is the shifting of the lower peak to higher temperatures and more importantly, the higher peak to lower temperatures, with increase in heating rate. For quiescent crystallization, the *morphological model* (a terminology used often in literature) explicates the dual-melting behavior on the basis of dual lamellar populations, the thicker lamellae being formed due to the primary crystallization while the later forming thinner lamellae are due to the secondary crystallization process. The higher melting point is then ascribed due to the thicker primary lamellae while the lower endotherm, which usually occurs 10-25°C above the crystallization temperature, is the result of the thinner secondary lamellae. One of the stronger evidences cited to support this model is that the higher melting endotherm appears to form first whereas the lower melting endotherm appears later. However, within the proponents of the ‘morphological model’, debate still exists as to the location of thinner lamellae. While some have argued for the existence of thinner lamellae within the stacks of thicker primary lamellae, others have postulated the existence of separate stacks of thinner lamellae^{43,48,51}.

This study addresses the crystallization and multiple melting behavior of this polyimide by using the techniques of DSC, optical microscopy and wide angle X-ray diffraction (WAXD). The polyimide is first introduced by showing some evidence concerning the thermal stability and recrystallization ability from the melt. Thereafter, the effects of crystallization temperature on the melting behavior are discussed. Regarding the kinetics of crystallization, while the detailed quantitative methods like Avrami analysis are not utilized in the present study, some qualitative arguments are made on the basis of the observed results. Reasons for the multiple melting behavior and how this behavior may depend upon the previous crystallization temperature are explained on the basis of the evidence obtained. In this regard, experimental evidence is discussed in order to explain the multiple melting behavior on the basis of different crystal unit cell structures, the ‘melting and recrystallization model’ and the ‘morphological model’. Results of the DSC experiments are shown for the isothermal crystallization for varying times at selected crystallization temperatures. Also, the effect of heating rate on the melting behavior when crystallized at these temperatures is discussed. Lastly, some results are presented regarding the isothermal thickening

phenomenon at relatively higher crystallization temperatures. The problem of estimating the equilibrium melting point using traditional methods is also discussed.

8.2 Experimental

8.2.1 Synthesis:

1,3-bis(4-aminophenoxy) benzene (TPER diamine) was supplied by Ken-Seika and was recrystallized from toluene before use. 3,3',4,4'-benzophenonetetracarboxylic dianhydride (BTDA) was supplied by the Occidental Chemical Corporation and was dried at 120°C prior to use. The endcapper phthalic anhydride (PA) was obtained from Aldrich and sublimed prior to use. N-methylpyrrolidinone (NMP) was obtained from Fisher and vacuum distilled after drying over P₂O₅ before use. The Carothers equation was utilized to calculate the monomer and endcapper concentration for synthesizing polymer samples with the desired number average molecular weight of 30,000 (30K) daltons. The reaction vessel was a three neck round bottom flask equipped with a mechanical stirrer, nitrogen inlet and a drying tube. Sufficient NMP was added to achieve a 10% solids concentration and the solution was allowed to stir for 24 hours, to afford a homogenous poly(amic acid) solution as shown in Figure 8.1. A stepwise thermal imidization procedure was utilized which others as well as workers in this laboratory has used successfully in the past⁴. The first step was the casting of the poly(amic acid) precursor on the pyrex glass plates. These plates were placed in the vacuum oven overnight until smooth non-tacky films were obtained. Thermal imidization was achieved by raising the temperature to 100°C, 200°C and 300°C and holding at each of these temperatures for 1 hour. The time to go from one temperature to the next was ca. one hour each at the fastest heating rate available with the oven. After the completion of the cycle, the plates were allowed to cool down to room temperature before being removed from the oven. The films were carefully stripped off the glass plates in hot water and stored in a desiccator before use.

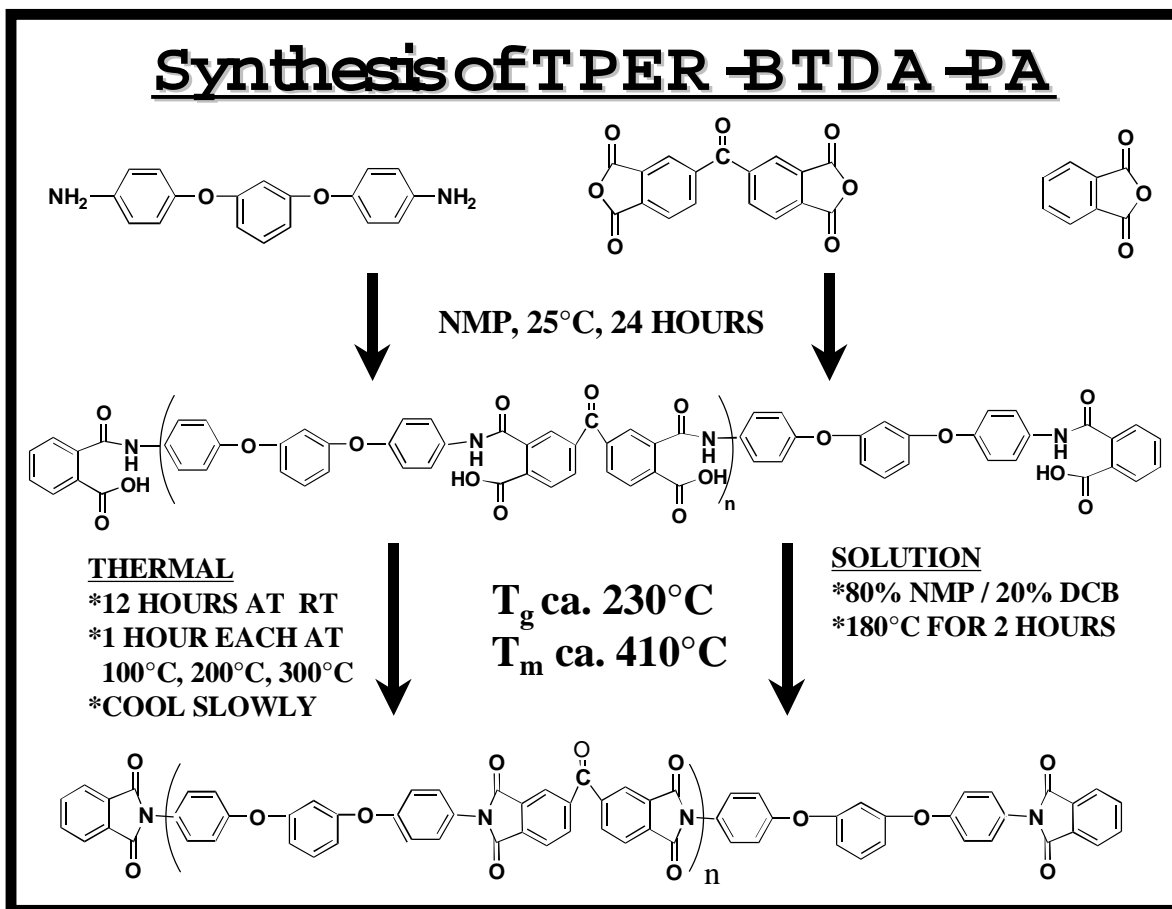


Figure 8.1 Scheme for synthesis of TPER-BTDA-PA polyimide.

8.2.2 Characterization

Thermogravimetric (TGA) studies utilized a Seiko TG/DTA and all experiments were carried in either a nitrogen or air atmosphere. The temperature was calibrated using indium and zinc standards and the dynamic experiments utilized a heating rate of 5°C/min. The isothermal experiments were performed for a duration of 180 minutes.

DSC experiments for both isothermal and non-isothermal crystallization were performed on a Perkin Elmer DSC-7. The amount of polymer utilized in a given thermal scan was kept between 6-8 mg. The DSC was calibrated with indium and zinc standards. All experiments were conducted under a nitrogen purge and a DSC baseline was determined by running empty pans. For isothermal crystallization experiments, the samples were kept at room temperature and purged with nitrogen for 5 minutes to remove air from the DSC cell. The samples were then rapidly heated to 450°C for 1 minute while cooling to below the glass transition temperature was done at the desired cooling rate or to the specific crystallization temperatures at 300°C/min. In this regard, data collection at high supercoolings was hampered by the initial instability of the DSC signal. This initial instability occurs on cooling to the crystallization temperature at fast cooling rates and may persist for ca. one minute on Perkin Elmer DSC 7 utilized in this study. To perform quantitative analysis like Avrami analysis or to calculate the value of $t_{1/2}$ (time to attain 50% of its total crystallinity), some extrapolation of the initial portion of the exotherm is then usually undertaken (for the higher supercoolings), which results in some degree of error in the final result. In this study however, the peak time for the crystallization exotherm t_m for various crystallization temperatures is only reported. These values behave similarly as the quantitatively more precise $t_{1/2}$ parameter and give a good indication of the crystallization kinetics at various supercoolings. For the variable heating rate studies, the DSC was first calibrated using zinc and tin standards at that heating rate using the onset of the melting points. For heating rates higher than 10°C/min, the sample mass was reduced to 2-3 mg to minimize the thermal lag that may

result at higher heating rates. All experiments were performed twice in order to maintain accuracy in the results. All reported DSC scans are normalized with respect to the sample mass (to 1 mg).

Polarized optical microscopy was carried out on a Zeiss optical microscope equipped with a Linkam 600 hot stage and 35mm camera. The hot stage was calibrated using indium, tin and zinc. The film (~2 mils) was sandwiched between two glass slides and a nitrogen purge was maintained inside the hot stage. The sample was taken to 450°C and kept there for 1 minute before being quenched to a 340°C, kept there for 20 minutes and then rapidly heated to and held at 370°C. The quenching to 340°C from 450°C was achieved by using a separate nitrogen source.

For wide angle X-ray diffraction experiments, a Siemens diffractometer equipped with a STOE Bragg-Brentano type goniometer was utilized. A wavelength of 1.54 Å was used after monochromitization through a graphite monochromator. Data was collected during a continuous scan at a speed of 0.5 degrees/minute between the angles of 10°-60°.

8.3 Results and discussion

Thermogravimetric analysis was first utilized to determine the thermal stability of the material as indicated by weight loss that may occur at higher temperatures. Dynamic experiments at a slow heating rate of 5°C/min were conducted from room temperature to 600°C in both air and nitrogen environments (Figure 8.2(a)). The 5% weight loss temperatures in air and nitrogen are 507°C and 529°C respectively. It is clear that the polymer exhibits significantly higher thermal stability in nitrogen than in air, as the onset of degradation accompanied by significant weight loss appears to start in air at lower temperatures. These high weight loss temperatures are not surprising and are usually obtained for such high temperature thermally stable polyimides. However, before weight loss temperatures are utilized to compare thermal stability of any two materials, it is important to recognize that the exact value of such temperatures would depend significantly on the heating rate utilized. For the higher and commonly utilized heating

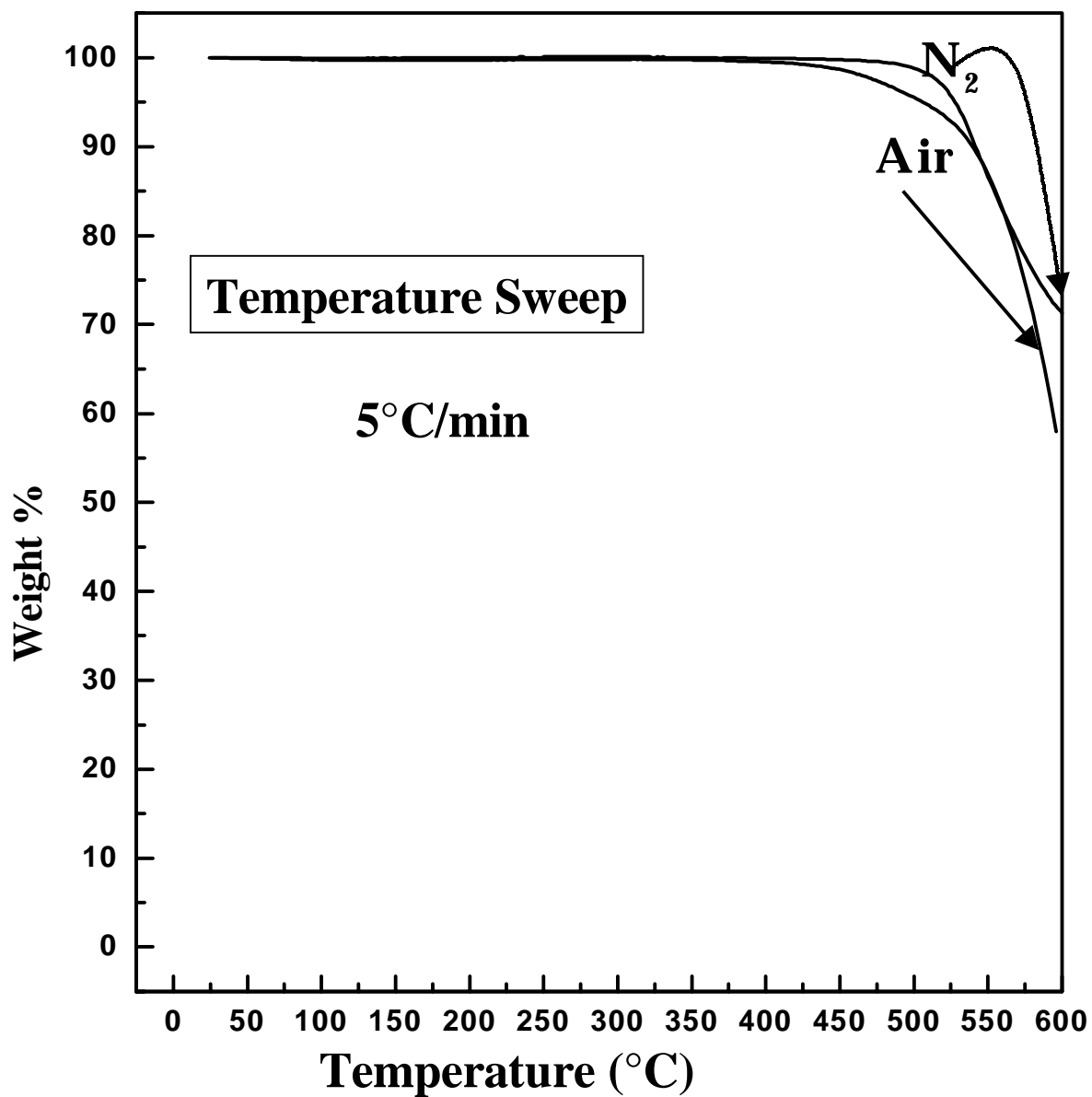


Figure 8.2(a) Dynamic heating profiles for weight loss in air and nitrogen when heated at 5°C/min.

rate of 10°C/min, the weight loss temperatures would obviously be higher as the polymer spends less time at any temperature. Similarly for a low heating rate of say 2°C/min, the weight loss temperatures may be significantly lowered due to the increased time spent at the previous temperatures.

While the degradation temperatures obtained in (at 5°C/min) are higher than the possible melt processing temperatures of ca. 450°C, it is important to understand the effect of prolonged exposure at melt processing temperatures. In this regard, the isothermal scans for weight loss vs. residence time in the melt, at a typical melt temperature of 450°C are shown for both in air and nitrogen (Figure 8.2(b)). While the weight loss begins to occur in air for low residence times, the polyimide shows very little weight loss even after 180 minutes in the melt at 450°C. The 5% weight loss time in air is 56 minutes, while 4.7% weight loss occurs in 180 minutes in nitrogen.

While the above traditionally utilized TGA experiments reveal the significant bulk thermal stability with respect to weight loss for this polyimide, no major inference can be made regarding the recrystallizability of the material from these temperatures. While TGA would detect the weight loss due to degradation reactions that are accompanied by emission of volatiles, other less severe reactions like crosslinking/chain branching may take place with little or no emission of volatiles, and thus little observable weight loss. These reactions, however, may significantly inhibit the ability of the material to crystallize from the melt. The increased viscosity that may result due to these reactions would also make the melt processing of the polymer difficult. Hence, TGA experiments, while serving as a gross measure of thermal stability, are of limited utility from understanding the stability from a recrystallization viewpoint.

To understand the initial melting behavior and recrystallization response once heated above the melting temperature, DSC experiments were conducted by heating the polymer to the melt temperature of 450°C for 1 minute and rapid quenching to below the glass transition temperature. The four consecutive scans are shown in Figure 8.3. The initial material, which is crystalline, shows only a weak and broad glass transition in the vicinity of 230-260°C. However, very interestingly, two prominent and widely spaced melting endotherms, with peak temperatures of 357°C and 416°C respectively are

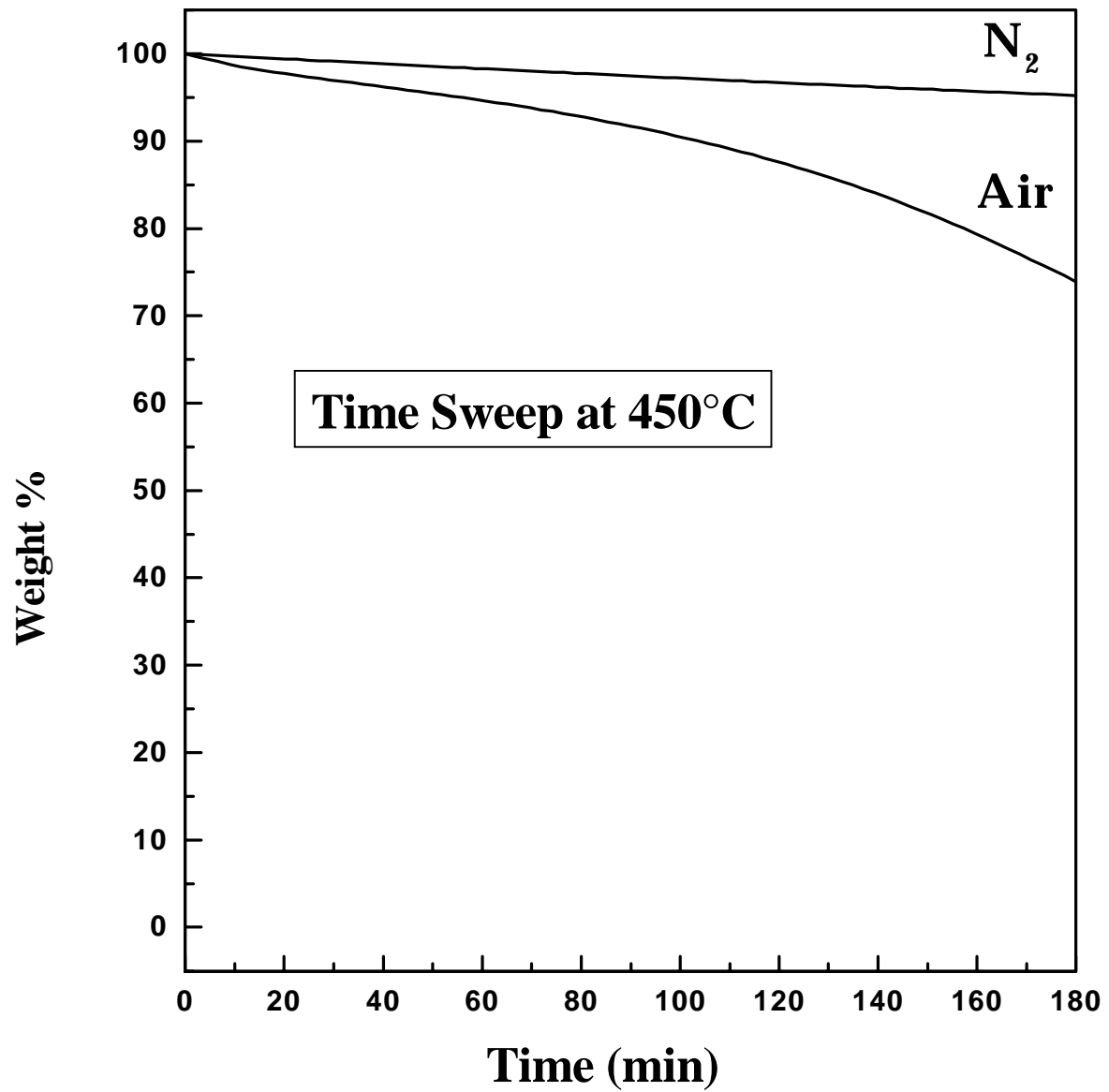


Figure 8.2(b) Weight loss profile with time in air and nitrogen when kept at a typical melt temperature of 450°C/min.

observed. The first melting endotherm is also rapidly followed by a recrystallization exotherm, which lies between the two melting endotherms. Such peculiar melting behavior has not often been observed for other semicrystalline polymers. It is also noticed that in the initial material, the higher melting endotherm is significantly larger than the lower melting endotherm.

Figure 8.3 also shows consecutive heating scans once the polyimide is *quenched* from the melt. In this regard, several features are observed, mainly:

- (1) The glass transition temperature becomes clearer (in terms of a narrow well-defined heat capacity jump) occurring at 230°C. The T_g is maintained for all the consecutive scans.
- (2) A prominent crystallization exotherm ca. 20°C above the T_g appears. The peak temperature of this exotherm shifts to slightly higher temperatures with consecutive scans. The relative magnitude however, does not change much.
- (3) The peak of the lower melting endotherm shifts downward to 347°C and both this peak temperature and the relative magnitude of this lower endotherm are maintained for the consecutive scans.
- (4) The recrystallization exotherm continues to appear after the first endotherm, and shifts slightly to higher temperatures accompanied with moderate decrease in size. The higher melting endotherm continues to decrease in size and shifts to lower temperatures with repeat heating.

For the consecutive heating scans, the overall heat of melting (as given by ‘area under the endotherms-area under the exotherms’) is close to zero, thus indicating that it was possible to quench the polymer to nearly an amorphous state from the melt. The well-defined T_g thus results from the removal of the constraints that were provided by the crystallites in the initial material. *The polyimide though, did not loose its ability to rapidly crystallize as evidenced by the crystallization exotherm just above the T_g .* However, the shift of this exotherm to higher temperatures with successive scans indicates that more thermal energy is required to introduce crystallization. This could possibly be in part the result of a small amount of crosslinking/chain branching reactions that may occur every time the polyimide is heated to 450°C for 1 minute. Such short

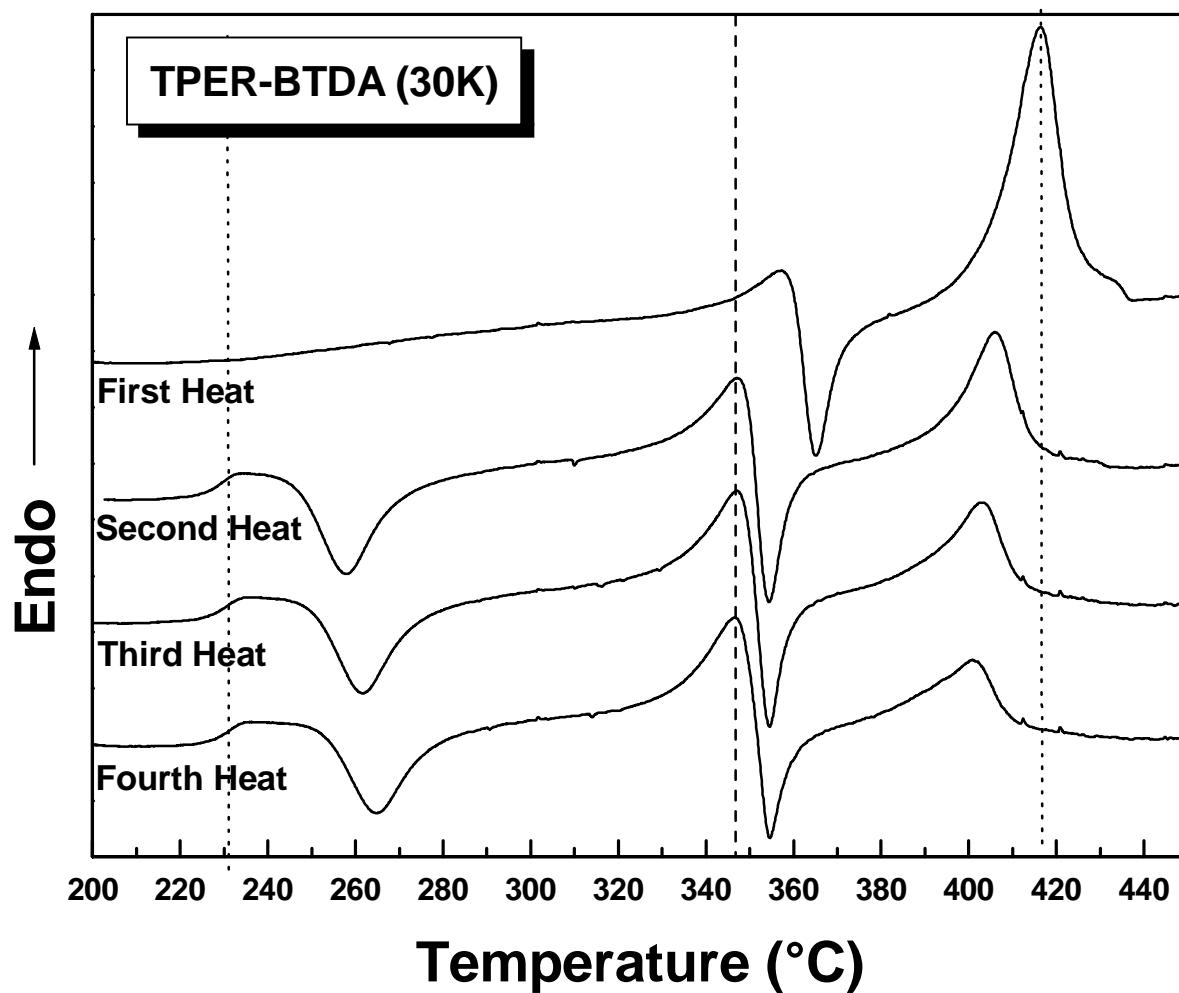


Figure 8.3 Consecutive DSC heating scans after heating to 450°C at 10°C/min, holding for 1 min, quenching to 100°C and reheating at 10°C/min.

time exposures though do not result in any observable weight loss, as already discussed previously. If any large-scale crosslinking reactions had occurred then the polyimide's ability to crystallize would be severely hampered, resulting in little or no crystallization during the heating scan. All experiments discussed henceforth in this chapter will only utilize the milder melt conditions of 450°C for 1 minute.

The construction of a baseline extending from just above the glass transition temperature to the end of the melting enables the calculation of the relative amount of crystal content associated with the respective crystallization exotherms and the melting endotherms. However, exact values are not tabulated here as results depend on slight variations in the placement of the baseline (due to the nature of the DSC curves). Nonetheless, some characteristics of the melting behavior are evident. Both the higher and lower melting forms are present in the initial material as the heat of melting associated with the higher temperature peak is clearly greater than the heat of crystallization of the intermediate exotherm. However, for the later scans, these amounts are nearly equal indicating that the higher melting form is primarily the result of recrystallization occurring after the lower melting endotherm. The lower melting form in this case is mainly the result of melting of the crystals formed after the glass transition. It is also important to note here that there exists some difference in the higher melting point of the initial film and the films crystallized from the melt. This is due to the solvent induced crystallization being operative when imidization is taking place. The enhanced mobility offered due to the solvent results in better packing and more perfect crystals. Secondly as the polymerization is not complete yet, the polyimide chains inherently possess a much greater degree of mobility thus enabling more perfect crystals (with respect to lesser defects inside the crystal lattice and a smoother surface-resulting in lower surface energies and higher melting points).

While this melting response is obtained after quenching from the melt, it is also important to understand the effect of varying cooling rates on subsequent melting behavior. Studying the effect of cooling rate also yields information on the crystallization kinetics of the polyimide. Figure 8.4 shows the heating scans after the polyimide was cooled from the melt at different rates. Decreasing cooling rates give the

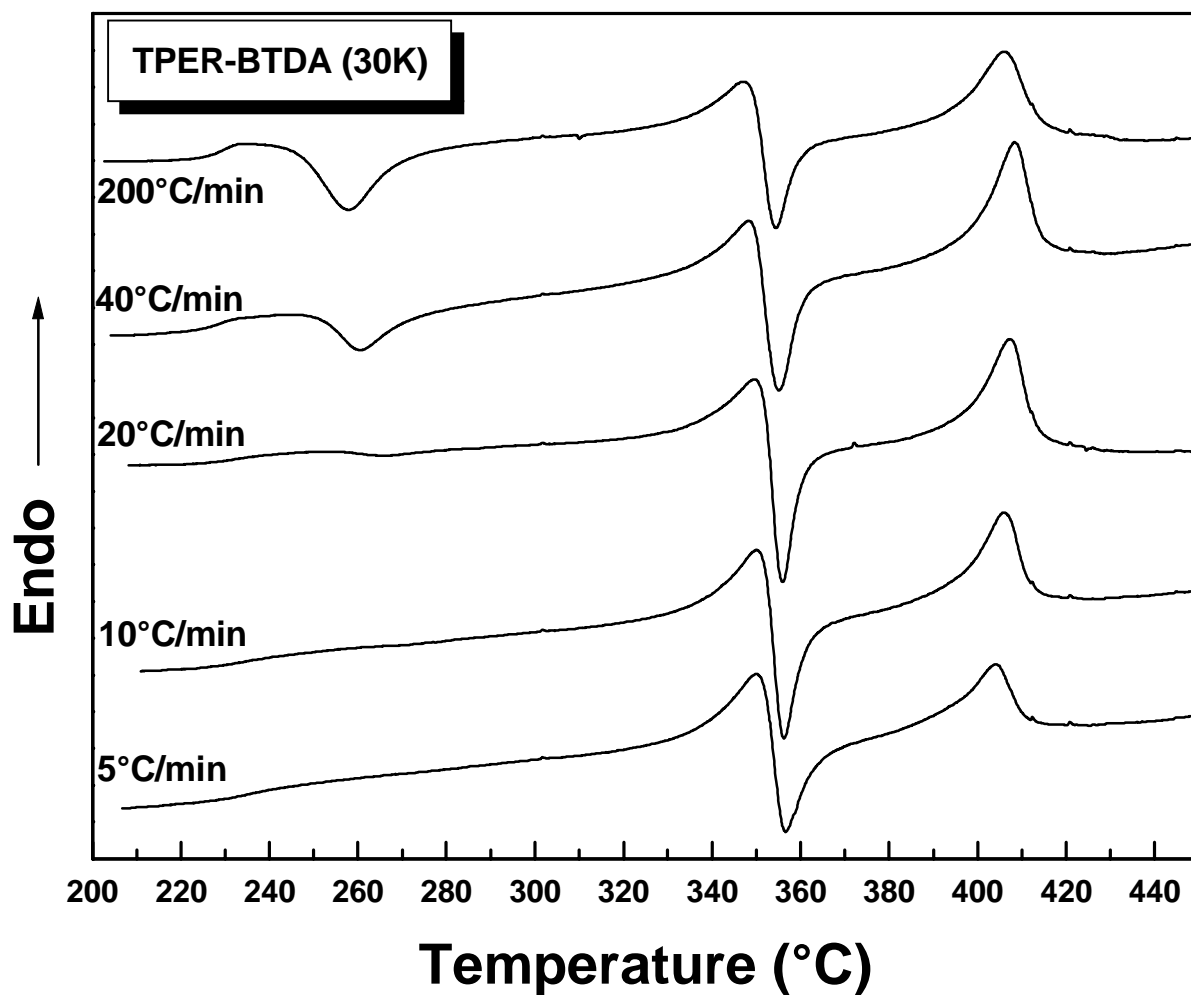


Figure 8.4 Second heat DSC scans at 10°C/min after cooling from 450°C, 1 min at different cooling rates.

polyimide more time to crystallize during the cooling scan. This is clear from the glass transition behavior and the crystallization behavior after the T_g . The heat capacity jump at the T_g becomes relatively smaller and the magnitude of the crystallization exotherm after the T_g decreases tremendously as the cooling rate is decreased and the polyimide is given enough time to crystallize. Interestingly though, the nature of the lower melting endotherm does not appear to change much. It is also immediately succeeded by a sharp recrystallization exotherm that appears to broaden somewhat for slower cooling rates of 5° and 10°C/min. This is due to the extended time that the polyimide experiences at high temperatures for these slower cooling rates, and the corresponding increased crosslinking/chain-branching that may ensue in such a case. A corresponding decrease in the magnitude of the higher melting endotherm, which results from this recrystallization process, is also observed. *However, it is interesting to observe that the higher melting crystals always form during the prominent recrystallization process during the heating process and not during the cooling process (even when the cooling rate is slow).* The adjacency of the intermediate crystallization exotherm with the lower melting endotherm also suggests that the crystallization is distinctly associated with melting of the previous crystals. One of the reasons for this could be that the fast recrystallization occurs at sites of just melted crystals. This proposal is further discussed in subsequent sections.

Several reasons to elucidate the overall melting behavior can be offered, of which the three important ones are: (a) a *continuous melting-recrystallization model* to explain the lower melting endotherm and the higher melting endotherm (b) a *morphological model* with the two endotherms representing melting of lamellae with different thickness', the thicker lamellae being formed due to the recrystallization at the higher crystallization temperature (c) different crystal unit cell structures being responsible for the two melting endotherms with the crystal transformation taking place during the recrystallization step. Subsequent discussion in this chapter will consider the applicability of these various reasons in addressing the melting behavior in light of the available experimental evidence. However, before such an exercise is undertaken it is first important to recognize the effect of various isothermal crystallization temperatures on how they may influence the melting behavior.

Figure 8.5 (a) and (b) show the heating scans after the polyimide was melt crystallized at temperatures ranging from 270°C to 380°C after quenching from the melt at 450°C for 1 minute. This range of crystallization temperatures covers the temperatures much below the position of the lower endotherm, at the position of lower endotherm and recrystallization exotherm and also temperatures intermediate between the recrystallization exotherm and the higher melting endotherm. Figure 8.5(a) shows the scans from room temperature after crystallizing at temperatures ranging from 270-330°C, all of which are below the position of the lower melting endotherm. The characteristic melting behavior of this polyimide with two widely spaced melting endotherms and an intermediate recrystallization exotherm are clearly observed for all crystallization temperatures. However, a third melting shoulder appears ca. 15°C above the previous crystallization temperature. Such behavior has often been observed for a large variety of other semicrystalline polymers, though the magnitude of this shoulder in the present case is quite small. For other polymers exhibiting this behavior, the widely argued models again rest on either the ‘continuous melting and recrystallization’ or the ‘difference in morphology’ being responsible for lower melting shoulder and subsequent main melting endotherm. According to the melting-recrystallization model then, the lower melting shoulder would be due to the onset of the melting of the crystals formed at the crystallization temperature, after which a continuous melting and recrystallization process ensues. The lower melting endotherm at ca. 350°C then appears when the rate of melting exceeds the rate of recrystallization. The ‘morphological model’ ascribes the lower melting shoulder to the melting of thinner lamellae formed during the secondary crystallization while the main primary lamellae lead to the primary endotherm (in this case the lower melting primary endotherm at ca. 350°C). *This author believes that the ‘morphological model’ and not the ‘melting recrystallization model’ is more appropriate in describing the lower melting endotherm.* It is useful to notice here that the position of the lower melting peak shifts to slightly higher temperatures as the crystallization temperature is raised. Such a behavior is inexplicable on the basis of a continuous melting-recrystallization approach, which if true would have resulted in the melting temperature being the same. For example, if the continuous

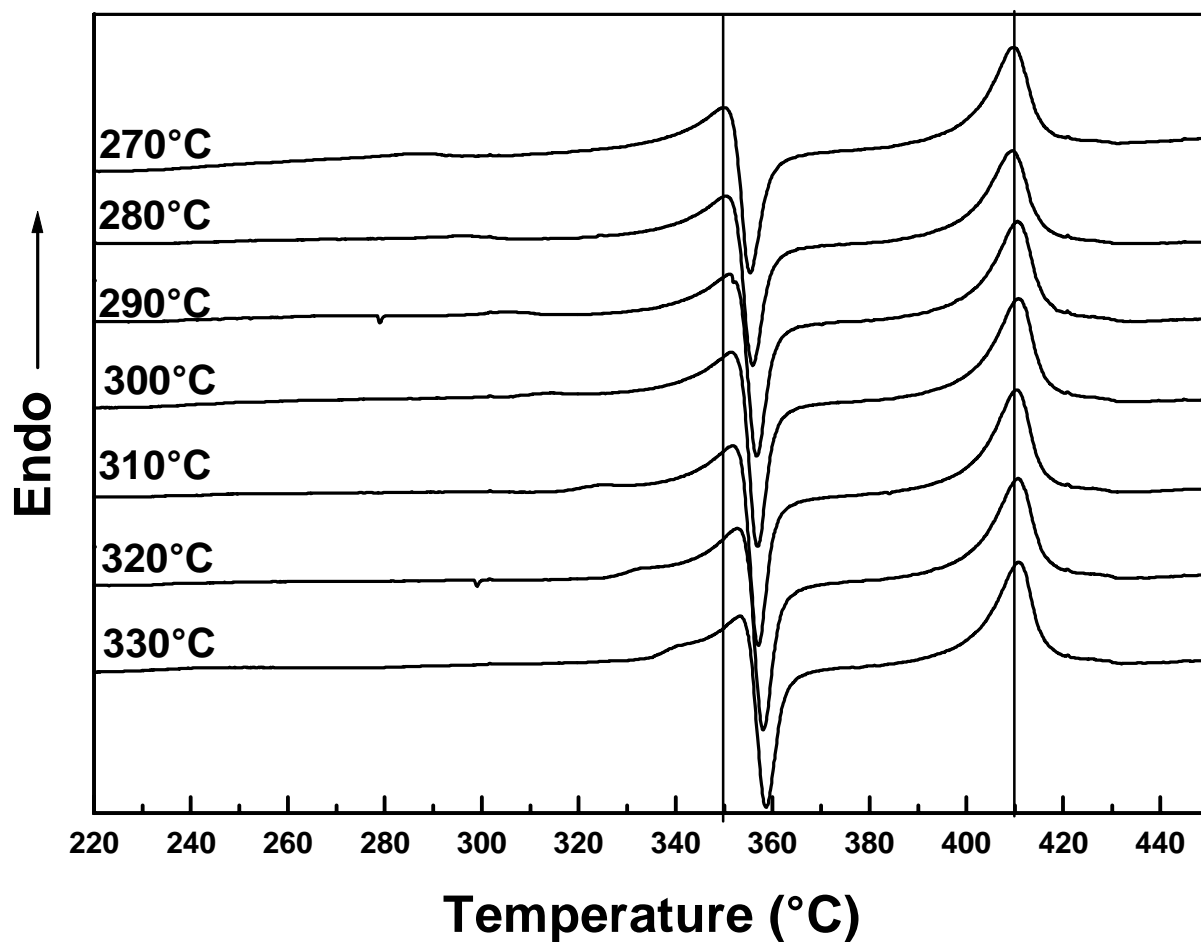


Figure 8.5(a) Scans from room temperature at 10°C/min after crystallizing at different temperatures from the melt at 450°C, 1min. Samples crystallized for 60 min.

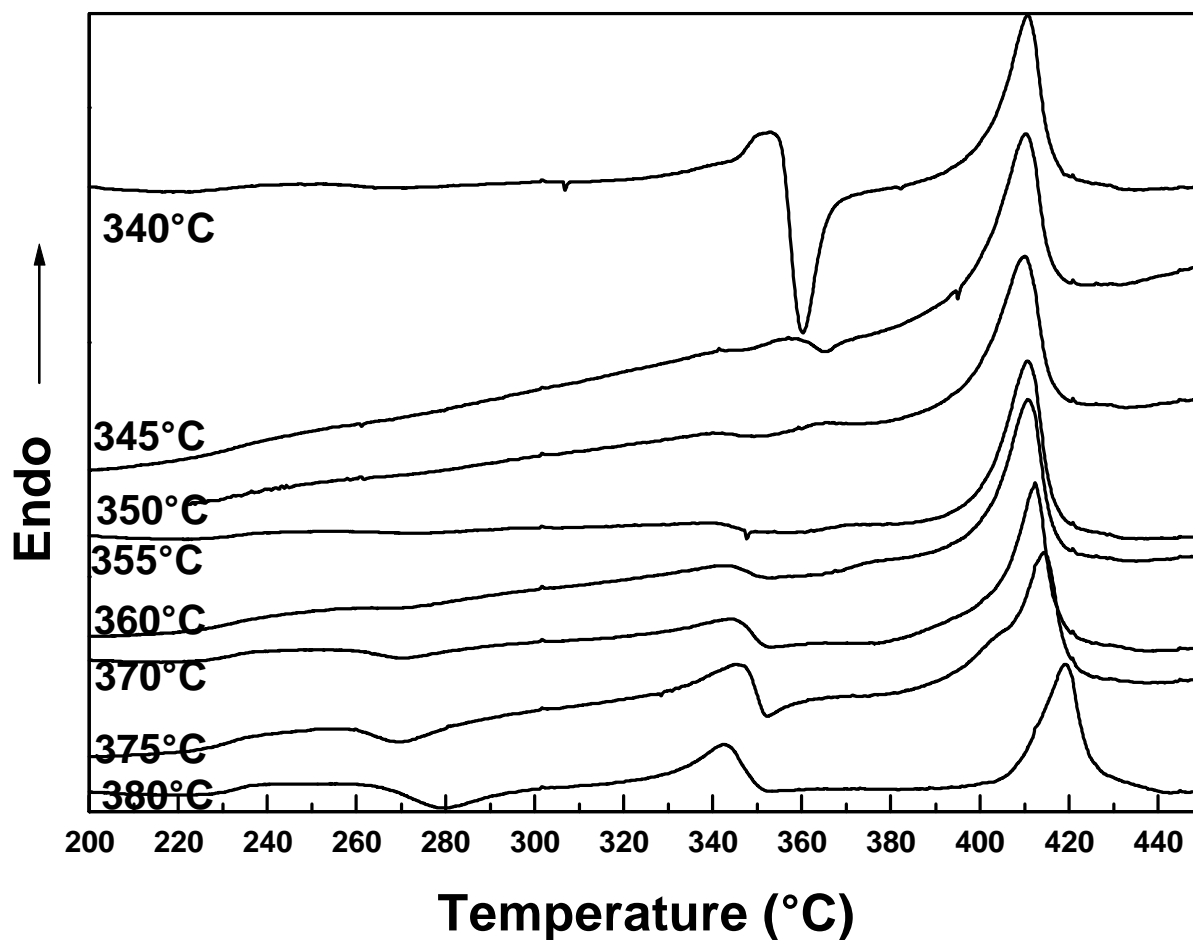


Figure 8.5(b) Scans from room temperature at 10°C/min after samples were melt crystallized at different temperatures and quenched to room temperature. The melt conditions utilized were 450°C for 1min. Samples for 340°C-360°C crystallized for 60 min. Samples for 370°C-380°C crystallized for 3 hours.

melting-recrystallization process was operative than the crystals formed at 270°C will start reorganizing at temperatures above 270°C. At a higher temperature then, say 330°C, these crystals should not be much different than crystals formed at 290°C (which start reorganizing above 290°C). The final melting temperature of the crystals then should have remained unchanged if such a phenomenon was taking place. These preceding arguments, however, rest on the assumption that kinetics of melting-recrystallization are faster compared to the heating rate utilized. This assumption usually holds good for the heating rate of 10°C/min utilized above. Other evidence supporting this conclusion (also from the DSC experiments) will be presented in the later sections.

It also needs to be recognized that the position of the observed peak temperature for the lower melting endotherm may depend upon the subsequent recrystallization exotherm to some extent. This may occur due to the possibility of the recrystallization starting with the onset of the melting process. The DSC signal obtained in such a case then results from these two simultaneous processes. The shape of the overall melting and recrystallization behavior observed during the DSC scan thus depends upon the relative position of these two processes. In this regard, the recrystallization exotherm, which depends upon the melting of the crystals at ca. 350°C, also shifts to higher temperatures. The final melting endotherm at ca. 410°C is independent of the previous crystallization temperature for this range of T_c 's.

Figure 8.5(b) shows the heating scans after the samples are crystallized in the range 340°C-380°C. The lower melting shoulder that appears at ca. 15°C above the previous crystallization temperature occurs very close to the main lower melting endotherm for $T_c=340^\circ\text{C}$, while the melting behavior changes drastically as the crystallization temperature is raised just 5°C to 345°C. It is noticed that for a sample crystallized at $T_c=345^\circ\text{C}$, only a small endotherm at ca. 350°C is produced followed by immediate recrystallization and a final larger melting endotherm at ca. 410°C. This indicates that at $T_c=345^\circ\text{C}$, most of the crystals that form are those that melt at higher temperatures. The small population of lower melting crystals that result in the small endotherm at 350°C may form during the fast cooling to room temperature or during the heating scan from the room temperature. Similar behavior is obtained for T_c 's greater

than 350°C. In fact, for T_c greater than 360°C, a crystallization exotherm begins to appear during the heating scan resulting in formation of lower melting crystals. Also, the peak position of the higher melting endotherm begins to shift to higher temperatures as the T_c is increased to 380°C. For the T_c 's above 350°C, the presence of any $T_c+15^\circ\text{C}$ endotherm is difficult to detect. This issue is elaborated in greater detail in the forthcoming sections where the isothermal experiments at 360°C are described. These overall results clearly illustrate the significant effect that small changes in T_c can have on the overall melting behavior. The peculiar-melting behavior, with two prominent endotherms, changes dramatically as the T_c is raised above 340°C. Indeed this has important ramifications from an application standpoint, where the polyimide may be used for example in high temperature adhesive and composite applications. The modulus of the material is expected to show dramatic changes at ca. 350°C for the samples which are crystallized below 345°C, while the modulus is expected to hold till much higher temperatures for samples crystallized above 340°C.

Another issue of significant importance is the crystallization kinetics at various isothermal temperatures. In this regard, the peak times for the isothermal crystallization exotherms are plotted in Figure 8.6 and give a good indication of the kinetics of crystallization at various temperatures. The data was obtained by utilizing a minimum of four experiments for each crystallization temperature and the average values of peak times as well as the error bars indicating the standard deviation are plotted. It is a well-established fact that when the crystallization takes place in the nucleation controlled region, the bulk crystallization rate increases as the degree of supercooling increases. In this regard, it is at first surprising to note the increase in peak crystallization times at intermediate crystallization temperatures. *This implies that the rate of crystallization starts to decrease with increasing supercooling in a narrow range of T_c 's close to 345°C!* These crystallization temperatures are close to the position of the lower melting endotherm. Also, as is previously discussed, melting behavior of the polyimide changes dramatically when crystallized at T_c 's above 340°C.

A likely reason for this peculiar behavior of crystallization half times is the presence of two crystal unit cell structures with different equilibrium melting points.

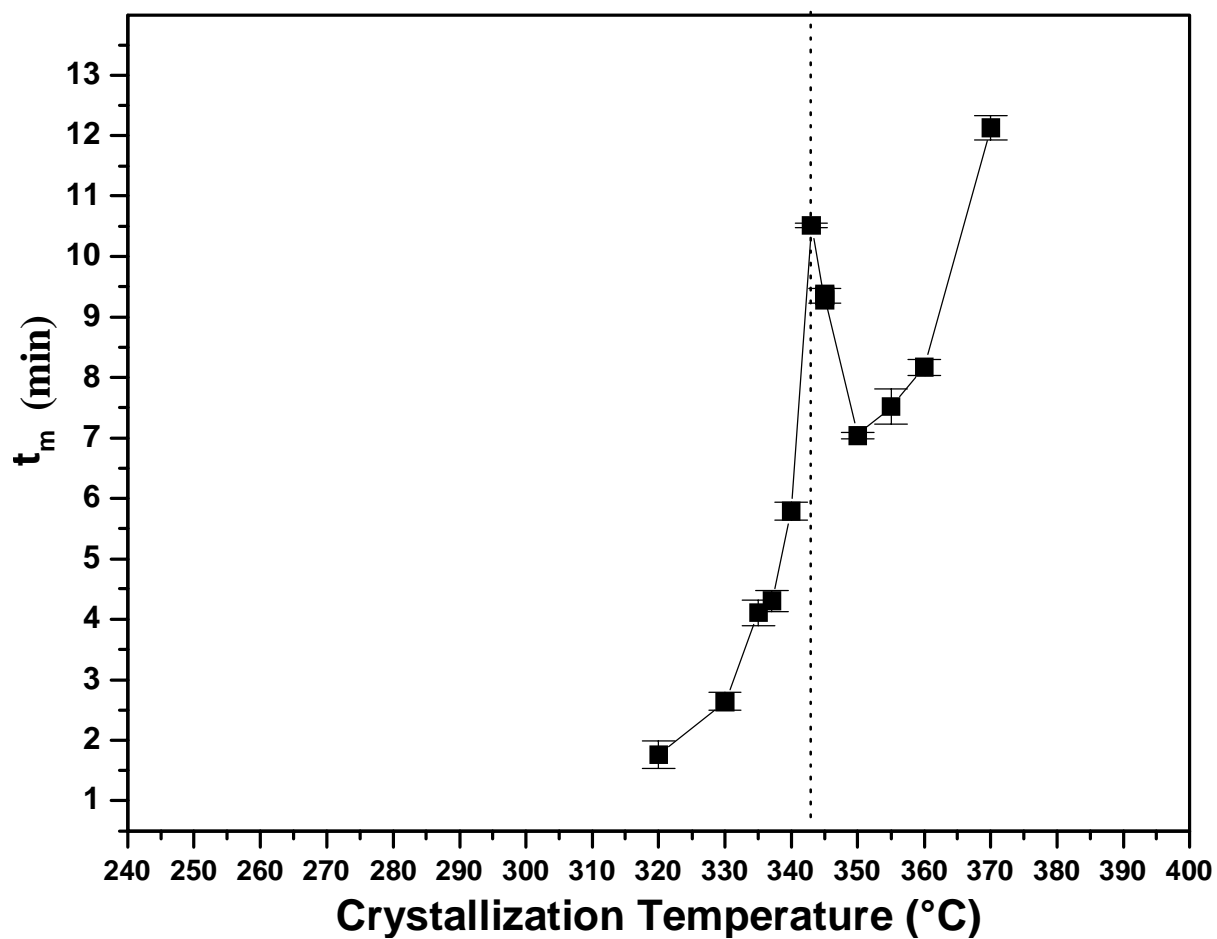


Figure 8.6 Peak times for isothermal crystallization exotherms, after quenching from 450°C, 1 min to different crystallization temperatures. The error bars indicate the standard deviation of at least four samples.

While the formation of lower melting crystals is favored at temperatures below 345°C, higher T_c 's promote the higher melting form. The rise in 'peak crystallization times' can then be explained due to a slower crystallization rate of lower melting crystals being formed at these temperatures. This slower rate is due to the lower 'effective supercooling' that is operative relative to the equilibrium melting point of these crystals. As the crystallization temperature is lowered further, the supercooling increases again and crystallization rate thus also increases. The peak crystallization times thus begin to decrease once more. During the heating scan the lower melting crystals, if present, completely melt at temperatures in the vicinity of 345°C-350°C and subsequently give rise to the higher melting form. In this case, the size of the recrystallization exotherm depends upon the size of the previous melting endotherm. This evidence and the immediacy of the recrystallization then suggest that the recrystallization process is closely associated with the previous melting of the lower melting form. It is possible to contemplate that only a small conformational rearrangement is needed of the chains constituting the lower melting crystals to give rise to higher melting crystals. Additionally, as there is relatively little melt disorder, the nucleation density 'in effect' is very high for the subsequent crystals to grow. This would then also explain the position and the fast rate of such a recrystallization process.

It is important to understand the morphological changes that may accompany this prominent bulk melting and recrystallization process. To this end, a hot stage polarized optical microscopy experiment was conducted where the polyimide was rapidly quenched from the melt to 340°C (where the low melting crystals form), crystallized at this temperature for 20 minutes and then *rapidly heated* to 370°C. A spherulitic morphology that appeared initially at 340°C, was then observed for any changes at 370°C. Also, a more severe melt condition of 460°C for 3 minutes was utilized to reduce the residual nuclei in the melt and thereby reduce the nucleation density at 340°C, thus facilitating easier observation. It was found that a very subtle and quick change occurred in the appearance of spherulites, when they were held at 370°C. This change is illustrated in Figure 8.7, where (a) illustrates the spherulitic morphology after 20 minutes at 340°C, and (b), (c) and (d) show the morphology at 370°C after 30s, 90s and 120s of holding

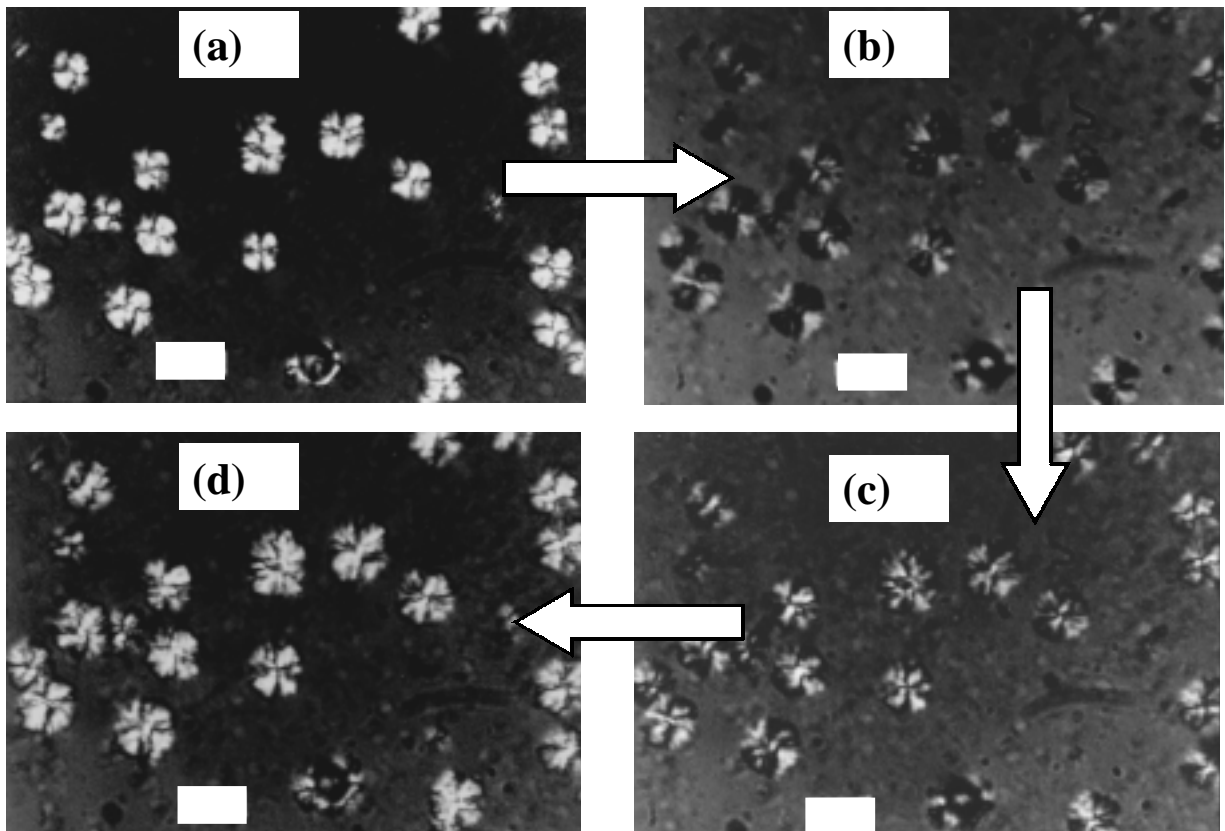


Figure 8.7 Polarized optical micrographs of sample (a) crystallized at 340°C for 20 min and (b, c, d) held at 370°C for (a) 30s (b) 90s (c) 120s. The white scale bars indicate 25 microns.

time respectively. A coarse spherulitic morphology with only a weakly defined maltese cross is observed at 340°C. *However, when heated to 370°C, these spherulites consisting of low melting crystalline form, melt and give rise to new spherulites at exactly the same position.* The melting and recrystallization of the initial spherulites is illustrated in Figure 8.7 (b and c), where the birefringence first changes on melting (compare Figure 8.7(a) and Figure 8.7(b)). However, following melting, immediate recrystallization leads to the reemergence of spherulites that finally melt at ca. 410°C. If the temperature is held at 370°C, then the spherulites continue to grow at this temperature. In fact, from a polarized optical microscopy viewpoint, there is not much difference between the spherulites in Figure 8.7(a) and Figure 8.7(d), an observation also born out by independent experiments at these two temperatures. This evidence also explains to a large extent the reason for a sharp and adjacent recrystallization exotherm immediately after the lower melting endotherm. It also supports the earlier proposal of recrystallization occurring at or about the same sites with a possible conformational rearrangement of the chains to give rise to a different crystal unit cell structure.

Subsequently WAXD experiments were performed on samples crystallized above and below the temperature of lower endotherm to verify if any noticeable difference in the x-ray patterns was obtained. The WAXD scans in Figure 8.8 show the results obtained for the initial material, samples crystallized at 360°C and also for samples crystallized at 330°C. It is important to recall at this stage, that while the samples crystallized at 360°C and 330°C are expected to respectively contain only the higher and lower melting crystalline forms, the DSC results indicate that the as-received initial polyimide contains both the higher and lower melting form. However, for the samples crystallized at the three different temperatures, no significant differences are visible in terms of position of the peaks or presence of new ones. Thus this WAXD experiment is therefore not able to distinguish between the two different crystal unit cell structures, which may be due to the close similarity between them. Such similar WAXD scans have been reported for other materials that show two different crystal unit cell structures. It has been shown that although PET shows two different crystal unit cell structures (with different melting points), only very sharply resolved WAXD experiments (on isotropic

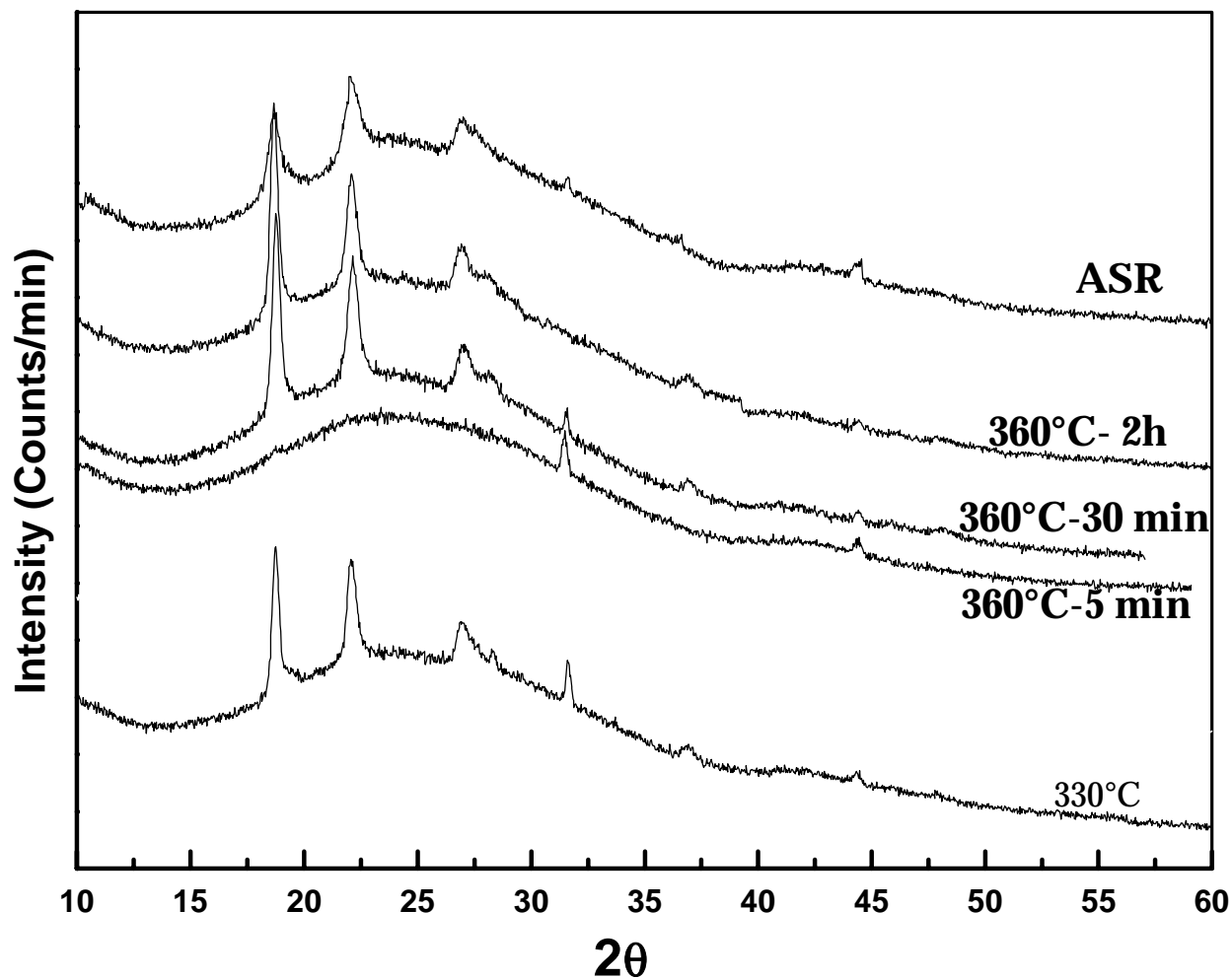


Figure 8.8 WAXD patterns of TPER-BTDA-PA –initial film and melt crystallized at different temperatures. Samples were precisely prepared in the DSC.

samples) are able to resolve that difference. It is likely that the diffractometer utilized in this study did not resolve a small difference that might exist in the crystal unit cell structures of the present polyimide. A more detailed information regarding the crystalline reflections, possibly from a fiber pattern is required to resolve this difference. Thus in light of evidence demonstrated earlier, it is contended that the presence of two prominent and widely spaced endotherms is the result of difference in crystal unit cell structures, though it did not lead to different WAXD results for the isotropic films in the present study.

While two different crystal unit cell structures have been ascribed for the two prominent endotherms, it remains unresolved whether the crystals undergo a continuous melting and recrystallization process before the melting endotherms appear or the melting endotherms represent the melting of crystals formed at the previous crystallization temperature. Further experiments were hence conducted to resolve this issue and correctly surmise the cause of the two melting endotherms. In this regard two different types of experiments were conducted- one consisting of isothermal crystallization for varying times at the selected crystallization temperature and heating from that temperature, and the other consisting of scans of previously crystallized specimens at varying heating rates. Also, two crystallization temperatures, 320°C (below the lower melting endotherm), and 360°C (between the two endotherms) were selected for this purpose. The results from the isothermal experiments are discussed first to see if convincing evidence supporting either of the two models is obtained.

Figure 8.9(a) shows the direct heating scans from 320°C after the specimens were crystallized at that temperature for times indicated in the figure. A short residence time of only 1-minute at 320°C is unable to induce any crystallinity in the polyimide. Also, no additional crystallization occurs during the heating scan from that temperature though it takes 8 minutes (at 10°C/min) for the polyimide to reach the onset of the higher melting endotherm at 400°C. Possibly, any incipient nuclei, if formed, are destroyed as the temperature is continuously raised, thus precluding any significant crystallization (at this heating rate). Also, the progressive slowing down of crystallization kinetics with increasing temperature (see Figure 8.6) further lowers the possibility of any significant

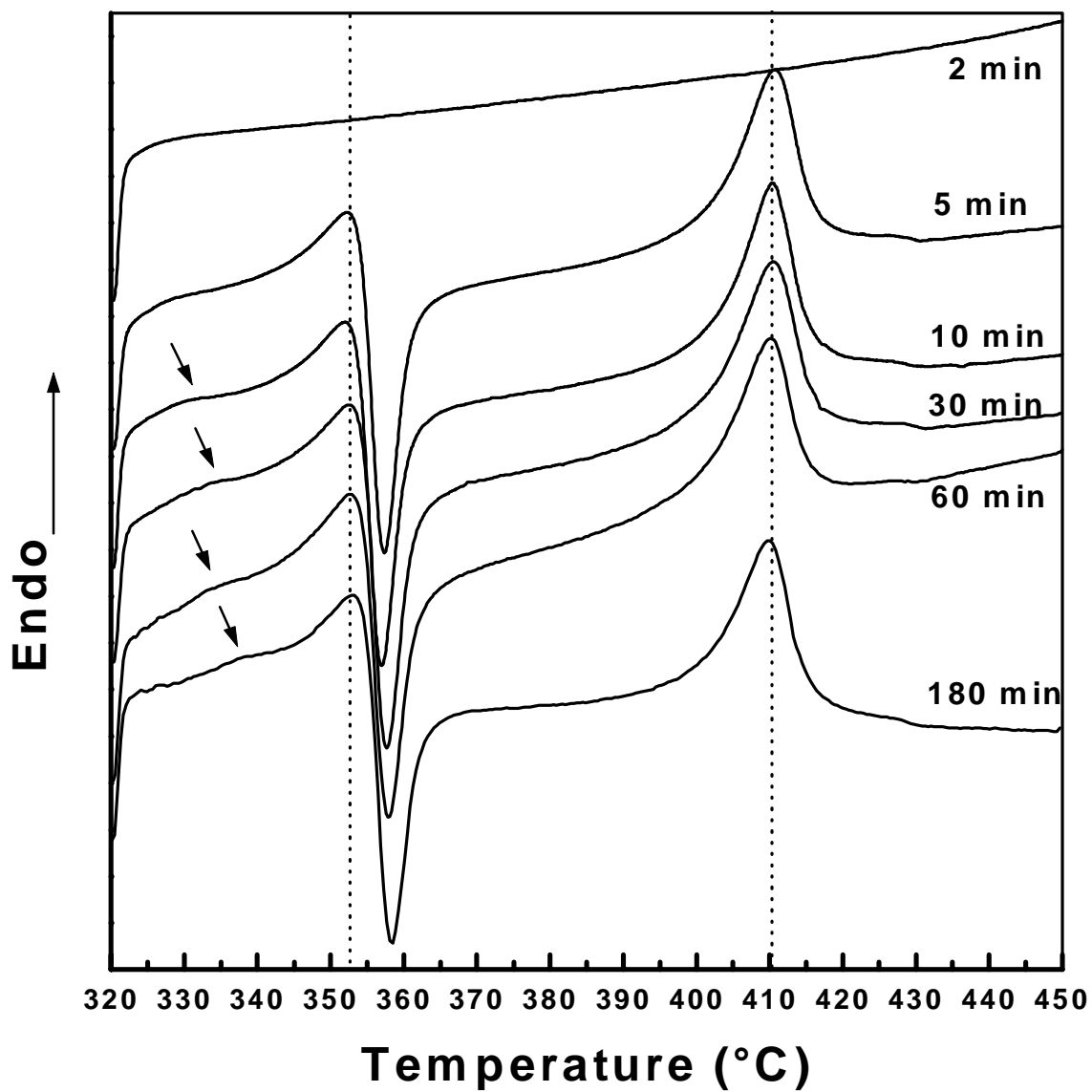


Figure 8.9(a) Direct DSC heating scans at 10°C/min after crystallizing for various times at 320°C.

crystallization occurring during the heating scan. However, crystallinity appears in the specimens for higher residence times of 5-180 minutes. No major changes, however, are observed between different specimens with respect to the position and size of the two prominent endotherms and the intermediate recrystallization exotherm. Additionally, a small but noticeable endotherm appears ca. 10-15°C above 320°C for times greater than 5 minutes, with its strength showing a small increase and its position slightly shifting to higher temperatures for increasing crystallization times. This is followed by the primary lower melting endotherm, whose peak position or size does not change with increasing time. There is a minor change in the position of the recrystallization exotherm that shifts to slightly higher temperatures. The higher melting endotherm, however, does not show any change in the peak melting point of 410°C.

The result that the main melting endotherm at ca. 353°C appears first and the much weaker melting shoulder at ca. 330°C later, suggests that the primary and first forming crystals at $T_c=320^\circ\text{C}$ are responsible for the melting endotherm at ca. 353°C. The later forming thinner crystals due to secondary crystallization are then responsible for the weaker lower melting shoulder. The absence or relative weakness of the lower melting shoulder for shorter crystallization times is thus an argument in favor of the difference in morphology (with respect to the thickness of the crystals) being responsible for the lower melting shoulder and the melting endotherm at 353°C. If, however, the melting-recrystallization model is defended here, then a commonly utilized argument for explaining absence or weakness of the small melting shoulder is that at shorter crystallization times, the amount of crystallinity is low and hence the shoulder representing melting of such crystals is correspondingly weak/absent. This argument, however, does not hold here as the population of crystals melting at ca. 353°C is similar for all times (except 2 min) and thus the lower melting shoulder should also have been similar for all crystallization times. The higher melting endotherm at 410°C remains unaffected by the crystallization times at 320°C, as it only represents the melting of crystals formed during the recrystallization at 355-360°C.

The direct heating scans from 360°C, when the sample is crystallized for different times are also shown in Figure 8.9(b). In this case no additional lower melting shoulder

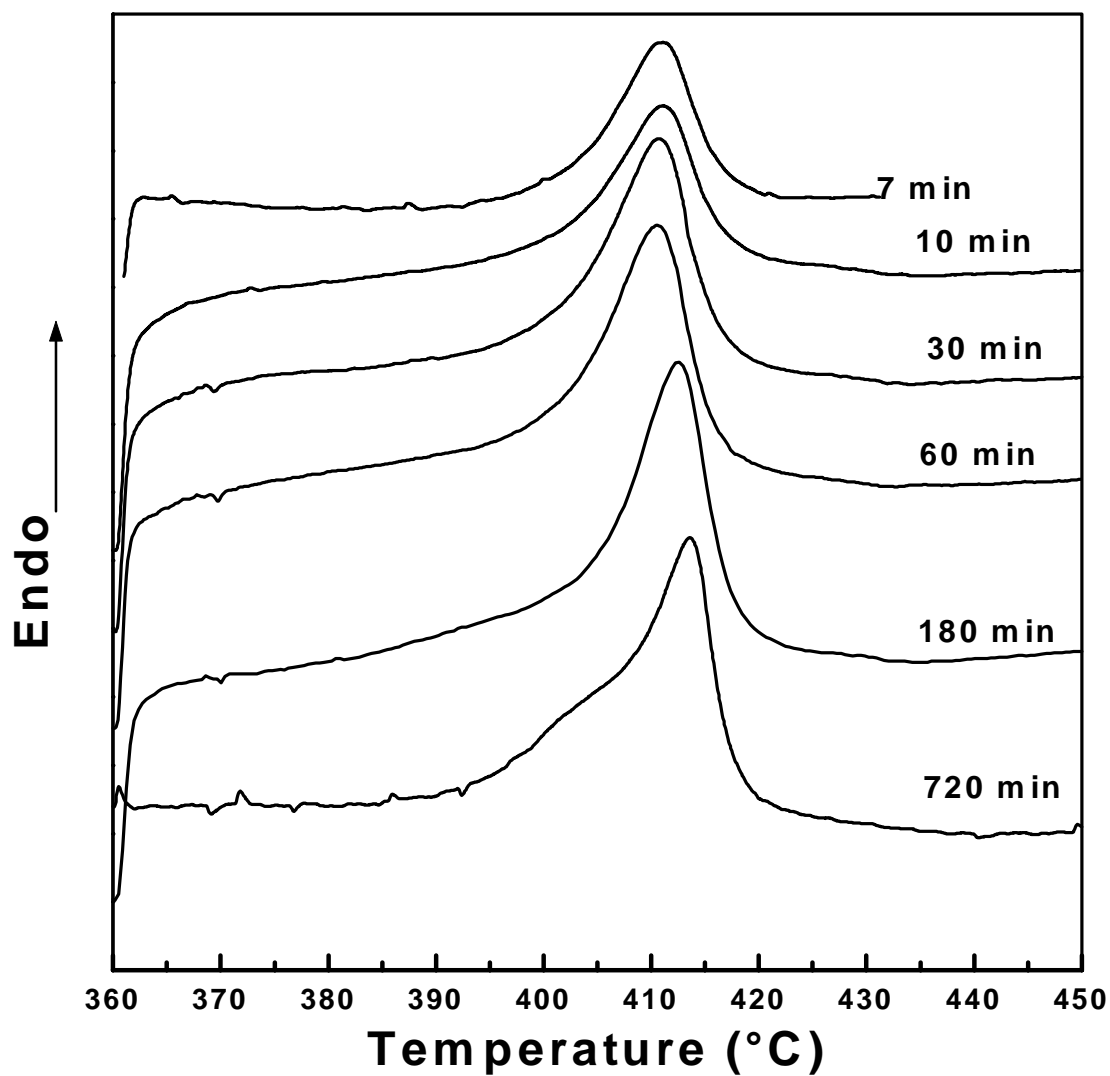


Figure 8.9(b) Direct DSC heating scans at 10°C/min after crystallizing for various times at 360°C.

is observed, but rather only a broad melting endotherm at ca. 410°C is obtained for all crystallization times. Also, for higher times of crystallization, the amount of crystallinity continues to increase (as indicated by the size of the endotherm) while a shift in the position of peak melting point is also observed. The absence of a well-defined smaller endotherm ca. 10-15°C above the crystallization temperature precludes assignment of the overall melting to either a 'continuous melting recrystallization process' or due to the 'melting of lamellae of two different thicknesses'. Rather it can only be said that a very broad melting population of crystals is obtained with the crystals starting to melt as the temperature is raised above 370°C.

To further substantiate the origin for the melting endotherms, experiments were conducted at varying heating rates for specimens originally crystallized at 320°C and 360°C respectively. Similar experiments were also conducted on the original as received polyimide film to detect any change in its melting behavior. Before conducting experiments at different heating rates, the DSC was carefully calibrated at each heating rate using zinc and tin standards. This minimizes any discrepancy in the DSC signal for varying heating rates although some error due to thermal lag effects may still result for faster heating rates. A lower weight of the samples was also used to minimize this error. Figure 8.10(a) shows the DSC scans for the initial film heated at rates ranging from 5-150°C/min. The overall shape of the DSC scan for the different rates does not change much and consists of the characteristic prominent dual endotherms and an intermediate recrystallization exotherm. It is important to note, however, that the position of the lower melting peak does not change with the heating rate. If this peak was the result of a continuous melting-recrystallization of previous crystals than the position of this peak is expected to shift to a lower temperature for faster heating rates, as lesser time is now available for the crystals to reorganize. Similar arguments can be extended for the behavior of the crystals associated with the higher melting peak, which also does not show much change in its position. Also, both the recrystallization exotherm and higher melting endotherm broaden somewhat as the heating rate is increased. It is, however, interesting to note that recrystallization process is not greatly reduced even for significantly faster heating rates of 80°C/min and 150°C/min, thereby indicating the

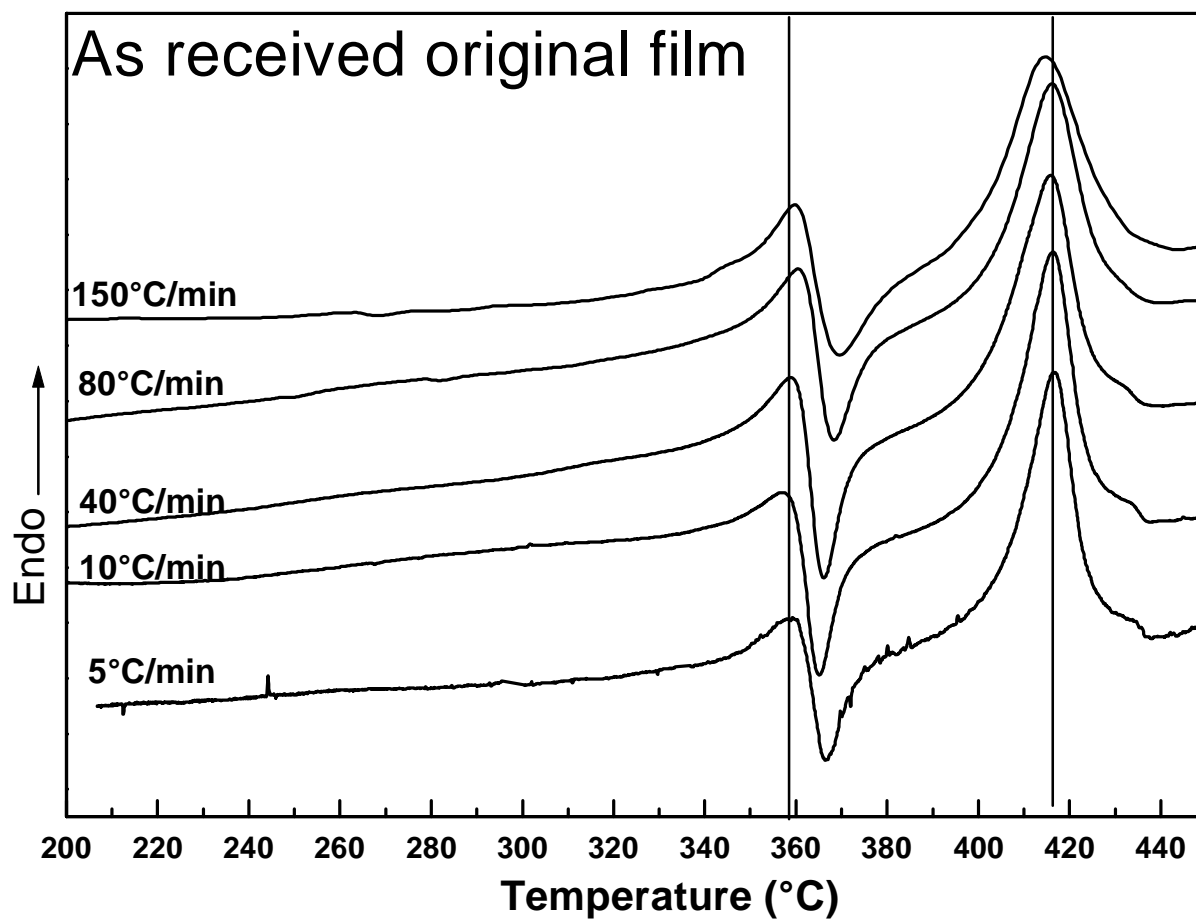


Figure 8.10(a) DSC heating scans at different heating rates for initial film after calibrating the DSC at different heating rates.

extremely fast kinetics associated with this process. It is also important to remember that the initial film undergoes a process of simultaneous polymerization and solvent aided crystallization during the synthesis process. The larger size of the higher peak clearly suggests that both higher and lower melting crystals form during the initial polymerization and simultaneous crystallization.

Figure 8.10(b) shows the DSC scans at different heating rates for films melt crystallized at 320°C for 1 hour-the crystallization temperature where only the lower melting form is expected to form. Expectedly the melting behavior is quite different from the initial film. Whereas the lower melting peak shows a slight shift to higher temperatures for faster heating rates, the size and position of the higher melting form depends significantly on the heating rate utilized. In fact, for the fastest heating rate of 150°C/min, the higher melting form is eliminated. This reduction in the higher melting form occurs concurrently with the reduction in the recrystallization process. It is interesting to note that although considerable broadening is visible for these two processes at faster heater rates, the peak position of the higher endotherm does not change much. This again contradicts the continuous melting-recrystallization being operative for the higher form, which if it had been true would have resulted in shifting of the higher melting peak to lower temperatures for faster heating rates. For the main lower melting peak at ca. 353°C, a lower melting shoulder discussed previously appears for the slower heating rates. If the lower melting shoulder represents the onset of the melting-recrystallization process, then it should gain strength (possibly even becoming a separate peak) and shift to higher temperatures for faster heating rates. Also, the main melting peak at ca. 353°C should shift to lower temperatures. None of these observations were made, thus indicating absence of a ‘continuous’ melting-recrystallization. The results can be readily explained on the basis of the ‘morphological model’. The lower melting shoulder due to thinner crystals gets less defined due to the natural broadening of the melting for faster heating rates. The lower peak that represents the melting of primary crystals shows a slight shift to higher temperatures due to the delayed melting and small thermal lag. Hence, these results provide strong support for the difference in morphology being responsible for lower peak and a small shoulder associated with it.

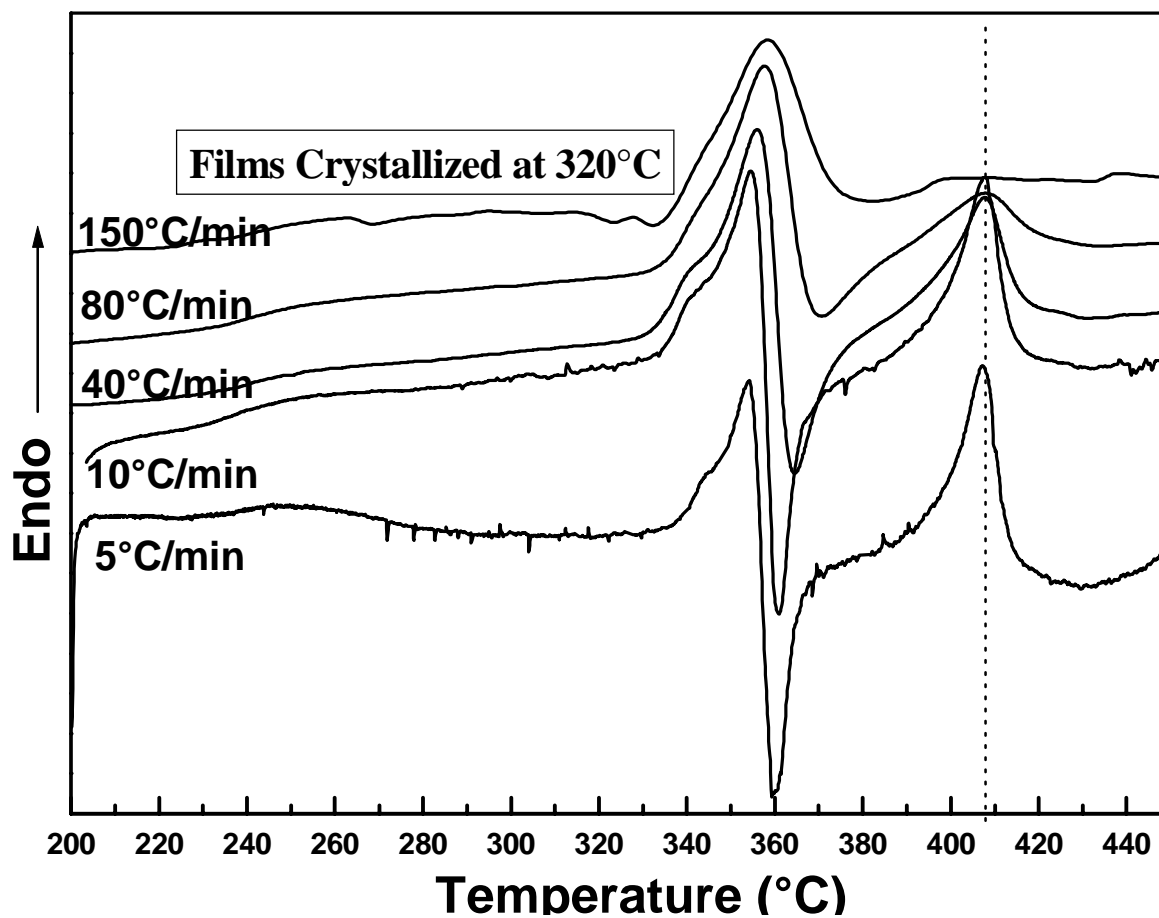


Figure 8.10(b) DSC heating scans at different heating rates for films crystallized at 320°C after calibrating the DSC at different heating rates.

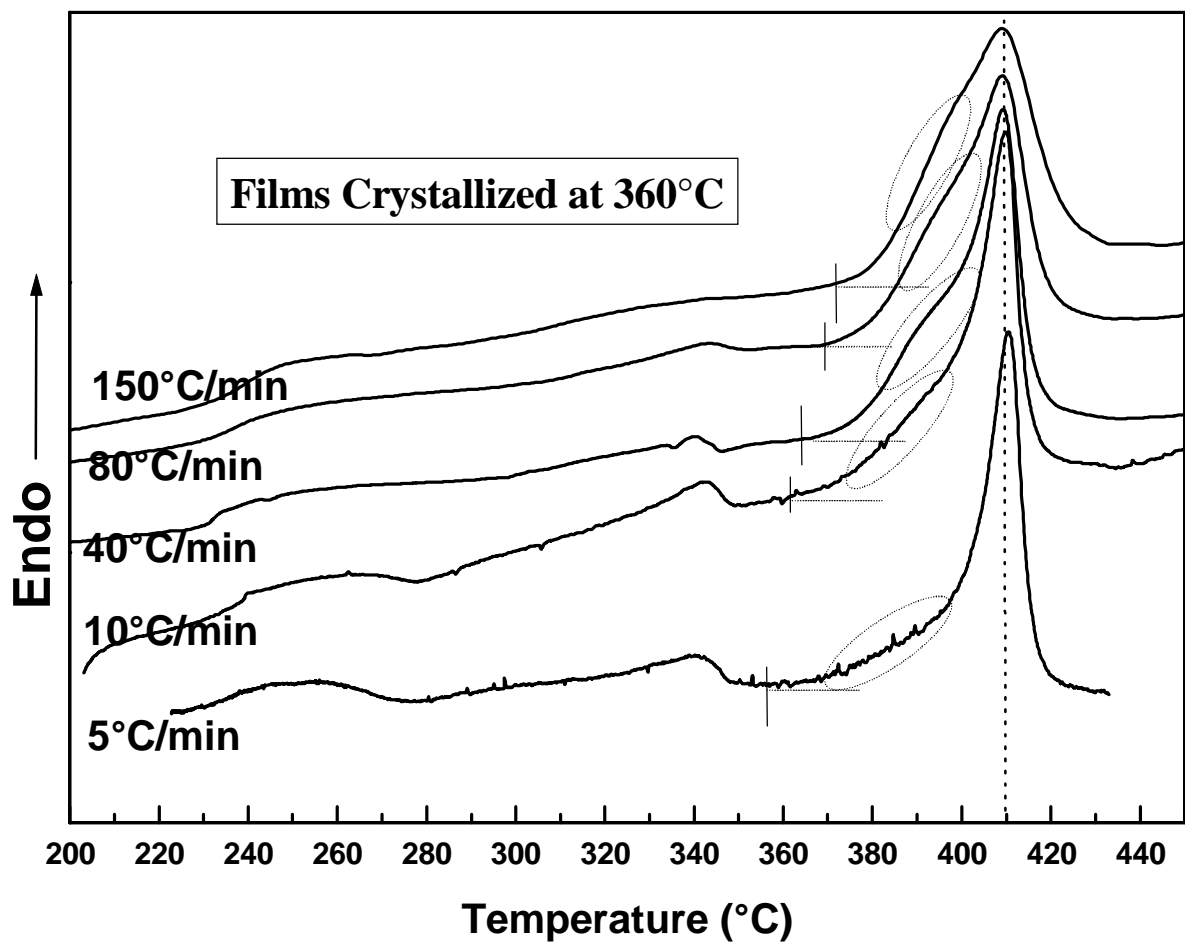


Figure 8.10(c) DSC heating scans at different heating rates for films crystallized at 360°C after calibrating the DSC at different heating rates. The encircled regions highlight the broad distribution of crystal thickness' which seems to broaden with increasing heating rate but does not become a separate peak in itself.

Figure 8.10(c) shows the DSC scans for polyimide crystallized at 360°C for 1 hr- a temperature where only the higher melting form is expected to form. The samples were quenched to room temperature before scanning at different rates. It is observed that while only one prominent endotherm at ca. 410°C is observed, a smaller endotherm at ca. 340°C appears for slower heating rates. The appearance of the lower endotherm is due to the crystallization that occurs above the glass transition temperature. Faster heating rates reduce this crystallization thereby resulting in a reduction of the melting endotherm at ca. 340°C. There is, however, no prominent recrystallization exotherm observed to give rise to higher melting crystals. It is useful to remember that this lower endotherm due to crystallization after T_g also occurred for T_c 's greater than 360°C. This suggests that there may be a population of chains that more easily crystallize into the lower melting form, but require much longer times to crystallize into the higher melting form when at crystallization temperatures that are greater than ca. 360°C. The higher melting endotherm broadens considerably as the heating rate is increased, although there is no effect on the peak position. It is also noted that there is a low temperature tail associated with the endotherms signifying the onset of melting of thinner crystals formed at 360°C. This melting starts after the temperature exceeds 360°C. The onset of melting seems to shift to slightly higher temperatures for faster heating rates due to delayed melting. The vertical bars drawn for various scans (Figure 8.10(c)) only roughly indicate the onset of this melting process rather than indicating its 'exact' position. For intermediate scanning rates, a shoulder appears on the low temperature side of the endotherm. However, this should not be identified as indicating the 'onset' for a continuous melting-recrystallization process (as has been done for other PEEK and other polymers by various workers). The author feels that this is a consequence of the natural broadening associated with faster heating rates. If a continuous melting-recrystallization process was occurring and the higher peak was a consequence of this process, than two events would have been taken place: (1) the lower melting shoulder would have tended to become a peak for faster rates (2) some shift to lower temperatures would have occurred for the higher peak. However, no such evidence supporting the continuous melting-recrystallization process is observed here. The effect of overall broadening of the various endotherms and

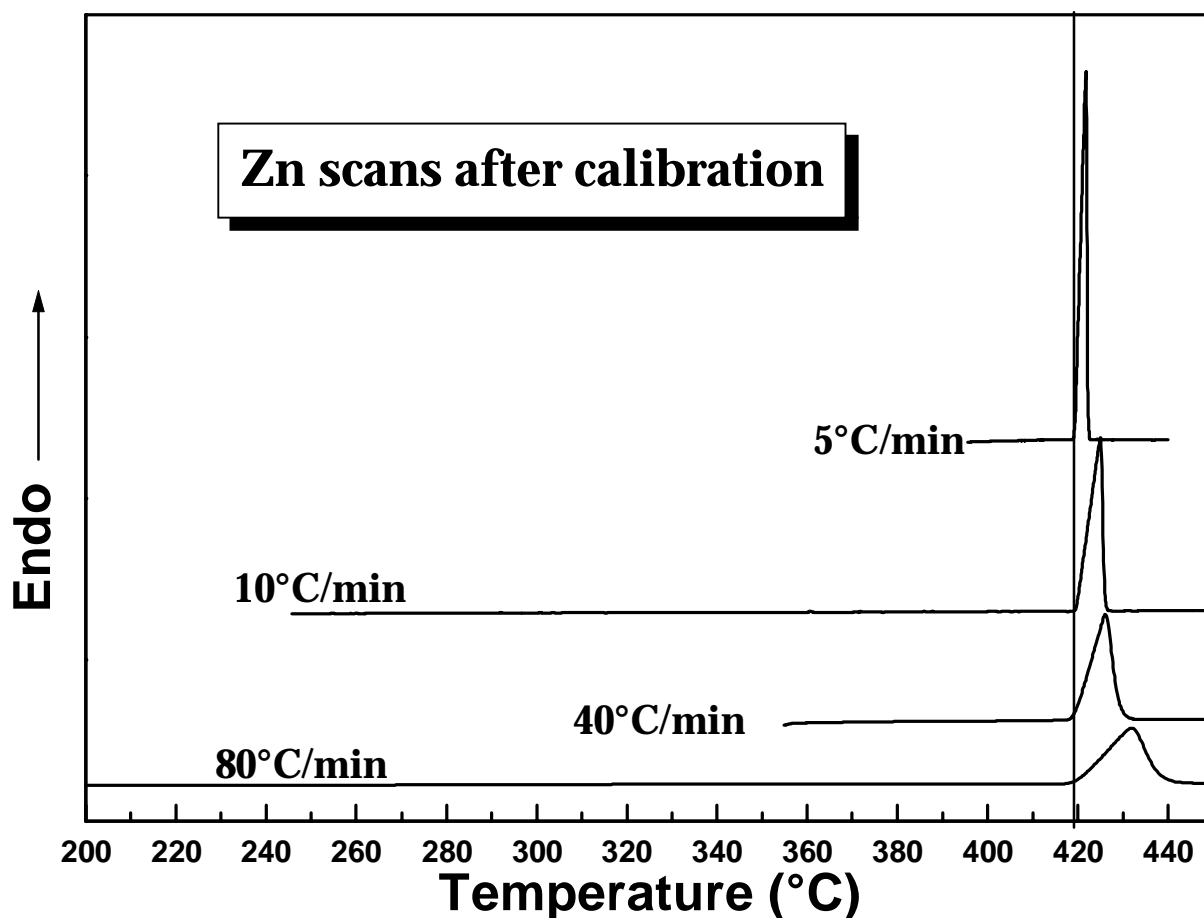


Figure 8.10(d) DSC heating scans at different heating rates for zinc after calibrating the DSC at different heating rates.

exotherms observed in Figure 8.10(a, b and c) is also shown for the zinc specimens in Figure 8.10(d) after calibrating at various heating rates. The onset of the melting point serves as a true measure of the calibration and is obtained to within 0.3°C for various heating rates. However, while a sharp peak is obtained for lower heating rates, the peak broadens for faster heating rates due to the thermal lag. Such an effect should be even more pronounced for the polymer samples and consequently a broadening is indeed observed in this case. However, it is surprising that the position of the various peaks do not show any major shift to higher temperatures for faster rates. This polyimide also demonstrates the commonly observed dependence of melting point on the previous crystallization temperature (see Figure 8.5(b)). For temperatures above 350°C, it is observed that higher T_c 's result in higher melting points.

It is earlier shown (Figure 8.9(b)) that there is some indication that the melting point of the polyimide crystallized at 360°C shifts to higher temperatures for longer times of crystallization. The increases in melting point can occur due to isothermal or non-isothermal thickening of the original crystals formed at 360°C. To further investigate this phenomenon, detailed experiments were conducted at 360°C and higher temperatures for longer crystallization times (Figure 8.11 and Figure 8.12). Also, the evolution of crystallinity was concurrently followed along with the variation in melting point as a function of time. Interestingly it was found that the melting point does not change much for residence times of ca. 100 minutes or less, while for longer crystallization times, a clear trend is observed in that the melting point increases as a logarithm of crystallization time. *In fact,, significant increases of 10-14°C in the melting point were observed for higher T_c 's and longer crystallization times.* It is also noted that these increases in melting point are not accompanied by any sharpening/narrowing of the endotherms and thus cannot be solely attributed to crystal perfection or narrowing of the crystal thickness distribution. Rather the endotherms at higher temperatures are broader indicating a wider distribution of crystal thickness with time. This phenomenon,, in the author's opinion, clearly reflects the 'crystal thickening' effects occurring at longer crystallization times in the polyimide. Also, there is an indication that the rate of thickening is faster for higher crystallization times, an observation commonly associated with such effects. However, it is peculiar to note that there seems to be an onset time associated with this crystal

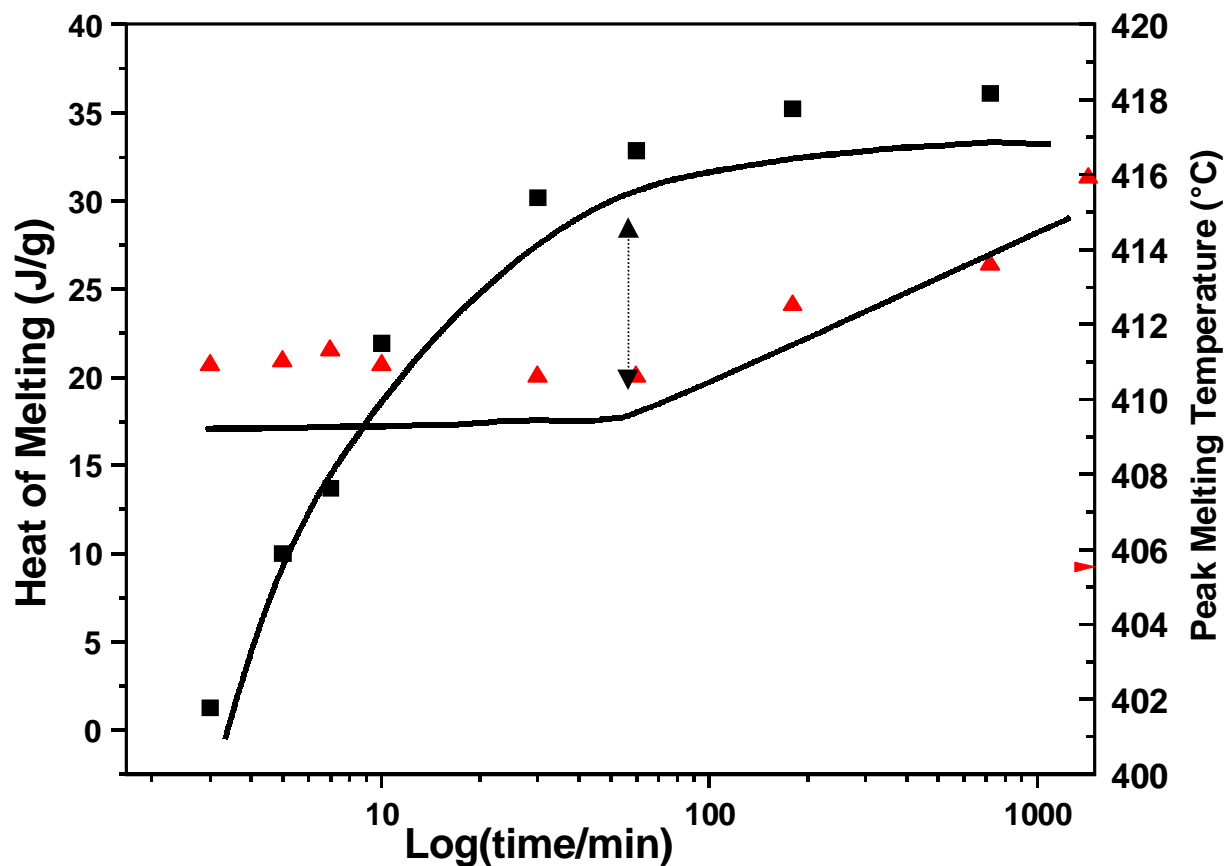


Figure 8.11 Isothermal crystallization at 360°C with respect to logarithm of time (■) heat of melting obtained after heating to melt (▲) the corresponding peak melting points obtained.

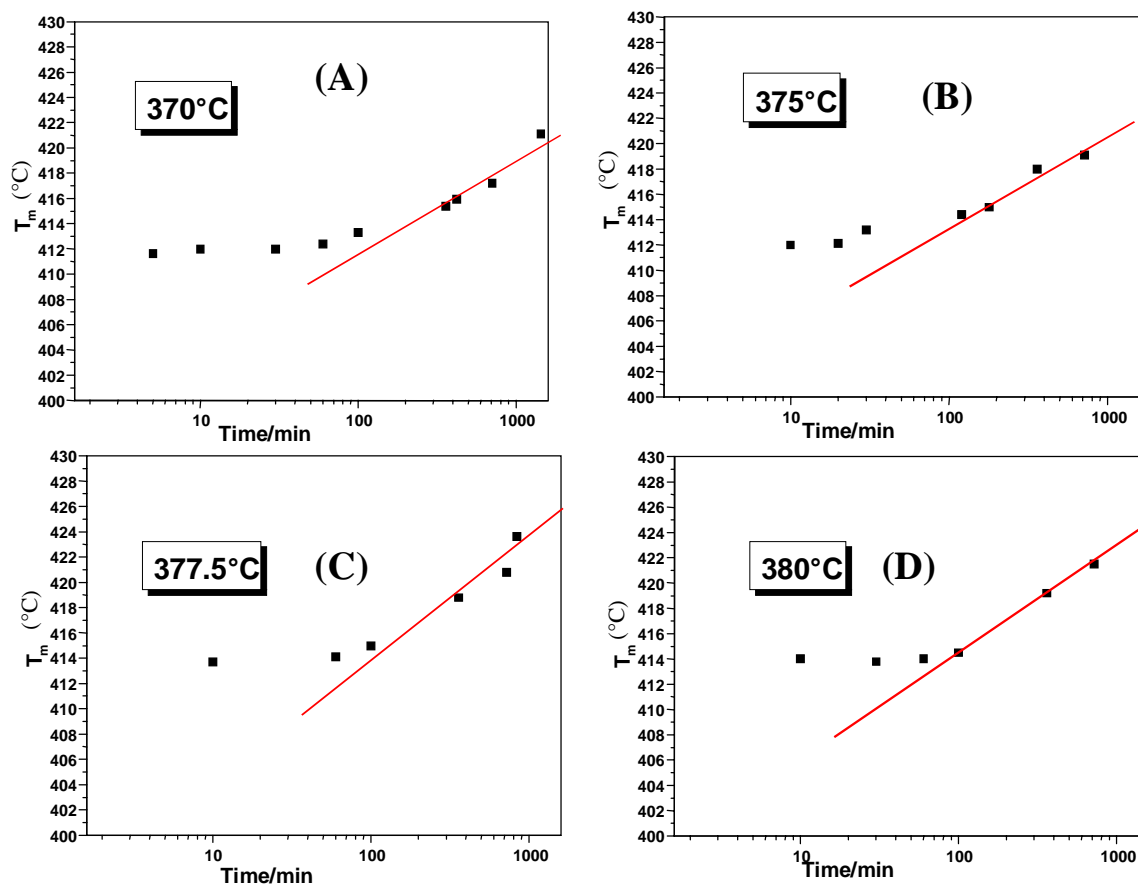


Figure 8.12 Isothermal crystallization was carried out at various crystallization temperatures for varying amounts of time after quenching from the melt (450 $^{\circ}\text{C}$, 1min). The plots show the peak melting points obtained on heating with respect to the logarithm of the crystallization time. The crystallization temperatures for various plots are (a) 370 $^{\circ}\text{C}$, (b) 375.5 $^{\circ}\text{C}$, (c) 377.5 $^{\circ}\text{C}$ and (d) 380 $^{\circ}\text{C}$.

thickening process. Figure 8.11 also shows the simultaneous evolution of crystallinity as indicated by heat of melting. For shorter times, the faster increase is associated with the primary crystallization process, while for longer times, the heat of melting begins to level off indicating the end of primary crystallization. It is important to note here that the onset of the thickening process is roughly associated with the ‘tapering off’ of the heat of melting curve. The results therefore suggest that the thickening phenomena depends somewhat on the end of the primary crystallization (see Figure 8.11). In this regard, it is relevant to first discuss the morphology of polyimide crystals. Other studies by this author using atomic force microscopy (AFM) and small angle x-ray scattering have indicated the presence of lamellar stacks within the material. However, the fold surfaces of these lamellae are not expected to be smooth. The long and semi-rigid nature of the chain will effectively block much adjacent or next neighbor reentry from taking place. It can therefore be conjectured that the nature of the fold surface is more akin to the switchboard model promulgated by Flory⁶³ and other workers⁶⁴. While this model has remained controversial for polyolefins and other flexible polymers, it is more applicable for such rigid chain polymers as the one used in this study, which inherently cannot demonstrate a smooth and regularly folded surface due to their long repeat units and relatively more rigid chains. Thickening of the crystals then can take place by the incorporation of the segments adjoining the ones already crystallized. At times shorter than needed for the primary crystallization to be over, the amount of such thickening (which itself depends on primary crystals) is expected to be small. This can then explain the absence of any noticeable crystal thickening effect for shorter times.

Determination of the equilibrium melting point, T_m° , is another aspect of fundamental importance in any crystallization study of a new polymer as it determines the undercooling dependence of the crystallization kinetics. This thermodynamic property determines the reference point for determining the driving force of crystallization and thus is also important when evaluating different crystallization theories, analyzing the spherulitic growth rates and nucleation density dependence. With respect to studying melt crystallization, it also determines the temperatures needed to erase the effect of previous thermal history and residual nuclei. In this regard, the

traditionally utilized method has been the Hoffman-Weeks analysis⁶⁵, which results from the Gibbs-Thomson equation and an expression derived from Lauritzen-Hoffman theory⁶⁵. However, this analysis, which was originally proposed for explaining the increases in melting points with crystallization temperature, is rigorously incorrect for predicting equilibrium melting points due to some fundamentally incorrect assumptions involved in its derivation⁶⁷. Another popular method of determining the equilibrium melting point consists of fitting the spherulitic growth rate data at low undercoolings using the classical Lauritzen-Hoffman theory⁶⁶. Also, Marand^{67,68} et. al. have recently proposed a fundamentally more rigorous non-linear Hoffman-Weeks analysis for polyethylene and other flexible polymers which is better able to predict the equilibrium melting temperature. Most of these methods, however, depend directly or indirectly on the classical Lauritzen-Hoffman theory and its various modifications, which were initially derived for polyethylene and other flexible polymers. The successful application of the theory itself in modeling the crystallization of such rigid-chain and long repeat unit polymers is doubtful. This author's own application of Hoffman-Weeks analysis yields a very low equilibrium melting point of ca. 430°C for the present polyimide. This value is clearly erroneous as the end of the melting endotherm itself in many cases extends beyond this temperature. Also, the recently proposed non-linear method could not be successfully applied for this polyimide. The melting temperatures utilized for these analyses were based on the initial melting points where the absence of any significant thickening can be reasonably assumed. Others thermodynamic methods like the Gibbs-Thompson method and the Flory-Vrij method also cannot be easily utilized for determining the equilibrium melting point. The Gibbs-Thompson method^{65,69} bases itself on presence of thin plate-like crystals where the lateral dimensions are significantly greater than the thickness of the crystals. This assumption is likely valid for the present polyimide (on the basis of independent AFM results). However, the lamellar thickness' at various T_c 's needs to be determined before such data, along with the melting data, is utilized to predict the equilibrium melting point using this analysis. Lastly, the Flory-Vrij method⁷⁰ requires preparation of a series of low molecular weight analogs. This demands synthesis and segregation of controlled molecular weight samples, an exercise not easy from a synthetic standpoint. Additionally, the molecular weight of the final polyimide is

difficult to determine (by conventional GPC analysis) due to insolubility of the final polyimide in common solvents.

8.4 Conclusions

This work introduces a new semicrystalline polyimide which is based on commercially available monomers. The polyimide displays high thermal stability both with regards to the TGA experiments and with respect to its ability to crystallize from the melt after repeated exposures to the high temperature of 450°C. A T_g of ca. 230°C, two distinct and widely spaced prominent melting endotherms at ca. 353°C and 416°C, and a prominent recrystallization process immediately proceeding the end of the lower melting crystals is evident. The two main crystallization endotherms are conjectured to be due to difference in crystal unit cell structures. The lower melting crystals form below ca. 350°C while the higher melting crystals form at higher temperatures. The abrupt increase in peak crystallization times (at ca. 340-345°C) is explained due to low supercooling experienced by the polymer at those temperatures with respect to the equilibrium melting point of the lower melting crystals. Hot stage polarized optical microscopy experiments reveal that the spherulites that develop at 340°C, melt and rapidly give rise to the higher melting spherulites at exactly the same site, when heated to 370°C. This also explains the occurrence of fast recrystallization exotherm immediately proceeding the lower melting endotherm. It is proposed that only a small conformational rearrangement is needed of the chains constituting the lower melting crystals (once heated above their melting point), to give rise to the higher melting crystalline form. The melting behavior depends significantly on the temperature of crystallization, with an additional low melting shoulder appearing 10-15°C above the crystallization temperature when crystallized at temperatures below the position of the lower melting endotherm. Only the higher melting crystals form at temperatures above 345°C leading to only one prominent melting endotherm at ca. 410°C.

For specimens crystallized at 320°C, the primary lower melting endotherm appeared first and the lower melting shoulder developed only for later times. While the strength and the position of the primary lower endotherm does not change much, the shoulder shows a slight increase in strength and temperature of appearance. These results are concluded to support the 'morphological model' where the main lower melting endotherm is due to the melting of the first forming primary crystals and the weak lower melting shoulder is due to the secondary crystallization, which results in thinner crystals. Heating rate studies show that for specimens crystallized at 320°C, the lower melting shoulder becomes part of the primary lower melting peak with increasing heating rate. The main lower melting peak does not shift to lower temperatures with faster heating rates but rather shifts slightly to higher temperatures due to thermal lag. The recrystallization process after the lower melting shoulder that is responsible for the higher melting crystals weakens and finally disappears for faster heating rates. For specimens crystallized at 360°C, a broadening of the higher melting endotherm occurs. However, the peak temperature remains unaffected and does not move to lower temperatures for faster heating rates. It is thus concluded that for both kinds of specimens, the 'morphological model' is applicable. There does not seem to be any evidence which lends credence to a 'continuous melting and recrystallization' process being operative for this polymer. A similar conclusion is reached from the heating rate experiments on the initial film. An isothermal thickening phenomenon occurs at crystallization temperatures in excess of 350°C (giving rise to the higher melting crystals), as concluded from significant increases in melting points (10-14°C) for samples crystallized for longer times. There, however, is an induction time for start of this thickening phenomenon. This time corresponds roughly to the time needed for completion of the primary crystallization at different temperatures.

Reference

¹ Hergenrother, P.M., Stenzenberger, H.D. and Wilson, D., *Polyimides*, Blackie & Sons Ltd., London, 1990.

-
- ² Mittal, K.L. and Ghosh, M.K., *Polyimides, Fundamentals and Applications*, Marcel Dekker Inc., 1996.
- ³ *Polyimides: Trends in Materials and Applications*, Ed. Feger, C., Khojasteh, M.M. and Molis, S.E., Proceedings of the Fifth International Conference on Polyimides, Ellenville, New York, Nov, 1994.
- ⁴ Ratta, V., Stancik, E.J., Ayambem, A., Parvattareddy, H., McGrath, J.E and Wilkes, G.L., *Polymer*, 1999, **40**, 1889.
- ⁵ Srinivas, S., Caputo, F.E., Graham, M., Gardner, S., Davis, R.M., McGrath, J.E. and Wilkes, G.L., *Macromolecules*, 1997, **30**, 1012.
- ⁶ Ratta, V., Ayambem, A., Young, R., McGrath, J.E. and Wilkes, G.L., *Polymer*, submitted for Publication, Nov, 1998.
- ⁷ Chang, A.C., Hou, T.H. and St. Clair, T.L. in *Polyimides: Trends in Materials and Applications*, Ed. Feger, C., Khojasteh, M.M. and Molis, S.E., Proceedings of the Fifth International Conference on Polyimides, Ellenville, New York, Nov, 1994, 3.
- ⁸ Sasuga, T., *Polymer*, 1991, **32**, 1012.
- ⁹ Tamai, S., Yamaguchi, A. and Ohta, M. *Polymer*, 1996, **37**, 3683.
- ¹⁰ Tamai, S., Oikawa, H., Ohta, M. and Yamaguchi, A. *Polymer*, 1998, **39**, 1945.
- ¹¹ Graham, M.J., Srinivas, S., Ayambem, A., Ratta, V., Wilkes, G.L. and McGrath, J.E., *Polymer Preprints*, April, 1997, **38(1)**, 306.
- ¹² Srinivas, S., Graham, M., Brink, M.H., Gardener, S., Davis, R.M., McGrath, J.E. and Wilkes, G.L., *Polym. Engg. Sci.*, 1996, **36**, 1928.
- ¹³ Mitoh, M. and Asao, K., *Polymeric Materials Encyclopedia*, **8**, 1996, 6220.
- ¹⁴ Holden, H.W., *J. Polymer Sci.* **6**, 1964, 53.
- ¹⁵ Mandelkern, L., Fatou, J.G., Denison, R. and Justin, J., *J. Polym. Sci. (B)* **3**, 1965, 803.
- ¹⁶ Bair, H.E., Salovey, R. and Huseby, T.W., *Polymer*, **8**, 1967, 9.
- ¹⁷ Harland, W.G., Khadr, M.M. and Peters, R.H. *Polymer*, **13**, 1972, 13.
- ¹⁸ Passingham, C., Hendra, P.J., Cudby, M.E.A, Zichy, Z. and Weller, M., *Eur. Polym. J.*, **26**, n6, 1990, 631.
- ¹⁹ Samuels, R.J. *J. Polym. Sci. (B)*, **13**, 1975, 1417.
- ²⁰ Edwards, B.C., *J. Polym. Sci. (B)*, **13**, 1975, 1387.
- ²¹ Groeninckx, G. and Reynaers, H., *J. Polym. Sci. (B)*, **18**, 1980, 1325.

-
- ²² Holdsworth, P.J. and Turner-Jones, A., *Polymer*, **12**, 1971, 195.
- ²³ Qiu, G., Tang, Z., Huang, N. and Gerking, L. *J. Appl. Polym. Sci.*, **69**, 1998, 729.
- ²⁴ Tan, S., Su, A., Li, W. and Zhou, E., *Macromol. Rapid Commun.* **19**, 1998, 11.
- ²⁵ Woo, E.M. and Ko, T.Y., *Colloid Polym. Sci.*, **274**, 1996, 309.
- ²⁶ Alfonso, G.C., Pedemonte, E. and Ponzetti, L., *Polymer*, **20**, 1979, 105.
- ²⁷ Zhou, C. and Clough, S.B., *Polym. Eng. Sci.*, **28**, n2, 1988, 65.
- ²⁸ Stein, R.S. and Misra, R.S., *J. Polym. Sci. (B)*, **18**, 1980, 327.
- ²⁹ Nichols, M.E. and Robertson, R.E., *J. Polym. Sci. (B)*, **30**, 1992, 755.
- ³⁰ Cheng, S.Z.D., Pan, R. and Wunderlich, B., *Makromol. Chem.*, **189**, 1988, 2443.
- ³¹ Yeh, J.T. and Runt, J., *J. Polym. Sci. (B)*, **27**, 1989, 1543.
- ³² Kim, H.G. and Robertson, R.E., *J. Polym. Sci. (B)*, **36**, 1998, 1417.
- ³³ Qudah, A.M.A. and Raheil, A.A., *Polymer Int.*, **38**, n4, 1995, 375.
- ³⁴ Chung, J.S. and Cebe, P., *Polymer*, **33**, n11, 1992, 2312.
- ³⁵ Chung, J.S. and Cebe, P., *Polymer*, **33**, n11, 1992, 2325.
- ³⁶ Lattimer, M.P., Hobbs, J.K., Hill, M.J. and Barham, P.J., *Polymer*, **33**, 1992, 3971.
- ³⁷ Lee, Y., Porter, R.S. and Lin, J.S., *Macromolecules*, **22**, 1989, 1756.
- ³⁸ Lee, Y. and Porter, R.S., *Macromolecules*, **20**, 1987, 1336.
- ³⁹ Jonas, A.M., Russell, T.P. and Yoon, D.Y., *Macromolecules*, **28**, 1995, 8491.
- ⁴⁰ Blundell, D.J., *Polymer*, **28**, 1987, 2248.
- ⁴¹ Blundell, D.J. and Osborn, B.N., *Polymer*, **24**, 1983, 953.
- ⁴² Cheng, S.Z.D., Cao, M.Y. and Wunderlich, B. *Macromolecules*, **19**, 1986, 1868.
- ⁴³ Verma, R.K., Velikov, V., Kander, R.G. and Marand, H., *Polymer*, **37**, 1996, 5357.
- ⁴⁴ Marand, H. and Prasad, A., *Macromolecules*, **25**, 1992, 1731.
- ⁴⁵ Marand, H., Velikov, V. and Netopilik, M., *Polymer Preprints*, **34(2)**, 1993, 239.
- ⁴⁶ Marand, H. and Velikov, V., *Polymer Preprints*, **34(2)**, 1993, 835.
- ⁴⁷ Marand, H. and Velikov, V., *J. Therm. Anal.*, **49**, 1997, 375.
- ⁴⁸ Verma, R., Marand, H. and Hsiao, B., *Macromolecules*, **29**, 1996, 7767.
- ⁴⁹ Hsiao, B.S., Sauer, B.B., Verma, R., Zachmann, H.G., Seifert, S., Chu, B. and Harney, P., *Macromolecules*, **28**, 1995, 6931.
- ⁵⁰ Hsiao, B.S., Gardner, K.H., Wu, D.Q. and Chu, B., *Polymer*, **34**, 1993, 3986.
- ⁵¹ Hsiao, B.S., Gardner, K.H., Wu, D.Q. and Chu, B., *Polymer*, **34**, 1993, 3996.

-
- ⁵² Kumar, S., Anderson, D.P. and Adams, W.W., *Polymer*, **27**, 1986, 329.
- ⁵³ Bassett, D.C., Olley, R.H. and Raheil, A.M.A., *Polymer*, **29**, 1988, 1745.
- ⁵⁴ Kroger, K.N. and Zachmann, H.G., *Macromolecules*, **26**, 1993, 5202.
- ⁵⁵ Deslandes, Y., Day, M., Sabir, N.F. and Suprunchuk, T., *Polym. Comp.*, **10**, 1989, 360.
- ⁵⁶ Brandom, D.K. and Wilkes, G.L., *Polymer*, **36**, 1995, 4083.
- ⁵⁷ Brandom, D.K. and Wilkes, G.L., *Polymer*, **35**, 1994, 5672.
- ⁵⁸ Kreuz, J.A., Hsiao, B.S., Renner, C.A. and Goff, D.L., *Macromolecules*, **28**, 1995, 6926.
- ⁵⁹ Hsiao, B.S., Kreuz, J.A. and Cheng, S.Z.D., *Macromolecules*, **29**, 1996, 135.
- ⁶⁰ Sauer, B.B. and Hsiao, B.S., *Polymer*, **36**, 1995, 2553.
- ⁶¹ Hsiao, B.S., Sauer, B.B. and Biswas, A., *J. Polym. Phys.*, **32**, 1994, 737.
- ⁶² Harrison, I.R., *Polymer*, **26**, 1985, 3.
- ⁶³ Yoon, D.Y. and Flory, P.J., *Faraday Discussions of the Chemical Society*, **n68**, *Organization of Macromolecules in the Condensed Phase*, 1979, 288.
- ⁶⁴ Mandelkern, L., *Characterization of Materials in the Research: Ceramics and Polymers*, Syracuse University press, Syracuse, New York, 1975, 369.
- ⁶⁵ Hoffman, J.D., Davis, G.T. and Lauritzen, J.I. *Treatise on Solid State Chemistry*, Ed Hannay, N.B., Plenum Press, New York, 1976, Vol. **3**, Chapter 7.
- ⁶⁶ Hoffman, J.D., Frolen, L.J., Ross, G.S. and Lauritzen, J.I., Jr. *J. Research NBS Sect. A* 1975, **79**, 671.
- ⁶⁷ Marand, H., Xu, J. and Srinivas, S., *Macromolecules*, **31**, 1998, 8219.
- ⁶⁸ Marand, H., Xu, J., Agarwal, P. and Srinivas, S., *Macromolecules*, **31**, 1998, 8230.
- ⁶⁹ Hoffman, J.D., *Polymer*, **32**, 1991, 2828.
- ⁷⁰ Flory, P.J. and Vrij, A.J., *J. Am. Chem. Soc.*, **85**, 1963, 3548.

Chapter 9

Summary and Recommendations for Future Work

9.1 Summary

The essence of this research work is well encapsulated by the title of this work, namely, “*Crystallization, Morphology, Thermal Stability and Adhesive Properties of Novel High Performance Semicrystalline Polyimides*”. Indeed the title is emblematic of the broad range of topics covered in this research. These topics were critically important in the way they were interrelated for the overall success of this work. In this regard, the present chapter concludes this thesis by summarizing the motivation and the achievements of this research and recommending future work in this area.

A number of advances have been made in the field of polyimides in the past two decades that have made possible their use in diverse applications ranging from ‘interlayer dielectric’ to ‘structural adhesive’ that helps to hold the wing panels and fuselage of aircraft together. Despite these advances, several research topics in this area have still not received adequate attention. One such major area has been the development of linear aromatic polyimides that are amenable to melt processing. It is thus no surprise, that to this day with very few exceptions like New-TPI^{1,2} and possibly some versions of LARC-TPI, which can be processed from the melt to a small extent, almost all polyimides (including the thermoplastic ones) are exclusively being processed by the solvent route. While polyimides offer tremendous opportunities due to the diverse range of useful properties, this limitation has certainly impeded their advancement with respect to large scale applications. Melt processing is obviously beneficial as it is (1) environmentally friendly (does not require handling dangerous solvents often associated with polyimides) (2) involves significantly shorter cycle times (3) processing is easier (4) often economically more attractive and (5) makes some large scale applications viable.

Another attractive feature desirable in linear aromatic thermoplastic polyimides is the presence of crystallinity, which leads to substantial improvement in many properties including solvent resistance, radiation stability and partial retention and enhancement of

certain mechanical properties much above the glass transition temperature. These attributes make semicrystalline polyimides especially attractive and efforts to develop these materials continue among various research groups around the world^{3, 4} and here at Virginia Tech^{5,6,7}. This work constitutes another step in this direction. In this regard, the present work has accomplished significant goals in this area both with regards to the fundamental viewpoint and with respect to future potential uses of these polymers as high temperature and high performance adhesives. The broad research objectives successively attained by the work presented within this dissertation can be briefly listed as:

- (1) High temperature and high performance semicrystalline polyimides that display superior solvent resistance and higher thermal stability, have been developed.
- (2) The polyimides are also melt processable. Melt viscosity was studied with respect to melt temperature, melt time (at different melt temperatures) and frequency (also at different melt temperatures).
- (3) One of these polyimides has been used extensively as a hot-melt adhesive. Some of the promising results of this study were:
 - Simple and economical grit blasting was a sufficient surface treatment.
 - Bonding process was simple, solvent free and involved relatively less times.
 - Very high lap-shear strengths of ca. 6600-8400 psi were obtained.
 - The strengths remained unaffected on exposure to various common solvents.
 - Considerable durability of these strengths was observed with respect to high aging and testing temperatures.
- (4) Wedge and DCB tests revealed the considerable solvent resistance and fracture toughness of this adhesive respectively.
- (5) Also, another attractive and distinguishing feature of the research has been that all the polyimides synthesized are based on monomers that are commercially available. This makes these polyimides potentially attractive from the commercial standpoint in the future.
- (6) One more important characteristic attained in these polyimides was the fast crystallization kinetics from the melt. This feature is particularly important as faster crystallization kinetics removes any need of a post annealing process to introduce crystallinity in the material. The semicrystalline morphology and bulk

crystallization kinetics was studied with respect to crystallization temperature, previous melt temperature and melt time.

- (7) A new polyimide based on the same diamine but a different dianhydride, BTDA was developed. Some features of this study were:
- The polyimide displayed considerable bulk thermal stability and recrystallization stability from high melt temperatures.
 - Intermediate dual melting behavior with an intermediate recrystallization exotherm.
 - Additional melting shoulders due to secondary crystallization and absence of a continuous melting-recrystallization process.
 - A crystal thickening phenomenon at high crystallization temperatures.

9.2 Recommendations for Future Work

While there were considerable doubts about the bulk melt processing of these materials at the start of this work, the research presented in this thesis has come a long way in removing many of these reservations. It has been proved that for at least one of the polyimides, TPER-BPDA, the melt processing can be effectively conducted. Although the lower molecular weight version of this polyimide ($M_n=15,000$ daltons) provided a sufficiently low viscosity for extensive testing as a hot melt adhesive, it also necessitated making large amounts of the polyimide film. For any such large applications of this material, the availability of large amounts of material in film form (which cannot be just made using the traditional film casting during synthesis) would be necessary. In this regard, there is an important need for film extrusion of this material. This could be a promising area of research as large scale film production, if possible, would make adhesive and other applications feasible. The melt extrusion itself could be attempted in two ways – (a) either the final polyimide could be extruded into a film form or (b) partially imidized polymer could be extruded (with the completion of imidization reaction during the extrusion process). For (a), the shear thinning behavior of the polyimide will make it easier to be extruded. For (b), the partially imidized polyimide

would provide lower viscosity and possibly a lower melt temperature requirement for extrusion. The molecular weight of the polyimide, its degree of imidization and the extrusion temperature will be important factors in this regard. Also, there is some possibility of foam formation due to evolution of water during the imidization reaction.

Before the above mentioned experiment are attempted, it may be often more useful to first extrude the material into a fiber form as it requires less material and is usually easier to carry out. Once the conditions for such a process are optimized, film extrusion could be carried out subsequently. WAXD experiments on such fibers may produce a significantly better defined (in terms of increased and sharper reflections) pattern, thus making it possible to determine the unit cell crystal structure with considerable accuracy. Additionally, the effect of either a film and fiber extrusion process on the percentage crystallinity and melting behavior could be studied. The study of percentage orientation and the crystalline morphology could be an important area of research. It would also be interesting to see the effect of melt extrusion process on the partial melting and recrystallization behavior during the heating scan in a DSC, as the nature of the crystalline morphology (to the lamellar level) is expected to be different.

Another exercise attractive from a fundamental viewpoint is molecular modeling of the various polyimides. Such a study may throw considerable light on the nature of the *conformation* of the overall chain and the individual repeat units. Such information may then be correlated with the information from SAXS experiments to check if the lamellar thickness' could be correlated with such information. Also, the information on chain conformation together with the crystal unit cell data could be useful in getting to the constitution of an average unit cell and subsequently the crystalline density. Obtaining the absolute crystalline and amorphous densities could be a very useful information for subsequent studies with this material. The percentage crystallinity for a given sample could then be easily calculated using density measurement techniques. This information, in conjunction with other DSC experiments, would also be useful in calculating another useful parameter, the heat of fusion for the 100% crystalline material.

TPER-BPDA polyimide has yielded encouraging adhesion results with respect to lap-shear, wedge and DCB tests. However, 'peel test', which is another important and widely utilized adhesion test has not so far been conducted. This test, if conducted, could

provide important information for this polyimide adhesive. The important parameters with respect to this study could include the bonding conditions, cooling rate from the melt and the peel rate. This study, however would require substantial amounts of the polyimide film and thin titanium alloy sheets (ca. 50 microns).

From an application viewpoint, another area of future research involves the potential use of this material as an interlayer dielectric. Obviously, the important parameter from this viewpoint is the 'dielectric constant' of the polyimide and will need to be determined first. The thermal expansion coefficient (CTE) is another important parameter from this viewpoint as a large CTE could cause significant mismatch between the bonded adherends. Some preliminary work by this author has yielded a very low CTE of $15 \times 10^{-6}/^{\circ}\text{C}$ (from room temperature till ca. 250°C), which is a very encouraging result. Further work, however, would need to be carried out in this regard.

While many polyimides and associated copolymers have been synthesized in this research work (see Table 8.1), only two of these polyimides have provided attractive properties. Especially, the results of the polyimide based on TPER diamine and BPDA dianhydride have been particularly encouraging from a thermal stability, crystallization and adhesion viewpoint. Thus, in this authors opinion, future work should focus more on the scaling up the synthesis of this polyimide rather than varying the chemical structure of the polyimide. Further work, that needs to be carried out in adhesion and other areas demands much larger quantities of this material than is presently available.

References:

-
- ¹ Hou, T.H. and Reddy, R.M. *SAMPE Journal*, **Jan** 1991, 38.
 - ² Hsiao, B.S., Sauer, B.B. and Biswas, A. *J. Polym. Sci., Part B*, 1994, **32**, 737.
 - ³ Tamai, S., Ohta, M. and Yamaguchi, A. *Polymer* 1996, **37**, 3683.
 - ⁴ Hsiao, B.S., Kreuz, J.A. and Cheng, S.Z.D. *Macromolecules* 1996, **29**, 135.
 - ⁵ Muellerleile, J. *Ph.D. Thesis*, Virginia Polytechnic Institute and State University, Sep, 1991, Blacksburg, VA.

⁶ Brandom, D.K. *Ph.D. Thesis*, Virginia Polytechnic Institute and State University, June 1996, Blacksburg, VA.

⁷ Srinivas, S. *Ph.D. Thesis*, Virginia Polytechnic Institute and State University, June 1996, Blacksburg, VA.